Josip Juraj Strossmayer University of Osijek

University of Dubrovnik

Ruđer Bošković Institute

Doctoral Study of Molecular biosciences

Maja Jirouš Drulak

Characterisation of the phenotype, transcriptional markers and T cell receptor repertoire of circulating MAIT and γδ T lymphocytes in psoriasis vulgaris

PhD thesis

Osijek, 2024.

BASIC DOCUMENTATION CARD

Josip Juraj Strossmayer University of Osijek **PhD thesis**
University of Dubrovnik
Ruđer Bošković Institute
Doctoral Study of Molecular biosciences

Scientific Area: Interdisciplinary area of science
Scientific Fields: biology, basic medical sciences

Characterisation of the phenotype, transcriptional markers and T cell receptor repertoire of circulating MAIT and γδ T lymphocytes in psoriasis vulgaris

Maja Jirouš Drulak

Thesis performed at: Laboratory for DNA analysis, Faculty of Medicine Osijek, J.J. Strossmayer University of Osijek, Croatia; Division of Biomedical Sciences, Warwick Medical School, University of Warwick, United Kingdom; Department of Immunology and Biotechnology, University of Pécs Medical School, Hungary.

Supervisor 1: Assoc. Prof. Stana Tokić
Supervisor 2: Assoc. Prof. Martin Davey

Short abstract: Psoriasis vulgaris is a chronic T-cell driven autoinflammatory dermatosis in which unconventional mucosal-associated invariant T (MAIT) and γδ T cells play poorly understood roles. Through a comprehensive characterisation of circulating MAIT and γδ T cells, this study revealed alterations in their frequencies, transcriptional profiles, TCR repertoires, and phenotypic and functional properties, influenced by disease duration, severity, age and sex, elucidating their contribution to disease pathogenesis.

Number of pages: 208
Number of figures: 74
Number of tables: 33
Number of references: 304
Original in: English
Key words: psoriasis vulgaris, γδ T cells, MAIT cells

Date of the thesis defense:

Reviewers:
1.
2.
3.
4. (substitute)

Thesis deposited in: National and University Library in Zagreb, Ul. Hrvatske bratske zajednice 4, Zagreb; City and University Library of Osijek, Europska avenija 24, Osijek; Josip Juraj Strossmayer University of Osijek, Trg sv. Trojstva 3, Osijek

TEMELJNA DOKUMENTACIJSKA KARTICA

Sveučilište Josipa Jurja Strossmayera u Osijeku **Doktorski rad**
Sveučilište u Dubrovniku
Institut Ruđer Bošković
Doktorski studij Molekularne bioznanosti

Znanstveno područje: Interdisciplinarno područje znanosti
Znanstvena polja: biologija, temeljne medicinske znanosti

Karakterizacija fenotipa, transkripcijskih biljega i repertoara T staničnih receptora cirkulirajućih limfocita MAIT i γδ T u vulgarnoj psorijazi

Maja Jirouš Drulak

Doktorski rad je izrađen u: Laboratoriju za analizu DNA, Medicinski fakultet Osijek, Sveučilište J. J. Strossmayera u Osijeku, Hrvatska; Odjelu za biomedicinske znanosti, Medicinski fakultet Warwick, Sveučilište Warwick, Ujedinjeno Kraljevstvo; Odjelu za imunologiju i biotehnologiju, Medicinski fakultet, Sveučilište u Pečuhu, Mađarska.

Mentor 1: izv. prof. dr. sc. Stana Tokić
Mentor 2: izv. prof. dr. sc. Martin Davey

Kratki sažetak doktorskog rada: Psorijaza vulgaris kronična je autoupalna dermatoza posredovana limfocitima T, u kojoj nekonvencionalne sluznici pridružene invarijantne T (MAIT) i γδ T stanice imaju još uvijek nedovoljno shvaćenu ulogu. Ovaj rad, kroz sveobuhvatnu karakterizaciju cirkulirajućih MAIT i γδ T stanica, otkriva promjene u njihovoj učestalosti, transkripcijskim profilima, TCR repertoarima te fenotipskim i funkcionalnim svojstvima, koje su pod utjecajem trajanja i težine bolesti, dobi i spola, čime se ističe njihov doprinos patogenezi bolesti.

Broj stranica: 208
Broj slika: 74
Broj tablica: 33
Broj literaturnih navoda: 304
Jezik izvornika: engleski
Ključne riječi: psorijaza vulgaris, γδ T limfociti, MAIT limfociti

Datum javne obrane:

Povjerenstvo za javnu obranu:

1.
2.
3.
4. (zamjena)

Doktorski rad je pohranjen u: Nacionalnoj i sveučilišnoj knjižnici Zagreb, Ul. Hrvatske bratske zajednice 4, Zagreb; Gradskoj i sveučilišnoj knjižnici Osijek, Europska avenija 24, Osijek; Sveučilištu Josipa Jurja Strossmayera u Osijeku, Trg sv. Trojstva 3, Osijek

This thesis was conducted at the Laboratory for DNA analysis, Faculty of Medicine Osijek, J.J. Strossmayer University of Osijek, Croatia, the Division of Biomedical Sciences, Warwick Medical School, University of Warwick, UK, and the Department of Immunology and Biotechnology, University of Pécs Medical School, Hungary. Financial support for this research was provided by the Croatian Science Foundation through the project "NGS analysis of MAIT and γδ T cell transcriptome: phenotype, function and TCR repertoire in the aetiology of psoriasis vulgaris" (UIP-2019-04-3494, PI: Assoc. Prof. Stana Tokić) and Royal Society Wolfson Fellowship (RSWF\R2\222002, PI: Assoc. Prof. Martin Davey). Additional support for travel and international collaboration was provided by the Croatian Science Foundation (MOBDOK-2023), European Federation of Immunological Societies (EFIS-IL Short-Term Fellowship) and Erasmus+ Mobility Program.

TABLE OF CONTENTS

1. INTRODUCTION

1.1. Clinical presentation, diagnosis and evaluation of psoriasis severity

Psoriasis is a highly variable disease, both in terms of clinical presentation and severity. There are five distinct clinical phenotypes: plaque, guttate, erythrodermic, pustular, and inverse/flexural psoriasis. Plaque psoriasis, also known as psoriasis vulgaris, is the most prevalent form of the condition, accounting for approximately 85–90% of psoriasis cases (1–4).

Psoriasis vulgaris is characterised by well-defined erythematous plaques covered with silvery-white scales (Figure 1), typically symmetrically distributed on predilection sites such as the elbows, knees, forearms, shins, trunk and scalp (1,3,5). The detachment of scales may lead to tiny spots of bleeding, referred to as the "Auspitz sign", although this sign is not specific to psoriasis (2,5). The diagnosis of psoriasis vulgaris is generally based on clinical findings, which are confirmed by histological examination of a skin biopsy (1,5,6).

Several scoring systems are used to assess disease severity, with the Psoriasis Area Severity Index (PASI) introduced in 1978 being the most widely validated tool (7). The PASI score is calculated by dividing the body into four regions (head (h), upper limbs (u), trunk (t), and lower limbs(l)) and assessing the severity of erythema (E), induration (I), and desquamation (D) in each region, as well as the percentage of area affected. Severity is scored on a scale from 0 to 4 (0 = none; 4 = very severe), and area involvement is scored on a scale of 1 to 6 (1 = less than 10 %; 2 = 10–29 %; 3 = 30–49 %; 4 = 50–69 %; 5 = 70–89 %; and 6 = greater than 90 %). The PASI score is calculated using the formula: PASI = 0.1(Eh + Ih + Dh)Ah + 0.2 (Eu + Iu + Du)Au + 0.3 (Et + It + Dt)At + 0.4 (El + Il + Dl)Al, with a maximum possible score of 72 (5,8,9).

The impact of skin disease on quality of life is most commonly assessed using the Dermatology Life Quality Index (DLQI), a self-assessment questionnaire that evaluates symptoms, daily activities, work, social life, and the burden of treatment (10). Each question is graded on a scale from 0 to 3 (0 = not relevant, 3 = very relevant), with scores ranging from 0 to 30. A DLQI score above 10 indicates a significant impairment in quality of life (8,9).

Psoriasis varies greatly in morphology and distribution, from a few localised plaques to involvement of almost the entire body surface (11). The disease may be chronic and stable, or rapidly progressive, affecting large areas of the body and often triggering comorbidities. This

wide heterogeneity among patients remains puzzling, and underlines the need to further investigate the genetic, environmental and immunological factors contributing to this phenomenon.

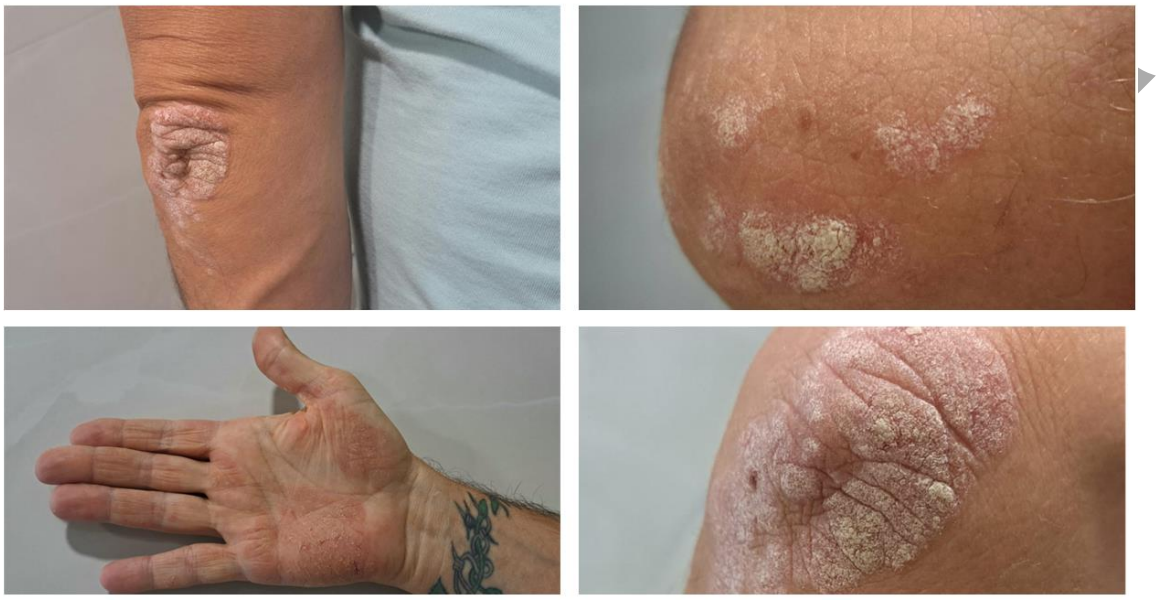

Figure 1. **Psoriatic plaques on elbows and hands.** *Author's work.*

1.2. Epidemiology and burden of psoriasis

1.2.1. Epidemiology and demographics

The worldwide prevalence of psoriasis is 2–3%, affecting over 125 million people of all age groups, ethnicities, and geographical regions (5,12). However, its prevalence varies significantly between populations, with higher rates in Western populations (American, Canadian, and European), compared to those of African and Asian descent (13,14). This variation most likely reflects the interaction between environmental factors and genetic predispositions.

Psoriasis can develop at any age, even in childhood, although the prevalence in children remains lower, at less than 1% (15). Interestingly, several studies suggest that about one third of cases begin in childhood (16). Psoriasis is most prevalent in adults aged 50–69 years (12), with several studies identifying a bimodal onset pattern. Early-onset psoriasis typically develops before the age of 40, most commonly between 15 and 30 years, while late-onset psoriasis presents after 40, with peak incidence between 50 and 60 years (3,7,8). This bimodal

distribution has been used to classify psoriasis into two subtypes: Type I, characterised by early onset, a positive family history, and a connection to the HLA-C*06:02 allele; and Type II, or late-onset psoriasis, which lacks a family history and is not linked to HLA-C*06:02 (19).

Although it is generally considered that psoriasis occurs with similar frequency in both sexes, several studies indicate a higher incidence in men (11,12,20). There are also indications that men exhibit more severe forms of the disease (21–23), as they are more likely to get systemic biologic therapy (24). Despite these findings, research on gender differences in psoriasis remains limited and the evidence is not yet conclusive.

1.2.2. Comorbidities

In addition to its visible impact on the skin, psoriasis is frequently associated with various comorbidities (25,26), with psoriatic arthritis being one of the most common, affecting 10–30% of patients. Although it often emerges after the onset of psoriatic skin lesions, in some cases, it may precede the manifestation of cutaneous symptoms (27,28). Psoriasis patients are also at higher risk of developing cardiovascular conditions, such as hypertension, atherosclerosis, and myocardial infarction, particularly in severe and prolonged disease (29). In addition, severely affected patients are more susceptible to autoimmune diseases, such as rheumatoid arthritis, systemic lupus erythematosus and inflammatory bowel disease (30).

While psoriasis alone typically has no impact on survival, severe disease forms are linked to increased risk of mortality and a reduced life expectancy, primarily due to associated comorbidities (17,20,31). Beyond physical symptoms, psoriasis imposes emotional and social challenges that can greatly diminish patient's quality of life. The chronic nature and discomfort of the disease also contribute to a higher incidence of psychiatric disorders, with over 5% of patients experiencing depression and suicidal thoughts (12,17). The treatment of psoriasis, especially in severe cases, leads in significant healthcare costs, both for direct psoriasis treatment and ongoing care of related comorbidities (32–34). Overall, psoriasis places a considerable burden on both physical and mental well-being, complicating long-term management.

1.3. Genetic and environmental factors in psoriasis pathogenesis

Psoriasis is a multifactorial disease with a complex aetiology, driven by the interplay between genetic predisposition and environmental factors. Although its precise causes are not fully understood, it is generally believed that psoriasis manifests in genetically susceptible individuals after exposure to certain external factors.

1.3.1. Genetic factors in psoriasis pathogenesis

Heritability plays a significant role in psoriasis susceptibility, with genetic factors estimated to account for 70–90% of the risk (35,36). Studies show a higher prevalence of psoriasis within families (37) and a 2-3 times greater risk of developing psoriasis among monozygotic twins compared to dizygotic twins (4,5,35,38). In addition, up to 71% of childhood psoriasis cases have a positive family history, which further emphasises the genetic influence (35,36).

In early genetic studies of psoriasis, linkage analyses were performed in families with a history of the disease, leading to the identification of nine psoriasis-associated loci (PSORS1 to PSORS9) (36,41,42). Among these, PSORS1 emerged as the most significant, with genome-wide linkage studies consistently showing that the HLA-C*06:02 is the primary susceptibility marker, contributing up to 50% to the disease heritability (4,18,41). Over 60% of patients carry this allele, which is linked to early onset, severe disease, and susceptibility to streptococcal infections (43,44). Other key genes associated with psoriasis are central to both adaptive and innate immunity. These include genes associated with antigen presentation (*ERAP1, ERAP2, MICA)*, NF-κB signalling (*TNFAIP3, TNIP1, TRAF3IP2, CARD14*), the type 1 interferon pathway (*RNF113, IFIH1*), T cell development and polarisation (*RUNX1, RUNX3, STAT3, TAGAP, IL4, IL13*), and the IL-23–Th17 axis (*IL23R, IL12B* and *TYK2, JAK2*) (3,5,18).

Despite the identification of over 80 genes associated with psoriasis, these account for only 30% of heritability. In addition, the incomplete concordance of psoriasis in monozygotic twins and the lack of a clear inheritance pattern suggests that remaining heritability may be due to cumulative impact of numerous minor genetic variations and environmental influences (5,13,35,42,45).

1.3.2. Environmental factors triggering psoriasis

External and internal triggers play a crucial role in the initiation and exacerbation of psoriasis. Factors such as infections, microbiome dysbiosis, physical trauma, medication, smoking, stress, and alcohol might significantly influence gene-environment interaction that contribute to disease onset, and can also provoke or worsen psoriasis symptoms (12,18).

The link between *Streptococcus pyogenes* infections and psoriasis, particularly guttate psoriasis, is well documented. Several studies have shown that throat infections often precede psoriasis onset or worsen its symptoms (44,46), with some patients experiencing significant improvement after tonsillectomy (44,47–49). Moreover, the discovery of identical T cell clones in both the tonsils and psoriatic plaques suggests that the cross-reactivity between the tonsil and skin immune response may be mediated by molecular mimicry (50,51).

Microbiome dysbiosis is also increasingly recognized in psoriasis pathogenesis. Psoriatic skin often shows reduced microbial diversity, with increased colonisation by species such as *C. simulans, C. kroppenstedtii*, *S. aureus* and *S. pyogenes*, along with a decrease in *Lactobacilus*. However, the inconsistent findings of several studies highlight the need for further research to clarify the role of microbiota in the development of psoriasis (52–54).

Physical trauma, such as tattoos or surgical cuts, can induce psoriatic lesions on previously unaffected skin, known as the Koebner phenomenon (55). Other stimuli, including radiotherapy, UV exposure, and even mild skin irritation, have also been reported to induce new lesions (47).

Lastly, smoking has been shown to influence psoriasis severity, especially in terms of comorbidities. Moreover, the interaction between HLA-C*06:02 and cigarette smoking or stress have been identified as potential factors in the development of the disease (13,56).

1.4. Histopathology of psoriatic plaques

The skin is composed of three main layers: the epidermis, the dermis and the hypodermis. The epidermis consists mainly of keratinocytes and is divided into five layers: the stratum basale, stratum spinosum, stratum granulosum, stratum lucidum, and stratum corneum, listed from the deepest to most superficial. Beneath the epidermis, the dermis provides a structural support through collagen fibres and hosts various immune cells, including dermal dendritic cells, αβ T cells, γδ T cells, natural killer cells, B cells, mast cells, and macrophages. The deepest layer, the hypodermis, is primarily made up of subcutaneous adipose tissue and

supportive stromal cells (57).

Psoriatic lesions display distinctive histopathological changes, including a significant thickening of the epidermis caused by increased keratinocyte proliferation and altered differentiation, resembling "regenerative maturation". Hallmark features include hyperkeratosis (thickening of the stratum corneum resulting in scales formation), acanthosis (thickening of the stratum spinosum), and parakeratosis (retention of cell nuclei in the cornified layer), often with a thin or absent granular layer. Additional characteristics include elongated rete ridges, dilated dermal capillaries, and abnormal stacking of corneocytes, impairing the skin barrier. Neutrophil clusters in the stratum corneum form Munro's microabscesses, while immune cell infiltration, primarily composed of T cells, is prominent in both dermis and epidermis (8,23,25,55–57).

1.5. Immunopathogenesis of psoriasis

Psoriasis was initially considered a keratinocyte disorder until research in the 1970s revealed the crucial role of immune cells. By the 1990s, the focus shifted to T cells, with Th1 and Th17 cells being identified as key drivers of inflammation through cytokines such as TNF-α, IFN-γ, IL-17, and IL-23 (61). Recently, several candidate autoantigens identification has opened new avenues, although their exact role in disease pathogenesis remain under investigation (62–65). At the same time, significant progress has been made in the development of biological therapies targeting key cytokine pathways involved in disease progression (57,63,64). Moreover, the recirculation of pathogenic T cells and the release of pro-inflammatory cytokines from inflamed lesions contribute to systemic inflammation, leading to the recognition of psoriasis as a systemic disease with distinct cutaneous and systemic aspects (2,68,69).

1.5.1. Cellular and molecular interactions driving psoriatic plaque formation

Psoriatic plaque formation involves a complex network of interactions between resident and infiltrating cells, including T cells, dendritic cells, NK cells, macrophages, keratinocytes, and endothelial cells. This crosstalk is driven by the persistent production of pro-inflammatory cytokines, sustaining chronic inflammation and contributing to the disease pathology.

Dendritic cells are thought to initiate psoriatic inflammation by responding to signals from stressed keratinocytes, which release antimicrobial peptides, especially LL-37, a key

mediator in plaque development (70,71). LL-37 binds to self-DNA/RNA fragments, forming immunostimulatory complexes that activate plasmacytoid dendritic cells (pDCs), which are usually not present in healthy skin but infiltrate early psoriatic lesions (63). Following activation, pDCs secrete large amounts of type I interferons (IFN-α and IFN-β) (72), which activate other immune cells, such as myeloid dendritic cells (mDCs). These mDCs produce proinflammatory cytokines like TNF-α, IL-23, and IL-12, which influence naïve T cells differentiation. In addition, dendritic cells may also directly activate T lymphocytes by presenting autoantigens (63).

Among dendritic cell-derived cytokines, IL-12 promotes Th1 differentiation, leading to IFN-γ production. IFN-γ amplifies the inflammatory cascade by activating macrophages and keratinocytes, further recruiting immune cells (73). In the past, psoriasis was considered a primarily Th1/Tc1 and IFN-γ-driven disease, supported by Th1 and Tc1 cell increases in psoriatic plaques (70, 71). However, more recent studies have shown that the IL-23/IL-17 axis plays a decisive role (76), as IL-23, in association with IL-6 and other cytokines, drives the differentiation and expansion of IL-17 producing cells (77). IL-17, in turn, acts on keratinocytes, and stimulates them to produce chemokines such as CXCL1, CXCL2, CXCL5, and CXCL8, which recruit neutrophils, and CCL20, which attracts $CCR6^+$ T cells. In addition, IL-17 stimulates the production of antimicrobial peptides like LL-37 and S100 proteins (S100A7/8/9/15), further fuelling the inflammatory response (78). Together, IL-17, and TNF-α, promote IL-23 production in keratinocytes (75), creating a feedback loop that drives sustained keratinocyte proliferation and continuous immune cell recruitment characteristic of psoriasis.

The immune reactions described here provide a brief overview of the complex molecular and cellular mechanisms underlying the formation and progression of psoriatic plaques. The discovery of these pathways was also of high importance for the development of targeted therapies. The discovery of TNF-α inhibitors, such as infliximab and etanercept, marked a significant breakthrough in psoriasis treatment (80,81). Later, the discovery of IL-23/IL-17 axis paved the way for new routes in biologics research, providing highly effective therapies targeting IL-23 and IL-17, such as ustekinumab and secukinumab (82). However, while these biologic therapies have transformed the treatment of moderate and severe forms of psoriasis, a subset of patients do not respond to them, underscoring the need for a better understanding of the heterogeneity of the psoriasis immunopathogenesis in order to allow for more personalised treatment (83,84).

1.5.2. T cells in psoriatic lesions

Psoriasis is undoubtedly recognised as a T cell-mediated pathology, with a complex network of T cell subtypes central to its pathogenesis. While the exact trigger for psoriatic plaque formation remains unclear, key players include tissue-resident memory T (T_{RM}) cells, as well as infiltrating effector T helper (Th) and cytotoxic (Tc) cells. In addition, regulatory T cells (T_{regs}), natural killer T (NKT), mucosal-associated invariant T (MAIT), and gamma delta T (γδ T) cells, though less studied, add to the complexity of the inflammatory response (85).

T_{RM} cells are considered significant in sustaining chronic inflammation within psoriatic plaques, as evidenced by the recurrence of lesions at the same sites after therapy discontinuation (86–88). In human skin, $CD4^+$ Th cells predominantly reside in the dermis, while $CD8^+$ Tc cells are concentrated in the epidermis (85). IL-17-producing $CD8^+CD69^+CD103^+$ Tc cells, linked with more severe and persistent disease, highlight the importance of cytotoxic TRM cells in psoriasis (87,89,90). Furthermore, Th17, Th1, and Tc1 cells have been extensively studied as these immune players are major sources of IL-17, IFN-γ, and TNF-α (74,91,92).

The increased activation of T cells in psoriasis, alongside its proposed autoimmune aspects, have prompted numerous research groups to seek out the autoantigens that drive autoreactive T cell responses. These studies have led to the identification of several candidate autoantigens, namely LL-37, ADAMTSL5, PLA2G4D, and keratin 17 (62–64,93,94). These proposed autoantigens, however, possess distinct molecular characteristics and are released by different cell types. For example, LL-37 and ADAMTSL5 are of peptide origin, with LL-37 largely produced by keratinocytes, while ADAMTSL5 is expressed in melanocytes. In addition, PLA2G4D is an enzyme elevated in psoriatic mast cells, and keratin 17, highly expressed in lesional epidermis, is associated with molecular mimicry due to high structural homology with M protein released by *S. pyogenes*. This diversity of autoantigens reflects the heterogeneity of the psoriatic immune response and suggests the absence of a singular, universal autoantigen. Furthermore, the variability in patient reactivity to these antigens fuels an ongoing debate as to whether psoriasis is primarily an autoimmune disease driven by specific autoantigen-T cell interactions or an autoinflammatory condition where innate immune activation may secondarily lead to autoreactive processes (65,78).

TCR sequencing has provided insights into T cell specificity in psoriatic lesions, revealing shared TCRα, TCRβ, and TCRγ clonotypes among psoriasis patients, but absent in healthy controls (95), and oligoclonal T cell populations in therapy-resolved lesions (96),

suggesting common drivers of psoriatic inflammation. However, polyclonal T cell infiltrates in untreated lesions indicated that many T cells in psoriatic lesions originate from the circulating pool and relocate to the site of inflammation (95,96). Single-cell transcriptomic profiling of cutaneous T cells further revealed a cytotoxic signature in psoriatic plaques, with elevated levels of *GZMA*, *GZMB*, *PRF1*, *CD8A*, *GZMK*, and *GNLY*, along with increased expression of chemotactic factors *CCL3*, *CCL4*, *CCL5*, and *CCL20*, all correlating with disease severity (97). These lesional T cells perpetuate chronic inflammation by mediating tissue damage and recruiting additional immune cells.

1.5.3. Circulating T cells in psoriasis

To migrate from the bloodstream into the skin, circulating T cells use a specific set of chemokine receptors. This "skin-homing barcode" that directs T cells toward the skin includes CCR4, CCR6, CCR8, CCR10, and CXCR3 (98). In addition, cutaneous lymphocyte antigen (CLA), a glycoprotein formed by the post-transcriptional modification of platelet selectin glycoprotein ligand-1, PSGL-1, promotes T cell interaction with endothelial E- and P-selectins, facilitating skin infiltration (99). CLA serves as a biomarker of T cells involved in cutaneous pathologies and is expressed on approximately 15% of αβ T and 30% of γδ T cells in circulation, and on up to 90% of T cells in the skin (98,100–105). Notably, the frequency of CLA^+ cytotoxic $CD8^+$ T cells is increased in the peripheral blood of psoriasis patients, correlates with disease severity (78,104,106,107) and suggests a key role in early plaque initiation (108).

Recirculation is a key concept in understanding the behaviour of CLA^+ T cells in psoriasis. Studies have demonstrated that circulating CLA^+ T cells correlate with disease severity and therapeutic outcomes. For instance, monoclonal antibody targeting CD11a, involved in T cell extravasation, has been shown to increase CLA^+ cells in the peripheral blood by preventing T cell redistribution into the skin (109,110). In contrast, systemic anti-TNF-α therapies (104) and localised UVB therapy have been shown to significantly decrease CLA^+ cell proportions (111). Collectively, findings underscore the importance of skin-blood recirculation in psoriasis-related inflammation, although direct mechanistic evidence for CLA^+ T cell recirculation remains limited. Recent studies have provided insight into T cell migration dynamics in psoriasis. Phenotypic analysis of peripheral T cells and gene expression profiling in psoriatic plaques revealed that the proportion of CLA^+ $CD4^+$ memory T cells

expressing chemokine receptors such as CCR6, CCR4, and CXCR3 negatively correlates with disease severity. In parallel, transcriptomic levels of lymph node-homing CCR7 and the CLA-encoding gene *SELPLG* increased in psoriatic lesions suggested a dynamic movement of T cells between skin and bloodstream (112). Moreover, animal model studies have shown that $CD4^+$ T_{RM} cells can downregulate CD69, enabling them to exit primary skin sites. Of note, $CD4^+$ CLA^+ $CD103^+$ T cells found in peripheral blood shared phenotypic, transcriptional and clonotypic features with those in the skin, underpinning the notion of recirculation. These cells, in addition, showed the ability to repopulate secondary skin sites and re-express CD69 (113), suggesting that such recirculation of pathogenic T cells in psoriasis may lead to the formation of new lesions.

While CLA plays a crucial role in T cell migration into the skin, not all T cells in psoriatic plaques express CLA, indicating that CLA is not essential for skin infiltration (108). This was recently confirmed by a single-cell TCR-coupled sequencing study which found that clonally expanded T cells in the skin lesions matched those of the circulating CLA^+ fraction, but also revealed significant clonotypic overlap between CLA^- and lesional T cells, suggesting that non-CLA^+ T cells also contribute to the inflammatory process in psoriasis. In addition, CLA^- T cells exhibited a higher degree of clonality, further emphasising the systemic nature of the disease (68). These findings were corroborated by studies comparing T cell clonotypes in peripheral blood and lesional skin from psoriasis vulgaris and atopic dermatitis patients, where psoriasis patients showed a greater overlap between peripheral and lesional clonotypes, with upregulation of genes associated with TNF-α and IFN-γ responses, cell adhesion, and cytolytic potential (97).

In addition to the single-cell sequencing, several studies have identified elevated levels of inflammatory T cells, including Th17, Th22, Th1 cells and Tregs (106,107,111,114–116), in the peripheral blood of psoriasis patients. In addition, bulk TCR-seq analyses revealed distinct TCR motifs in psoriasis patients, along with subtle differences in V gene usage and CDR3 nucleotide length (117), underscoring the need for further investigation of the peripheral T cell receptor repertoire in psoriasis. Moreover, the premature immunosenescence of peripheral T cells driven by chronic inflammation has been hypothesised in a study where a higher proportion of terminally differentiated or senescent $CD8^+$ T_{EMRA} cells was found, particularly in patients with a longer disease (78). In addition, perforin expression was found notably elevated in circulating cytotoxic $CD8^+$ T cells of psoriasis vulgaris patients, especially in severely affected individuals (114,117).

To summarise, psoriasis results from a complex interplay of various T cell subsets at different stages of disease progression. Autoreactive T cells likely initiate inflammation in psoriatic lesions, while tissue-resident memory T and IL-17-producing T cells sustain chronic inflammation. Furthermore, recirculating T cells contribute to spreading inflammation beyond the skin by linking local and systemic immune responses (Figure 2). Although unconventional T cells, such as MAIT and γδ T cells, have been implicated in psoriasis, their roles remain primarily explored in animal models or using a limited number of phenotypic markers in human studies (105,107,119,120).

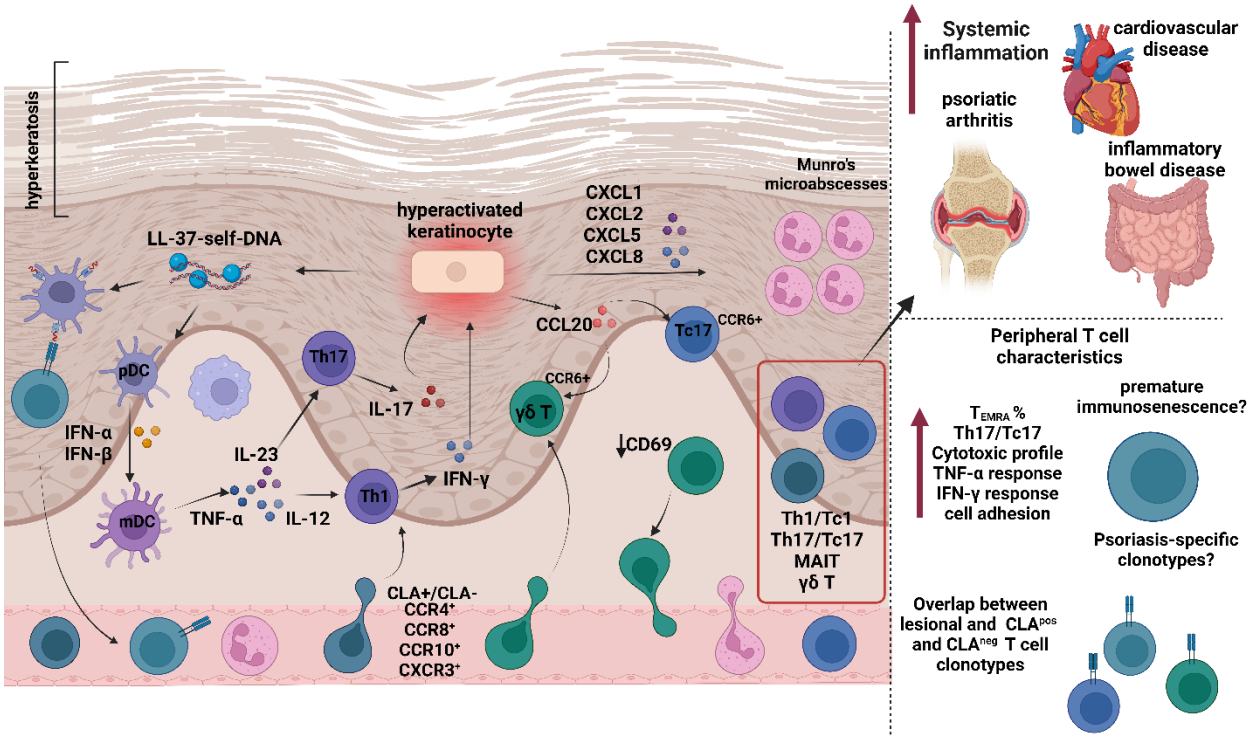

Figure 2. T cell-mediated interactions in psoriatic plaque formation and systemic inflammation. *This schematic shows the key cellular and molecular interactions in psoriatic plaque formation, focusing on the role of skin-infiltrating and circulating T cells. Plasmacytoid dendritic cells (pDCs) release type I interferons (IFN-α, IFN-β) in response to LL-37-self-DNA complexes (72), activating myeloid dendritic cells (mDCs) to secrete TNF-α, IL-23, IL-12. These cytokines drive the Th1 and Th17 differentiation, leading to IFN-γ and IL-17 secretion, which amplify keratinocyte activation and chemokine release (CXCL1, CXCL2, CXCL5, CXCL8, CCL20). Skin-homing T cells expressing CLA, CCR4, CCR8, CCR10, and CXCR3, migrate to the skin, exacerbating inflammation. CD69 downregulation facilitates recirculation of T cells into the bloodstream, contributing to systemic inflammation* (113). *Peripheral T cells show heightened activation, effector functions, and signs of accelerated senescence*

(78,97,115). *Overlap between lesional and circulating CLA⁺/CLA⁻ T cell clonotypes suggests recirculation of activated T cells between the skin and blood stream (68). Created with Biorender.*

1.6. Characteristics, functions and roles of unconventional T cells

The immune system is traditionally divided into two main arms: innate and adaptive immunity. However, a third component, unconventional T cells, blurs the line between these classifications. These cells exhibit the spectre of features from both innate and adaptive ends, with significant phenotypic and functional diversity across its subsets.

Unconventional T cells include γδ T cells, which express a distinct γδ T cell receptor (TCR) and αβ TCR-expressing invariant natural killer T (iNKT) and mucosal-associated invariant T (MAIT) lymphocytes. Together, these subsets constitute approximately 10–30% of peripheral T cells and are enriched in the epithelial and mucosal surfaces of the liver, respiratory tract, digestive system, and reproductive organs (121,122).

Unlike conventional αβ T cells, which rely on previous antigen exposure to generate memory and drive responses, unconventional T cells are poised for rapid effector functions. Upon encountering an antigen, they can respond swiftly without prior sensitization, similar to cells of the innate immune system. In addition, unconventional T cells can be stimulated by cytokines independently of TCR-antigen interaction, further aligning them with innate-like immunity.

Despite their innate-like properties, the presence of TCRs enables unconventional T cells to mount specific antigen responses. In contrast to adaptive αβ T cells, which are restricted to recognising peptide antigens presented by major histocompatibility complex (MHC) molecules, unconventional T cells can be activated beyond the peptide-MHC interaction. In particular, they detect a completely different set of antigens, including lipids, phosphoantigens, or bacterial-derived molecules, presented by distinct non-polymorphic (non-MHC) antigen presenting molecules (3,4). This non-redundant mode of antigen recognition makes unconventional T cells unique and functionally significant in immune responses.

It is not surprising that the unique immunobiology of unconventional T cells has attracted increasing interest in various fields of research, including diseases like psoriasis, where their distinct responses may play an important role in pathogenesis (105,107,119,120,125).

1.7.T cell receptors

T cell receptors (TCRs) are molecules expressed on the surface of T cells, consisting of either an α and β chain (αβ TCRs) or a γ and δ chain (γδ TCRs). Each TCR has a constant region, which defines its structure, and a variable region, responsible for antigen recognition. The variable region comprises three hypervariable complementary-determining regions (CDRs), CDR1, CDR2, and CDR3. CDR1 and CDR2 interact with antigen presenting molecule, while CDR3 directly contacts the antigen and is the most variable part of the TCR (126), featuring conserved cysteine at the C-terminal and phenylalanine at the N-terminal.

Functional variable regions of TCRs are generated during T-cell development in the thymus through a process of V(D)J recombination. This somatic recombination process involves the rearrangement of variable (V), diversity (D), and joining (J) gene segments. The α and γ chains are encoded by V and J genes, while the β and δ chains are assembled through V, D, and J segments recombination. The genes are located at distinct loci, namely TRA, TRB, TRG, and TRD.

In addition to the random combination of V(D)J gene segments, the V(D)J recombination also includes junctional diversity - deletion or insertion of palindromic sequences (P nucleotides) and non-templated nucleotides at the junctions between the V, D, and J regions. This process, together with chain pairing, generates an estimated range of $1x10^{15}$ to $1x10^{20}$ distinct αβTCRs, far exceeding the estimated $5x10^{11}$ T cells in the human body (11–13). The final product of V(D)J recombination, a unique V(D)J nucleotide sequence in the CDR3 region, is defined as a clonotype and the collection of all clonotypes in an individual is referred to as the TCR repertoire (14).

The TCR repertoire can alter significantly during disease, reflecting responses to infections, cancer, or inflammation, including autoimmunity. TCR repertoires also change due to physiological changes in the body, the most notable of which is aging. Specifically, the proportion of naïve T cells declines with advancing age, leading to a less diverse TCR repertoire, fuelled further by the higher content of hyperexpanded clonotypes from experienced memory cells (15).

TCR repertoire analysis can provide valuable insights into the composition of TCR repertoires in diseases, and hence improve understanding of disease aetiology, especially in diseases with unknown antigenic triggers. Nowadays, high-throughput next generation sequencing (NGS) technologies offer the simultaneous analysis of millions of TCRs, serving as a window into the previously unreachable complexities of TCR repertoires (128).

1.8. γδ T cells

Since their discovery in the 1980s (132,133), γδ T cells have gained attention for their multifunctional capacities in immune surveillance, tissue repair, antimicrobial defence, anticancer immunity, and involvement in various diseases. In healthy adults, they comprise 0.5–10 % of peripheral $CD3^+$ T cells, with frequencies influenced by age, gender and disease. A defining feature of γδ T cells is their unique TCR, composed of γ and δ chain, which allows the sensing of phosphoantigens (pAg), lipid molecules, and stress-induced proteins (134–139). However, the full spectrum of antigens these cells recognise remains enigmatic (124). In addition, unlike αβ T cells, γδ T cells usually lack CD4 or CD8 co-receptors, though cytotoxic subsets may express CD8.

Human γδ T cells can be classified by the variant of the δ chain they express, with $Vδ1^+$, $Vδ2^+$, and $Vδ3^+$ being the most studied subsets. While often considered innate-like, recent advances in γδ T cell immunobiology, supported by single-cell sequencing and detailed phenotypic profiling, have revealed that not all γδ T subsets exhibit innate-like behaviour (140–142) (Figure 3). Specifically, $Vδ1^+$ and $Vγ9^-Vδ2^+$ subsets align more closely with adaptive-like responses, including greater TCR repertoire diversity, clonotypic expansion in response to viral infections (e.g. CMV), and lack of TCR motifs linked with pAg sensing (141,143–145). In contrast, the predominant peripheral blood subset, Vγ9Vδ2 cells, typically conforms to innate-like immunobiology, expressing PLZF and possessing an invariant TCR associated with pAg reactivity (140,146–148).

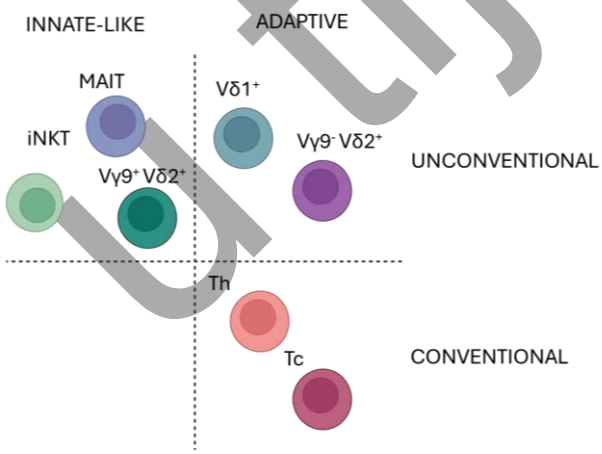

Figure 3. Classification of T cells based on their innate-like and adaptive-like properties. *While $Vδ2^+$ T cells co-expressing the Vγ9 chain cluster with innate-like MAIT and iNKT cells, $Vδ1^+$ and $Vγ9^-Vδ2^+$ exhibit features that align more closely with conventional adaptive T cells.*

1.8.1. The characteristics of γδ T cell receptors

According to the ImMunoGeneTics information system (IMGT), the human TRG locus on chromosome 7 contains 14 variable genes, of which only TRGV2, TRGV3, TRGV4, TRGV5, TRGV8, and TRGV9 are functional, while others are pseudogenes. The locus also includes 5 joining (TRGJP1, TRGJP, TRGJ1, TRGJP2, and TRGJ2) and two constant segments (TRGC1 and TRGC2). The TRD locus, nested within the TRA locus on chromosome 14, contains eight TRDV genes: *TRDV1*, *TRDV2*, *TRDV3*, *TRAV14/TRDV4*, *TRAV29/TRDV5*, *TRAV23/TRDV6*, *TRAV36/TRDV7*, *TRAV38/TRDV8*, with the last five dual annotated V segments used to generate both the α and δ chains. Furthermore, three TRD (TRDD1, TRDD2, and TRDD3), and four TRDJ (TRDJ1, TRDJ2, TRDJ3, TRDJ4) alleles contribute to the TCRδ chain (Figure 4) (149).

Although γδ T cells have fewer variable Vγ and Vδ genes than αβ T cells, they can generate an estimated 10^{17}-10^{18} different TRG/TRD combinations (145,150). However, the diversity of human γδ TCRs appears constrained, as shown by the predominance of Vγ9Vδ2 cells in peripheral blood. These cells feature TCRs with semi-invariant characteristics, with specific chain pairings adapted for pyrophosphate antigen reactivity. TCRγ chains derived from TRGV9 and TRGJP segments show constrained diversity and are highly "public", i.e. commonly found in many healthy individuals. Conversely, Vδ2 chains show greater CDR3 diversity, typically formed through the recombination of TRDV2, TRDD3, and TRDJ1 genes, often with a hydrophobic amino acid (Val, Leu, Ile) at the fifth position from the C-terminus cysteine (140,141,147,151).

The TCR repertoires of $V\delta1^+$ and $V\gamma9^-V\delta2^+$ cells, in contrast, exhibit much higher diversity. Vδ1 clonotypes feature more flexible and typically longer CDR3 regions due to increased nucleotide addition, resulting in a highly private repertoire with minimal overlap between individuals. Unlike Vγ9Vδ2 TCRs, Vγ-Vδ1 pairings are not restricted to a specific gamma variant, and Vγ9 chains that form TCR of Vδ1 cells usually do not express JγP variant (140,141,143).

In summary, the TCR repertoires of $V\delta1^+$, $V\gamma9^+V\delta2^+$, $V\gamma9^-V\delta2^+$, and $V\delta3^+$ cells show distinct structural properties, arising from both the differences in the gene segments used for their construction and variations in the introduction of non-templated and palindromic sequences. These distinctions are further associated with variations in the "publicness" and the potential for clonotypic focusing. Moreover, these variations in TCRs not only tailor their

antigen specificities but are also linked to specific phenotypic signatures of different γδ T cell subsets and their functional states.

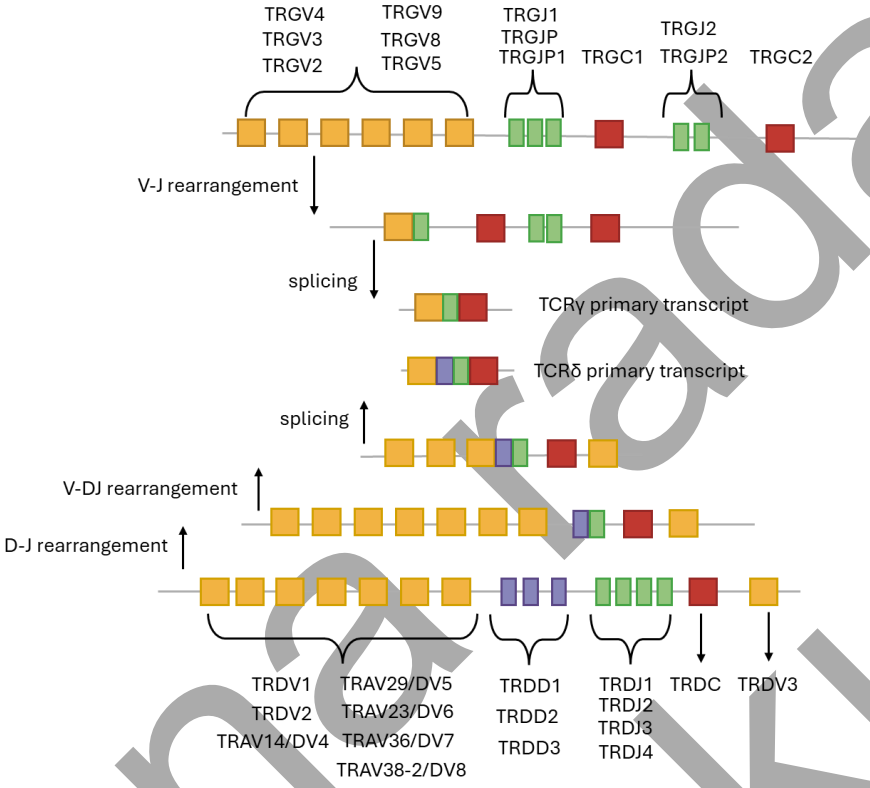

Figure 4. The schematic illustration of the γδ T cell receptor assembly.

1.8.2. γδ T cell subsets

Recent insights into the link between T cell receptor variants, phenotypic traits, and clonal expansion have greatly advanced our understanding of γδ T cell heterogeneity. Despite shared roles in rapid response, immunosurveillance and effector potentials, γδ T cell subsets display distinct phenotypic and clonotypic traits, tissue distributions, activation requirements, and antigen recognition mechanisms. The following sections will outline the defining characteristics of the most common and best characterised γδ T cell subsets.

1.8.2.1. Vγ9Vδ2 subset

The Vδ2^{+} γδ T cell population comprises two distinct subtypes, distinguished by the expression of Vγ9 chain. Innate-like Vγ9Vδ2 T cells are the most abundant circulating γδ T cells, accounting for 50–90% of peripheral population. They respond to microbial phosphoantigens, such as (E)-4-hydroxy-3-methyl-but-2-enyl pyrophosphate (HMB-PP), a

metabolite of the non-mevalonate isoprenoid biosynthesis pathway found in many bacteria and protozoa (152). Vγ9Vδ2 T cells can also recognise isopentenyl pyrophosphate (IPP), an endogenous molecule that accumulates in transformed or infected cells due to mevalonate pathway dysregulation (153). Importantly, Vγ9Vδ2 TCRs do not bind phosphoantigens directly but instead require interactions with butyrophilin (BTN) subfamily members BTN3A1 and BTN3A2. In short, the accumulated pAgs bind the intracellular domain of BTN3A1, inducing a conformational change and association with BTN3A2, which is necessary for the activation of Vγ9Vδ2 TCR (154,155).

The Vγ9Vδ2 subset displays distinct innate-like characteristics, including a heightened responsiveness to cytokine-mediated (IL-12 and IL-18) activation, in line with their innate-like biology (140,141). These cells uniquely express high levels of CCR5 and show elevated CCR6 and CD161 expression compared to other γδ T cell subsets (156,157). Vγ9Vδ2 T cells also frequently express IL7Rα, granzyme A and CX_3CR_1 (140).

Functional heterogeneity within the Vδ2 compartment has been observed, as reflected in variable responses observed in clinical trials of autologous Vγ9Vδ2 anti-tumour immunotherapies (158,159). Detailed analysis of peripheral Vδ2 cells has revealed four distinct subsets based on the CD28, CD27, and CD16 expression. These subsets, which vary in frequency between individuals, exhibit unique functional capacities. The most divergent subsets are $CD27^+CD28^+CD16^-$, which constitute the majority of circulating Vγ9Vδ2 T cells, and $CD27^-CD28^-CD16^+$, which represent a smaller portion of the population. $CD28^-CD27^-CD16^+$ cells are highly cytotoxic, expressing high levels of perforin, granzymes B and H, granulysin, KIR receptors, and CX_3CR_1. On the other end, $CD28^+CD27^+CD16^-$ cells produce more GzmK and express IL-7Rα, CCR2, CCR7, CCR6, CCR5, and IL-18Rα. These phenotypic differences align with functional capabilities, as exemplified by distinct efficacy against various cancer cell lines (160). Following HMB-PP stimulation, $CD28^+CD27^+CD16^-$ cells showed a tenfold higher expansion than $CD28^-CD27^-CD16^+$ Vδ2 cells (160), consistent with distinct TCR characteristics observed between Vγ9Vδ2 subsets defined by CD27 expression. Specifically, δ chains in the $CD27^-$ subset lacked key pAg-sensing features, occasionally joined with the *TRDJ3* gene, and contained non-hydrophobic amino acids at position 5 of the CDR3 region. Additionally, the $CD27^-$ subset displayed markedly lower CDR3δ diversity compared to $CD27^+$ cells, indicative of clonal expansion (159).

1.8.2.2. Vγ9⁻Vδ2 subset

Vγ9⁻Vδ2 cells, which represent ~2-6% of peripheral γδ T cells, predominantly exhibit $CD27^{hi}CCR7^{+}CD28^{+}IL7R\alpha^{+}$ naïve-like phenotype. During clonal expansion, these naïve cells transition to an effector-like state, marked by the downregulation of CD27 and increased expression of chemokine receptor CX3CR1, as well as increased production of cytolytic granules granzyme A and granzyme B (140). The $CD27^{hi}$ to $CD27^{lo}$ transition upon CMV infection was paralleled by changes in transcriptional programs, with significant upregulation of T-bet, Hobit, and Blimp-1 transcriptional factors associated with effector functions (142).

Unlike Vγ9⁺Vδ2, Vγ9⁻Vδ2 cells lack the response to HMB-PP and are unresponsive to IL-12/IL-18 stimulation, which illustrates their adaptive-like behaviour and different antigen targets. In addition, the highly private TCRγ repertoires and clonal expansion during acute CMV infections indicate their characteristics highly resemble those of $V\delta1^{+}$ cells (147).

1.8.2.3. Vδ1 subset

As previously described, Vδ1 T cells are marked by an adaptive-like immunobiology. The proportions of this subset in peripheral blood are typically lower than that of Vδ2 cells, presenting 10–30 % of γδ T cells. However, the Vδ2/Vδ1 ratio may decrease in certain conditions, such as during viral infections like CMV, or with aging (161,162). In addition, Vδ1 T cells are more frequent in solid tissues, where they play important role in epithelial tissue immunosurveillance (163,164).

The Vδ1 T cells in peripheral blood exhibit either a naïve $CD27^{hi}$ or effector-like $CD27^{lo/neg}$ phenotype, with $CD27^{hi}$ profiles associated with unexpanded clonotypic variants, while $CD27^{lo/neg}$ phenotype is characteristic of clonally expanded cells that have undergone antigen-driven differentiation (141,156). In addition to CD27, naïve-like $V\delta1^{+}$ T express markers such as IL7Rα, CD28, CCR7, and CD62L, and transcription factors like TCF7, LEF1, JAML, and MYC, which are vital for maintaining stem-like properties and self-renewal. Effector-like $V\delta1^{+}$ cells, on the other hand, upregulate T-bet, and BLIMP-1, which are essential for effector functions and cytotoxicity. $CD27^{neg}$ effector $V\delta1^{+}$ T cells also show higher levels of CD8, CD56, CD16, and TIGIT, along with increased Granzyme A/B, perforin, and CX_3CR_1, altogether indicating enhanced cytotoxic potential, tissue migration, and NK-like properties (141,142,156). Furthermore, the identification of over 1,000 differentially expressed genes

illustrates the profound molecular changes that Vδ1 T cells undergo as they shift from a naïve to an effector state (142).

Vδ1 T cells have demonstrated a remarkable versatility in their reactivity, displaying both antigen-dependent and antigen-independent reactivities toward diverse antigen-presenting molecules, but also molecules that do not serve a conventional antigen-presenting role. To date, Vδ1 T cells have been shown to recognise lipid-presenting molecules like CD1b (165), CD1c (166), and CD1d (136), either in an autoreactive or antigen-bound manner. Similarly, Vδ1 cells also demonstrated antigen-independent binding to MR1 (167), a molecule that presents microbial metabolites to MAIT cells. In addition, like Vδ2 cells, Vδ1 cells express NKG2D receptors through which they respond to stress-inducible molecules such as MICA and MICB (168).

In summary, human $V\delta1^+$ cells portray unique blend of adaptive and unconventional characteristics which are reflected in the private and focussed TCR repertoires, combined with the flexible, rapid, and non-MHC restricted unconventional immune monitoring.

1.8.2.4. Vδ3 subset

Unlike Vδ2 and Vδ1 subsets, Vδ3 lymphocytes are rare in peripheral blood, which has led to far less research on this subset. Nevertheless, Vδ3 cells have been found at higher proportions in the liver (163) and gut epithelia (169), where they are believed to play important roles in antimicrobial responses, which is supported by their expansion and upregulation of cytotoxic phenotypes in individuals with infections like CMV (170), HIV (171) and hepatitis C (57).

Although the phenotypic characteristics of Vδ3 cells have not been extensively characterised, a few studies suggested their phenotypes resemble those of Vδ1 and iNKT cells. For example, in a flow cytometry study investigating the roles and phenotypes of peripheral γδ T cells during malaria infection, Vδ3 cells did not form a distinct population, but instead clustered with Vδ1 cells, indicating their similarities. Vδ3 cells displayed either naïve $CD27^+$ $CD127^+$ or $CD27^{neg}$, $CCR7^{neg}$, $CD45RA^+CD16^+$ effector-like profile. However, when compared to Vδ1 cells, the Vδ3 subset demonstrated a higher frequency of CD94 and CCR6 expression. In another study, Vδ3 cells exhibited variable expression of NK-associated receptors like CD56, CD161, CD94, and NKG2D. In addition, following the recognition of CD1d, activated Vδ3 cells produced pro-inflammatory cytokines including TNF-α, INF-γ, and

IL-17(173).

Aside from the reactivity to CD1d, a subset of Vδ3 cells have showed antigen-independent MR1 reactivity, another feature shared with Vδ1 cells (167,174). This autoreactivity, together with the findings of increased proportions of Vδ3 cells in autoimmune disease like SLE (60) may suggest their involvement in autoimmunity. However, further investigations are needed to elucidate the functionalities, phenotypes, and antigen specificities.

1.8.3. γδ T cells in psoriasis

The involvement of γδ T cells in psoriasis has been defined in many studies, presenting them as major producers of IL-17, through which they significantly contribute to skin inflammation. However, most of these findings stem from psoriasiform murine models, where psoriasis-like lesions are induced by topical application of imiquimod (120,125,176). Although these lesions display pathohistological homology to those seen in humans, such as epidermal thickening and immune cell infiltration (177), this model lacks certain key elements for studying of the role of T cells in psoriasis, especially γδ T cells. In particular, murine skin comprises γδ T cells called dendritic epidermal T cells (DETC) which make about 50–70% of epidermal T compartment. In contrast, human skin does not have a direct equivalent to DETCs and contains relatively low proportions of γδ T cells in the skin (<10 % of cutaneous T cells) (96,105). In addition, as the psoriasis does not develop in mice naturally, the antigen specificities and, more importantly, systemic effects of the disease reflected in circulating T cells could not be investigated.

Human studies investigating the contribution of γδ T cells in psoriasis are relatively scarce, however, there is a consensus on the involvement of the Vγ9Vδ2 subset. It has been found that the proportions of Vγ9Vδ2 cells among circulating $CD3^+$ T cells are significantly decreased in psoriasis patients, with this reduction being particularly pronounced in individuals with more severe forms of the disease. Interestingly, when dissecting Vγ9Vδ2 cells based on the CLA expression, only CLA^+ circulating cells were found to be contracted in psoriatic patients, while the frequencies of CLA^- cells remained unchanged. Moreover, Vγ9Vδ2 cells were enriched in both psoriatic lesions and non-lesional skin compared to healthy controls. Additionally, peripheral CLA^+ Vγ9Vδ2 cells were found to produce pro-inflammatory cytokines such as IFN-γ, TNF-α, and IL-17, although IL-17-secreting cells comprised only 0.4 % of all CLA^+ Vγ9Vδ2 cells (105).

A recent study confirmed that Vγ9Vδ2 cells were significantly less frequent in the blood of PV patients, with an inverse correlation to PASI score, and higher proportions of Vδ2 cells in psoriatic lesions (119). This study further yielded the concept that heightened Vγ9Vδ2 activation in lesions was linked to a substantial up-regulation of BTN3A1 on monocytes. Further phenotypic analysis revealed an acquisition of a "more experienced" character of Vγ9Vδ2 in psoriasis patients, marked by a decrease in $CD27^{+}CD45RA^{-}$ populations and an expansion of the $CD27^{-}CD45RA^{+}$ subset. Interestingly, the RNA-sequencing of peripheral Vγ9Vδ2 cells revealed over 2000 differentially expressed genes, with genes associated with inflammatory response, TNF-mediated signalling, T cell activation and proliferation being upregulated. Regarding cytokine production, peripheral Vγ9Vδ2 cells produced IFN-γ and TNF-α, while IL-17 production was minimal (less than 0.01% of Vδ2 cells). In contrast, immunofluorescence analysis of skin biopsies estimated that about 40% of cutaneous Vδ2 cells express IL-17, indicating their functional plasticity in psoriatic lesions (119). Another research on γδ T lymphocytes in psoriasis supports this finding by demonstrating that about 15% of *in vitro* IL-23-stimulated dermal γδ T cells produce IL-17 (120).

In contrast, a recent study of peripheral γδ T cells in psoriasis found no reduction in Vδ2 proportions but revealed sex-based differences. Specifically, altered γδ T cell proportions were seen only in male patients, with an expansion of $Vδ2^{+}γδ\ TCR^{hi}$ and $Vδ1^{-}Vδ2^{-}\ γδ\ TCR^{int}$ cells among diseased individuals compared to controls. In addition, RT-qPCR transcriptomic profiling revealed lower expression of *RUNX3*, *IL18R*, and *PLZF* in bulk γδ T cells (178).

A recent study examining γδ TCR repertoires in skin samples from psoriasis patients found higher diversity of TRG/TRD clonotypes, with no significant differences in the V, D, or J gene usage in CDR3 regions. Additionally, immunostaining of psoriatic lesions confirmed prior findings of high γδ T cell infiltration in affected skin, which positively correlated with PASI scores (179).

In summary, the composition and blood-to-skin redistribution of γδ T cells, particularly Vγ9Vδ2 cells, appear to be altered in psoriasis, implicating these cells in the pathogenesis of the disease. Recent studies indicate that the proportions of Vδ1 cells remain stable in psoriasis, and therefore the phenotypic and functional characteristics of this subset, as well as other γδ T cell populations such as $Vδ3^{+}$, have not been probed. On a similar vein, while the involvement of Vγ9Vδ2 cells in psoriasis has been appreciated, an in-depth characterisation of their transcriptomic and phenotypic profiles would provide critical insights into their specific contributions to the underlying immune perturbations in the disease.

1.9. MAIT cells

Mucosal-associated invariant T (MAIT) cells are a population of innate-like T cells highly abundant in human liver and various epithelial and mucosal sites, including the skin, intestine, respiratory, and urogenital tracts (180,181). In peripheral blood, MAIT cells typically account for an average of 2% of the total T cell population, with reported ranges varying from 0.1% to 10% (181–185). MAIT cells are defined by an invariant TCRVα7.2 chain and conserved ability to recognize bacterially derived intermediates of riboflavin (vitamin B2) biosynthesis displayed by the monomorphic MR1 (MHC class I-related protein) molecule (186,187). These cells are crucial in antimicrobial immunity, responding to a broad range of bacterial and fungal ligands. Their activation is primarily driven by the presentation of microbial metabolites, such as 5-OP-RU (5-(2-oxopropylideneamino)-6-D-ribitylaminouracil), a potent MR1 ligand that effectively stimulates MAIT cells (188,189). In contrast, other MR1-presented molecules, such as 6-formylpterin (6-FP), a derivative of vitamin B9 (folate), generally fail to elicit MAIT cell activation (187).

In addition to their invariant TCR, MAIT cells are characterised by high expression levels of the C-type lectin-like receptor CD161 and the transcription factors PLZF and RORγt, which contribute to their innate-like properties and their capacity for rapid cytokine production. They also express high levels of receptors for the pro-inflammatory cytokines IL-12 and IL-18, important in TCR-mediated activation and MR1-independent innate responses (181,184,190,191). Circulating MAIT cells express high levels of CD127 (IL-7Rα), CD95 (Fas), NKG2D, CD26, and chemokine receptors such as CCR2, CCR5, CCR6, and CXCR6, which likely guide their trafficking to mucosal and inflamed tissues (181,182).

Based on the expression of CD8 and CD4 co-receptors MAIT cells can be classified into distinct subsets: $CD8^+$, $CD4^+$, double-negative (DN, $CD4^-CD8^-$), and double-positive (DP, $CD4^+CD8^+$). The majority of MAIT cells (~70-80%) express CD8, while a smaller proportion (~15%) are DN. $CD4^+$ MAIT cells are comprising only a small fraction of the population (~5%), with the DP subset being equally or even less common (180–182,184,185,190,192).

The proportion of MAIT cells in peripheral blood exhibits significant age-dependent variation, with frequencies peaking around 25–30 years and subsequently declining in later decades, reaching very low levels in the elderly (184,185,193–195). This decline is most pronounced in the $CD8^+$ subset (184,185,193–195), while the frequency of DN MAIT cells is more variable, with some studies reporting stable levels (185,195) and others showing a gradual decrease with age (184). The frequency of $CD4^+$ MAIT cells also displays inconsistent

findings, with studies reporting an age-associated increase (185,195), or no clear correlation with age (184). Alongside the reduction in MAIT cell frequency, there is a shift in cytokine production from a Th1-dominant response to an increased Th2-like profile, evidenced by a higher IL-4/IFN-γ ratio in $CD8^+$ and DN subsets (185). Despite the overall decrease in frequency, MAIT cells retain key effector functions with age, as indicated by higher baseline levels of GzmB, IFN-γ, and CD107a (195). Interestingly, the frequencies of MAIT cells are positively correlated with those of $V\delta2^+$ cells, suggesting that both populations may be similarly influenced by genetic or environmental factors (184).

1.9.1. Heterogeneity of MAIT subsets

Due to their invariant TCR, which is highly specific for MR1-bound riboflavin metabolites, and a conserved set of surface markers, MAIT cells initially appeared to constitute a homogenous population. However, studies from the early 2010s, along with more recent advances in single-cell transcriptomics, proteomics, and refined functional assays, have revealed substantial heterogeneity within the MAIT cell population. This heterogeneity is reflected in phenotypically distinct subsets, characterised by variations in CD8/CD4 expression, diverse functional profiles, and transcriptomic programs, indicating specialized roles in immune responses (182,184,196).

For example, $CD8^+$ MAIT cells show higher basal levels of IL-12R and IL-18R than DN cells, along with increased expression of co-stimulatory molecules CD2, CD9, and the inhibitory receptor PD-1. Furthermore, $CD8^+$ MAIT cells are characterised by strong type 1 effector functions, producing slightly higher levels of IFN-γ and TNF-α than DN cells, and possess significant cytotoxic potential through elevated levels of granzyme B, granulysin, and perforin. They also express higher levels of cytotoxicity-associated receptors CD94A/NKG2A and NKG2D and transcriptional factors T-bet and Eomes, aligning with a robust effector profile (182,184,196,197). Despite similar cytotoxic functions, transcriptomic analyses have revealed that $CD8^+$ and DN subsets differ by approximately 600 genes, with $CD8^+$ MAIT cells displaying elevated expression of genes such as *KLRK1*, *NKG7*, *CCL5*, and *IL12RB2* (182,196). In contrast, DN MAIT cells display higher levels of *PLZF* and increased propensity for apoptosis, along with an elevated RORγt/T-bet ratio and increased IL-17 production upon stimulation, consistent with type 3 immune profile (196).

The $CD4^+$ MAIT subset, though rare, shows a unique profile with reduced type 1

effector functions and decreased cytotoxic potential, as indicated by lower production of IFN-γ and TNF-α and an almost absent expression of cytotoxic markers (e.g., CD69, CD56, NKG2A, NKG2D, NKG7, GzmA, GzmK, GzmB, perforin) compared to $CD8^+$ and DN populations (182,184,198). Furthermore, transcription factors linked to effector function like Eomes, PLZF, and RORγt are expressed at lower levels in $CD4^+$ MAIT cells. Instead, $CD4^+$ MAIT cells exhibit higher levels of CD25 (IL-2Rα), CD127 (IL7R), CTLA4, CCR4, CCR7, CD62L, and TNFRSF4 (OX40), and display enhanced ability to produce IL-2, suggesting distinct costimulatory signals, potentially greater sensitivity to IL-2 signalling, and tissue-homing potential (182,184,198).

The TCR repertoire of MAIT cells also shows distinct characteristics according to the phenotype defined by the expression of CD8/CD4 costimulatory molecules, with reports indicating greater diversity within $CD8^+$ MAIT cells compared to their DN counterparts (196,199). In particular, the TCRβ chain of $CD8^+$ MAIT cells encompasses a broader range of TRBV segments and a higher number of unique TCRα and TCRβ clonotypes compared to DN subset, indicating a more diverse antigen recognition potential. Despite differences in clonotypic diversity, both $CD8^+$ and DN subsets share overlapping clonotypes within their TCRα and TCRβ repertoires, indicating a conserved capacity for antigen recognition (196,199).

While murine MAIT cells comprise distinct MAIT1 and MAIT17 subsets (200), recent comprehensive research of human blood and liver MAIT gene signature has revealed that analogous human MAIT subsets could not be detected. Specifically, human MAIT cells were found to possess the ability to produce IL-17 under dual TCR and cytokine stimulation conditions, displaying a unique gene expression profile compared to $IL\text{-}17^-$ cells. However, the largely similar transcriptional and functional profiles of $IL\text{-}17^+$ and $IL\text{-}17^-$ cells, along with overlapping TCR repertoires and no significant differences in TRAJ and TRBV usage, indicate that IL-17 producing MAIT cells represent an activation state rather than a distinct subset (199).

1.9.2. MAIT T-cell receptor characteristics

In contrast to the extensive diversity of T-cell receptors found in conventional αβ T cells, MAIT cells exhibit a more restricted TCR repertoire due to their semi-invariant TCRα chain. In conventional αβ T cells, the TCRα chain is generated through recombination of 54 functional TRAV gene segments with 61 functional TRAJ variants (201). By contrast, in MAIT

cells, the TCRα chain is mainly formed by TRAV1-2 recombination with TRAJ33, with less frequent pairings involving TRAJ12 and TRAJ20, very rare associations with other joining segments, and minimal junctional variability (184,190,199) (Figure 5). Crystallographic studies have revealed that the recognition of riboflavin metabolites by the MAIT TCR is primarily mediated through a direct interaction between the conserved Tyr95α residue within the J region of the CDR3α loop (202,203), with this interaction being critical for MR1 binding. Meanwhile, sequence variations in CDR3β loop subtly modulate antigen recognition in an antigen-dependent manner (186,188). The MAIT TCRβ chain provides greater diversity, although with a significant bias to TRBV6 and TRBV20 gene families (190,204). Initially, MAIT cells were thought to express a limited range of TCRβ chains, however, advances in TCR sequencing have revealed a broader array of TRBV genes that contribute to increased variability within the MAIT TCR repertoire (190,199,205,206).

MAIT cells also exhibit distinct αβ chain pairing patterns. For example, TCRα chains containing TRAJ12 or TRAJ20 preferentially pair with TRBV6-4 TCRβ chains, while TRAJ33 TCRα chains pair more frequently with TRBV20-1 or TRBV4 TCRβ chains (190,199,206). Due to the restricted nature of the MAIT TCRα repertoire, many MAIT cells share identical CDR3α sequences but differ in their TCRβ chains, which are more variable. Consequently, CDR3α sequences are often shared across different donors, while TCRβ clonotypes tend to remain largely private, contributing to individual uniqueness of MAIT TCR repertoires (199).

The emerging understanding of MAIT cell diversity is further expanded by the identification of MR1-autoreactive and folate-reactive MAIT cells in peripheral blood which exhibit greater TCR diversity and antigen specificity than previously appreciated. While some of these cells express the conventional MAIT-specific TRAV1-2 chain, others lack this variant and are thus referred to as ‘atypical MR1-restricted’. These atypical MR1-restricted cells are rare in the peripheral blood (~0.01-0.05% of $CD3^+$ T lymphocytes) (192,207), display phenotypic heterogeneity, more diverse TCRα and TCRβ chains than canonical MAIT cells, and lack the canonical Tyr95a residue (186).

In summary, the MAIT TCR repertoire, though semi-invariant, exhibits considerable diversity, especially in TCRβ usage and CDR3β composition. This variability potentially broadens the scope of antigen recognition and MR1-restricted reactivity by MAIT cells, raising new questions about the range of antigens that MAIT cells may detect and respond to.

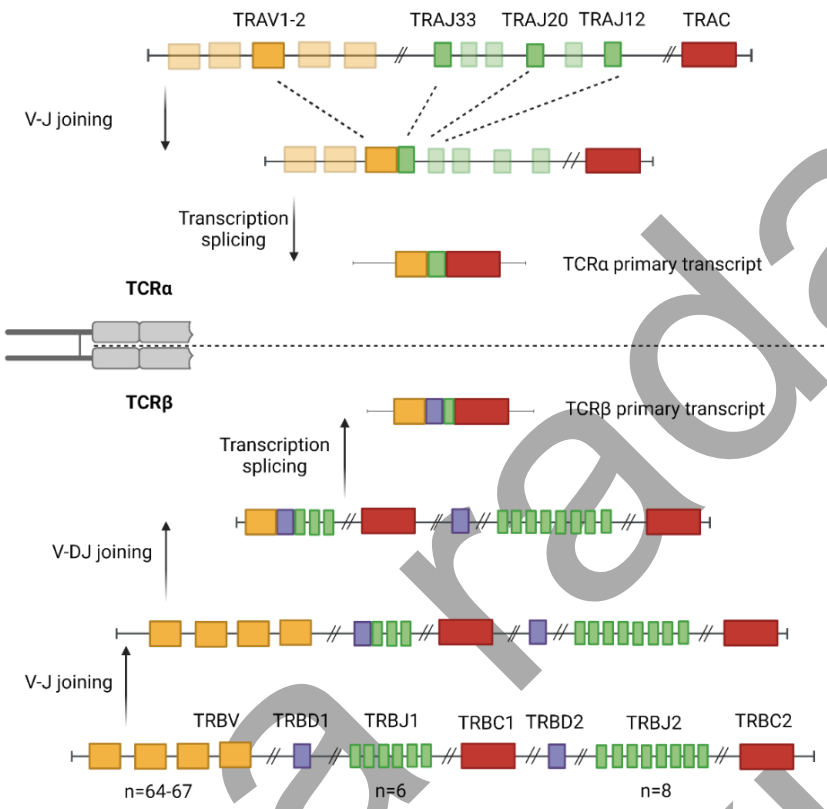

Figure 5. The schematic illustration of the MAIT T-cell receptor assembly.

1.9.3. TCR-dependent and cytokine-induced modes of MAIT cell activation

MAIT cells can be activated through TCR-dependent antigen recognition or through cytokine signalling, particularly via IL-12 and IL-18, independent of direct antigen engagement (Figure 6). Upon activation, MAIT cells rapidly produce type 1 cytokines (IFN-γ, TNF-α) and, under specific conditions, type 3 cytokines (IL-17, IL-22). They also display potent cytotoxic activity mediated by the expression of cytolytic molecules such as perforin and granzymes (GzmA, GzmK, GzmB). In their resting state, MAIT cells predominantly express GzmA and GzmK, with low levels of perforin and granulysin, and minimal or absent GzmB expression (181,182,190,208,209).

TCR and cytokine-mediated activation induce distinct signalling pathways that lead to specific transcriptional and functional profiles. TCR stimulation triggers a rapid, polyfunctional response, with elevated expression of TNF-α, IFN-γ, IL1-7A and IL-22. In contrast, cytokine-driven activation produces IFN-γ with a delayed response (210). TCR engagement promotes pro-inflammatory cytokine genes (*IL1B*, *IL2*, *IL6*, *IL10*, *IL17A*, *IL17F*,

IL21, *IL22*), transcription factors (EGR1, EGR2, RORγt, ZBTB16), chemokines (CCL3, CCL4, CCL20), and co-stimulatory molecules (CD25, and TNFRSF9), supporting immune cell recruitment, proliferation, and effector function (199,210). In contrast, cytokine-driven activation preferentially induces genes such as *BATF*, *STAT1*, *IKZF1*, *IFNG*, and *IL26*. Notably, genes like *GZMB*, *TBX21*, *NFATC1* and *STAT4*, are upregulated in both activation contexts, reflecting a core MAIT cell response (199,210).

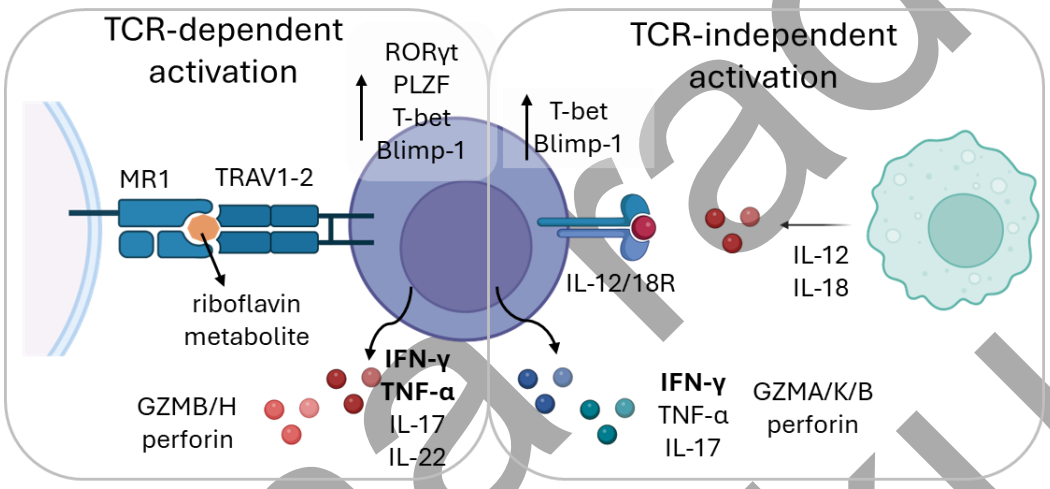

Figure 6. TCR-dependent and cytokine-induced modes of MAIT cell activation. *TCR-dependent activation occurs through MR1-antigen presentation, leading to the upregulation of transcription factors RORγt, PLZF, T-bet, and Blimp-1, and multiple cytokines, while cytokine-induced activation involves upregulation of T-bet and Blimp-1, resulting in predominant IFN-γ secretion. Created with Biorender.*

1.9.4. MAIT cells in psoriasis

Accumulating evidence implicates MAIT cells in autoimmune and inflammatory diseases, with studies frequently reporting reduced frequencies in peripheral blood and increased presence in lesional tissues (192,211,212). However, results vary, with some studies finding no overall frequency changes but rather shifts in subset composition or functional capacities (192). Whether changes in MAIT cell numbers and functions in autoimmune diseases reflect MR1-mediated self-antigen recognition or cytokine-driven responses within the inflammatory milieu remains unclear.

The role of MAIT cells in psoriasis, however, remains largely underexplored, with only a few studies addressing their involvement in the disease. Early research relied on surrogate

markers for MAIT cell identification (107), while more recent studies have employed MR1-tetramer based approaches, albeit with modest sample sizes (205) or limited phenotypic markers (178).

The first targeted investigation of MAIT cell presence and characterisation in psoriatic lesions was conducted in 2014 (107). This study identified MAIT cells within psoriatic plaques, defined as $CD3^+CD8^+CD161^+IL18R\alpha^+$, though at frequencies comparable to those found in healthy skin. This finding was later supported in a study investigating various cutaneous inflammatory diseases, which reported a slight, yet statistically insignificant increase in MAIT cells within psoriatic lesions compared to healthy skin (213). Notably, however, lesional MAIT cells were found to produce IL-17, a characteristic rarely observed among MAIT cells in normal skin (107). In addition, a higher proportion of circulating MAIT cells expressed CLA compared to conventional $CD8^+$ αβ T cells, suggesting a potential enrichment in their skin-homing capacity.

A more recent study examining circulating MAIT cells of psoriasis patients found no significant differences in the frequency of total circulating MAIT cells, nor within the largest $CD8^+$ and DN populations when compared to healthy controls. However, male psoriasis patients exhibited significantly lower proportions of $CD4^+$ and DP MAIT cells. At the transcriptional level, circulating MAIT cells of PV patients displayed reduced levels of *EOMES* and *CCR6*, alongside upregulation of *RORC*, suggesting a potential shift toward a Th17-like phenotype (178).

Further investigation of the TCRβ repertoire of circulating MAIT cells revealed TRB repertoires in psoriasis patients undergo significant age-related reshaping, characterised by heightened clonal expansion, an effect not observed in age-matched healthy controls. Additionally, the identification of psoriasis-enriched clonotypes, with overlap to previously reported clonotypes in peripheral blood as well as lesional and non-lesional skin, pointed to a potential presence of psoriasis-specific clonotypes and plausible recirculation of MAIT cells between lesional skin and peripheral blood (205).

Overall, while these studies have provided foundational insights into the involvement of MAIT cell in psoriasis, particularly regarding numeric and phenotypic alterations, the functional implications and underlying mechanisms driving these changes remain poorly understood. To address these gaps, larger, more comprehensive studies are needed to confirm frequency alterations, uncover transcriptomic signatures, and enable detailed phenotypic characterisation.

2. AIMS AND HYPOTHESES

Psoriasis vulgaris is a common, chronic, inflammatory skin disease characterised by multifaceted aetiology that encompasses genetic, environmental and immune components. Due to a range of associated comorbidities and signs of systemic inflammation, psoriasis is increasingly recognised not merely as a localised skin condition, but as a systemic disorder with broader implications for overall health.

Among the diverse immune cells implicated in the pathogenesis of psoriasis, T cells have emerged as central players. While the roles of conventional T cell subsets in initiation, progression and amplification of the inflammatory processes are well-established, the specific contributions of unconventional T cells, such as mucosal-associated invariant T (MAIT) cells and γδ T cells, remain poorly understood. Although these cell populations have been implicated in the pathogenesis of psoriasis, research in human subjects remains limited, often relying on a modest range of markers for their characterisation.

To address these gaps, this study aims to provide a comprehensive analysis of MAIT and γδ T cells, including their phenotypic, transcriptomic, and T cell receptor (TCR) repertoire profiles. This detailed characterisation seeks to deepen our understanding of their roles in disease pathophysiology and contribute to guiding future research efforts.

Building on previous findings regarding the characteristics of unconventional T cells in psoriasis and other autoimmune/autoinflammatory diseases, this study hypothesizes that:

1. The proportions, phenotype and gene expression profiles of circulating MAIT and γδ T cells, specifically markers related to activation, differentiation, migration and effector function, will differ significantly between patients with psoriasis and healthy controls.
2. The TCR repertoire of these unconventional T cells will display distinct clonal patterns in psoriasis patients compared to healthy individuals.
3. These differences will correlate with anthropometric and biochemical characteristics, as well as indicators of disease severity.

3. MATERIALS AND METHODS

3.1. Subjects

Peripheral blood samples from patients with psoriasis vulgaris and healthy control subjects were collected as part of the Croatian Science Foundation (CSF) project "NGS analysis of MAIT and γδT cell transcriptome: phenotype, function and TCR repertoire in the aetiology of psoriasis vulgaris" (CSF-UIP-2019-04-3494, PI: Assoc. Prof. Stana Tokić). A total of 101 samples used in this case-control study (66 psoriasis vulgaris patients and 35 healthy examinees) were obtained between February 2020 and December 2023.

Participants were recruited at the Department of Dermatology and Venereology, University Hospital Osijek during routine diagnostic procedures. Eligible patients were treatment-naïve adults over 18 years of age with a confirmed diagnosis of psoriasis vulgaris, verified through both clinical and histopathological assessment. The control group comprised healthy adults, matched by age and gender to the psoriasis cohort, who were selected during routine dermatological consultations for benign, non-infectious, and non-allergic skin conditions.

To ensure the validity of the study and avoid confounding factors, exclusion criteria for both groups included the presence of autoimmune, malignant, or infectious diseases, as well as any allergic reactions within six weeks prior to sample collection.

Before sample collection, participants were given detailed oral and written explanations of the study's objectives, methods, and expected outcomes. They were also informed of their right to withdraw from the study at any point. All participants provided written informed consent prior to their involvement in the study. Each participant was assigned a unique coded identification number to maintain data confidentiality throughout the collection, processing, and data analysis. Ethical approval was obtained from the Ethics Committee of the Faculty of Medicine in Osijek (Certificate No. 2158-61-07-19-126, October 11, 2019) and the Ethics Committee of the Clinical Hospital Centre Osijek (Certificate No. R2-12487/2019, September 12, 2019).

For all participants, demographic data (name, age, and gender) were recorded, and anthropometric measurements (height and weight), were taken to calculate body mass index (BMI). A detailed medical history was also obtained, including the age of psoriasis onset, presence of comorbid conditions, and current medication use. For psoriasis patients, disease

severity was assessed using the Psoriasis Area Severity Index (PASI) (9,214), while the impact on quality of life was evaluated with the Dermatology Life Quality Index (DLQI) (10).

As part of the diagnostic evaluation, the following diagnostic tests were conducted: complete blood count, high-sensitivity C-reactive protein (hsCRP), erythrocyte sedimentation rate (ESR), cholesterol, and triglyceride levels. In addition, serological markers for Mycobacterium tuberculosis (QuantiFERON-TB Gold test), hepatitis B (anti-HBs, HBsAg, anti-HBc IgG, anti-HBc IgM, HBeAg, anti-HBe), hepatitis C (anti-HCV), and cytomegalovirus (anti-CMV IgG/IgM) were analysed.

3.2. Peripheral blood mononuclear cell (PBMC) collection, cryopreservation, and thawing

Peripheral blood samples (20 ml) were drawn from fasting subjects in the morning and collected in heparin-coated tubes. The samples were immediately processed for PBMC separation using Lymphoprep gradient density medium (Stemcell Technologies, Vancouver, Canada). Lymphoprep, with a density of 1.077 g/mL, is specifically formulated to separate lymphocytes and other mononuclear cells from whole blood through density gradient centrifugation. During centrifugation, the density gradient formed by Lymphoprep allows for the separation of blood components: denser granulocytes and erythrocytes pass through the Lymphoprep medium, while less dense lymphocytes and monocytes remain at the interface between the Lymphoprep medium and plasma. This interface is then carefully collected to isolate PBMCs.

PBMC isolation and cryopreservation protocol:

Whole blood was diluted with an equal volume of saline solution (0.9% NaCl). Subsequently, up to 20 ml of the diluted blood was gently layered onto 15 ml of Lymphoprep medium. The tubes were then centrifuged at 800 × g for 25 minutes at room temperature, with the centrifuge set to break-off. Following centrifugation, the PBMC layer, which formed at the interface between the Lymphoprep medium and the plasma, was carefully collected and transferred into a new 15 ml tube (Figure 7). Phosphate-buffered saline (PBS) was added to the PBMCs to approximately 15 ml. A subsequent centrifugation was performed at 400 × g for 10 minutes at room temperature. The supernatant was discarded, and the PBMC pellet was resuspended in 5 ml of PBS. The number and viability of the cells were determined using the

LUNA-II Automated Cell Counter (Logos Biosystems, South Korea), following the manufacturer's protocol. Briefly, cell suspension was mixed with Trypan blue dye at a 1:10 dilution ratio, and 10 µl of this mixture was used for cell counting. Following this, the resuspended PBMCs were centrifuged again at 400 × g for 5 minutes to pellet the cells. The PBMC pellet was then resuspended in pre-chilled (4°C) cryopreservation medium (10% dimethyl sulfoxide (DMSO [Sigma Aldrich, Germany]) in foetal bovine serum [Sigma Aldrich, Germany]), in aliquots of 4-5 × 10^6 cells per vial.

Cryovials were placed in a Mr. Frosty container (Thermo Fisher Scientific, USA) at -80°C for 48 hours before being transferred to a liquid nitrogen tank for long-term storage.

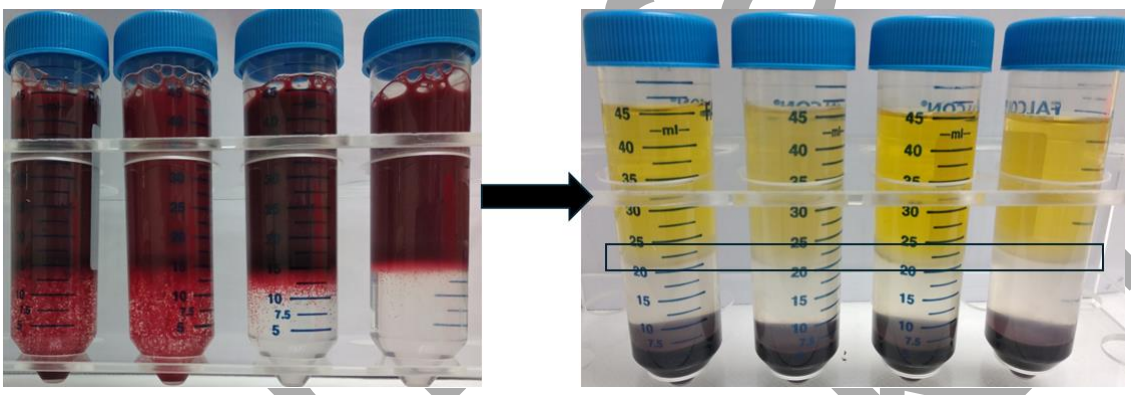

Figure 7. Separation of PBMCs from blood using Lymphoprep. *The left panel shows a blood sample layered onto the Lymphoprep medium before centrifugation. The right panel shows the separation after centrifugation, with PBMC layer outlined. Author's work.*

PBMC thawing protocol:

Cryopreserved PBMCs were rapidly thawed in a 37°C water bath and subsequently transferred to a 15 ml Falcon tube. For each millilitre of thawed cell suspension, 4 ml of pre-warmed (37°C) supplemented RPMI-1640 medium (10% foetal bovine serum [FBS], 1% sodium pyruvate [Capricorn Scientific, Germany], and 0.01M HEPES [Sigma Aldrich, Germany]) was added. The cell suspension was then centrifuged at 350 × g for 5 minutes to pellet the cells. The resulting cell pellet was resuspended in 5 ml of MACS buffer (1x PBS, 0.075% EDTA, and 0.05% BSA). The number and viability of the cells were determined using the LUNA-II Automated Cell Counter (Logos Biosystems, South Korea).

3.3. Flow cytometry

Cryopreserved PBMCs (1 x 10^6 cells) were used for γδ T and MAIT cell immunophenotyping. To identify MAIT cells, the cells were stained with a combination of anti-CD3ε, MR1-5-OP-RU-loaded tetramer and anti-TCRVα7.2 antibodies. MAIT cells were then further characterised based on CD4 and CD8 expression, classifying them into $CD4^+$, $CD8^+$, $CD4^-CD8^-$ double negative (DN) or $CD4^+CD8^+$ double positive (DP) subsets. CD3 and pan-γδTCR antibodies were used to identify γδ T cells, while $Vδ2^+$, $Vδ1^+$, and $Vδ1^-$ $Vδ2^-$ subpopulations were distinguished by TCRVδ2 and TCRVδ1 antibodies, respectively. Antibodies used are listed in Table 1.

Staining protocol:

For the staining procedure, 0.5 x 10^6 cells were aliquoted into 1 ml of PBS, and 0.25 µl of Live/Dead Fixable Near IR Dead fluorescent dye (ThermoFisher Scientific, USA) was added to stain dead cells. The cells were incubated for 15 minutes at +4°C in the dark, followed by a wash with 1 ml of PBS and centrifugation at 350 × g for 5 minutes. The supernatant was then removed. To block non-specific binding, 2.5 µl of human FcR blocking agent (TruStain FcX, Biolegend, USA) was added, and the cells were incubated for 5-10 minutes at room temperature in the dark. For the staining of γδ T cells, an antibody cocktail including CD3, γδ TCR, TCRVδ1, and TCRVδ2, was added to an aliquot of cells. MAIT cells were stained through a two-step process. First, 20 µl of a 1:100 dilution of the MR1-5-OP-RU tetramer was added, followed by incubation at + 4°C in the dark for 20 minutes. After this, 80 µl of a MAIT cell antibody cocktail containing CD3, CD4, CD8, and TCRVα7.2 was added, and incubation continued under the same conditions for an additional 20 minutes. After incubation, the cells were washed twice with 2 ml of PBS and centrifuged at 350 × g for 5 minutes.

Table 1. Antibodies used in γδ T and MAIT cell immunophenotyping.

Antibody	Fluorochrome	Clone	Source / manufacturer	Dilution	Panel
MR1-5-OP-RU loaded tetramer	APC	-	NIH Tetramer Core Facility, as permitted to be distributed by the University of Melbourne (189)	1:100	MAIT

TCRVα7.2	PE	3C10	Biolegend	1:100	MAIT
CD4	PE-Cy7	SK3	eBiosciences	1:200	MAIT
CD8	PerCP	RPA-T8	eBiosciences	1:200	MAIT
CD3	FITC	UCHT1 gamma	Department of Immunology and Biotechnology, University of Pécs, Hungary	1:250	MAIT and γδ T
γδTCR	PE-Cy7	B1	BioLegend	1:100	γδ T
TCR Vδ1	APC	TS8.2	eBiosciences	1:100	γδ T
TCR Vδ2	PerCP/Cy5.5	B6	BioLegend	1:200	γδ T

The cells were acquired on BD FACS Canto II cytometer (FACS Canto II, Becton Dickinson, San Jose, CA, USA) at the Szentágothai Research Centre in Pécs, Hungary.

Compensation parameters were established based on single-stained controls, while gating strategies were optimized using fluorescence-minus-one (FMO) controls and MR1-6-FP isotype controls. Data analysis was performed using OMIQ Platform (Dotmatics, USA). The representative gating strategies are depicted in figures below (Figures 8 and 9).

The median viability of thawed PBMC samples, as assessed by flow cytometry, was 98.7% (IQR: 97.28-99.5%).

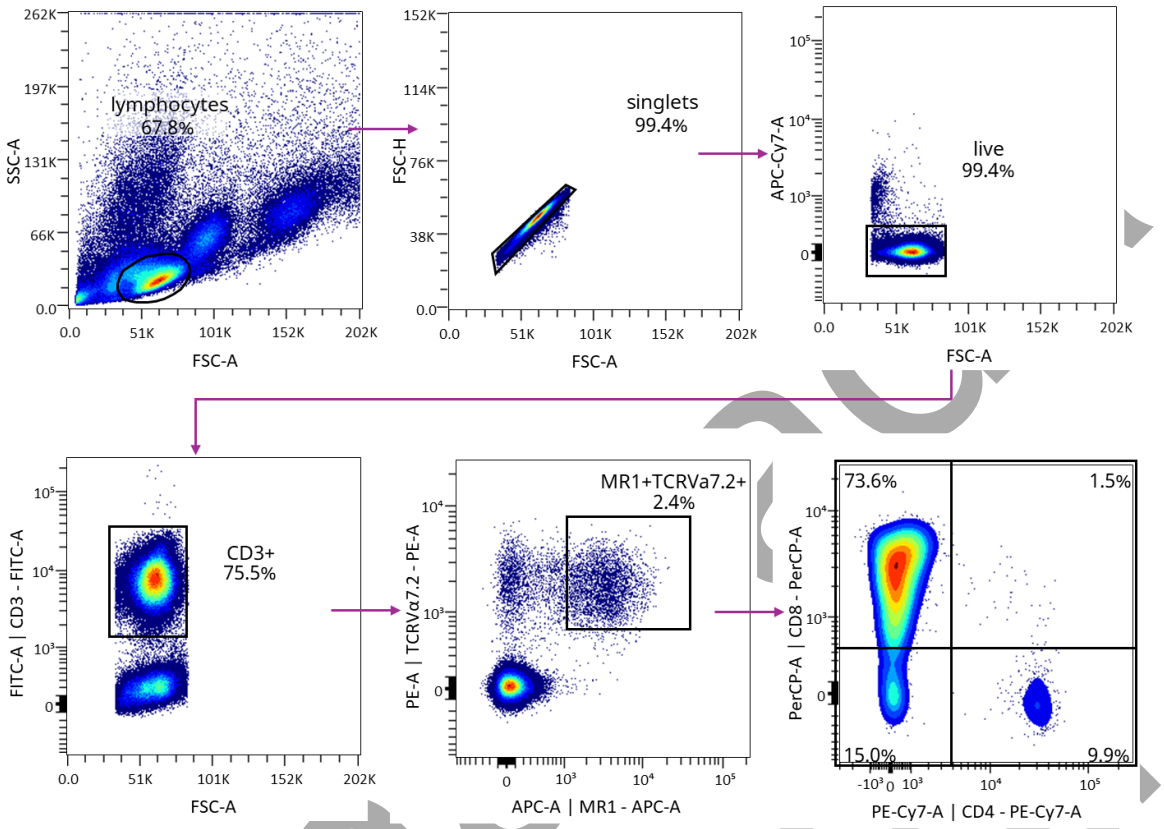

Figure 8. **Representative gating strategy of MAIT cells**. *First, lymphocyte population was selected based on forward scatter (FSC) and side-scatter (SSC) properties. Then, FSC-area vs. FSC-height settings were used to exclude doublets and aggregates. Live cells were detected based on the absence of staining with viability dye that penetrates dead cells and binds their free amines. CD3$^+$ T cells were further gated based on a positive CD3 labelling, and MAIT cells were defined by dual staining with MR1-5-OP-RU tetramer and TCRVα7.2. MAIT cells subsets were subsequently defined based on the CD4 and CD8 expression. The sample acquisition was conducted using BD FACS Canto II cytometer and data analysis performed using the OMIQ Platform.*

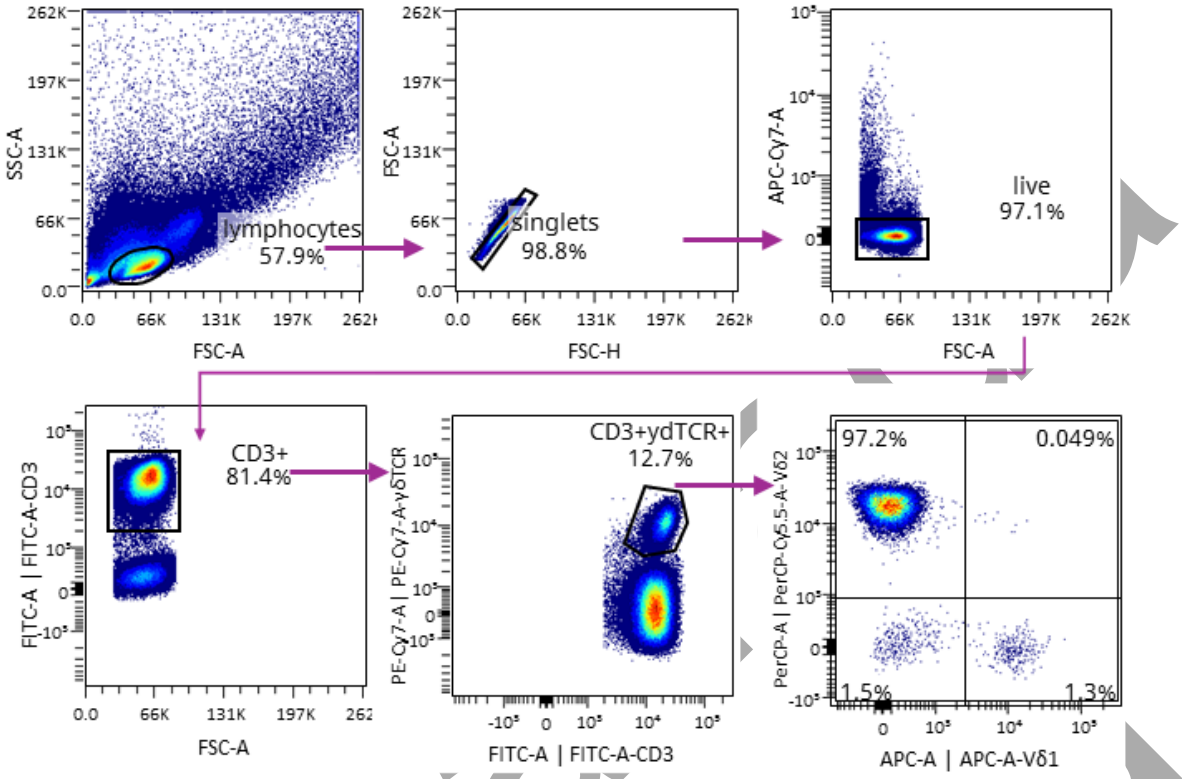

Figure 9. Representative gating strategy of γδ T cells. *$CD3^+$ T cells were gated from live, single lymphocytes using the same gating methods previously described for MAIT cells. γδ T cells were then identified by labelling with γδTCR antibody and were further classified based on the expression of TCR Vδ1 and TCR Vδ2. The sample acquisition was conducted using BD FACS Canto II cytometer and data analysis performed using the OMIQ Platform.*

3.4. Fluorescence-activated cell sorting of peripheral MAIT and γδ T cells

MAIT and γδ T cells typically comprise between 1% and 20% of peripheral T cells, depending on factors such as age, gender, disease status, and the physiological condition of individual (144,161,185,194,215,216). To explore the transcriptomic profiles of these T cell subsets through bulk RNA-sequencing, it was necessary to enrich them from PBMCs. This was achieved via fluorescence-activated cell sorting (FACS).

Two-way FACS sorting was conducted using the same staining settings as those employed for flow cytometry. Briefly, MAIT cells were identified and sorted as $CD3^+$ $TCRV\alpha7.2^+$ MR1-5-OP-RU-tet^+ lymphocytes, while γδ T lymphocytes were selected based on positive staining with CD3 and γδTCR antibodies. The sorted cells were collected directly into 500 µl of TRI reagent (Sigma Aldrich, Germany) for immediate RNA extraction. The sorting

process was performed using a Bio-Rad S3e cell sorter (Bio-Rad Laboratories, USA) at the Department of Immunology and Biotechnology, Medical School Pécs, Hungary.

On average, 13.6 x 10^6 (range: 5.65 x 10^6 - 24.4 x 10^6) thawed PBMCs were used for sorting, yielding a median of 142, 591 (interquartile range (IQR): 71, 655 – 249, 979) γδ T cells and 37, 266 (IQR: 12, 408 - 69, 909) MAIT cells. The gating strategies and compensation controls were based on previously validated protocols, using fluorescence-minus-one (FMO) and single-stain controls, respectively.

To ensure accuracy and post-sort purity, the sorted MAIT and γδ T cell were collected into 100% FBS and analysed using a flow cytometer (DxFLEX, Beckman Coulter, USA). The median purity of sorted MAIT and γδ T cell populations exceeded 95%, with median values of 95.88% (IQR: 94.12% - 97.7%) for MAIT cells and 95.62% (IQR: 89.33% - 96.95%) for γδ T cells.

3.5.RNA extraction

Total RNA was extracted from flow-sorted cells collected in TRI reagent using Direct-zol™ RNA MicroPrep kit (Zymo Research,USA), following manufacturer's instructions.

RNA extraction protocol:

The cells were initially sorted into 500 µl of TRI reagent. For samples with a high yield of sorted cells, the cells were sorted in multiple tubes were used to prevent over-dilution of the TRI reagent. To prepare the sample for RNA extraction, 100% ethanol was added to the TRI reagent in a 1:1 ratio (500 µl), and thoroughly mixed. Next, 700 µl of this solution was transferred to a column and centrifuged at 13,000 x g for 30 seconds. The flow-through was discarded, and the process was repeated by transferring additional 700 µl portions to the column until the entire sample had been processed. Following this, the column was transferred to a new tube, and the flow-through was discarded. For purification, 400 µl of Direct-zol™ RNA PreWash was added to the column. This was followed by centrifugation at 13,000 x g for 30 seconds, with the flow-through being discarded. The washing step was repeated once. Subsequently, 700 µl of RNA Wash buffer was added to the column, and centrifugation was carried out for 1 minute. After the wash, the column was transferred to a new 1.5 ml RNase-free tube. Finally, 7 µl of DNase/RNase-free water was added to the column, and a final centrifugation at 13,000 x g for 30 seconds was performed to elute the RNA. RNA samples were stored at -80 °C until further use.

RNA quantification was performed using the DeNovix QFX Fluorometer (DeNovix Inc., USA) and the Qubit RNA High Sensitivity Assay kit, according to the manufacturer's guidelines. Briefly, the reagent solution was prepared by adding Qubit™ RNA HS reagent to Qubit® RNA HS Buffer in a 1:200 ratio. For each RNA measurement, 1 µl of RNA sample was resuspended in 199 µl of the reagent solution. A calibration curve was generated by measuring two standards, Qubit™ RNA HS Standards 1 and 2, which were prepared by mixing 10 µl of each standard with 190 µl of the reagent solution.

The RNA yield from sorted MAIT cells ranged from 2.15 ng to 286.16 ng, with a median value of 38.7 ng (IQR: 23.85 ng - 64.95 ng). For sorted γδ T cells, the RNA yield varied from 8.83 ng to 1342.32 ng, with a median value of 84.67 ng (IQR: 41.4 ng - 162.9 ng).

3.6. Amplicon-based bulk RNA sequencing

In order to explore transcriptomic alterations in γδ T and MAIT cells in patients with PV, a targeted, amplicon-based RNA sequencing was employed. Specifically, the commercially available Immune Response Panel kit from Illumina was used, designed to simultaneously analyse the expression of 395 immunologically relevant genes. This method allows for a detailed examination of immune-related gene activity, encompassing key molecular processes such as cell activation, effector functions, adhesion, migration, and differentiation. Additionally, it provides insights into T cell receptor (TCR) signalling pathways, the expression of antigen-presenting molecules, and the regulation of immune responses through co-stimulatory and inhibitory receptors, along with chemokine and cytokine receptors.

3.6.1. Library preparation

To investigate the immunotranscriptomes of MAIT cells and γδ T lymphocytes, a total of 48 sequencing libraries were prepared. Specifically, 24 libraries (12 from patient samples [PV] and 12 from healthy controls [HC]) were constructed for MAIT cells, and additional 24 libraries (12 PV and 12 HC) were prepared for γδ T cells. The Immune Response Panel kit is suitable for RNA inputs ranging from 1 to 100 ng, with a standard recommendation of 10 ng of high-quality RNA. Sequencing libraries were prepared following the protocol outlined in the AmpliSeq for Illumina Immune Response Panel Reference Guide (v06, February 2019).

Library preparation protocol:

The selected RNA samples were diluted with nuclease-free water to a final volume of 7 µl, using 20 ng of RNA from γδ T cells and 10 ng from MAIT cells as input for cDNA synthesis. A reverse transcription master mix was prepared by combining 5X AmpliSeq cDNA Reaction Mix and 10X AmpliSeq RT Enzyme Mix, with 3 µl of this master mix added to each RNA sample and mixed thoroughly. The reverse transcription (RT) program was initiated on the thermal cycler.

Reverse transcription (RT) program:

	Temperature (°C)	**Time (min)**
Reverse transcription (RT)	42°C	30 min
Enzyme inactivation	85°C	5 min
Hold	10°C	-

For amplification of target regions, 4 µl of 5X AmpliSeq HiFi Mix, 4 µl of 5X AmpliSeq Immune Response Panel, and 2 µl of Nuclease-free water were added to each cDNA sample, and the amplification program (AMP) was run.

Amplification program (AMP):

	Temperature (°C)	**Time (min)**	**Number of cycles**
Initial denaturation	99°C	2 min	1
Denaturation	99°C	15 sec	20
Annealing/Extension	60°C	4 min	
Hold	10°C	-	-

To digest primer dimers and partially digest amplicons, 2 µl of FuPa Reagent was added to each target amplification reaction, and the FUPA program was executed on the thermal cycler.

FUPA program:

	Temperature (°C)	**Time (min)**
Digestion Step 1	50°C	10 min
Digestion Step 2	55°C	10 min
Digestion Step 3	62°C	20 min
Hold	10°C	Up to 1 hour

Next, ligation of Index 1 (i7) and Index 2 (i5) flow cell adapters was performed to uniquely index each library for dual-index sequencing. This was achieved by sequentially adding 4 µl of Switch Solution, 2 µl of AmpliSeq UD Indexes for Illumina, and 2 µl of DNA Ligase. The LIGATE program was then run on the thermal cycler.

LIGATE program:

	Temperature (°C)	**Time (min)**
Adapter Annealing	22°C	30 min
Ligation Reaction	68°C	5 min
Ligation Extension	72°C	5 min
Hold	10°C	Up to 24 hours

For library cleanup, 30 µl of MagSi-NGSPREP Plus beads (Magtivio, Netherlands) were added to each library, followed by vortexing and brief centrifugation. After a 5-minute incubation at room temperature, the plate was placed on a magnetic stand until the solution cleared. The supernatant was carefully removed and discarded, and the wells were washed twice with 150 µl of 70% ethanol. The plate was then sealed, briefly centrifuged, and returned to the magnetic stand.

In the second amplification step, 50 µl of amplification master mix (45 µl of 1X Lib Amp Mix and 5 µl of 10X Library Amp Primers) was added to the beads, and the AMP_7 program was run.

AMP_7 program:

	Temperature (°C)	**Time (min)**	**Cycles**
Initial denaturation	98°C	2 min	1
Denaturation	98°C	15 sec	7
Annealing/Extension	64°C	1 min	
Hold	10°C	Up to 24 h	-

The second cleanup involved two rounds of purification using MagSi-NGSPREP Plus beads. In the first round, high molecular-weight DNA was captured by the beads and discarded, while the library and primers remained in the supernatant and were transferred to a fresh plate. In the second round, the libraries were captured by the beads, while the primers remained in

the supernatant. The bead pellet, containing the libraries, was saved and eluted. The plate was briefly centrifuged and unsealed, after which 25 µl of MagSi-NGSPREP Plus beads were added to each well containing ~50 µl of the library. Following a 5-minute incubation, the supernatant (~75 µl) was transferred to a new plate, and 60 µl of MagSi-NGSPREP Plus beads were added. After incubation and clearing, the supernatant was discarded, and the wells were washed with ethanol, dried, and re-eluted in 30 µl of Low TE buffer. Finally, 27 µl of the library supernatant was transferred to a new PCR plate for further quality control analysis.

3.6.2. Library quantification and size assessment

To evaluate the quality and yield of the synthesized sequencing libraries, both concentrations and fragment sizes were evaluated. Quantitative PCR (qPCR) was employed to measure the library concentrations, while agarose gel electrophoresis was used to determine fragment sizes.

3.6.2.1. qPCR quantification

Library quantification was carried out using the KAPA Library Quantification Kit for Illumina® platforms (Kapa Biosystems, USA), following the manufacturer's guidelines. The KAPA SYBR FAST qPCR Master Mix, used in the KAPA Library Quantification Kit, contains primers specifically designed to target the Illumina P5 and P7 adapter sequences ligated to the ends of successfully prepared sequencing libraries. By using these primers, only DNA fragments that have been properly ligated with these Illumina adapters are amplified and quantified. This makes qPCR-based quantification more specific and accurate compared to fluorometric methods (such as Qubit), which measure the total DNA content in the sample, including any unused adapters, primer dimers, or other non-library DNA fragments. The quantification process is based on the amplification of a set of six pre-diluted DNA standards that are used to generate a standard curve. The concentrations of diluted library samples are then calculated against the standard curve, using absolute quantification. Libraries with concentrations greater than 0.0002 pM can be quantified, regardless of the library type, preparation method, or Illumina sequencing platform.

qPCR quantification protocol:

Two microliters from each library were serially diluted twice (1:100) in 10 mM Tris-HCl (pH 8.0), resulting in a final dilution of 1:10000, to bring the sample concentration within the range of the KAPA standards (0.0002–20 pM). The qPCR mixture comprised 12 µl of KAPA SYBR FAST qPCR Master Mix, 4 µl of PCR-grade water, and 4 µl of the diluted library, resulting in a total volume of 20 µl. All qPCR reactions were run in triplicate using QuantStudio 5 real-time PCR instrument (Thermo Fisher Scientific, USA), with data analysis performed using QuantStudio Design & Analysis Software v 1.5.2 (Thermo Fisher Scientific, USA).

KAPA quantification qPCR program:

	Temperature (°C)	Time (min)	Cycles
Initial denaturation	95 °C	5 min	-
Denaturation	95 °C	30 s	35
Annealing/Extension	60 °C	45 s	
Hold	4 ° C	∞	-

3.6.2.2. Agarose gel electrophoresis

The size of NGS libraries plays a critical role in both the efficiency and accuracy of the sequencing process, as each sequencing platform has an optimal library size range that ensures optimal performance. For example, Illumina platforms typically require fragment sizes between 200-600 bp. Assessing library size prior to sequencing is essential to confirm the success and consistency of the library preparation, ensuring that fragments fall within the desired range. Moreover, library size assessment is needed for further molarity calculations.

Agarose gel electrophoresis protocol:

Library fragment sizes were assessed via 1.5% agarose gel electrophoresis. The gel was prepared by dissolving 0.75 g of agarose (Bio-Rad, USA) in 50 ml of 1X TBE buffer, and adding 5 µl of SYBR Safe gel stain (Thermo Fisher Scientific, USA). For sample loading, 4 µl of each library sample was mixed with 1 µl of DNA stain (6x MassRuler Loading Dye, Fermentas Life Sciences, USA). A 5 µl of 50 bp DNA ladder (Takara, Japan) was included as a size marker. The gel was run at 150 V for 25 minutes, and fragment sizes were estimated relative to the DNA marker.

The average library size was approximately 300 base pairs. The molarity of the libraries was next calculated using the following formula: $Molarity\ (nM) = \frac{ng/\mu l x\ 106}{660\frac{g}{mol}\ x\ average\ library\ size\ (bp)}$.

In accordance with the manufacturer's protocol, the libraries were further diluted to a final concentration of 2 nM. Following this, they were denatured and diluted in line with the MiniSeq System Denature and Dilute Libraries Guide, Protocol A: Standard Normalization Method (v08, September 2020). Only the libraries with a concentration higher than 0.2 nM/µl were used for sequencing.

3.6.3. Library denaturation and dilution

Library denaturation and dilution are essential in preparing NGS libraries for optimal hybridization to the flow cell. During denaturation with NaOH, the double-stranded DNA is converted into single strands, which will attach to the flow cell surface. Proper dilution adjusts the library concentration to the appropriate concentration, ensuring optimal cluster density for sequencing.

Library denaturation and dilution protocol:

For library denaturation and dilution, equal volumes (10 µl) of each 2 nM library were pooled into a 1.5 ml tube. Denaturation was achieved by combining 10 µl of the pooled libraries with 10 µl of 0.2 M NaOH and incubating at room temperature for 5 minutes. Following denaturation, 10 µl of 200 mM Tris-HCl (pH 7.0) was added to neutralize the NaOH. To achieve a final concentration of 20 pM, 970 µl of prechilled HT1 buffer was added to the denatured library pool. The 20 pM library solution was further diluted to a final loading concentration of 1.5 pM, which falls within the recommended range of 1.1–1.9 pM.

Simultaneously, PhiX control was prepared for sequencing. PhiX is an adapter-ligated library derived from a well-characterized bacteriophage, commonly used in next-generation sequencing as a control to monitor cluster generation, sequencing, and alignment. Initially, a 10 nM PhiX stock was diluted to 4 nM. PhiX was then denatured by mixing 5 µl of PhiX with 5 µl of 0.1 M NaOH and incubated at room temperature for 5 minutes. After denaturation, 5 µl of 200 mM Tris-HCl (pH 7.0) was added to neutralize the NaOH, and the denatured PhiX was diluted to a final loading concentration of 1.5 pM.

Finally, a mixture consisting of 495 µl of the diluted libraries and 5 µl of PhiX control, resulting in a PhiX spike-in of 1%, was pipetted into the reagent cartridge for sequencing.

3.6.4. Sequencing

High-throughput paired-end sequencing with a read length of 2 × 150 bp was carried out on MiniSeq Illumina platform using the MiniSeq High-Output Reagent Kit (Illumina, USA). The sequencing process included FASTQ file generation, demultiplexing, and adapter trimming.

3.6.5. Sequencing run quality control assessment

After sequencing, the Sequencing Analysis Viewer Software (SAV) v2.1 (Illumina, USA) was used to evaluate the quality metrics of the sequencing run. SAV is a specialised tool designed for quality control, providing a visual interface to assess data generated from Illumina sequencing platforms. It offers insight into various QC metrics, of which the Qscore (or Phred quality score) distribution is particularly critical. This metric indicates the reliability of base calls at different positions in the reads, and a high-quality Qscore distribution (≥ Q30 for more than 80 % reads) ensures confidence in the accuracy of the sequencing data.

In addition to Qscore distribution, the number of bases sequenced, cluster density, percentage of reads passing the filter, and the proportion of reads per sample were assessed to evaluate the overall quality and performance of sequencing runs. The number of bases sequenced indicates sequencing depth and coverage, with higher base counts enhancing the reliability of the analysis. Cluster density, defined as the number of clusters of DNA fragments generated per unit area on a flow cell, is crucial for optimal run quality, as it affects the percentage of reads passing the filter, Q30 scores, and total data output. While underclustering can preserve data quality but reduce output, overclustering may lower Q30 scores, introduce artifacts, and decrease overall output. The percentage of reads passing the filter (PF%) indicates the proportion of high-quality clusters retained after Illumina's chastity filter. Finally, the proportion of reads per sample helps ensure data balance, as a lower proportion in one sample may indicate issues such as poor library quality or sequencing artifacts.

3.6.6. RNA-seq alignment

The RNA-seq alignment pipeline was developed using the Galaxy platform (217). Initially, raw FASTQ files containing RNA-seq reads were imported into Galaxy and subjected to quality control using FastQC. FastQC provides comprehensive quality control metrics for sequencing data by evaluating various several key metrics. It checks the quality scores of each base in the reads, summarises overall sequence quality scores to determine if a significant portion of reads falls below acceptable threshold, and examines the base composition at each position to reveal any biases or contamination. It also analyses the distribution of GC content to detect potential sequencing biases, reports the proportion of ambiguous bases ('N') indicate issues with base calling, and assessed sequence duplication levels. Overrepresented sequences that may suggest contamination are also flagged.

Following quality assessment, the reads were pre-processed using Cutadapt to remove low-quality sequences or adapters, with a minimum length cutoff of 20 bp and Q20 quality cutoff. This way, all reads shorter than 20 bp or with quality score below Q20 were discarded. The cleaned reads were then aligned using the STAR aligner (218), with the GRCh38 reference genome sourced from the UCSC Genome Browser. STAR employs a two-step alignment process: seed searching and clustering. It initially identifies the longest exact matches between read sequences and the reference genome, termed Maximal Mappable Prefixes (MMPs), treating these as 'seeds.' The aligner sequentially searches for additional matches in the unmapped portions of the reads. When exact matches are not found, STAR extends or soft clips sequences to handle mismatches or contaminants, ultimately stitching seeds together based on alignment quality.

After alignment, the resulting alignment files (BAM files) were processed using featureCounts to quantify gene expression levels. FeatureCounts generates a count table that contains the information on the number of reads mapped to each gene across each sample. This matrix was subsequently used in downstream analysis. All evaluated metrics indicated the quality of both sequencing runs.

3.6.7. Differential gene expression and enrichment analyses

The R package Deseq2 was applied to analyse differential gene expression (DEG) in PV samples relative to healthy controls. Deseq2 is specifically designed for high-dimensional RNA-seq count data, performing differential expression analysis based on a negative binomial

distribution model. The package provides robust normalization, visualization, and differential analysis by employing empirical Bayes methods to estimate priors for log fold change and dispersion, and to calculate posterior estimates for these quantities (219).

Before proceeding with the analysis, the read counts across samples were assessed to identify potential outliers, specifically samples with read depths that significantly deviated from the others. Samples exhibiting anomalously low read counts were removed to ensure the accuracy and robustness of the analysis.

The analysis was performed using the standard functions provided by the DESeq2 package. Before executing the DEG analysis, the low-abundant transcripts were removed to enhance the accuracy and reliability of the results. Transcripts with less than 10 reads, in at least 5 samples within a group (PV or HC) were filtered-out.

The final output of the DESeq routine provides several key metrics for each gene, including the baseMean, which represents the average normalized expression across all samples, the log2FoldChange (log2FC) which quantifies the difference in gene expression between two conditions, the p-value to assess the significance of these changes, and the adjusted p-value (padj), calculated using the Benjamini-Hochberg (BH) method to account for multiple testing.

To identify patterns and biological functions associated with differentially expressed genes, enrichment analysis was conducted using various gene sets and pathway analyses. This included Gene Ontology (GO) term enrichment (220,221), functional annotation through the Kyoto Encyclopedia of Genes and Genomes (KEGG) (222), and analysis of Hallmark and Reactome gene sets from the Molecular Signatures Database (MSigDB) (223,224). GO term enrichment analysis evaluates which biological processes (BP), molecular functions (MF), or cellular components (CC) are overrepresented in a set of differentially expressed genes. KEGG functional annotation links genes with specific metabolic and signalling pathways. Additionally, Hallmark gene sets represent well-defined biological states or processes, while Reactome gene sets provide curated pathways and reactions.

The analyses were carried out using *clusterProfiler*, *AnnotationDbi*, and *msigdbr* packages, while visualisation of the results was enabled using *ComplexHeatmap*, *enrichplot*, *pathview*, and *ggplot* function.

3.7. Immune repertoire sequencing

To investigate the distinct characteristics of T cell receptor repertoires in peripheral MAIT and γδT cells in psoriasis, high-throughput TCR sequencing was performed. This methodology provides a thorough analysis of various aspects of TCR repertoires, including diversity, preferential gene usage, and detailed CDR3 metrics such as length variations, insertions, and convergence. Additionally, TCR sequencing provides insights into V(D)J pairing, clonotype overlap, and clonotype publicness, i.e. sharing of clonotypes between samples, amongst others. The robustness of TCR sequencing lies in its ability to capture a comprehensive view of TCR repertoire dynamics, revealing how T cell populations are shaped by disease processes.

3.7.1. TCR-seq library preparation

For library preparation, the Archer® Immunoverse™-HS TCR kit was used. This kit enables simultaneous sequencing of the CDR3 regions from the α-, β-, γ-, and δ-chains of TCR receptors. TCR sequences are selectively enriched during the cDNA synthesis step, thus minimizing the interference of non-immune cell genetic material and ensuring that the analysis focuses specifically on the TCR repertoire. The Immunoverse panel employs anchored multiplex PCR (AMP) chemistry in conjunction with molecular barcoded (MBC) adapters. AMP chemistry utilizes unidirectional gene-specific primers (GSPs) to amplify both known and novel mutations within the TCR sequences. To ensure accurate sequencing and analysis, MBC adapters are used to tag each DNA molecule with a unique barcode and a common region prior to amplification. This tagging enables precise deduplication and correction of PCR sequencing errors, thereby improving the accuracy of the TCR repertoire analysis.

Library construction protocol:

Sequencing libraries were prepared following the Archer® Immunoverse™-HS TCR Protocol (November 2022). All reagents were provided in designated reaction tubes, each containing lyophilised components pre-formulated for the specific reaction.

A total of 40 RNA samples extracted from MAIT cells and 40 RNA samples from γδ T cells were used for library construction. Specifically, 25 ng of RNA from MAIT cells and 50 ng of RNA from γδ T lymphocytes were used in the cDNA synthesis reactions, exceeding the recommended minimum input of 20 ng of RNA.

In the initial step, TCR-specific RT priming was performed to selectively synthesise TCR cDNA using TCR-specific primers. RNA samples were diluted with nuclease-free water to the desired concentrations, resulting in a final reaction volume of 20 µl. These diluted RNA samples were then transferred to TCR Specific RT Priming tubes, which were then placed in a thermal cycler for 5 minutes incubation at 65°C.

Following the RT priming, a two-step cDNA synthesis was carried out. In the first step, 20 µL of RT priming product was transferred to First Strand cDNA Synthesis tubes. The synthesis reaction was conducted according to the specified thermal cycling program.

First Strand cDNA Synthesis program:

	Temperature (°C)	Time (min)
Reverse transcription	50	30
Enzyme inactivation	80	20
Hold	4	Hold

After the first-strand synthesis completion, 20 µL of nuclease-free water was added to each tube, doubling the volume to 40 µL. This mixture was then transferred to Second Strand cDNA Synthesis tubes, and the second strand was synthesized by running the appropriate thermal cycler program.

Second Strand cDNA Synthesis program:

	Temperature (°C)	Time (min)
Second strand synthesis	16	60
Enzyme inactivation	75	20
Hold	4	Hold

To ensure that the cDNA was suitable for downstream adapter ligation, an end repair reaction was performed to correct any "ragged" or non-blunt ends that may have arisen during the synthesis process. The 40 µL of cDNA was mixed with lyophilised End Repair reagents and incubated at 25 °C for 30 minutes in a thermal cycler.

To purify the cDNA and remove small fragments or reaction by-products, a bead-based cleanup was performed. First, 100 µL of resuspended AMPure beads were added to each

sample. After thorough mixing and a five-minute incubation at room temperature, the samples were placed on a magnetic stand for four minutes to pellet the beads. The supernatant was carefully removed, and the beads were washed twice with 200 µL of 70% ethanol, ensuring complete removal of the supernatant between washes. After air drying the beads for five minutes, the DNA was eluted in 20 µL of 10 mM Tris-HCl (pH 8.0), followed by a two-minute incubation on the magnet to separate the beads from the eluted DNA.

Following the cleanup, the ligation of MBC adapters was performed. This was achieved by first transferring 20 µL of purified DNA to Ligation Step 1 tubes and incubating for 15 minutes at 37°C to prepare cDNA ends for efficient ligation with the adapters. Then, 20 µL of 10mM Tris-HCL (pH 8.0) was added to each reaction, and the 40 µL of cDNA mixtures were transferred to tubes containing MBC adapters. The MBC adapters included P5 index tag for multiplexed tracking of samples. Subsequently, the entire reaction mixture was transferred to Ligation Step 2 Tubes, mixed with reagents and incubated at 25 °C for 15 minutes.

To remove unligated adapters and by-products, the cleanup step was performed using Ligation Cleanup Beads. The entire volume of the Ligation Step 2 reaction was mixed with the 50 µL of pre-washed beads, incubated at room temperature for five minutes, and the process was repeated. The samples were spun down, placed on a magnet, and the supernatant was discarded. The beads were washed twice with 200 µL of Ligation Cleanup Buffer and once with 200 µL of nuclease-free water. After each wash, the supernatant was removed, ensuring all liquid was discarded. Finally, DNA was eluted by resuspending the beads in 36 µL of 5 mM NaOH.

To enrich the libraries specifically for TCR products, 36 µL of the eluted DNA was combined with First PCR reagents and 4 µLof the Immunoverse GSP mix. The mixture was then placed in a thermal cycler.

First PCR program:

	Temperature (°C)	Time (min)	Cycles
Initial denaturation	95	3	1
Denaturation	95	0.5	24
Annealing	65	3	
Extension	72	3	1
Hold	4	Hold	1

This was followed by the cleanup step with MagSi-NGSPREP Plus beads. The 48 µL of beads was added to each reaction, mixed thoroughly, and incubated at room temperature for five minutes. The samples were then placed on a magnet for four minutes to pellet the beads, and the supernatant was discarded. The beads were washed twice with 200 µL of 70% ethanol, with each wash followed by a 30-second incubation and removal of the ethanol. After air-drying the beads, DNA was eluted in 44 µL of 10 mM Tris-HCl (pH 8.0). After placing the tubes on the magnet for two minutes, 42 µL of the purified eluate was transferred to a new PCR tube.

The second PCR was then conducted to incorporate the Index 1 (P7 index) tag. In this step, 40 µLof the purified first PCR eluate was added to a Second PCR tube, and the Second PCR program was started on the thermal cycler.

Second PCR program:

	Temperature (°C)	Time (min)	Cycles
Initial denaturation	95	3	1
Denaturation	95	0.5	8
Annealing	65	3	
Extension	72	3	1
Hold	4	Hold	1

The final step included cleanup with MagSi-NGSPREP Plus beads, as described previously. This resulted in 18 µL of purified TCR libraries.

3.7.2. Library quantification and size assessment

The libraries were quantified using qPCR (KAPA Library Quantification Kit) and their sizes determined using 1.5 % agarose gel electrophoresis, as detailed in the previous chapter. The molarity of libraries was calculated applying the previously described formula, and the libraries were diluted to 2 nM concentrations prior to denaturation and dilution step.

3.7.3. Library denaturation and dilution

The denaturation and dilution of sequencing libraries were performed according to the Protocol A: Standard Normalization in NextSeq 500 and NextSeq 550 Sequencing Systems Denature and Dilute Libraries Guide (December 2022).

Denaturation and dilution protocol:

First, 10 µl of each 2 nM libraries were pooled together and thoroughly mixed. To denature the pooled libraries, 10 µL of pool was combined with 10 µL of 0.2M NaOH and incubated at room temperature for 5 minutes. Following incubation, 10 µL of 200 mM Tris-HCl (pH 7) was added to neutralize the reaction, and 970 µL of prechilled HT1 buffer was then added, resulting in a final concentration of 20 pM denatured libraries. To dilute this further, 97 µL of the 20 pM denatured library solution was mixed with 1203 µL of HT1, yielding 1.3 ml of a 1.5 pM library solution. Simultaneously, the PhiX control was prepared by diluting 10 nM PhiX to 4 nM, followed by denaturation with 5 µL of 0.2 M NaOH. After a 5-minute incubation at room temperature, 5 µL of 200 mM Tris-Hcl (pH 7.0) was added. Next, 985 µL of HT1 buffer was added to the denatured PhiX, generating 1 ml of 20 pM PhiX solution. This was then diluted to 1.5 pM by mixing 97 µL of denatured PhiX with 1203 µL of prechilled HT1. Finally, 1040 µL of denatured and diluted library solution was combined with 260 µL of the diluted Phix to achieve a 20 % PhiX spike-in.

3.7.4. Sequencing

Paired-end sequencing with a read length of 2 × 150 bp was performed on the Illumina NextSeq 550 platform at Sestre milosrdnice University Hospital Center using the NextSeq 500/550 Mid-output kit. The sequencing workflow included adapter trimming, demultiplexing, and FASTQ file generation.

3.7.5. Sequencing run and sample quality control

The quality of the sequencing run was evaluated using the Illumina SAV (Sequencing Analysis Viewer) software, as detailed in the previous section. Each FASTQ file was additionally examined using FastQC within the Galaxy platform.

3.7.6. TCR sequencing alignment and clonotype assembly

To align TCR sequences, MiXCR, a specialised tool for the analysis of TCR and BCR receptor repertoires from NGS data (225), was used. MiXCR processes FASTQ files by aligning raw sequencing reads against a built-in reference database of V, D, J, and C gene segments, performs error correction to improve accuracy, and assembles CDR3 sequences to identify and characterize clonotypes effectively. The alignment process begins by aligning the raw sequencing data to the reference gene segments. For paired-end data, MiXCR merges overlapping sequences using subsequence or alignment-aided overlap methods. It also trims low-quality nucleotides and corrects barcode sequences. MiXCR performs CDR3 reconstruction by assembling the V, D, and J segments into full-length CDR3 sequences. It enhances accuracy through two layers of error correction: quality-guided mapping to address sequencing errors and a heuristic clustering to correct PCR errors. The output from MiXCR provides detailed information on clonotype frequency, which indicates the abundance of each TCR clonotype within the sample,V(D)J gene segment usage, which provides insights into the diversity of gene segments utilised, and CDR3 nucleotide and amino acid sequences.

MiXCR is a command-line tool that offers a broad range of alignment options tailored to different wet-lab conditions, such as the library preparation and sequencing methods. Since MiXCR does not support *preset* for Archer Immunoverse, the *analyze* function with "*generic-amplicon-with-umi" preset* was used to execute alignment and clonotype assembly.

3.7.7. TCR repertoire analysis

The clonotype tables generated by MiXCR were used as input for further analysis. This included utilization of the VDJTools (226) command-line platform and the immunarch (227) R package to conduct comprehensive downstream analyses, such as evaluating clonotype diversity, expansion, and the distribution of T-cell receptor gene segments.

Initially, the *Correct* function in VDJTools was used to filter residual erroneous clonotypes by merging low-abundance clonotypes with similar high-abundance ones. This function identifies clonotype pairs with up to a specified number of mismatches and merges them if their size ratio falls below a set threshold. This correction is performed without altering the original data, ensuring accurate comparison and removal of erroneous clonotypes only after the procedure.

Then, using *FilterNonFunctional* command was used to remove non-coding clonotypes, including those with stop codon or frameshift in their receptor sequences. Additionally, the *FilterBySegment* function was applied to discard clonotypes with pseudogene segments (e.g. *TRGV10*), retaining only those with known functional V/D/J segments (positive selection) or removing those lacking specified V/D/J segments (negative selection).

The clonotype tables generated through these pre-filtering steps were used for downstream analyses with VDJTools and immunarch.

Several key functions from VDJTools were used to analyse various aspects of TCR repertoire characteristics. The *CalcBasicStats* routine provided fundamental sample statistics, including read counts, the number of clonotypes, and the average CDR3 length. The *CalcSegmentUsage* function was used to determine the usage patterns of Variable (V) and Joining (J) gene segments. To assess the distribution of CDR3 nucleotide lengths, *CalcSpectratype* function was applied. Additionally, *PlotFancyVJUsage* was used to display the V-J pairing frequencies within individual repertoires. For diversity analysis, *CalcDiversityStats* provided various repertoire diversity metrics, such as D50 value, Efron-Thisted estimate, and Shannon-Wiener index. The output from *JoinSamples* function was used to explore public, i.e., shared clonotypes across samples. Furthermore, for calculating the Jaccard overlap index, *repOverlap* function from immunarch was employed, while *trackClonotypes* was used for visualisation of clonotype and gene usage across samples.

3.8. Spectral flow cytometry analysis

To get comprehensive and more detailed insights into the phenotypes of circulating MAIT and γδ T cells in PV at the single-cell protein expression level, spectral flow cytometry was employed. Utilising a broad range of surface and intracellular markers, the spectral flow cytometry analysis aimed to explore the functional and activation profiles of these cells, as well as their trafficking patterns, cytotoxic potentials, and levels of exhaustion.

A total of 34 samples (20 from PV patients and 14 from healthy controls) were stained using two high-resolution panels. The first panel was designed to label 34 surface markers, including T cell lineage markers (CD45, CD3), MAIT cell markers (TCRVα7.2, MR1-5-OP-RU-loaded tetramer, CD4, CD8), and γδ T cell markers (γδTCR, Vδ1, Vδ2, Vδ3, Vγ9). Additional markers were used to assess various aspects such as functional status, activation, chemotaxis, trafficking and adhesion, NK-like functions, and exhaustion, comprising CD27, CD28, CD45RA, CD127, CD25, CD69, CD38, HLA-DR, CCR6, CCR7, CD11a, CD103, CXCR3, CXCR5, CX3CR1, CLA, CD16, CD56, CD94, CD161, CD57, and PD-1.

The second panel was focused on a more in-depth investigation of the effector and cytotoxic potentials of γδ T populations. This panel combined surface markers (CD3, CD4, CD8a, αβTCR, CD16, CD56, CD11a, CD27, CD28, CD45RA, CX3CR1, PD-1, CD127 (IL-7Rα), γδTCR, Vδ1, Vδ2, Vδ3) with intracellular labelling of proliferation markers (Ki67), transcription factors (T-bet, EOMES, TOX, BLIMP-1), and cytotoxic molecules (granzyme A, granzyme B, granzyme K, granulysin, perforin). The antibodies used in both panels are listed below (Tables 2 and 3).

Samples were processed using high-parameter spectral analyser Sony ID7000 at the University of Warwick Medical School, United Kingdom, and data analysis was performed using the OMIQ platform.

Table 2. Antibodies used for surface staining

Antibody	Fluorochrome	Clone	Source / manufacturer	Dilution
CD4	Spark UV387	SK3	Biolegend	1:100
CD45	BUV395	HI30	eBioscience	1:100
CD16	BUV496	3G8	BD Bioscience	1:200
CD56	BUV563	NCAM16.2	BD Bioscience	1:100
CD25	BUV615	2A3	BD Bioscience	1:100
CD11a	BUV661	G-25.2	BD Bioscience	1:1000
CD3	BUV805	UCHT1	BD Bioscience	1:30
PD-1	BV421	EH12.1	Biolegend	1:50
CD94	BV480	HP-3D9	BD Bioscience	1:200
αβTCR	VioBlue	REA652	Miltenyi Biotec	1:100
CD57	BV510	QA17A04	Biolegend	1:100
HLA-DR	BV570	L243	Biolegend	1:100
Va7.2	BV605	3C10	Biolegend	1:30
CCR7	BV650	G043H7	Biolegend	1:50
CD45RA	BV711	HI100	Biolegend	1:200
CD69	BV750	FN50	Biolegend	1:100

CXCR3	BV786	G025H7	Biolegend	1:50
Vδ1	FITC	REA173	Miltenyi Biotec	1:200
CXCR5	RB545	RF8B2	BD Bioscience	1:200
CD103	BB700	Ber-ACT8	BD Bioscience	1:100
CLA	PerCP Vio700	REA1101	Miltenyi Biotec	1:50
Vδ3	AF555	P11.5B	Beckman Coulter	1:300
MR1-tet	PE		Monash Biomedicine Discovery Institute, Monash University, Clayton, Australia (189)	1:50
CD127	Spark YG 581	A019D5	Biolegend	1:100
CD27	PE-Dazzle594	M-T271	Biolegend	1:200
Vγ9	PE-Cy5	IMMU 360	Beckman Coulter	1:400
CX3CR1	PE-Cy7/vio770	2A9-1	Biolegend	1:150
CD8a	Pe-Fire 700	SK1	Biolegend	1:200
CD28	PE-Fire 810	CD28.2	Biolegend	1:50
CD161	APC	W18070C	Biolegend	1:100
CCR6	Alexa Fluor 647	11A9	BD	1:50
Vδ2	VioBright R720	REA771	Miltenyi Biotec	1:20
γδTCR	APC-Vio 770	REA591	Miltenyi Biotec	1:100
CD38	APC-Fire 810	HIT2	Biolegend	1:200

Table 3. Antibodies used for intracellular staining

Antibody	Fluorochrome	Clone	Source / manufacturer	Dilution
CD4	Spark UV387	SK3	Biolegend	1:100
CD16	BUV496	3G8	BD Bioscience	1:200
CD56	BUV563	NCAM16.2	BD Bioscience	1:100
CD11a	BUV661	G-25.2	BD Bioscience	1:1000
CD3	BUV805	UCHT1	BD Bioscience	1:30
αβTCR	VioBlue	REA652	Miltenyi Biotec	1:100
CD27	BV605	M-T271	BD Bioscience	1:300
CD45RA	BV711	HI100	BioLegend	1:200
CX3CR1	BV750	2A9-1	BD Bioscience	1:50
PD-1	BV786	EH12.1	BD Bioscience	1:50
Vδ1	FITC	REA173	Miltenyi Biotec	1:200
Vδ2	PerCP Vio700	REA771	Miltenyi Biotec	1:50
Vδ3	AF555	P11.5B	Beckman Coulter	1:300
CD127	Spark YG 581	A019D5	Biolegend	1:100
CD8a	Pe-Fire 700	SK1	Biolegend	1:100
CD28	PE-Fire 810	28.2	Biolegend	1:100
γδTCR	APC-Vio770	REA591	Miltenyi Biotec	1:50

Ki67	BUV395	SolA15	eBioscience	1:100
Granzyme B	RB545	GB11	BD Bioscience	1:200
Granzyme K	RB780	G3H69	BD Bioscience	1:50
Perforin	PeCP Cy5.5	dG9	Biolegend	1:30
EOMES	Pe-eFlour610	WD1928	eBioscience	1:50
T bet	PE-Cy5	4B10	eBioscience	1:100
Granzyme A	PE-Cy7	CB9	eBioscience	1:100
TOX	PE	TXRX10	eBioscience	`1:50
Granulysin	APC	DH2	Biolegend	1:100
BLIMP-1	R718	6D3	BD Bioscience	1:50

3.8.1. Surface staining protocol

PBMCs were thawed in 3 ml of pre-warmed RPMI medium and centrifuged at 400 x g for 4 minutes. The cells were transferred to a 96-well plate, washed and centrifuged again. Next, 50 µl of Zombie NIR™ Fixable Viability Dye (Biolegend, USA) was added at 1:400 dilution, and the cells were incubated on ice for 15 minutes. After incubation, the cells were washed with 150 µl of FACS buffer, followed by the application of an Fc block, which was incubated for 5 minutes at room temperature in the dark. For surface staining, a mix of MR1-tetramer and CCR7 (10 µl) was first added and incubated at room temperature for 30 minutes. After washing, an antibody cocktail containing the remaining surface marker antibodies was added (50 µl) and the cells were incubated on ice for 20 minutes, followed by another wash with FACS buffer. For fixation, the cells were resuspended in 100 µl of intracellular fixation buffer (Thermo Fisher Scientific, USA) and incubated on ice for 10 minutes. Finally, the cells were washed with 130 µl of FACS buffer and resuspended in 150 µl of FACS buffer for further analysis.

3.8.2. Intracellular staining protocol

Thawed and washed PBMCs were transferred to 96-well plate and incubated with a Zombie NIR™ Fixable Viability Dye (1:400) for 15 minutes on ice, followed by a wash. Then, an Fc block was applied and incubated for 5 minutes at room temperature in the dark. The cells were then labelled with 50 µl of a surface antibody cocktail for 15 minutes on ice and washed with FACS buffer. For intracellular staining, components of eBioscience™ Foxp3 / Transcription Factor Staining Buffer Set (Thermo Fisher Scientific, USA) were used. The cells were resuspended in 100 µl of Fix/Perm buffer (diluted 1:4) and incubated on ice for 15 minutes,

followed by a wash with 100 µl of Perm buffer (1:10 dilution). Intracellular staining was carried out by adding 50 µl of an intracellular antibody cocktail diluted in Perm buffer (1:10) and incubating at room temperature for 30 minutes. The cells were then washed with 150 µl of FACS buffer and resuspended in 150 µl of FACS buffer for analysis.

3.8.3. Spectral reference library

Spectral flow cytometry differs from conventional flow cytometry by capturing the full emission spectrum of each fluorochrome, rather than detecting signals within individual channels. This allows the simultaneous detection of multiple fluorochromes, even those with overlapping emission spectra, by combining signals from all detectors into a comprehensive spectral profile.

To effectively separate fluorophores with overlapping emission spectra, a spectral reference library must be constructed. The library contains the unique spectral signatures of all fluorochromes used in an experiment and is crucial for the process of spectral unmixing, where mathematical algorithms separate combined signals into individual fluorophores.

To prepare spectral reference libraries, single-color controls were prepared by staining compensation beads (Invitrogen™ UltraComp eBeads, Thermo Fisher Scientific, USA) with each antibody used in the staining panel.

3.9. Statistical analysis

The normality of the numerical variables was assessed using the Shapiro-Wilk test. Non-parametric tests were used when data did not follow a normal distribution, and parametric tests were used otherwise. The Mann-Whitney U test and Student's T-test were used to compare differences between the test and control groups, while Fisher's exact test was applied for contingency tables. Spearman's rank correlation coefficient (ρ) was used to assess variable correlations. Multiple comparisons were adjusted using the Benjamini-Hochberg procedure. Descriptive statistics were presented as medians and interquartile ranges (IQR). The statistical significance was set to $p < 0.05$. All analyses were conducted in R using the *stats* library.

For graphical representation, R software v4.2.0 in the RStudio v2024.04 (RStudio Inc., USA) environment was used, along with the *ggplot2*, *ggpubr*, *ggstatsplot*, *treemap*, *ComplexHeatmap*, *cowplot*, and *RColorBrewer* packages. In addition, BioRender and Microsoft PowerPoint v2408 were used to create illustrations, while *Inkscape* (Brooklyn, New York, USA) was used for final figure editing.

4. RESULTS

4.1.Investigation of the proportion and composition of circulating γδ T cell compartment

The proportions of γδ T cells and their $V\delta1^+$, $V\delta2^+$, and $V\delta1^-V\delta2^-$ subsets in peripheral blood were analysed by flow cytometry in a set of 96 PBMC samples, comprising 63 samples from psoriasis vulgaris (PV) patients and 33 from healthy controls (HC). Upon assessing basic anthropometric and clinical metrics, psoriasis patients were found to have higher body mass index (BMI) scores and elevated leukocyte counts (within the reference range of 3.4–9.7 x 10^9/L), as well as a greater proportion of smokers and CMV negative examinees compared to healthy controls. There were no differences in age, sex distribution, hsCRP, or CMV IgG levels between the two groups. The psoriasis group was characterised by heterogeneity in terms of severity, onset, and duration. Positive correlations were observed between PASI score and hsCRP levels (Sperman's rho $\rho = 0.51$, $p = 6 \times 10^{-4}$), as well as between PASI and psychological burden measured by the DLQI questionnaire ($\rho = 0.67$, $p = 7.34 \times 10^{-9}$). Additionally, psoriasis patients who reported smoking displayed significantly higher leukocyte count (Me (IQR): 8.15 (7.33-10.38) vs. 6.6 (5.75-7.95) x 10^9/L, p=0.008, Mann-Whitney U test) and PASI scores (19.05 (9-23.4) vs. 8.2 (4.95-17.8), p=0.029) compared to non-smoking psoriasis participants. Detailed descriptive statistics of the participants' characteristics are presented in Table 4.

Table 4. Study subjects.

	PV (N = 63)	**HC (N = 33)**	**P**
Age	43 (33 – 56)	37 (29 – 43)	0.164*
Sex (M/F)	47/16	24/9	1**
BMI	30.2 (25.5 – 32.9)	27 (25.7 – 29.6)	**0.043***
hsCRP (mg/L)	1.65 (0.71 – 3.79)	1.2 (0.7 – 2.39)	0.422*
L (N x10^9/L)	7.6 (6.4 – 9.7)	6.4 (5.1 – 7)	**0.001***
CMV IgG (U/mL)	96.5 (42.9 – 126)	109 (89.7 – 129)	0.188*
CMV IgG (pos/neg)	47/14	27/1	**0.031****
Smoker (yes/no)	24/27	6/26	**0.010****
PASI	16.1 (7.1 – 22)	-	-
DLQI	10 (4 – 16)	-	-
Disease onset (years)	31 (19 – 44)	-	-
Disease duration (years)	9 (5 –17)	-	-

*Continuous data are shown as median (interquartile range). BMI - body mass index, hsCRP – high sensitivity C-reactive protein, L – leukocyte count, CMV – cytomegalovirus; PASI – psoriasis area and severity index, DLQI – dermatology life quality index * Mann-Whitney U test, ** Fisher's Exact Test*

The analysis of peripheral γδ T cells distribution revealed no statistically significant differences between affected and healthy individuals. The proportions of Vδ1$^+$, Vδ2$^+$, and Vδ1$^-$ Vδ2$^-$ subsets were consistent across both groups (Table 5). As anticipated, Vδ2$^+$ cells constituted the majority of peripheral γδ T cells, followed by Vδ1$^+$ and Vδ1$^-$Vδ2$^-$, with median percentages of 74.8 (Q1–Q3: 53.05–88.03) %, 14.15 (6.67–25.98) %, 6.89 (3.02–15) %, respectively (Figure 10).

Table 5. The distribution of peripheral γδ T cells in PV and HC samples

	PV (N = 63)	HC (N = 33)	P
% γδTCR$^+$ of CD3$^+$	2.82 (1.51-4.64)	4.12 (2.26 – 6.22)	0.099
% Vδ2 of CD3	1.68 (0.93-4.11)	2.31 (1.28 – 5.2)	0.107
% Vδ1 of CD3$^+$	0.32 (0.15-0.69)	0.41 (0.3 – 1.47)	0.062
%Vδ1$^-$Vδ2$^-$ of CD3$^+$	0.2 (0.09-0.43)	0.17 (0.12 – 0.35)	0.966
% Vδ2 of γδTCR$^+$	73.1 (49.7-88.1)	77.9 (56 – 83.8)	0.663
% Vδ1 of γδTCR$^+$	13.9 (5.82-26.05)	14.7 (9.71 – 24.7)	0.447
% Vδ1$^-$Vδ2$^-$ of γδTCR$^+$	7.2 (3.47-19.7)	6.46 (2.81 – 11.8)	0.312

Data are shown as median with interquartile range. Mann-Whitney U test

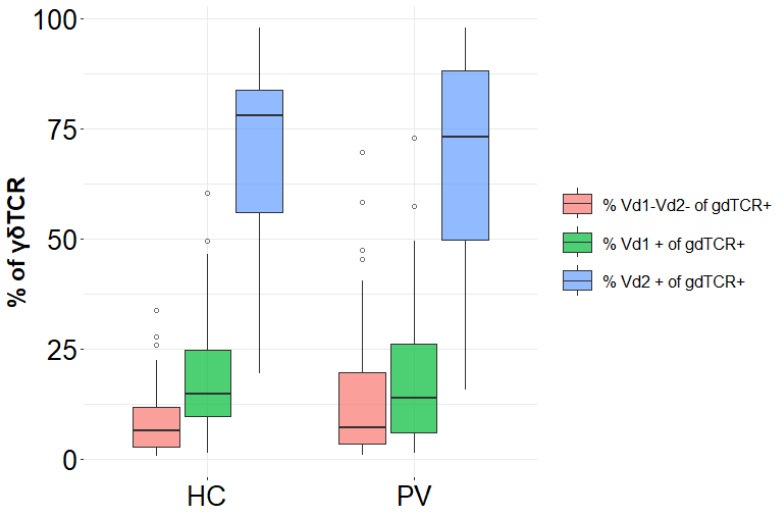

Figure 10. Vδ2$^+$ cells dominate the peripheral γδ T cell population, followed by Vδ1$^+$ and Vδ1$^-$Vδ2$^-$ subsets, with no significant case-control differences. *N (PV) = 63, N(HC) = 33*

In both psoriasis and control group, the proportion of total γδ T cells within CD3$^+$ T lymphocyte population, as well as the percentage of Vδ2$^+$ cells in both total CD3 and γδ T cells, declined with advancing age (Figure 11 B). In psoriasis patients, this reduction in Vδ2$^+$ cells was accompanied by a weak increase in the Vδ1$^+$ subset (Figure 11 A), whereas healthy individuals exhibited a slight expansion of the Vδ1$^-$Vδ2$^-$ population (Figure 11 C). Moreover,

CMV IgG levels positively correlated with the proportion of Vδ2^{neg} populations (Vδ1^{-}Vδ2^{-} and Vδ1^{+}), coinciding with the decline of Vδ2^{+} subset in both groups (Figure 11 D). The decrease in the Vδ2/Vδ1 ratio with advancing age and CMV IgG levels is in line with previous reports on the effect of age and CMV infection on reshaping of the γδ T cell population (121,162,228,229). No significant associations were found between PASI, DLQI, hsCRP, or disease duration and γδ T proportions. In addition, smoking status did not affect the distribution of the peripheral γδ T cell compartment.

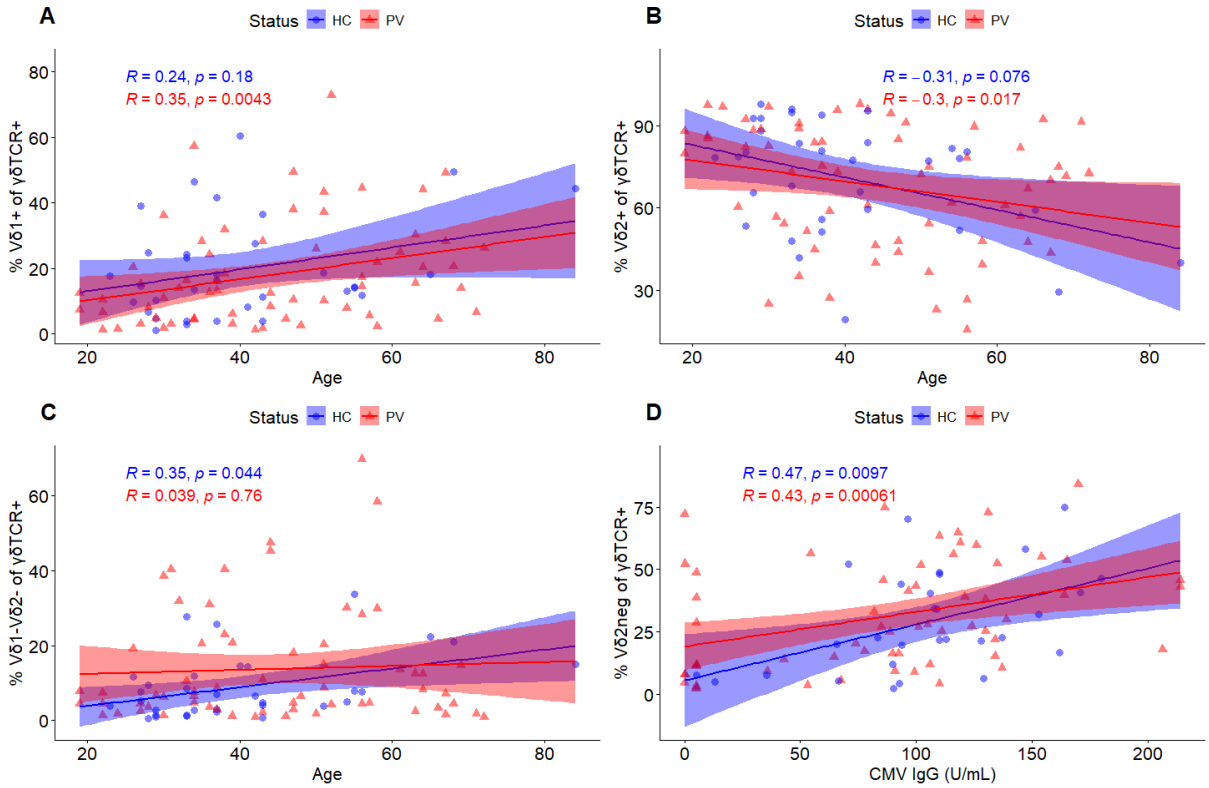

Figure 11. Age and CMV IgG levels influence γδ T cell compartment composition. *A) Vδ1^{+} cell proportions increase with age in psoriasis (PV). B) Vδ2^{+} cell frequencies decrease with age in PV patients C) Advancing age is associated with higher proportions of Vδ1^{-}Vδ2^{-} cells in healthy controls. D) CMV IgG levels positively correlate with increased proportions of the Vδ2^{neg} subset.*

Next, the analysis explored sex-based differences in the composition of γδ T cells. Notably, distinct variations emerged when focusing on male participants only. Specifically, male PV patients exhibited significantly lower levels of total γδ T cells and Vδ2^{+} cells in CD3^{+} T compartment compared to healthy men (Figure 12).

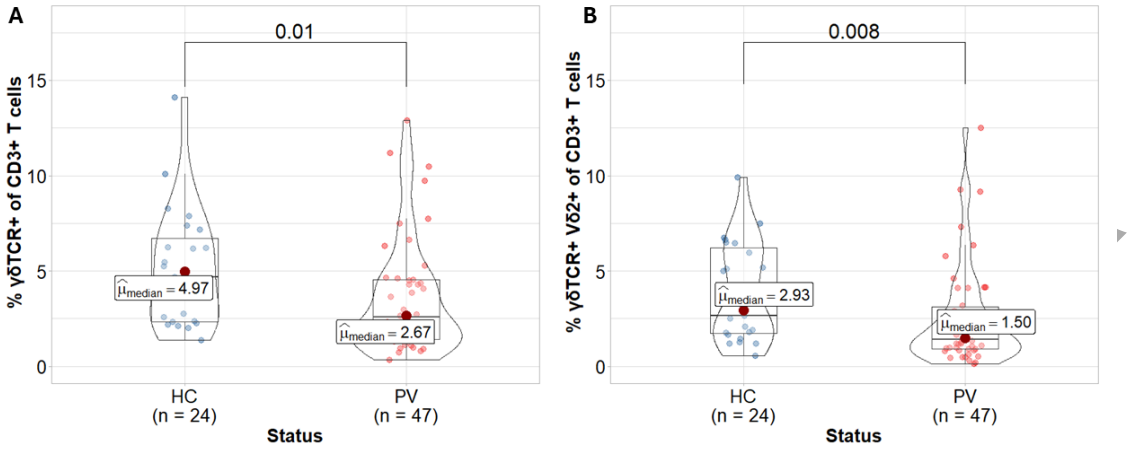

Figure 12. Male psoriasis patients show reduced γδ T cell proportions compared to healthy men. *Proportions of A) total γδ TCR$^+$ and B) Vδ2$^+$ cells within CD3$^+$ T cells are significantly lower in male psoriasis patients (PV) compared to healthy male controls (HC). Mann-Whitney U test*

In addition, the analysis revealed that healthy women displayed significantly lower proportions of γδ T and Vδ2$^+$ cells in total CD3$^+$ T cells compared to healthy men (Figure 13 A and B). In contrast, female psoriasis patients did not demonstrate significant differences in the proportions of γδ T or Vδ2 subset compared to affected men (Figure 13 C and D). Furthermore, there were no significant differences in the proportions of γδ T cells subsets between healthy and psoriasis-affected women.

To determine whether the decline of Vδ2$^+$ proportions observed in male psoriasis patients was influenced by confounding factors like age, further analyses were carried out. While no difference in median age was found between psoriasis group and healthy controls ($p = 0.164$), the psoriasis cohort contained a higher proportion of men aged over 60. Therefore, further analysis was restricted to participants under the age of 60. In this newly formed age-balanced group, the results remained consistent, showing significantly lower levels of γδ T and Vδ2$^+$ cells within the CD3$^+$ T population in psoriasis male patients, suggesting this decrease is disease-driven (Figure 14).

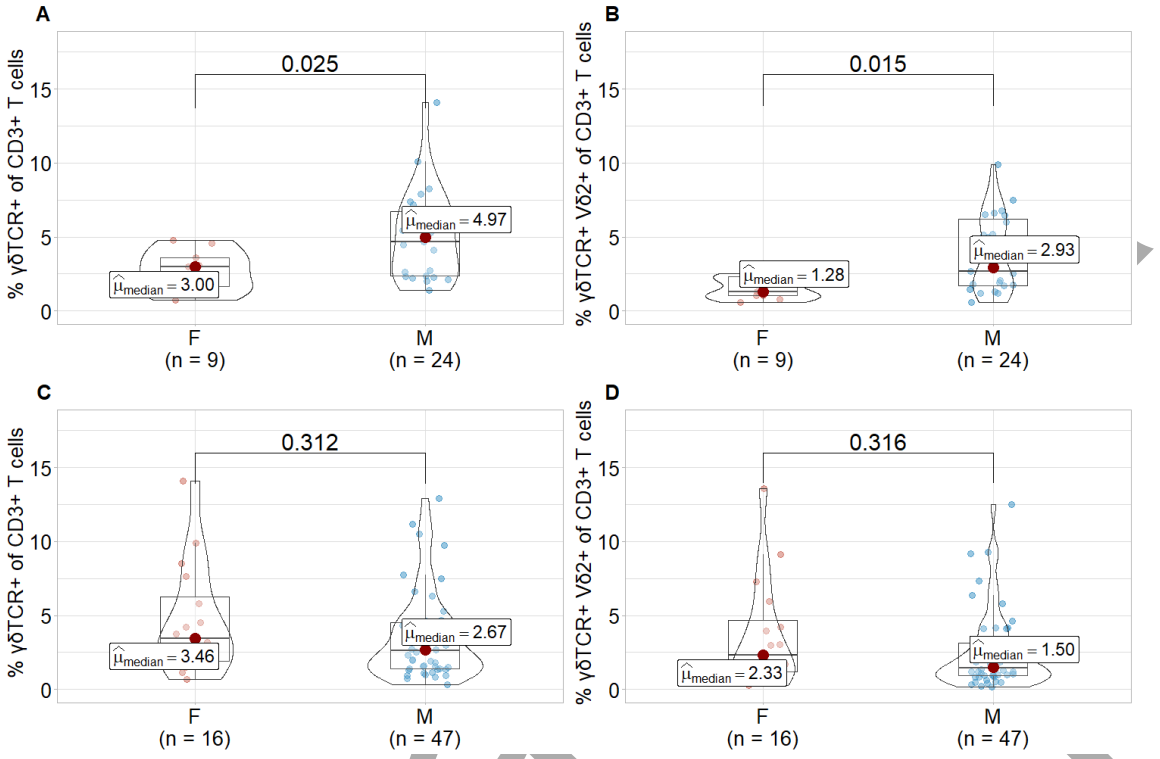

Figure 13. Lower proportions of γδ T cells and Vδ2⁺ subset in healthy women compared to men, with no significant differences in psoriasis patients. *Proportions of γδ T cells in women (F) vs men (M) in A) healthy and C) psoriasis patients. Proportions of Vδ2+ cells in women (F) vs men (M) in B) healthy and D) psoriasis patients. Mann-Whitney U test.*

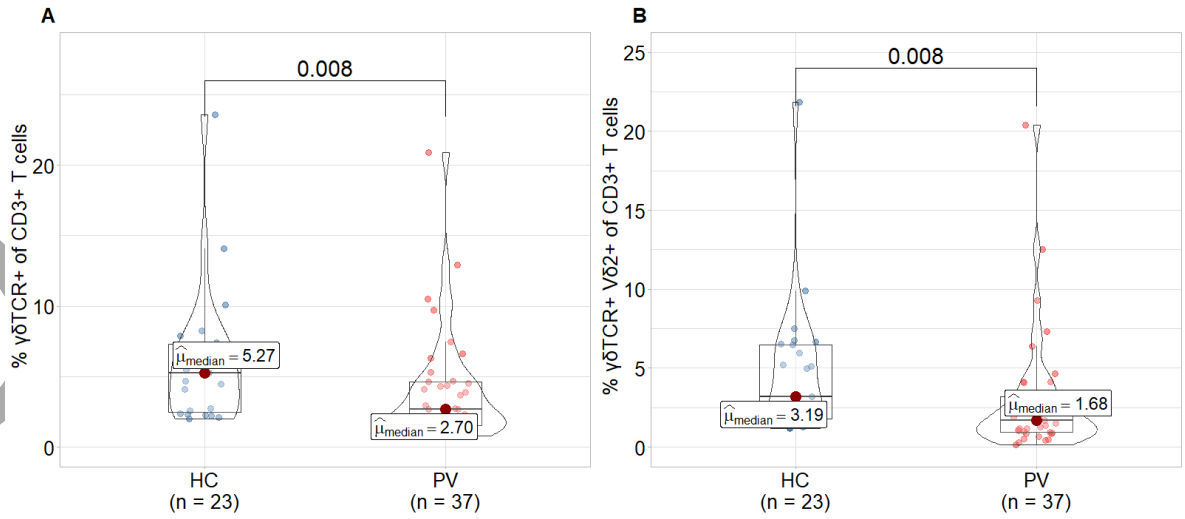

Figure 14. Reduced proportions of γδ T cells and Vδ2⁺ subset in male psoriasis patients persists in an age-balanced cohort (≤ 60 years). *A) Percentage of γδ T and B) Vδ2⁺ cells within the CD3⁺ T cell compartment. Mann-Whitney U test*

4.2.Profiling of γδ TCR repertoires

4.2.1. Sequencing quality metrics and participant characteristics

The composition of peripheral γδ T-cell receptor (TCR) repertoires in psoriasis patients was investigated to explore how the diversity and clonality of γδ TCR repertoires are shaped in the disease. This was achieved using 40 RNA samples (25 psoriasis vulgaris patients [PV] and 15 healthy controls [HC]) extracted from flow-sorted γδ T cells, with successful library construction achieved for 39 samples (24 PV + 15 HC).

The sequencing run and all sequenced libraries passed the initial quality control criteria, however, upon reviewing the read counts and the proportions of TRG/TRD reads in each sample, four samples with 'outlier' properties were found. Specifically, two samples were excluded due to an extremely low number of total clonotypes (< 60), and additional two samples were filtered out because their sequences were predominantly composed of TRA/TRB CDR3 transcripts (> 67 %). Importantly, there was no significant correlation between the number of sequences and the observed clonotype count for either TRG or TRD clonotypes, assuring that the read count did not influence clonotype diversity. A summary of the sequencing metrics is provided in Table 6.

Table 6. γδ TCR sequencing metrics

	PV (N = 20)	HC (N = 15)	P
TRG reads	631,219 (443,787 – 726,651)	511,311 (346,524 – 571,758)	0.067
TRD reads	248,937 (160,673 – 351,775)	267,126 (169,681 – 294,735)	0.498
TRG/TRD reads (%)	89.2 (84 – 92.7)	81.6 (75.7 – 89.5)	0.116
TRG clonotypes	748 (351 – 1738)	1235 (897 – 1617)	0.170
TRD clonotypes	497 (157 – 1192)	772 (534 – 1224)	0.204

Data are shown as median with interquartile range. Mann-Whitney U test

The baseline characteristics of the participants are summarised in Table 7. In brief, psoriasis patients exhibited a higher leukocyte count in their whole blood count (WBC) measurements, though the values remained within the normal reference range (3.4 – 9.7 x 10^9/L). No statistically significant differences were observed between psoriasis patients and healthy controls with respect to age, gender distribution, CMV status, CMV IgG levels, BMI, or hsCRP levels.

Table 7. Baseline subjects' characteristics

	PV (N = 20)	HC (N = 15)	P
Age	41 (32 – 55)	34 (29 – 37)	0.129*
Sex (M/F)	13/7	11/4	0.721**
BMI	30.12 (27.29 – 32.72)	26.59 (25.88 – 28.24)	0.089*
hsCRP (mg/L)	1 (0.58 – 2)	1.39 (0.81 – 2.28)	0.625*
L (N x10^9/L)	7.5 (6.58 – 8.53)	5.5 (4.8 – 6.75)	**0.001***
CMV IgG (U/mL)	105.5 (66.75 – 124.5)	106 (89.95 – 121)	0.751*
CMV IgG (pos/neg)	17/3	14/1	0.619**
PASI	8.6 (5.3 – 21.7)	-	-
Disease duration (years)	8 (3 – 15)	-	-

*Continuous data are shown as median (interquartile range). BMI - body mass index, hsCRP – high sensitivity C-reactive protein, L – leukocyte count, CMV – cytomegalovirus; PASI – psoriasis area and severity index * Mann-Whitney U test, ** Fisher's Exact Test*

4.2.2. Clonotype data preprocessing

The preprocessing of sequencing data included the removal of erroneous and non-coding clonotypes. Despite this, TRG clonotype tables still contained some pseudogene sequences (e.g. TRGV10), and TRAV-incorporating variants were occasionally assembled into TRD clonotype tables. To reduce the noise, only clonotypes containing either of six functional TRGV variants (TRGV2, TRGV3, TRGV4, TRGV5, TRGV8, TRGV9) and TRD clonotypes containing either of eight TRDV genes were included. This filtering process did not significantly impact the overall composition of the clonotype tables, with 99.1 ± 1.9% TRD and 97.5 ± 4.1% TRG sequencing reads retained for downstream analysis. Furthermore, the presence of pseudogene-containing TRG clonotypes was not significantly different between diseased and healthy participants (P = 0.93, Mann-Whitney U test).

Since TRG and TRD repertoires consist of diverse clonotypic variants with distinct structural and functional properties, the analysis was performed on both total CDR3γ and CDR3δ clonotype repertoires, as well as those stratified by variable segment usage. Clonotypes were categorized based on TRGV or TRDV variants, focusing specifically on the three most common TRDV variants (TRDV1, TRDV2, TRDV3) and six TRGV variants (TRGV2, TRGV3, TRGV4, TRGV5, TRGV8, TRGV9). For age-associated correlation analyses, the four oldest PV patients were removed to eliminate the interpretation bias as no appropriate age-matched healthy controls were available for comparison. Due to the limited number of CMV-negative participants (4 out of 35 individuals), a robust statistical comparison between CMV-

positive and CMV-negative groups was not feasible. Instead, to assess the impact of immune response intensity to CMV, correlation analyses using CMV IgG values were performed on the 31 CMV-positive participants.

4.2.3. Gene usage analysis

The composition of TCR repertoires was investigated with respect to the frequencies of TRGV/TRDJ, and TRDV/TRDJ gene segments used in the formation of TCRγ and TCRδ clonotypes, respectively. As expected, the TRGV9 variant was predominantly expressed in the majority of TRG repertoires, followed by lower expression levels of TRGV4, TRGV2, TRGV8, TRGV3, and TRGV5 variants (Figure 15 A). Among the joining variants, TRGJP was the most expressed, followed by TRGJ1, TRGJP1, TRGJP2, and TRGJ2 (Figure 15 B). The case-control comparison revealed no significant differences in the usage of TRGV or TRGJ segments (Table 8). The clonotypes containing paired TRGV9-TRGJP variants were the most common across most repertoires, however, some repertoires contained increased proportions of clonotypes formed by other rearrangements, such as TRGV9-TRGJ2, TRGV4-TRGJ2, TRGV2-TRGJ2, TRGV5-TRGJP2, and TRGV8-TRGJ2 (Figure 16).

Table 8. The TRGV / TRGJ segment usage frequencies in psoriasis and healthy repertoires.

	PV (N = 20)	HC (N = 15)	P
TRGV9	83.18 (74.19 – 88.22)	88.29 (74.17 – 91.98)	0.559
TRGV4	2.04 (0.49 – 5.38)	3.41 (1.75 – 5.61)	0.317
TRGV2	2.57 (1.14 – 7.03)	2.40 (0.73 – 3.35)	0.359
TRGV8	2.48 (1.24 – 6.08)	2.61 (1.69 – 3.85)	0.726
TRGV3	1.10 (0.35 – 4.11)	0.87 (0.42 – 4.31)	0.751
TRGV5	0.62 (0.19 – 1.66)	0.58 (0.31 – 3.77)	0.726
TRGJP	61.42 (50.66 – 70.74)	68.14 (43.06 – 74.56)	0.803
TRGJ1	16.07 (9.87 – 18.20)	17.63 (15.17 – 24.91)	0.113
TRGJP1	7.88 (4.47 – 15.40)	4.73 (3.28 – 8.46)	0.211
TRGJP2	5.62 (2.36 – 17.85)	6.79 (3.61 – 13.03)	0.494
TRGJ2	0.01 (0 – 0.23)	8.15×10^{-5} (0 – 1.13)	0.692

Data are shown as the median percentage with interquartile range. Mann-Whitney U test

Figure 15. Circulating TCRγ repertoires are predominantly composed of TRGV9 and TRGJP segment-containing clonotypes, with variable TRGV and TRGJ segment usage observed across both psoriasis patients (PV) and healthy controls (HC). *A) TRGV segment usage and B) TRGJ segment usage*

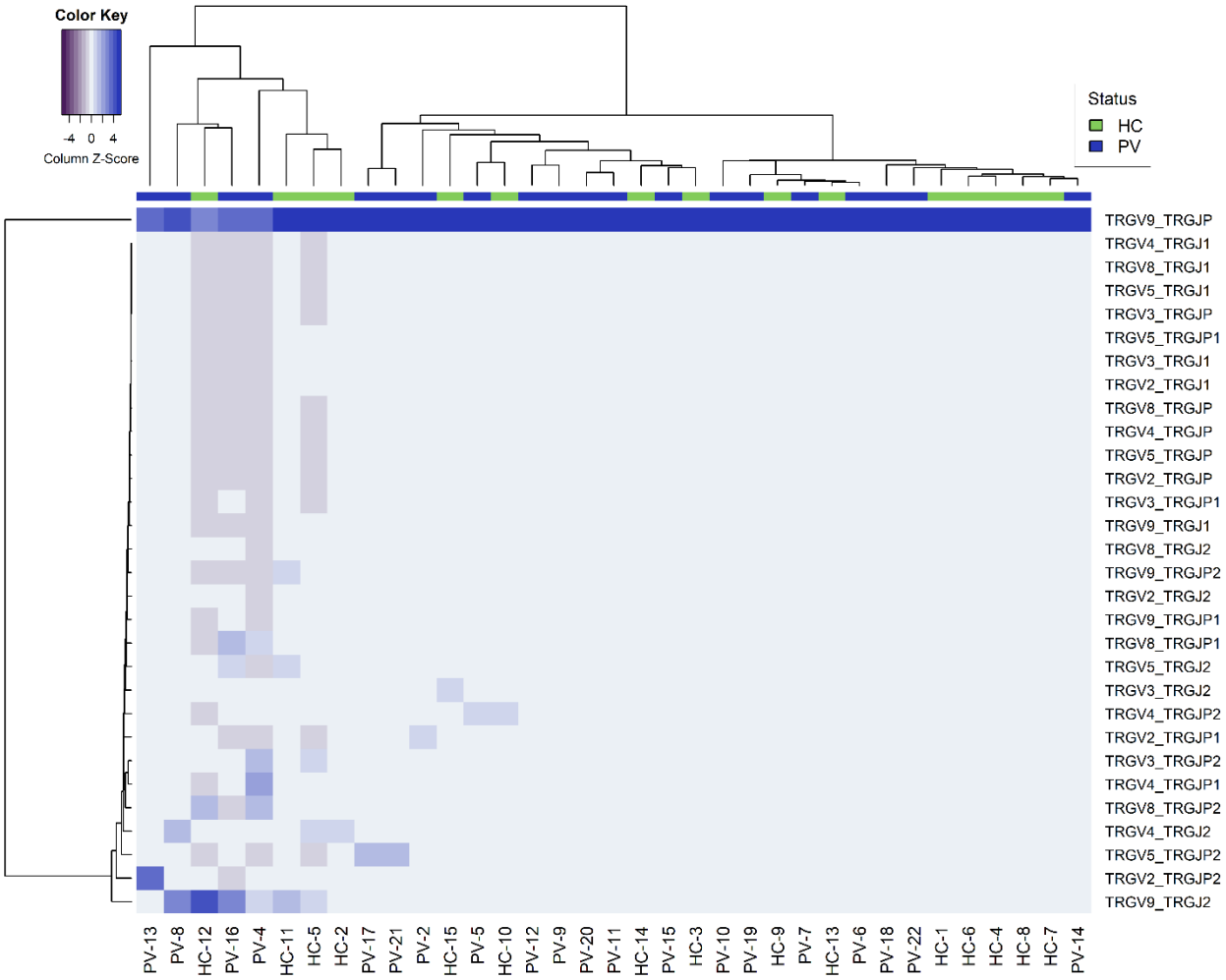

Figure 16. Heatmap of TRGV-TRGJ gene pairing frequencies in TCRγ repertoires highlighting the predominance of TRGV9-TRGJP clonotypes and variability in other rearrangements across samples. *Data were clustered using Euclidean distance based on TRGV-TRGJ segment usage. Z-scores represent the relative frequency of each TRGV-TRGJ clonotype within individual samples. Dendrograms illustrate hierarchical clustering of both samples and gene segments.*

Although there were no significant differences in segment usage between healthy and psoriasis-affected participants, a positive correlation was observed between the proportion of TRGV4 clonotypes and the duration of psoriasis (Figure 17). More specifically, the frequencies of clonotypes containing TRGV4-TRGJ2 ($\rho = 0.669$, $P = 0.001$) and TRGV4-TRGJP ($\rho = 0.503$, $P = 0.024$) rearrangements were increasing with disease duration, along with TRGV5-TRGJP1 ($\rho = 0.470$, $P = 0.036$) clonotypes. Interestingly, the TRGV2-TRGJP1 clonotypes expression increased with age in healthy repertoires ($\rho = 0.548$, $P = 0.035$) but decreased significantly with advancing age in psoriasis cohort ($\rho = -0.756$, $P = 7 \times 10^{-4}$).

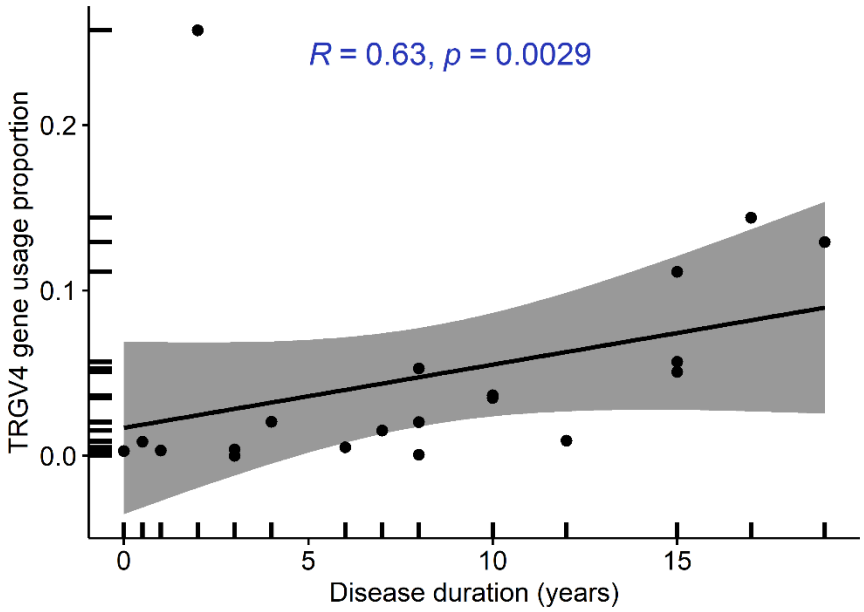

Figure 17. Proportion of TRGV4 segment-containing clonotypes increases with disease duration. *Spearman's correlation analysis*

The TRD repertoires predominantly consisted of TRDV2 clonotypes, followed by TRDV1 and TRDV3 variants, with the latter two occupying significant portions in some repertoires (Table 9). The TRDV4 – TRDV8 segments were infrequently expressed, generally accounting for less than 1% of the repertoire, although in certain samples these clonotypes were found at relatively higher frequencies than expected (Figure 18 A). The TRDJ1 variant was the most prominently expressed joining segment, whereas TRDJ2, TRDJ3, and TRDJ4 were expressed to a lesser extent (Table 9, Figure 18 B). Consequently, the TRDV2-TRDJ1 clonotypes emerged as the most dominant across all repertoires, with TRDV2-TRDJ3, TRDV2-TRDJ2, TRDV1-TRDJ1, and TRDV3-TRDJ1 rearrangements making up a smaller yet significant portions of the repertoires (Figure 19). No significant differences in TRDV/J gene usage composition were observed between psoriasis patients and healthy controls, however there was a modest negative correlation between the duration of disease and the proportion of TRDV2-TRDJ3 rearranged clonotypes ($\rho = -0.499$, $P = 0.025$).

Table 9. The TRDV and TRDJ segment usage frequencies in psoriasis and healthy repertoires.

	PV (N = 20)	HC (N = 15)	P
TRDV2	73.61 (68.97 – 93.36)	87.19 (64.89 – 94.67)	0.881
TRDV1	9.36 (2.43 – 22.38)	8.91 (2.89 – 28.08)	0.751
TRDV3	3.67 (0.55 – 11.16)	1.18 (0.5 – 4.02)	0.516
TRDV5	0.24 (0.13 – 0.46)	0.62 (0.18 – 0.79)	0.167
TRDV8	0.29 (0.04 – 0.61)	0.18 (0.02 – 0.60)	1
TRDV4	0 (0 – 0.06)	0 (0 – 0.02)	0.554
TRDV6	$2x10^{-3}$ (0 – 0.03)	0 (0 – 0.01)	0.628
TRDV7	0 (0 – 0.02)	0 (0 – 0.02)	0.899
TRDJ1	93.40 (90.51 – 94.30)	92.60 (89.47 – 94.26)	0.414
TRDJ3	4.93 (2.75 – 7.32)	4.35 (3.80 – 6.16)	0.907
TRDJ2	1.78 (0.62 – 2)	1.46 (1.36 – 2.62)	0.414
TRDJ4	0.11 (0.07 – 0.20)	0.12 (0.05 – 0.24)	0.665

Data are shown as the median percentage with interquartile range. Mann-Whitney U test

Figure 18. Circulating TCRδ repertoires are predominantly composed of TRDV2 and TRDJ1 segment-containing clonotypes- *A) TRDV segment usage and B) TRDJ segment usage*

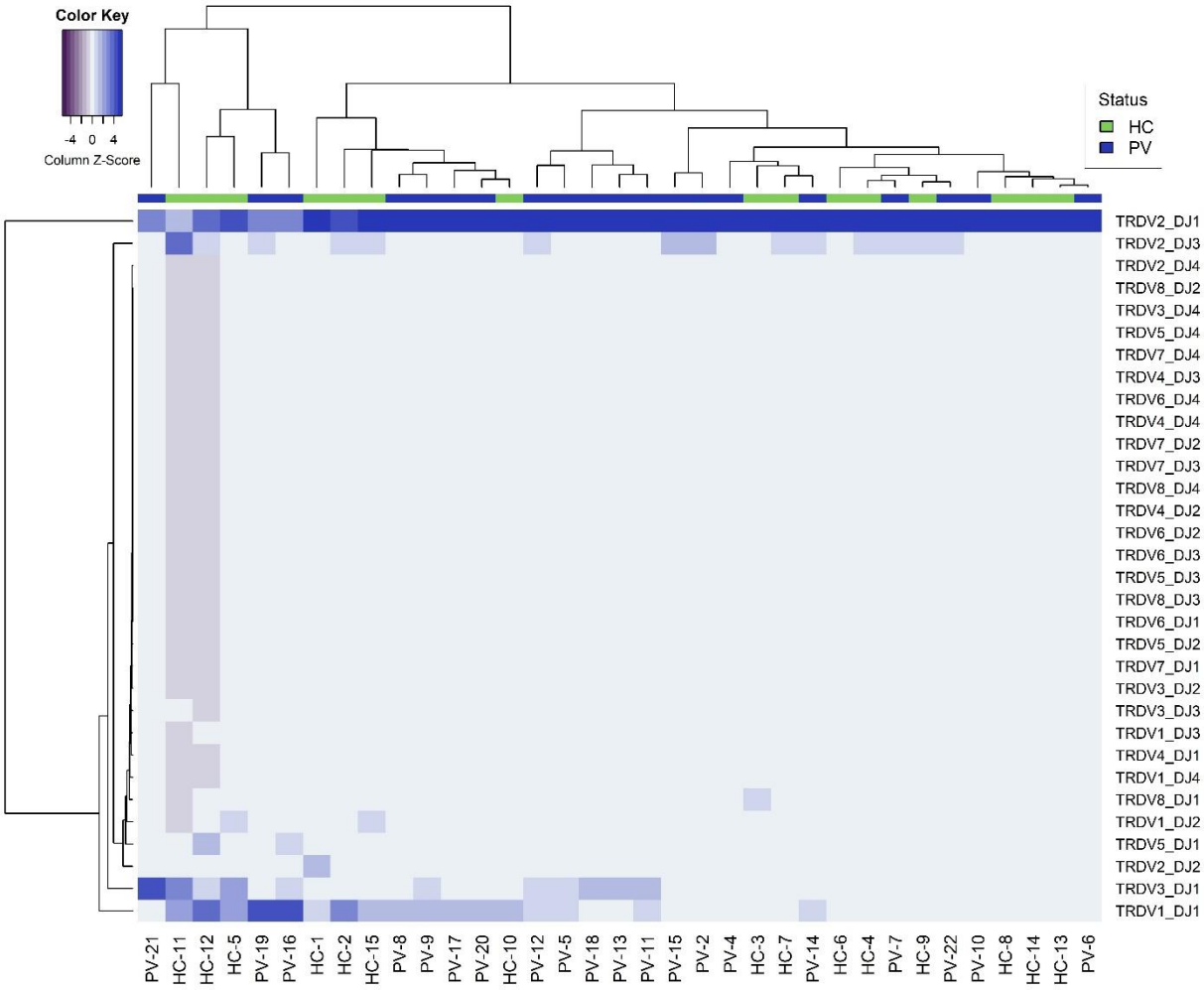

Figure 19. Heatmap of TRDV-TRDJ gene pairing frequencies in TCRδ repertoires, highlighting the predominance of TRDV2-TRDJ1 clonotypes and variability in other rearrangements across samples. *Data were clustered using Euclidean distance based on TRDV-TRDJ segment usage. Z-scores represent the relative frequency of each TRDV-TRDJ clonotype within individual samples. Dendrograms illustrate hierarchical clustering of both samples and gene segments.*

The expression of TRDV1, TRDV2, and non-TRDV1/2 gene segments was evaluated in relation to the corresponding flow cytometry data. A moderate association was observed, indicated by Lin's concordance correlation coefficient (CCC) of approximately 0.7, suggesting a favourable alignment between TRDV transcript levels and protein expression as measured by flow cytometry (Figure 20).

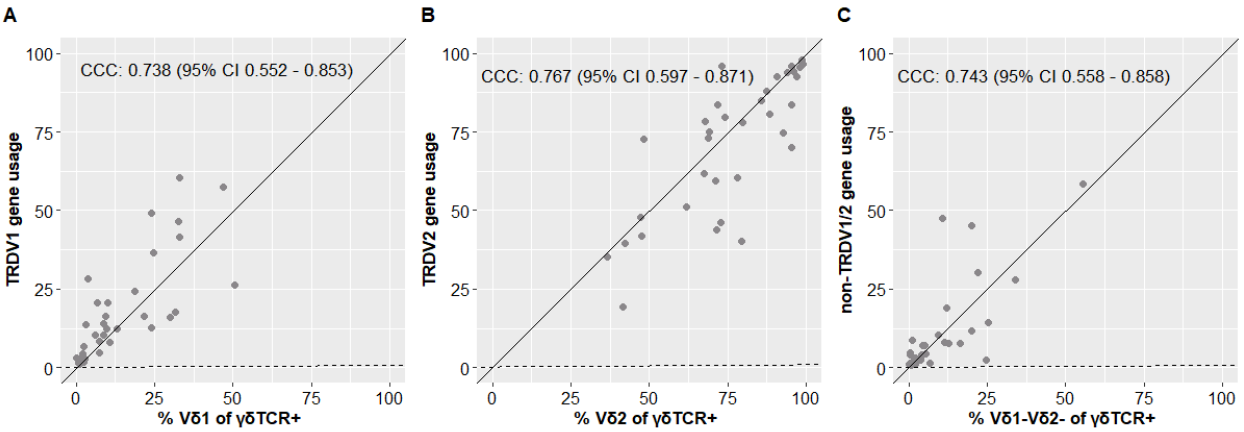

Figure 20. Lin's concordance correlation coefficient (CCC) suggests a favourable alignment between TRDV transcript levels and corresponding γδ T cell subset proportions. *A) TRDV1, B) TRDV2, and C) non-TRDV1/2 transcript levels correlate with the proportions of TCRVδ1^{+} TCRVδ2^{+}, and Vδ1^{-}Vδ2^{-} cells, respectively. γδ T cell subset proportions were measured by flow cytometry based on TCRVδ1 and TCRVδ2 chain expression.*

4.2.4. TRG and TRD CDR3 region metrics

The characteristics of TRG and TRD repertoires were examined using several metrics to capture their diversity and complexity, including the count of unique clonotypes, as an indicator of overall diversity and the average length of CDR3 regions, which influences antigen specificity and binding. In addition, the average clonotype frequency was assessed to understand the distribution of clonotypes. Convergence, defined as the generation of identical amino acid sequences from different nucleotide sequences, was also analysed. Junctional diversity was measured by the number of nucleotides inserted at V-D and D-J joints, along with the number of nontemplated nucleotides (NDN) introduced by terminal deoxynucleotidyl transferase (TdT), to evaluate structural variability.

Upon examination of the clonotypic characteristics in both TRG and TRD variants, no statistically significant differences were observed between the two groups (Table 10). The further analysis across individual TRD and TRG clonotype variants also did not reveal any significant differences in case-control comparison.

Table 10. Basic TRG and TRD repertoire characteristics

	PV (N = 20)	HC (N = 15)	P
TRG			
Clonotypes (N)	723(416 – 1325)	872 (633 – 1189)	0.726
Clonotype frequency (%)	0.14 (0.08 – 0.25)	0.11 (0.09 – 0.16)	0.726
Clonotype geomean frequency (%)	0.017 (0.012 – 0.022)	0.019 (0.016 – 0.023)	0.286
CDR3 length (nt)	46.9 (46.2 – 47.8)	47.6 (45.9 – 47.6)	0.987
NDN size	3.7 (3.4 – 4.7)	3.4 (2.9 – 3.9)	0.051
Convergence	1.133 (1.109 – 1.199)	1.121(1.089 – 1.173)	0.803
TRD			
Clonotypes (N)	856 (445 – 1442)	874 (636 – 1297)	0.653
Clonotype frequency (%)	0.12 (0.07 – 0.23)	0.11 (0.08 – 0.16)	0.653
Clonotype geomean frequency (%)	0.029 (0.019 – 0.035)	0.026 (0.022 – 0.029)	0.726
CDR3 length (nt)	49.3 (47.9 – 50.6)	49.2 (48.1 – 50.5)	0.987
Inserted nucleotides (N)	6.9 (5.9 – 8.7)	6.9 (6.3 – 8.9)	0.881
NDN size	15.9(15.3 – 17.8)	16.5 (15.5 – 18.5)	0.751
Convergence	1.028 (1.018 – 1.037)	1.024(1.019 – 1.039)	0.537

Data are shown as median with interquartile range. Mann-Whitney U test

The spectratyping analysis revealed the distinct distribution of CDR3 lengths within the TRG and TRD clonotypes. TRG clonotypes were characterised by CDR3 regions ranging from 7 to 23 amino acids (AA), with a significant proportion (~70%) falling within the 13–17 AA range (Figure 21 A). Among the TRG variants, TRGV9 clonotypes displayed a broader CDR3 length distribution, spanning from 10 to 20 AA, with most clonotypes (approximately 80%) concentrated between 15 and 18 AA (Figure 21 B). In contrast, TRGV4 and TRGV8 clonotypes showed more restricted CDR3 lengths, predominantly between 11 and 15 AA, indicating less variability in these variants (Figure 21 C and D).

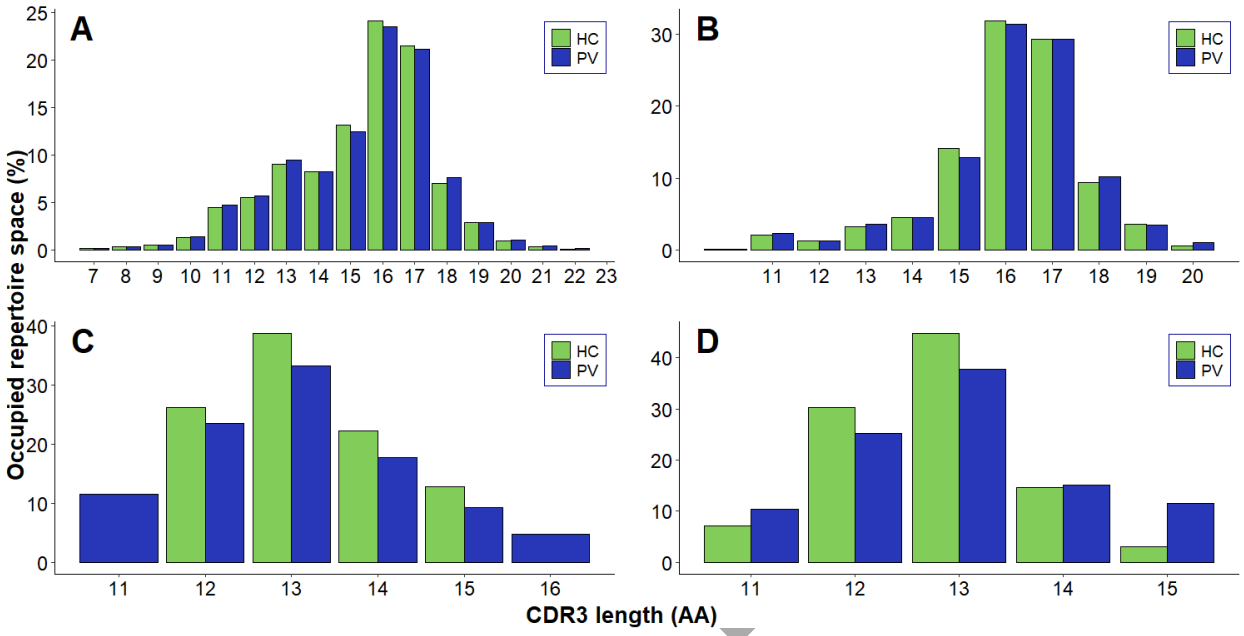

Figure 21. TRG clonotypes show broad CDR3 length distribution, with TRGV9 exhibiting a wider range TRGV4 and TRGV8 clonotypes, and no significant case-control differences. *Spectratypes of A) all TRG clonotypes, B) TRGV9, C) TRGV4, and D) TRGV8 clonotypes. N(PV) = 20, N(HC) = 15.*

For TRD clonotypes, the CDR3 regions ranged from 11 to 26 AA, with the majority (~60%) clustering between 14 and 17 AA (Figure 22 A). This distribution was primarily driven by the dominant TRDV2 clonotypes, which had a relatively narrow CDR3 length range of 13 to 22 AA (Figure 22 C). In comparison, TRDV1 and TRDV3 clonotypes demonstrated a more complex bimodal distribution. The TRDV1 clonotypes were primarily concentrated between 14 and 17 AA, with a secondary peak of longer clonotypes ranging from 19 to 25 AA (Figure 22 B). Similarly, TRDV3 clonotypes displayed a dominant population with CDR3 lengths of 13 to 15 AA, alongside a secondary peak ranging from 17 to 23 AA (Figure 22 D). The length distribution patterns were not significantly different between psoriasis patients and healthy controls.

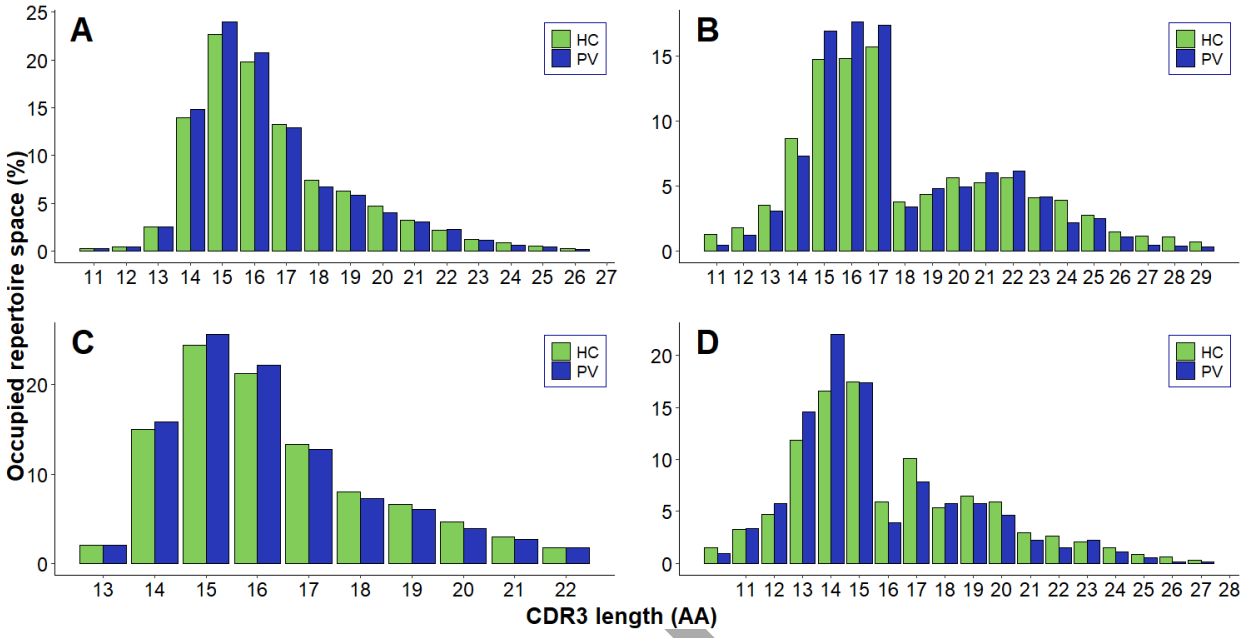

Figure 22. Spectratypes of TRD clonotypes show a broad CDR3 length distribution, with TRDV1 and TRDV3 exhibiting distinct bimodal patterns, compared to the more restricted distribution of TRDV2 clonotypes. *Spectratypes of A) total TRD, B) TRDV1, C) TRDV2, and D) TRDV3 clonotypes. N(PV) = 20, N(HC) = 15.*

The correlation analysis between basic repertoire characteristics and clinical parameters of the examinees revealed a significant decline in the number of unique clonotypes with increasing PASI scores, observed in both TRG and TRD repertoires (Figure 23). The age in psoriasis group was furthermore negatively associated with clonotype count in both TCRγ and TCRδ repertories, a relationship not observed in healthy controls (Figures 24 and 25). In addition, the convergence, defined as the presence of distinct nucleotide sequences which give rise to the same amino acid sequences in the CDR3 region, significantly decreased with the advancing age of psoriatic patients, in both TRG ($\rho = -0.55$, $P = 0.028$) and TRD ($\rho = -0.69$, $P = 0.003$) clonotypes.

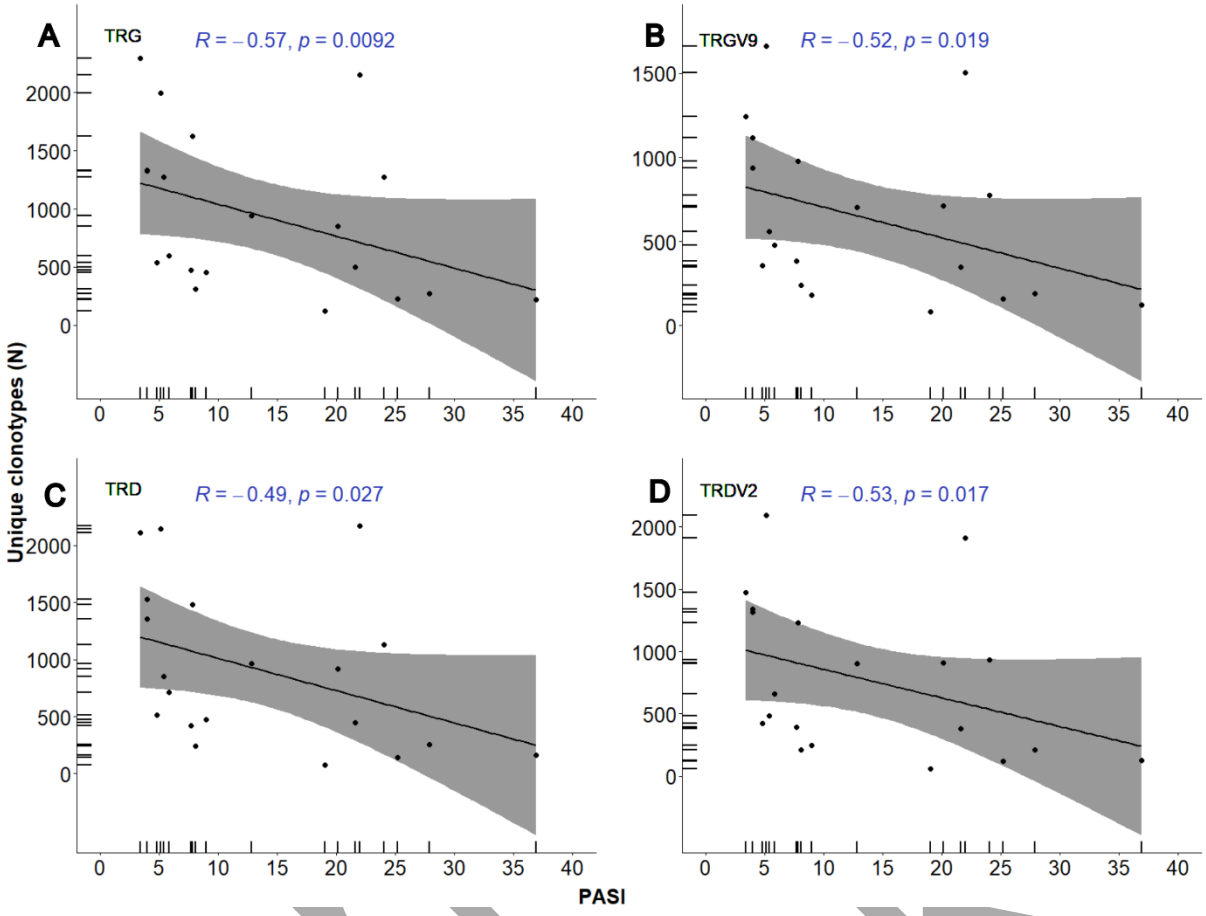

Figure 23. The number of unique TCRγ and TCRδ clonotypes decreases significantly with increasing PASI score. *Spearman's correlation analysis between PASI score and A) total TRG, B) TRGV9, C) total TRD, and D) TRDV2 clonotypes.*

When stratifying TRG clonotypes based on the TRGV variant expressed, a negative correlation between unique clonotype count and the age of psoriasis patients was observed in all clonotypic variants except for TRGV5. Interestingly, this trend was absent in healthy controls, who even exhibited an increase in clonotype count with advancing age across all TRGV9^{neg} variants (Figure 24). In addition, the advancing age of psoriasis patients also negatively correlated with the mean CDR3 length of TRGV9 clonotypes (ρ = -0.67, P = 0.005). Of interest, the number of unique TRGV9 clonotypes correlated negatively with disease severity, as indicated by the PASI score (Figure 23). The PASI score also demonstrated a positive association with the mean CDR3 length of TRGV8 clonotypes (ρ = 0.511, P = 0.021), while disease duration correlated negatively with the geometric mean frequency of TRGV4 clonotypes (ρ = -0.545, P = 0.016).

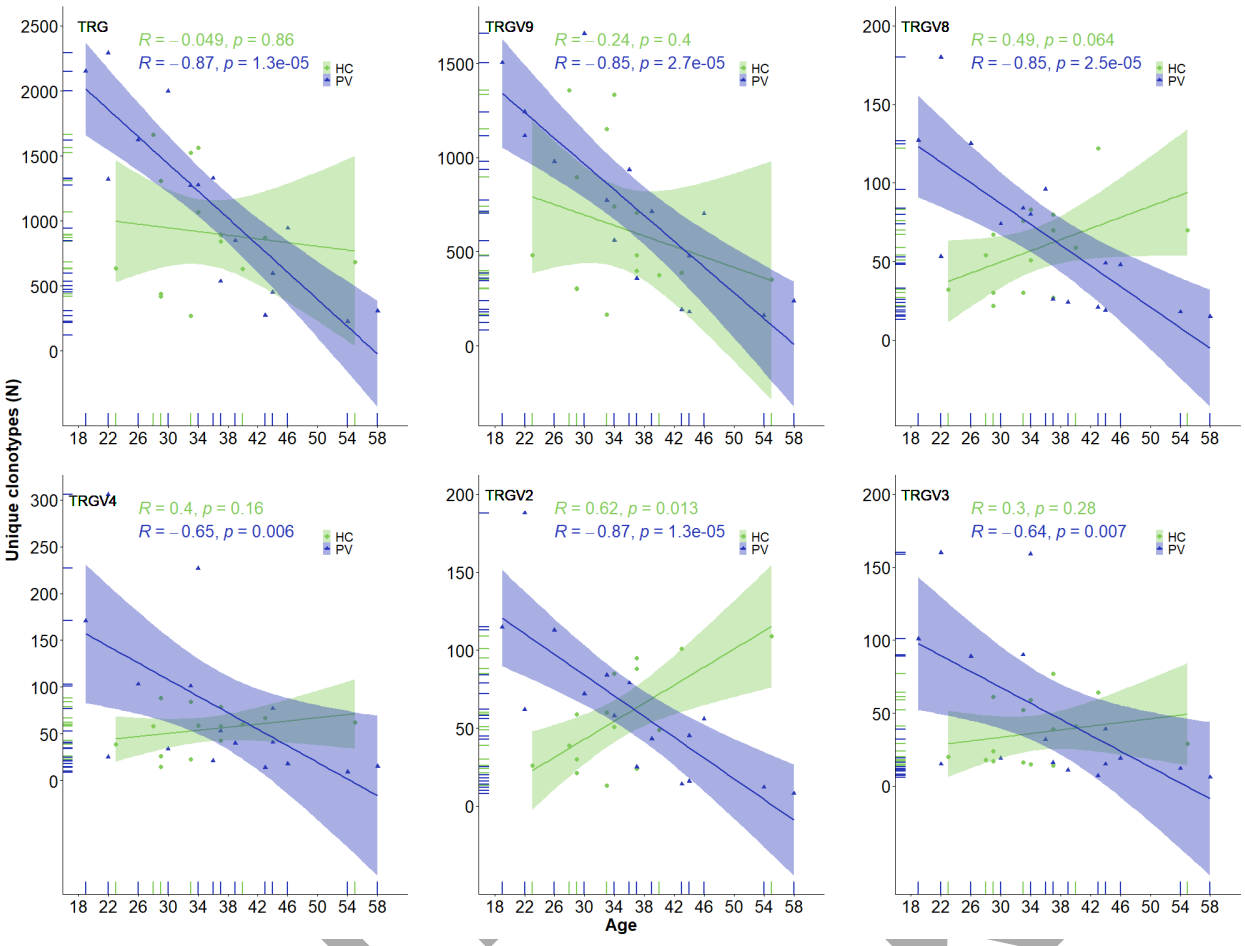

Figure 24. The number of unique TRG clonotypes, including TRGV-9/8/4/2/3 clonotypes, declines significantly with age in psoriasis patients, while this trend is absent or opposite in healthy controls. *Spearman's correlation analysis. N(PV) = 16, N(HC)=15.*

TRD clonotypes of psoriasis patients displayed a similar age-dependent dynamic, with significant decline of clonotype count across both total and individual TRDV clonotype variants. In contrast, the diversity of healthy TRD repertoires did not follow the same trend, moreover, the number of TRDV1 clonotypes was higher in older healthy subjects (Figure 25). The CDR3 length of TRDV1 was also affected by the age of psoriasis patients, as indicated by a positive correlation ($\rho = 0.611$, $P = 0.027$). Moreover, the PASI score influenced diversity within the TRD repertoire, particularly affecting TRDV2 clonotypes (Figure 23), but not TRDV1 or TRDV3. Interestingly, the proportion of Vδ2+ cells within γδ T cell compartment, as assessed by flow cytometry, did not decline with increasing PASI scores ($\rho = -0.09$, $P = 0.74$) or advancing age ($\rho = -0.36$, $P = 0.17$), suggesting the reduced TRDV2 clonotype count was not a result of the diminished proportion of $V\delta2^+$ cells, but rather reflects a contraction in clonotypic diversity within the $V\delta2^+$ population itself.

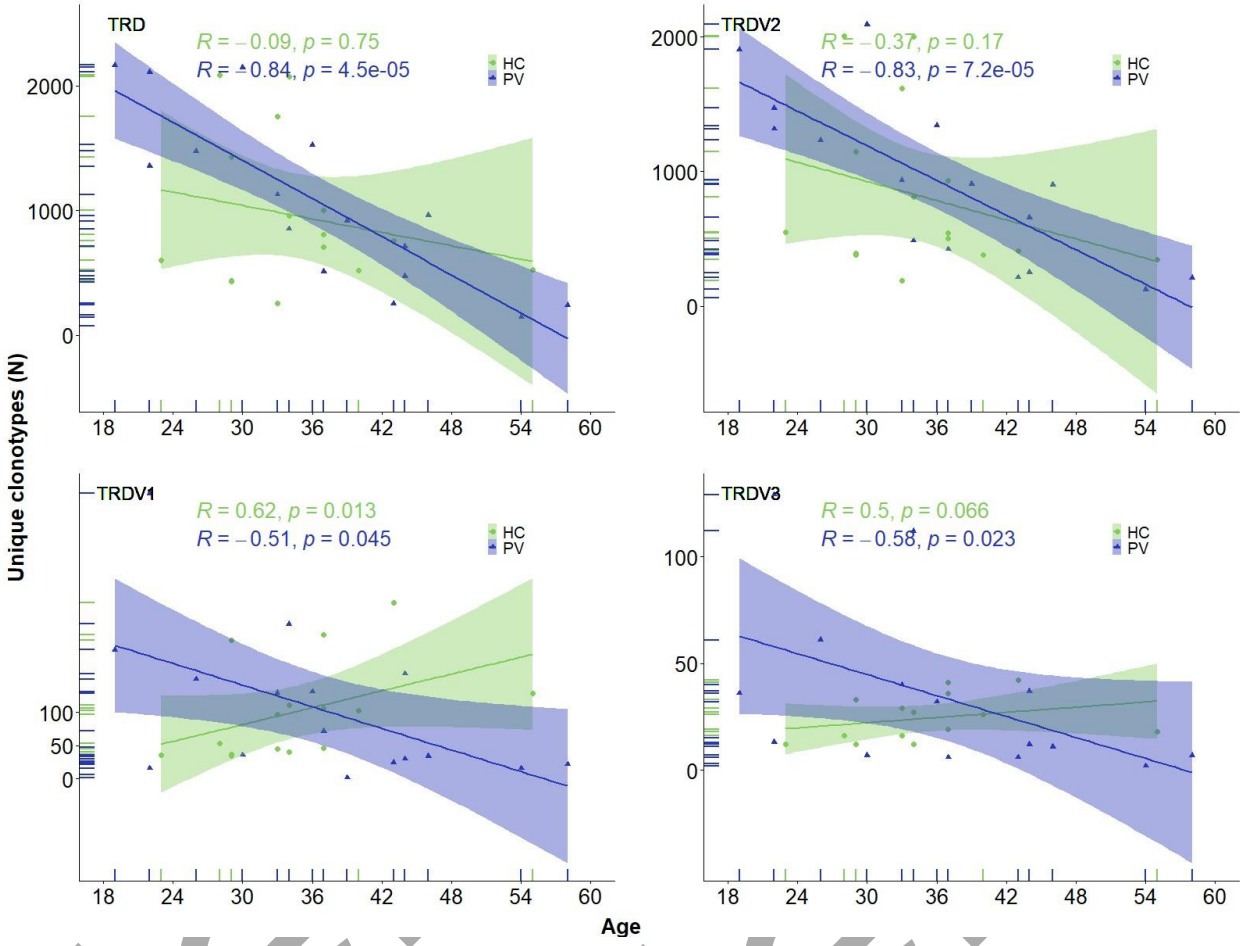

Figure 25. The number of unique TRD clonotypes, including TRDV-2/1/3 clonotypes, declines significantly with age in psoriasis patients, while this trend is absent or opposite in healthy controls. *Spearman's correlation analysis. N(PV) = 16, N(HC)=15.*

4.2.5. Assessment of clonal distribution and diversity metrics

The absolute number of unique clonotypes serves as a general metric for comparing individual TCR repertoires, however, a higher clonotype count does not necessarily reflect a greater abundance of rare variants or reduced presence of expanded clonotypes but can be affected by variations in sequencing depth between samples. To obtain a more nuanced understanding of the repertoire composition shifts, clonotypes were classified into four frequency groups: hyperexpanded (>5%), large (0.5–5%), medium (0.05–0.5%), and small (<0.005%).

Since TRGV9 and TRDV2 clonotypes dominate the peripheral blood repertoire, this frequency-based approach primarily detects shifts in these major variants. Consequently, changes in less frequent clonotypes, whose distribution across repertoires can vary widely, may be overlooked, especially if these shifts do not significantly impact the overall repertoire distribution. To address this, a complementary diversity index assessment was conducted. For the purpose of this analysis, clonotypes were filtered by their variable domain segments, forming independent repertoires for each variant, thus allowing the detection of diversity shifts within each clonotypic variant, regardless of their original frequency in the overall repertoire.

The diversity metrics used to estimate the number of rare clonotypic variant were Efron-Thisted and Chao1 indices, with higher values indicating a greater abundance of low-frequent clonotypes. Furthermore, the Shannon-Wiener and Inverse Simpson indices were included, accounting for both clonotype richness (total unique clonotypes) and evenness (distribution of their frequencies). The Shannon-Wiener index is more sensitive to low-frequency clonotypes, while the Inverse Simpson index emphasizes the dominance of expanded clonotypes, providing complementary insights. The D50 metric was also incorporated to measure the number of clonotypes that cumulatively account for 50 % of the total sequences, serving as an indicator of clonal expansion. Lower values of the Shannon-Wiener and Inverse Simpson indices indicate a higher proportion of dominant or expanded clonotypes, while higher values reflect a more even distribution of clonotypes. Similarly, the D50 index ranges from 0 to 0.5, where lower values indicate higher clonality and higher values indicate more diversity.

Diversity of TCRγ clonotypes

The diversity metrics for total TRG repertoires did not show significant differences between healthy and psoriasis-affected examinees. However, TRGV4 (Me [IQR]: 0.11 [0.06 – 0.13] vs. 0.05 [0.03 – 0.09], PV vs HC, P = 0.039) and TRGV8 (0.12 [0.08 – 0.14] vs. 0.07 [0.03 – 0.09], PV vs HC, P = 0.013) clonotypes demonstrated higher D50 values in the PV repertoires, suggesting TRGV4 and TRGV8 clonotypes in psoriasis samples may represent a more diverse set of clonotypic variants.

Analysis of TRG repertoire diversity with lower-bound estimators such as Chao1 and the Efron-Thisted estimator showed a decline corresponding to higher PASI scores, which was additionally associated with a reduced proportion of ‘small’ clonotypic variants (Table 11). In a similar manner, the Shannon-Wiener and Inverse Simpson indices exhibited modest negative correlations with PASI scores, confirming the presence of a higher proportion of

hyperexpanded clonotypes (Table 11). These patterns of diversity reduction and clonal expansion were evident in specific TRGV subtypes, including TRGV9, TRGV2, TRGV4, and TRGV8, as assessed by diversity indices. Notably, an increase in the proportion of TRGV9 clonotypes was observed in the 'hyperexpanded' group, alongside a corresponding decrease in the representation of 'small' clonotypic variants (Table 11). Conversely, other TRGV variants did not display significant changes across any of the four defined clonotype frequency groups. These results thus indicate that disease severity impacts the loss of diversity within all TRGV clonotypic variants, with the most pronounced effect being the expansion of TRGV9 clonotypes.

Table 11. Statistically significant correlations between PASI score and diversity indices or frequency groups in total TRG and individual TRGV repertoires

	Index or frequency group	ρ	P
TRG	Efron-Thisted	-0.533	0.015
	Chao1	-0.566	0.009
	Shannon-Wiener	-0.493	0.027
	Inverse Simpson	-0.457	0.04
	Small	-0.545	0.013
	Hyperexpanded	0.549	0.012
TRGV9	Efron-Thisted	-0.524	0.018
	Chao1	-0.517	0.019
	Shannon-Wiener	-0.475	0.034
	Inverse Simpson	-0.519	0.019
	Small	-0.516	0.020
	Hyperexpanded	0.587	0.006
TRGV2	Efron-Thisted	-0.466	0.038
TRGV8	Shannon-Wiener	-0.478	0.033
TRGV4	Shannon-Wiener	-0.513	0.025
	Inverse Simpson	-0.649	0.003

Spearman's rank correlation coefficient.

Interestingly, disease duration was associated with a reduction in the diversity of TRGV4 clonotypes, as evidenced by the negative correlation with D50 values ($\rho = -0.538$, $P = 0.018$). Furthermore, a strong positive correlation was observed between disease duration and the proportion of TRGV4 clonotypes within the 'medium' frequency compartment ($\rho = 0.702$, $P = 8 \times 10^{-4}$), indicating that the previously documented increased usage of TRGV4 clonotypes and the corresponding decrease in D50 values predominantly occur within the 'medium' frequency range.

In addition to disease severity and duration, age had a substantial impact on the diversity of TRG clonotypes in psoriasis patients. Strong negative associations were observed between age and the diversity of total TRG clonotypes, particularly in the TRGV9, TRGV2, and TRGV8 subtypes, as displayed by decreasing Efron-Thisted index (Figure 26). Moderate inverse relationships were also observed between age and the diversity of TRGV3, TRGV4, and TRGV5 clonotypes (Table 12). These age-related declines were consistent across both lower-bound estimators (Chao1 and Efron-Thisted) and Shannon-Wiener and Inverse Simpson indices, coinciding with a reduction in the proportion of rare ('small') clonotypic variants (Table 12). While elevated frequencies of hyperexpanded clonotypes with age of PV patients were evident in the analysis of total TRG repertoires, this pattern was not observed within individual TRGV variants, reflecting the fact that hyperexpanded compartments among different individuals are composed of distinct TRGV clonotypic variants.

Of interest, the same age-associated diversity correlations were again not present in healthy controls. In fact, TRGV2 clonotypes of healthy participant showed an opposite trend, with higher proportions of 'small' clonotypes as age increased ($\rho = 0.524$, $P = 0.044$), aligned with Efron-Thisted ($\rho = 0.548$, $P = 0.035$) and Chao1 indices ($\rho = 0.578$, $P = 0.024$).

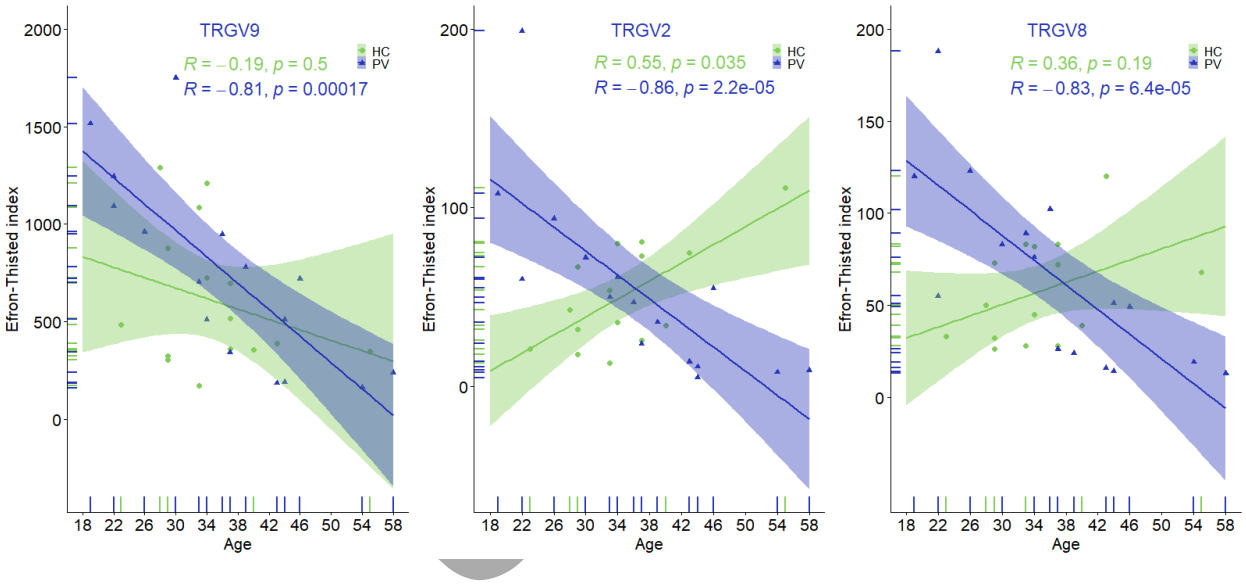

Figure 26. TRGV9, TRGV2, and TRGV8 repertoire diversity, assessed by the Efron-Thisted index, declines significantly with age in psoriasis patients, whereas healthy controls show significant diversity enrichment in TRGV2 clonotypes. *Spearman's correlation analysis. N(PV) = 16, N(HC)=15.*

Table 12. Statistically significant correlations between age and diversity indices or frequency groups in total TRG and individual TRGV repertoires of psoriasis patients

	Index	ρ	P
TRG	Efron-Thisted	-0.887	4.77×10^{-6}
	Chao1	-0.884	5.66×10^{-6}
	Shannon-Wiener	-0.828	7.57×10^{-5}
	Inverse Simpson	-0.711	0.002
	Small	-0.829	7.16×10^{-5}
	Medium	-0.652	0.006
	Hyperexpanded	0.644	0.007
TRGV9	Efron-Thisted	-0.805	1.66×10^{-4}
	Chao1	-0.853	2.71×10^{-5}
	Shannon-Wiener	-0.789	2.77×10^{-4}
	Inverse Simpson	-0.676	0.004
	Small	-0.816	1.16×10^{-4}
	Medium	-0.733	0.001
TRGV2	Efron-Thisted	-0.857	2.21×10^{-5}
	Chao1	-0.881	6.45×10^{-6}
	Small	-0.720	0.002
TRGV8	Efron-Thisted	-0.832	6.39×10^{-5}
	Chao1	-0.832	6.39×10^{-5}
	Shannon-Wiener	-0.541	0.031
	Inverse Simpson	-0.501	0.048
	Small	-0.797	2.2×10^{-4}
TRGV3	Efron-Thisted	-0.635	0.008
	Chao1	-0.689	0.003
	Small	-0.564	0.023
TRGV4	Efron-Thisted	-0.652	0.006
	Chao1	-0.668	0.005
	Shannon-Wiener	-0.509	0.044
	Small	-0.626	0.009
TRGV5	Efron-Thisted	-0.566	0.022
	Chao1	-0.566	0.022
	D50	0.518	0.039

Diversity of TCRδ clonotypes

Similar negative associations between PASI scores and repertoire diversity metrics were evident in TRD repertoires. Moderate correlations were found among the Efron-Thisted, Chao1, Inverse Simpson, and Shannon-Wiener indices with disease severity, both in the total TRD clonotypes and within TRDV2 clonotypes. These finding indicate that disease-related alterations in the repertoires lead to a reduction in the abundance of rare clonotypic and an

increase in the prevalence of dominant ones. In addition, TRDV3 repertoires demonstrated a negative relationship with the Shannon-Wiener and Inverse Simpson metrics, suggesting that patients with more severe forms of the disease tend to contain less diverse, more expanded TRDV3 clonotypes (Table 13). These trends were accompanied by a loss in the abundance of 'small' TRD clonotypes within the dominant TRDV2 fraction, but not TRDV1 or TRDV3, highlighting that the loss of rare TRDV2 variants is the primary factor reshaping the repertoires in patients with severe disease.

Table 13. Statistically significant correlations between PASI score and diversity indices or frequency groups in total TRD and individual TRDV repertoires

	Index	ρ	P
TRD	Efron-Thisted	-0.519	0.019
	Chao1	-0.495	0.027
	Shannon-Wiener	-0.529	0.017
	Small	-0.530	0.016
TRDV2	Chao1	-0.537	0.015
	Efron-Thisted	-0.524	0.018
	Shannon-Wiener	-0.463	0.040
	Small	-0.513	0.021
TRDV3	Inverse Simpson	-0.602	0.006
	Shannon-Wiener	-0.589	0.008

Furthermore, longer disease duration was moderately associated with an increase of D50 index among TRDV1 variants ($\rho = 0.561$, $P = 0.013$) and the increased proportion of TRDV3 clonotypes within the 'medium' frequency category ($\rho = 0.498$, $P = 0.029$).

Similar to the trends observed in TRG clonotypes, age significantly influenced shifts in TRD repertoires, leading to a marked reduction in 'small' clonotypic variants within the TRDV2 and TRDV3 compartments, associated with an increased proportion of hyperexpanded clonotypes in total TRD repertoires, particularly TRDV2 variant. In addition, strong negative correlations were observed between all assessed diversity metrics and the advancing age of affected individuals, present in total both total TRD, and within the TRDV2 and TRDV3 repertoires (Table 14, Figure 27), whereas in TRDV1 clonotypes, only a moderate relationship was observed between Chao1 and patients' age. The corresponding age-related changes were not observed in healthy repertoires (Figure 28). The immune response to CMV, assessed here by CMV IgG values, demonstrated a modest yet statistically significant negative correlation with TCRδ diversity in TRDV2 ($\rho = -0.571$, $P = 0.019$) and TRDV3 ($\rho = -0.534$, $P = 0.029$)

clonotypic subsets, as indicated by the Inverse Simpson index. Interestingly, no significant association was observed between CMV IgG levels and TRDV1 clonotype diversity, despite prior evidence that TRDV1 clonotypes expand in response to CMV infection (5,6).

Table 14. Statistically significant correlations between age and diversity indices or frequency groups in total TRD and individual TRDV repertoires of psoriasis patients

	Index	ρ	P
TRD	Efron-Thisted	-0.856	2.37×10^{-5}
	Chao1	-0.841	4.49×10^{-5}
	Shannon-Wiener	-0.800	2.01×10^{-4}
	Inverse Simpson	-0.624	9.72×10^{-3}
	Small	-0.834	6.03×10^{-5}
	Medium	-0.566	0.022
	Hyperexpanded	0.638	0.008
TRDV1	Chao1	-0.540	0.038
TRDV2	Efron-Thisted	-0.838	5.06×10^{-5}
	Chao1	-0.815	1.19×10^{-4}
	Shannon-Wiener	-0.741	0.001
	Inverse Simpson	-0.579	0.019
	Small	-0.813	1.29×10^{-4}
	Medium	-0.542	0.03
	Hyperexpanded	0.583	0.018
TRDV3	Efron-Thisted	-0.642	0.010
	Chao1	-0.626	0.013
	Shannon-Wiener	-0.626	0.013
	Inverse Simpson	-0.542	0.037
	Small	-0.756	4.58×10^{-4}

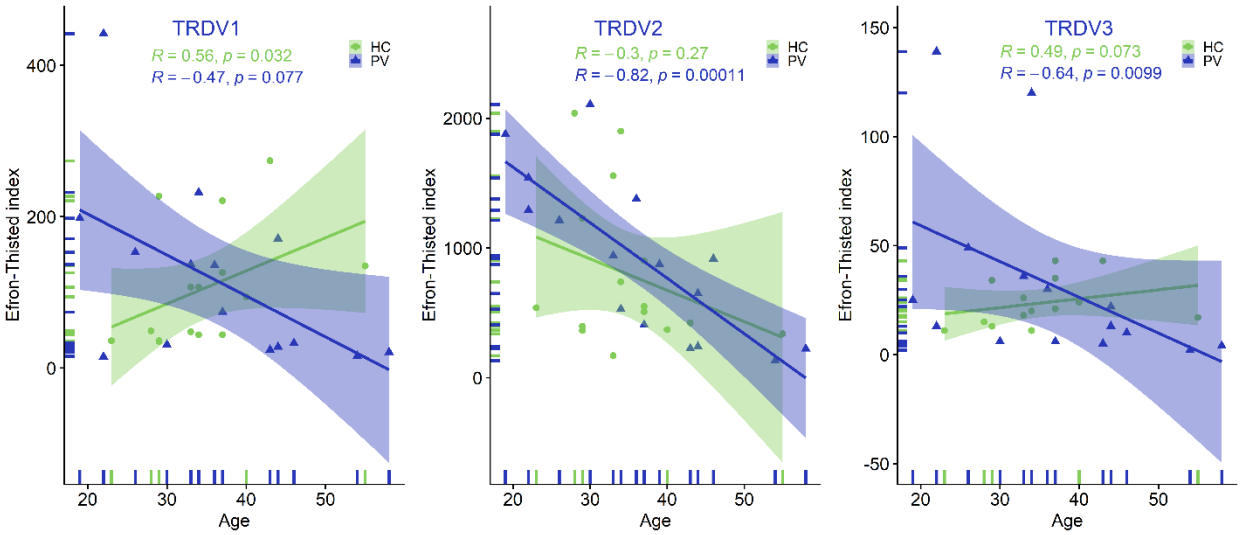

Figure 27. TRDV1, TRDV2, and TRDV3 repertoire diversity, assessed by the Efron-Thisted index, declines significantly with age in psoriasis patients, whereas healthy controls show significant diversity enrichment in TRDV1 clonotypes. *Spearman's correlation analysis. N(PV) = 16, N(HC)=15.*

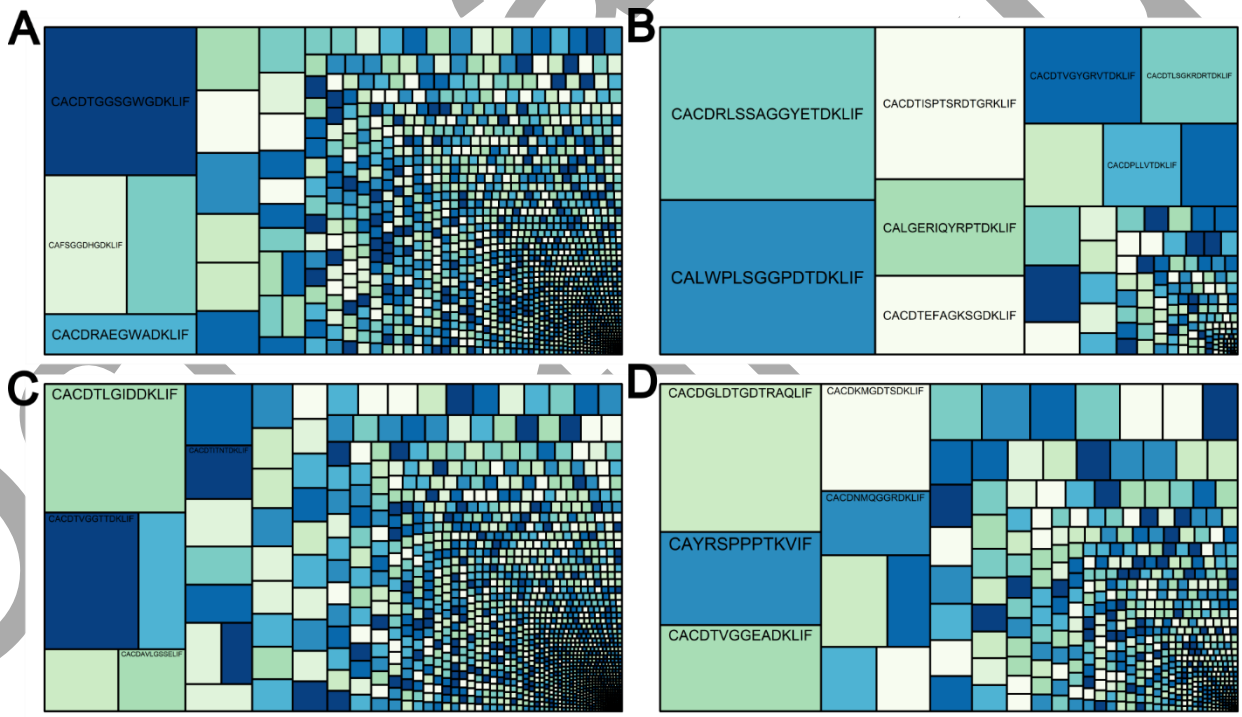

Figure 28. Representative treemaps illustrating greater TCRδ clonal focusing in psoriasis vulgaris (PV) patients (A, B) compared to age-matched healthy controls (HC) (C, D). *A) 26-year-old PV patient, B) 54-year-old PV patient, C) 29-year-old HC, and D) 55-year-old HC. Each rectangle represents a clonotype, with size corresponding to its relative frequency in the repertoire.*

The assessment of diversity metrics and frequency-based segregation of clonotypic groups indicates psoriasis is associated with enhanced clonal focusing and reduced TRG and TRD diversity, particularly with a greater disease severity, duration, and age, suggesting a disease-induced reshaping of the γδ TCR repertoires. Notably, the cumulative frequencies of the top ten TRD clonotypes occupied over 70% of the repertoire space exclusively in psoriasis patients, especially those with high PASI scores (Figure 29). Similarly, the top 10 TRG clonotypes accounted for over 80% of the repertoires in these patients. However, caution is warranted in interpreting hyperexpansion within TRG clonotypes as the high prevalence of specific Vγ9 clonotypes may not indicate clonal expansion, but rather suggest that these clonotypes could have resulted from multiple independent convergent recombination events, each pairing with various Vδ2 chains (140).

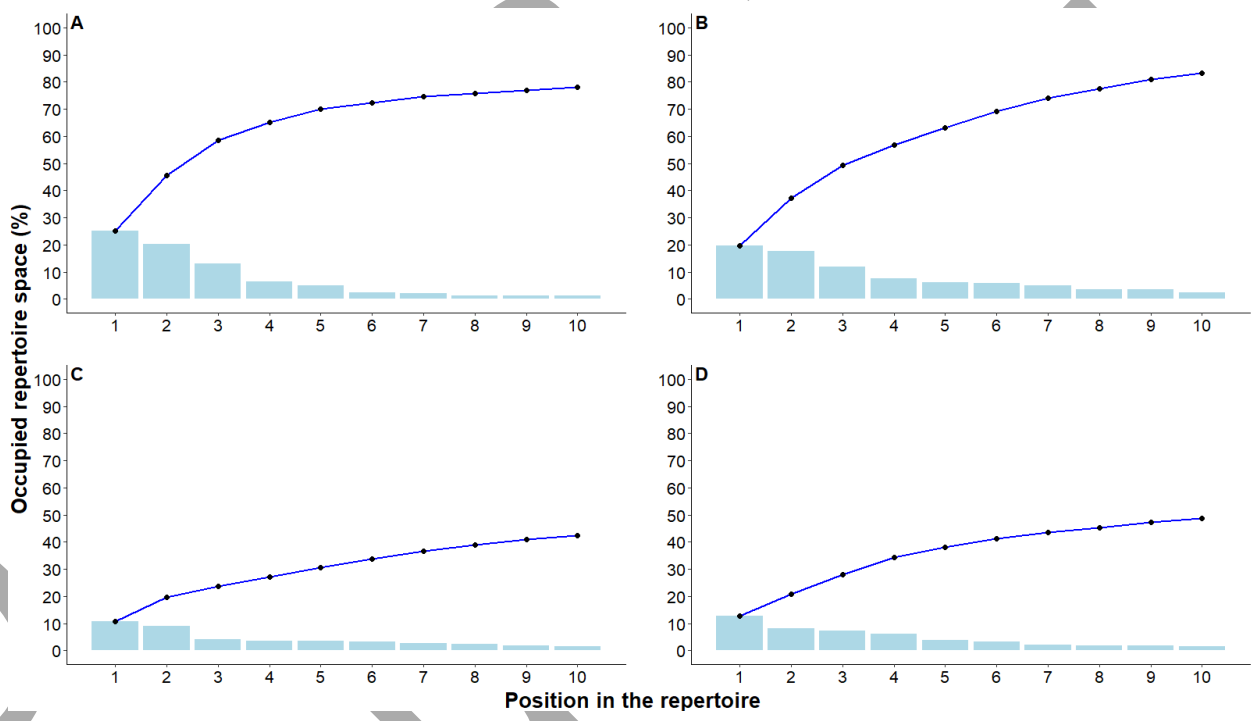

Figure 29. Cumulative frequencies of the ten most abundant TCRδ clonotypes occupy more repertoire space in psoriasis (PV) patients (A, B) compared to age-matched healthy controls (HC) (C, D). *A) 43-year-old PV patient with PASI score 27.5, B) 54-year-old patient with PASI score 25.2 C) 43-year-old HC, and D) 55-year-old HC.*

4.2.6. Analysis of public and disease-associated clonotypes

A total of 27,073 unique TCRδ clonotypes were identified across all samples, with 15,740 unique clonotypes found in the repertoires of psoriasis vulgaris (PV) patients and 12,647 in healthy controls (HC). Similarly, 15,364 unique TCRγ clonotypes were detected, with 9,906 in PV and 7,528 in healthy repertoires.

As expected, most TRD clonotypes were private, with 2,031 (7.5%), shared across all samples, of which 1,314 (4.8%) clonotypes were found in both PV and HC groups. In addition, 985 (7.8%) clonotypes were shared exclusively among PV patients, while 744 (5.9%) clonotypes were shared only among healthy individuals. Consistent with previous findings, clonotypes containing the TRDV2 segment predominated among shared (public) clonotypes, whereas TRDV1 and TRDV3 clonotypes were infrequently shared, typically appearing in only two repertoires. Clonotype overlap was further evaluated using the Jaccard index, which quantifies the proportion of clonotypes shared between two samples relative to the total number of unique clonotypes observed in both samples. The median Jaccard index value for TRDV2 clonotypes in PV group was 0.01 (IQR range: 0.006–0.017), while only four pairs of samples exhibited a Jaccard index greater than 0 for TRDV1 clonotypes (Figure 30). In addition, one TRDV5 clonotype was found to be shared between two donors, whereas other TRDV variants were strictly private. The top 10 most frequently observed clonotypes were rearranged with Jδ1 and featured a hydrophobic amino acid at the fifth position in the CDR region (Figure 30), with the germline-encoded CACDTLGDTDKLIF being the most prevalent, aligning with previous reports (159,230).

Interestingly, two clonotypes were found to be present in six (30%) psoriasis repertoires while being absent in the healthy controls. However, the identification of clonotypes in four healthy individuals (26.7%) that were not present in any psoriasis samples raises questions about the uniqueness of these findings, thereby reducing the likelihood that these two clonotypes can be definitively associated with psoriasis. This conclusion was further supported by a Fisher's exact test, which, after correcting for multiple comparisons, revealed no clonotype was significantly more or less prevalent in psoriasis patients than in healthy controls.

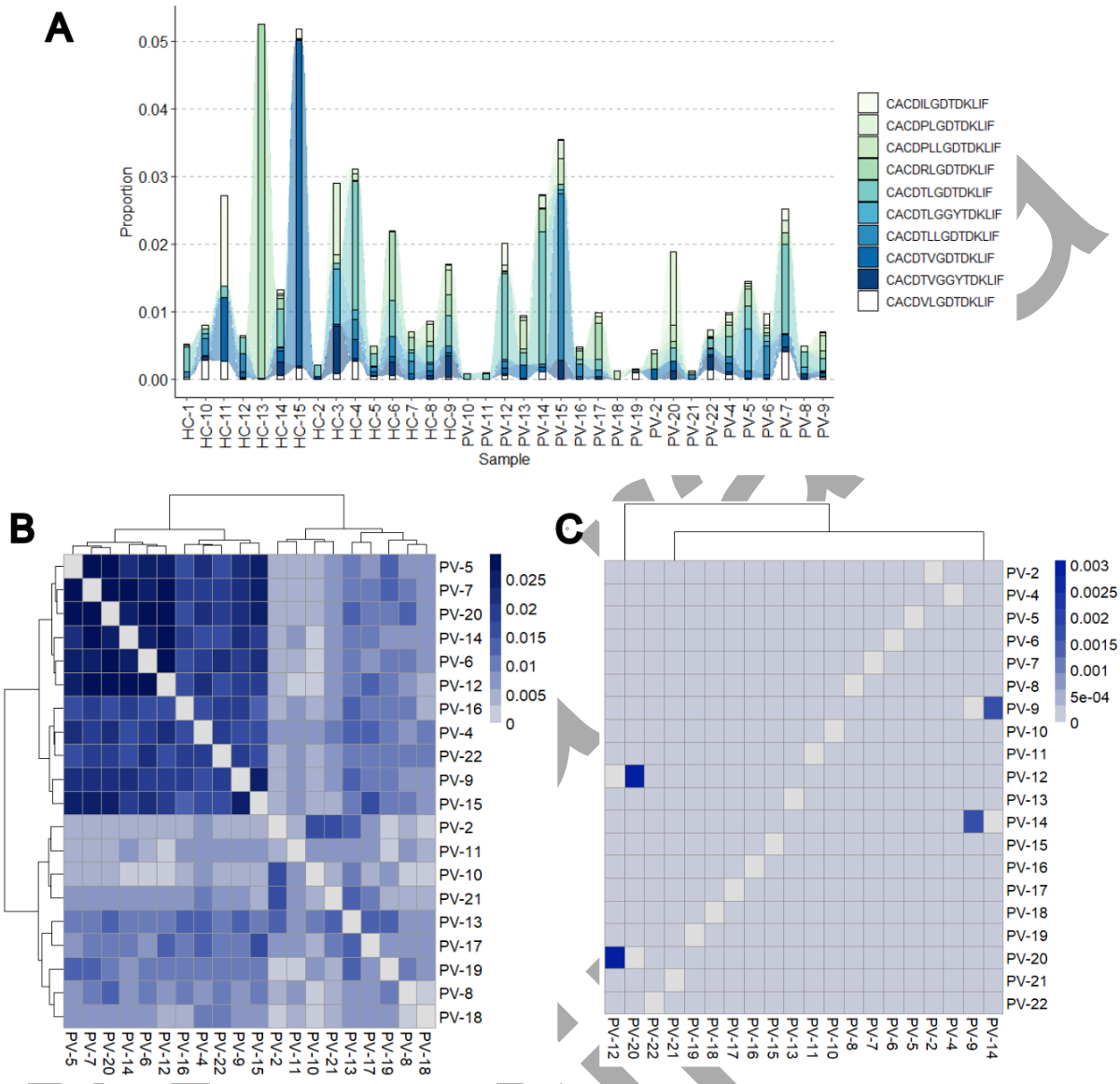

Figure 30. Public TRD clonotypes occupy low frequencies of individual repertoires, with TRDV2 clonotypes exhibiting public profiles in contrast to the private nature of TRDV1 clonotypes. *A) Proportion of the 10 most frequent TRD (TRDV2) clonotypes across all samples. Heatmap of pairwise Jaccard index for B) TRDV2 and C) TRDV1 clonotypes in the PV group.*

TRG clonotypes displayed a higher degree of publicness, with 18.8% (2,886/15,364), shared among study participants and 2,070 (13.5%) shared between at least one PV and one HC repertoire. The proportions of shared clonotypes were comparable within the PV group (1,724/9,906, 17.4%) and HC group (1,270/7,528, 16.9%). TRGV9 clonotypes were the most widely shared (Figure 31, median Jaccard index: 0.072 [IQR: 0.054, 0.086]), with the

CALWEVQELGKKIKVF and CALWEVRELGKKIKVF clonotypes present in all repertoires, consistent with previous studies documenting the widespread abundance of these clonotypic variants (1,7). Clonotypes with *TRGV2*, *TRGV3*, *TRGV4*, *TRGV5*, and *TRGV8* gene segments were also commonly shared, although displaying lower Jaccard index values.

A comparison with a publicly available dataset of TCRγ sequences from lesional, non-lesional, and healthy human skin (95) revealed noteworthy overlaps with clonotypes identified in the peripheral blood of psoriasis patients within our cohort. Namely, 297 clonotypes were shared with those from lesional skin, four of which exhibited significantly higher representation in the psoriatic peripheral repertoires compared to healthy controls (Table 15). However, these findings lost statistical significance following correction for multiple comparison. Conversely, five clonotypes were found to be more prevalent in healthy repertoires compared to psoriatic ones, but again, the significance was lost after multiple comparison correction. These observations hint a potential link between lesional and peripheral TCRγ clonotypes in psoriasis, however, larger studies involving paired peripheral blood and skin samples will be essential to clarify the biological relevance of these clonotypes.

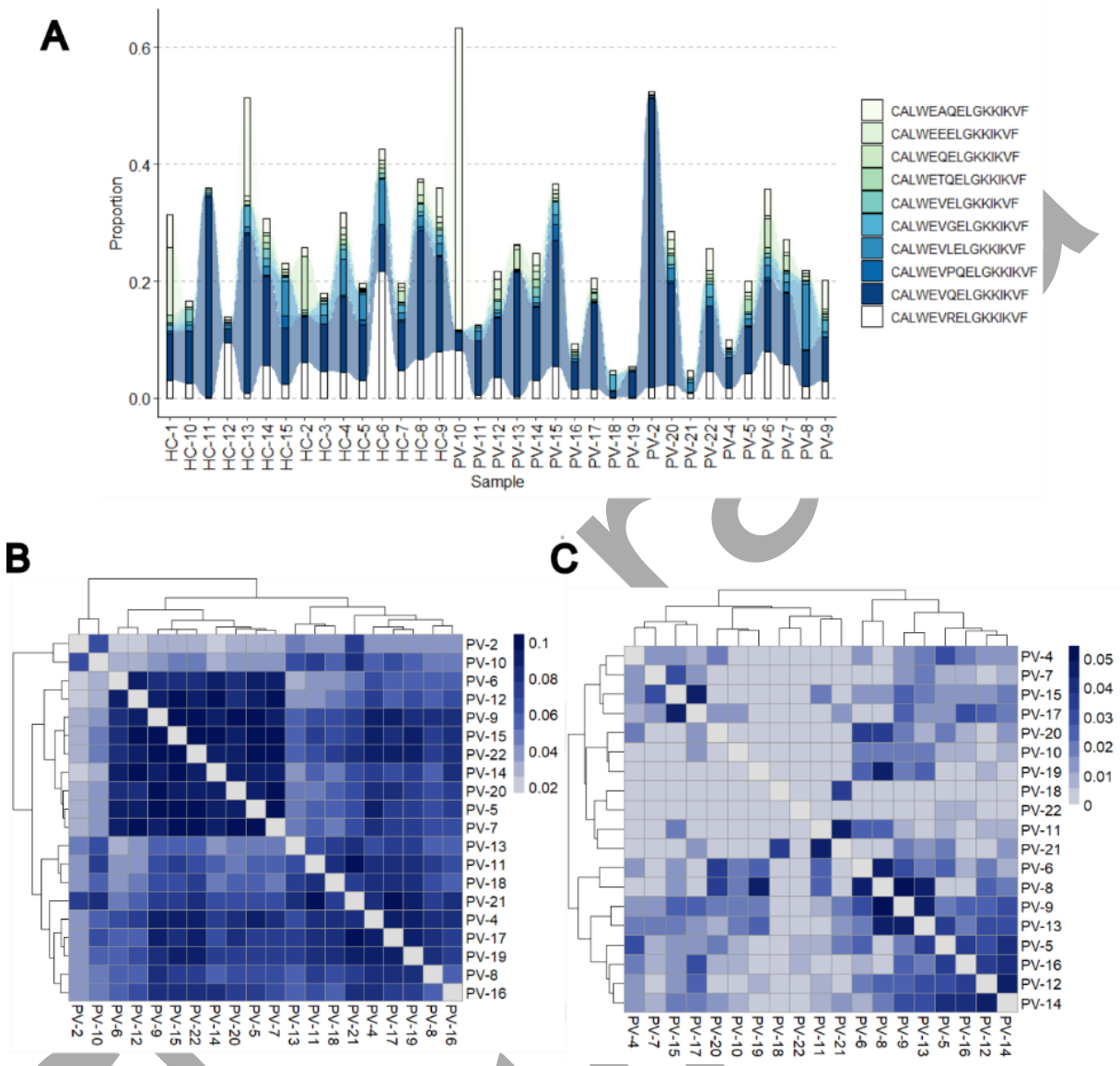

Figure 31. Public TRD clonotypes occupy significant portions of individual repertoires, with TRGV9 clonotypes exhibiting the highest degree of sharing. *A) Proportion of the 10 most frequent TRG (TRGV9) clonotypes across all samples. Heatmap of pairwise Jaccard index for B) TRGV9 and C) TRGV4 clonotypes in the PV group.*

Table 15. Clonotypes with differential presence in psoriatic versus healthy repertoires

Clonotype	TRGV	TRGJ	PV occurence	HC occurence	Match (95)	Fold change
CALWENELGKKIKVF	TRGV9	TRGJP	11/20	2/15	lesional skin	4.1*
CALWEVQPELGKKIKVF	TRGV9	TRGJP	9/20	1/15	lesional skin	6.8*
CATWEYYKKLF	TRGV5	TRGJ2	6/20	0/15	lesional skin	NA
CALWEVGYYKKLF	TRGV9	TRGJ2	6/20	0/15	lesional skin	NA
CALWGKQELGKKIKVF	TRGV9	TRGJP	8/20	0/15	-	NA
CALWEEIQELGKKIKVF	TRGV9	TRGJP	3/20	9/15	-	4**
CALWEAYYKKLF	TRGV9	TRGJ2	3/20	8/15	lesional skin	3.6**
CALWASQELGKKIKVF	TRGV9	TRGJP	1/20	8/15	-	10.7**
CALWEAPPQELGKKIKVF	TRGV9	TRGJP	1/20	6/15	-	2.7**
CALWEEMQELGKKIKVF	TRGV9	TRGJP	0/20	6/15	-	NA

The comparison was conducted using available sequences from Harden et al. (95) *The fold change is expressed as either * PV occurrence / HC occurrence or ** HC occurrence / PV occurrence. NA values were assigned when no occurrences were observed in the group being compared.*

4.3. Exploring the transcriptomic landscape of circulating γδ T cells

Transcriptomic profiling of circulating γδ T cells was conducted using commercially available panel designed to investigate 395 different immunologically relevant genes. This approach provided comprehensive overview of a wide range of immune response markers, including molecular indicators of activation, effector functions, adhesion, migration, differentiation, TCR signalling, antigen-presenting molecules, as well as chemokine and cytokine receptors. The immunotranscriptome of peripheral γδ T cells was analysed using 24 sequencing libraries, prepared from RNA extracted from flow-sorted γδ T cells of 12 psoriasis patients and 12 healthy controls. The sequencing run and individual samples passed the quality control criteria, with an average Phred score of >30 being 95.71 ± 0.51% of the bases and the average alignment rate of 79.98 ± 7.63%. One sample from the healthy control group was excluded from further analysis due to a low total read count (<64,000), which deviated significantly from the other samples. Basic sequencing characteristics are summarised in the table below.

Table 16. Basic sequencing metrics

	PV (N = 12)	**HC (N = 11)**	**P***
Sequencing reads	2,718,052 (1,757,418 – 4,008,349)	1,383,464 (1,109,603 – 2,740,868)	0.045
> Q30 bases (%)	95.96 (95.59 – 96.01)	95.86 (95.62 – 95.89)	0.309
Aligned reads (%)	83.55 (75.63 – 89.75)	80 (77.9 – 81.45)	0.424

*Data are shown as median with interquartile range. *Mann-Whitney U test*

No significant differences were observed between the two groups regarding age, sex distribution, BMI, hsCRP, CMV serostatus or CMV IgG levels, however, psoriasis patients exhibited a higher leukocyte count. Descriptive statistics for the characteristics of the participants are presented in Table 17.

Table 17. Baseline subjects' characteristics

	PV (N = 12)	**HC (N = 11)**	**P**
Age	38 (32 – 44)	37 (31 – 39)	0.578*
Sex (M/F)	9/3	8/3	1**
BMI	28.47 (26 – 31.46)	26.59 (26.31 – 28.24)	0.559*
hsCRP (mg/L)	1.10 (0.6 – 2.5)	1.4 (1.2 – 2.28)	0.307*
L (N x10^9/L)	7.05 (6.38 – 9.78)	5.40 (4.65 – 6.9)	**0.021***
CMV IgG (U/mL)	101 (34.75 – 122)	110 (96.93 – 125)	0.306*

CMV IgG (pos/neg)	8/3	10/0	0.214**
PASI	7.4 (5.03 – 24.3)	-	-
Disease duration (years)	7.5 (5.5 – 10.5)	-	-

*Continuous data are shown as median (interquartile range). BMI - body mass index, hsCRP – high sensitivity C-reactive protein, L – leukocyte count, CMV – cytomegalovirus; PASI – psoriasis area and severity index * Mann-Whitney U test, ** Fisher's Exact Test*

The composition of the γδ T cell compartment did not differ between the healthy and diseased groups, indicating that any observed transcriptional differences were not attributable to variations in the relative abundance of the Vδ1, Vδ2, or Vδ1-Vδ2- subsets (Table 18).

Table 18. γδ T cell compartment composition

	PV (N = 12)	**HC (N = 11)**	**P**
Vδ2 of γδ T (%)	74.15 (44.75 – 95.98)	80.6 (68.7 – 88.8)	0.712
Vδ1 of γδ T (%)	9.44 (2.79 – 16.15)	14 (7.58 – 27.15)	0.372
$Vδ1^{-}$ $Vδ2^{-}$ of γδ T (%)	6.08 (2.05 – 15.4)	3.98 (2.59 – 5.97)	0.309

Data are shown as median (interquartile range). Mann-Whitney U test

4.3.1. Analysis of differentially expressed genes

For the differential expression analysis using DESeq2, an initial pre-filtering step was applied to remove transcripts with low counts, retaining those with at least 10 counts in a minimum of five samples in either the psoriasis or control group. After this filtering, a total of 300 genes remained for the differential expression analysis.

The analysis identified 36 differentially expressed genes in peripheral γδ T cells of psoriasis patients in psoriasis patients, with 30 upregulated and 6 downregulated (Figure 32). The upregulated genes included activation markers (*CD3D/E/G*, *CD247*, *ZAP70*, *CD48*, *IL2RB*) and type-1 immune profile (*TBX21*, *IRF1*, *GADD45G*), associated with enhanced effector and cytolytic functions (*PRF1*, *GZMA*, *NKG7*, *SRGN*), increased tissue migration potential (*KLF2*, *SELL*, *CXCR4*, *ITGAL*) and improved survival (*CD47*, *HLA-E*, *CORO1A*). The downregulated genes were primarily associated with antiviral responses (*MX1*, *OAS3*, *IFI44L*) and activation (*ICOS*, *IL2RG*).

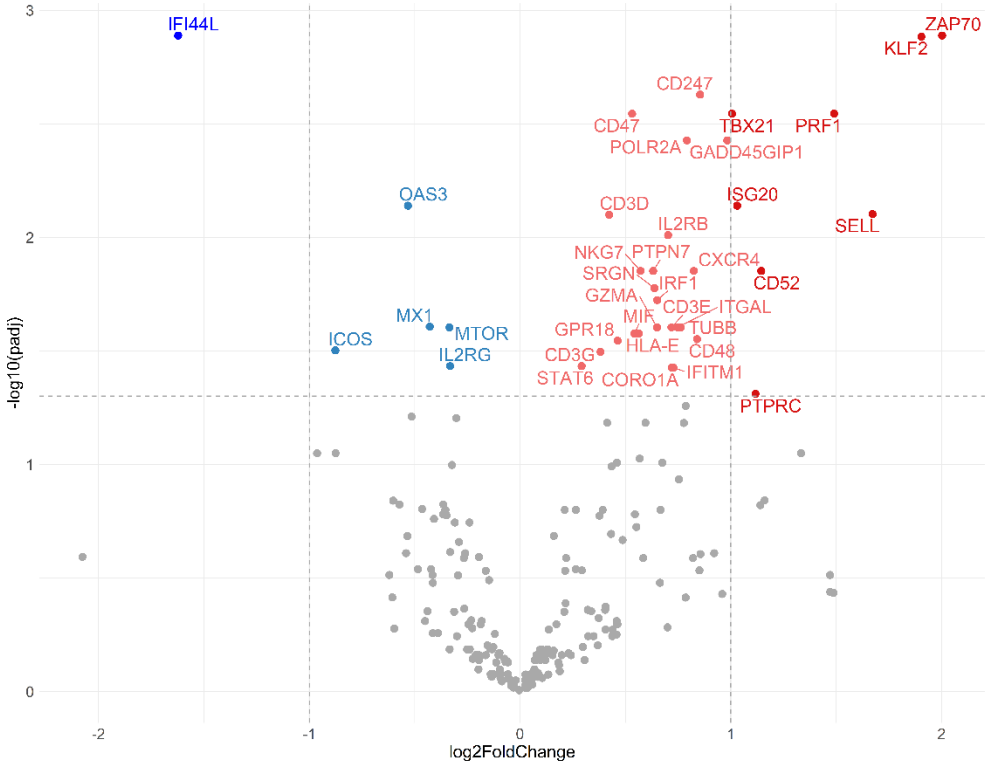

Figure 32. Differential gene expression in peripheral γδ T cells from psoriasis patients versus healthy controls. *The volcano plot shows log2 fold change (X-axis) and -log10 adjusted p-value (Y-axis). Genes significantly upregulated (log2FC > 1, adj. p-value < 0.05) are in dark red, with less significant upregulated (log2FC > 0, adj. p-value < 0.05) genes in light red. Similarly, significantly downregulated genes (log2FC < –1, adj. p-value < 0.05) are in dark blue; less significant downregulated genes (log2FC < 0, adj. p-value < 0.05) are in light blue. Non-significant genes are grey. Dashed lines indicate thresholds for fold change and adjusted p-value.*

4.3.2. Gene ontology (GO) analysis

Gene ontology (GO) analysis of the upregulated genes revealed significant enrichment in biological processes related to cell migration, activation, and differentiation (Figure 33). Most of the upregulated genes were associated with cellular components localized to the plasma membrane, particularly as part of the T cell receptor (TCR) complex or immunological synapse, as well as within cytolytic granules. Furthermore, GO analysis identified two significant enriched molecular functions: T cell receptor binding and major histocompatibility complex (MHC) binding activities (Figure 34).

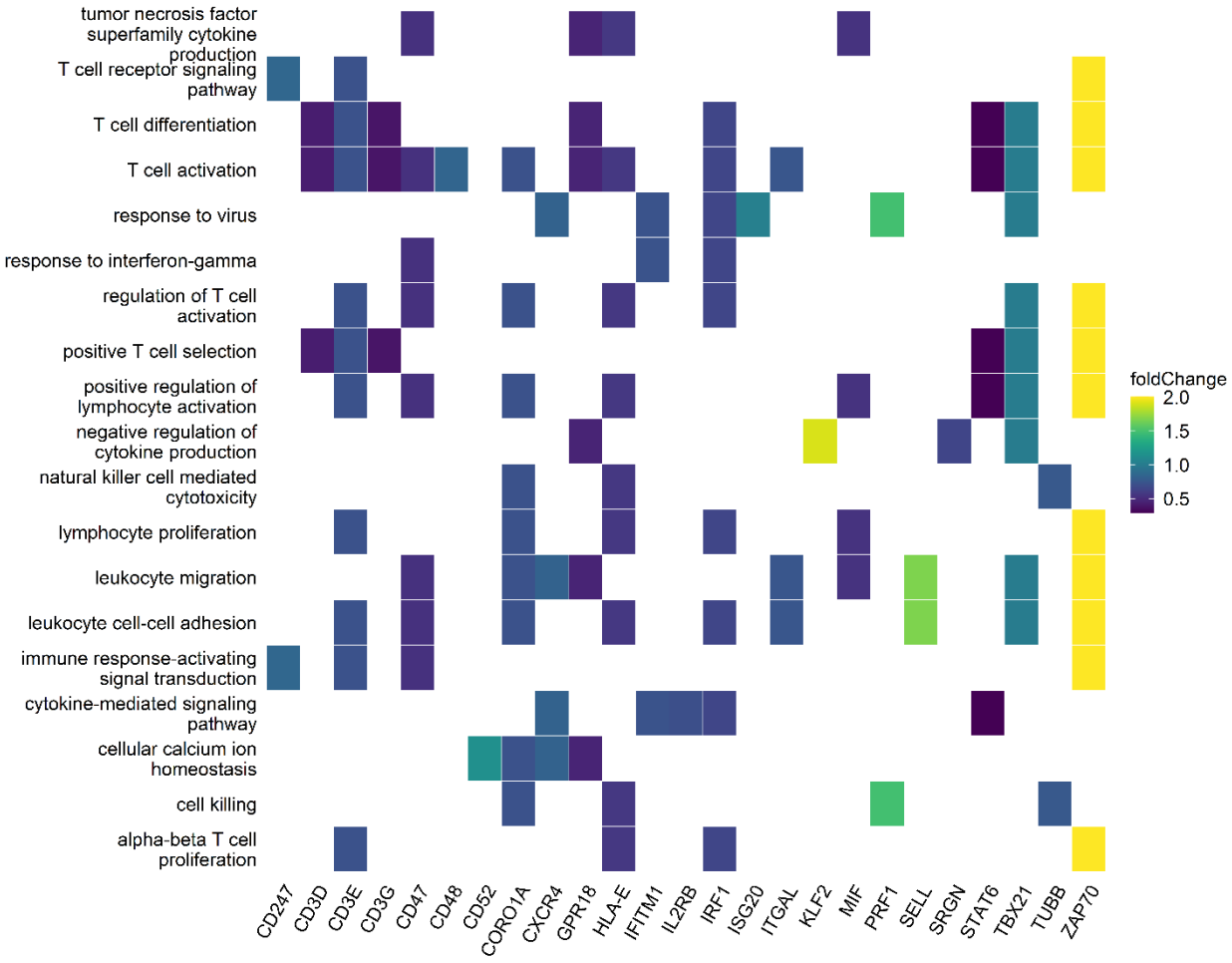

Figure 33. GO-BP enrichment analysis of upregulated genes in psoriasis. *Rows represent enriched Gene Ontology Biological Process (GO-BP) terms, while columns correspond to upregulated genes associated with these terms. The colour intensity reflects the fold change of each gene.*

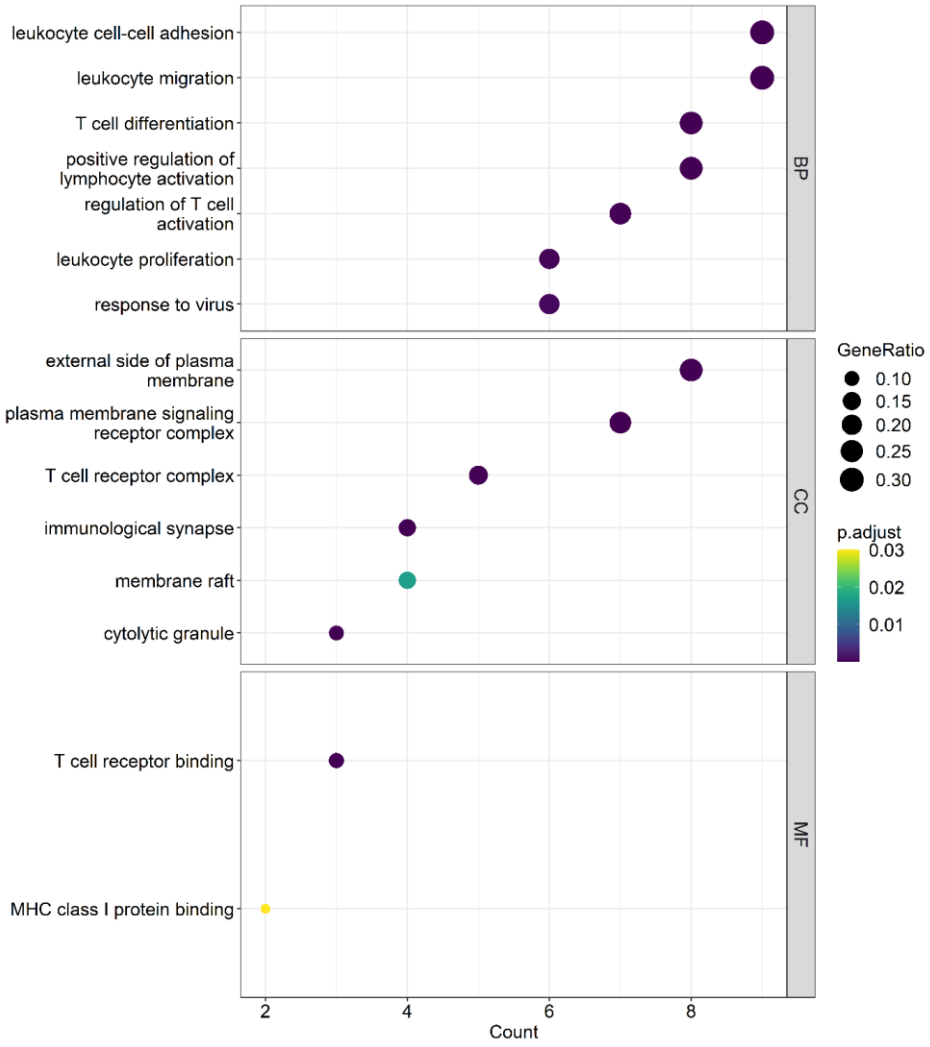

Figure 34. Gene Ontology (GO) enrichment analysis of upregulated genes. *Dot size represents the gene ratio, which is the proportion of upregulated genes within each GO category. GO categories are grouped into BP (Biological Process), CC (Cellular Component), and MF (Molecular Function). Dot colour reflects the adjusted p-value.*

4.3.3. Gene set enrichment analysis

The upregulated genes were mostly enriched within KEGG pathways related to "Natural killer cell mediated cytotoxicity" (Gene ratio: 6/20, adjusted p value: 2.53 x 10^{-4}) (Figure 35) and the "T cell receptor signalling pathway" (Gene ratio: 5/20, adjusted p value: 6.34 x 10^{-4}). In addition, comparison with the Biocarta gene set showed enrichment in the cytotoxic T lymphocyte (CTL) pathway (Gene ratio: 6/14, adjusted p value: 8.3 x 10^{-9}) and TCR pathway (Gene ratio: 6/14, adjusted p value: 4.93 x 10^{-6}) (Figure 36).

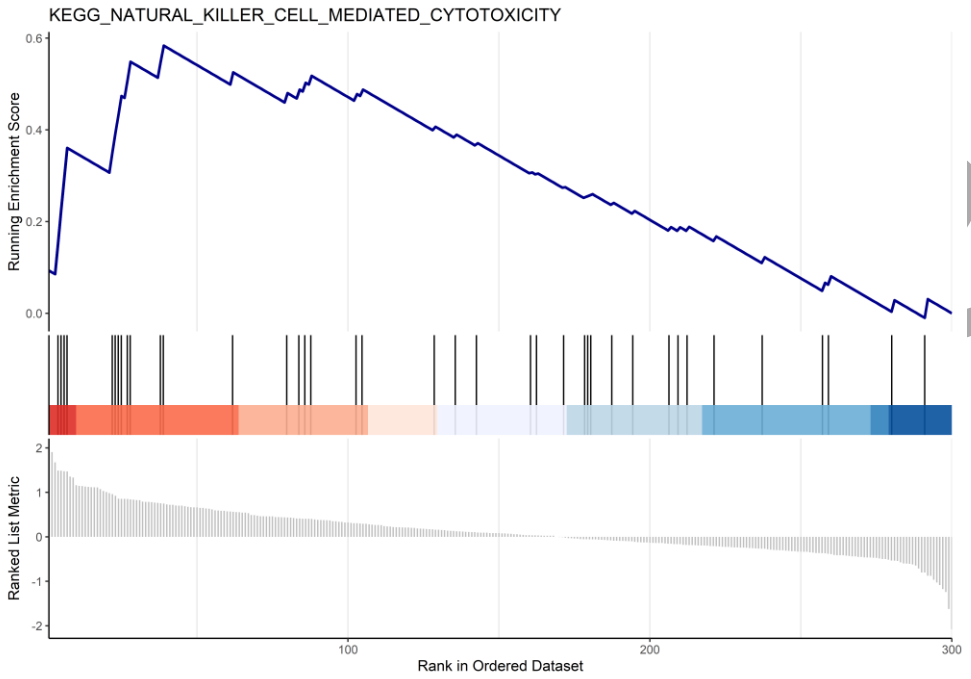

Figure 35. Gene Set Enrichment Analysis (GSEA) for the KEGG "Natural Killer Cell Mediated Cytotoxicity" pathway. *The top panel shows the running enrichment score (y-axis) across a pre-ranked list of genes (x-axis), with peaks indicating significant enrichment of pathway-associated genes. The bottom panel displays the ranked list metric, where the x-axis represents gene ranks based on differential expression, and the y-axis corresponds to the log2 fold change.*

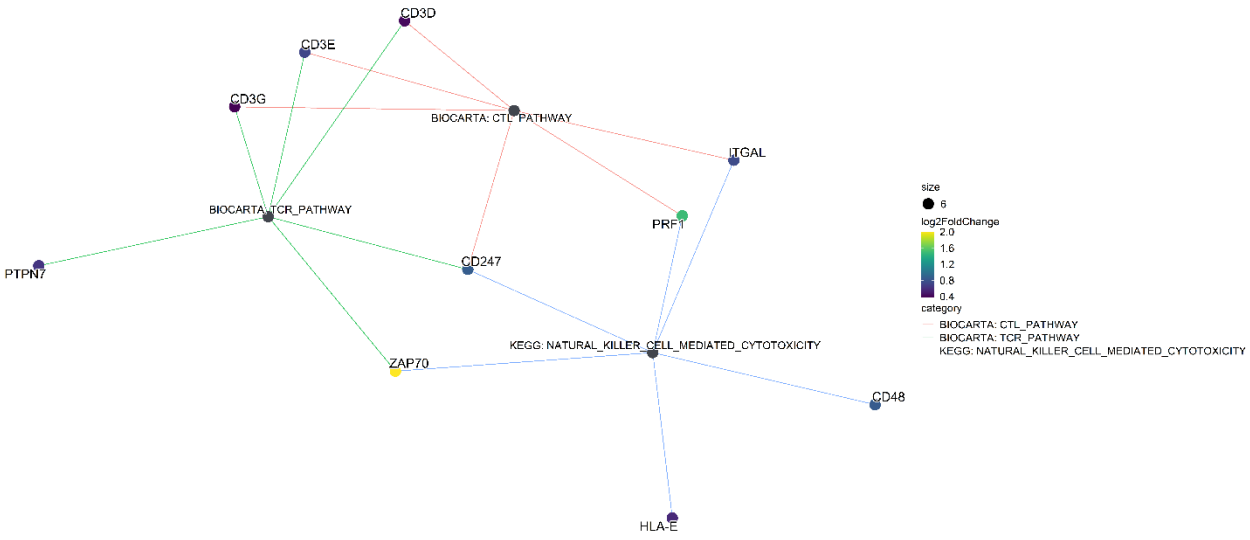

Figure 36. Cnet plot linking genes to enriched KEGG and Biocarta pathways. *Nodes represent genes (coloured by log2 fold change) and pathways (grey), with edges showing the association of each gene with one or more pathways.*

Interestingly, examination of upregulated gene expression patterns across individual samples revealed that the signature of these genes was particularly pronounced in a subset of the psoriasis group (Figure 37). This distinction was further supported by principal component analysis (PCA), where samples PV-4, PV-5, PV-6, PV-7, PV-8, and PV-9 formed a distinct cluster, while the remaining psoriasis samples were dispersed among the healthy control group (Figure 38).

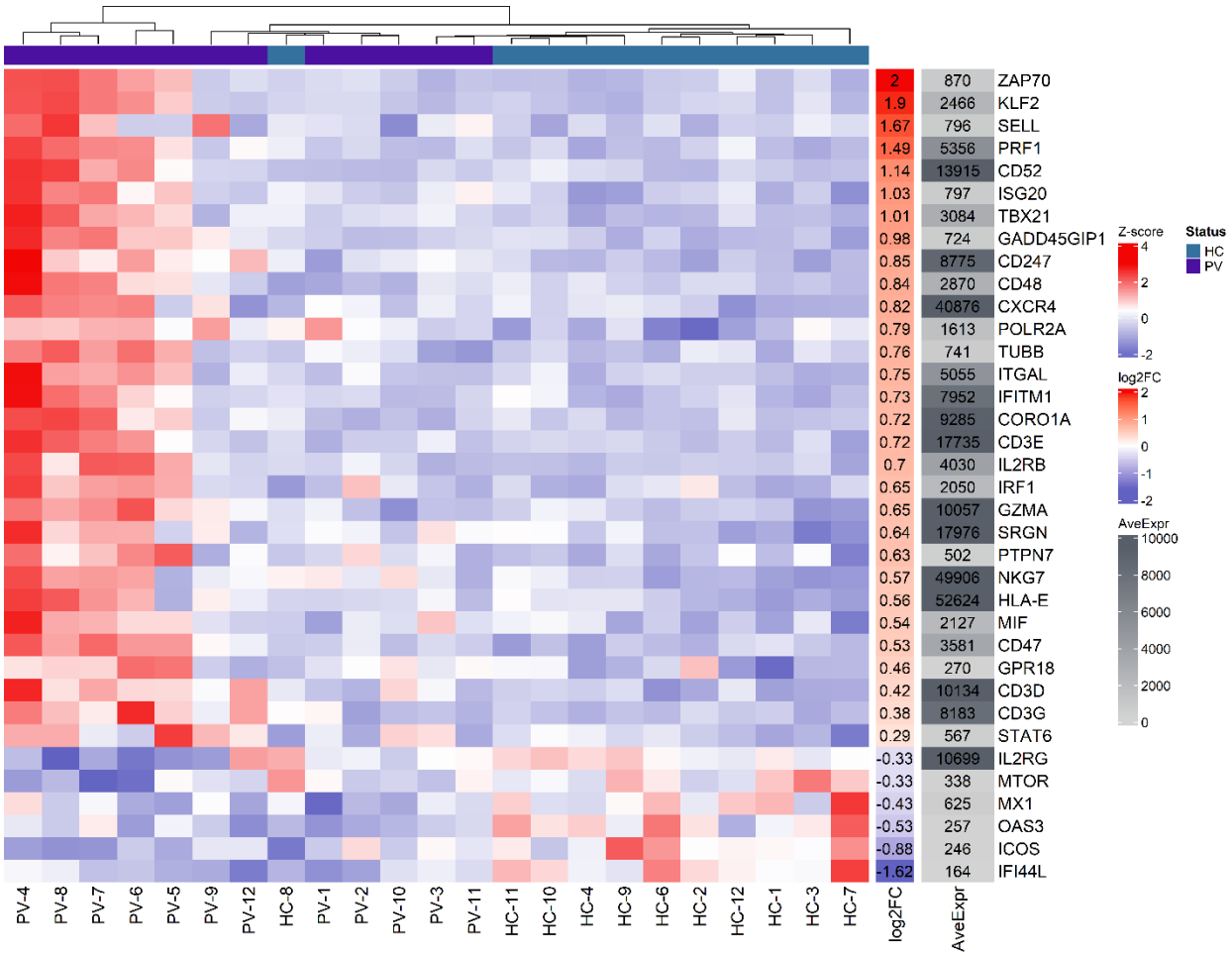

Figure 37. Heatmap of differentially expressed genes in psoriasis patients and healthy controls. *Rows represent genes ranked by descending log2 fold change (log2FC), while columns represent individual samples. Colour intensity indicates the Z-score of gene expression. The dendrograms at the top reflects hierarchical clustering of samples, while the colour bar indicates sample grouping (PV: psoriasis vulgaris, HC: healthy controls). "AveExpr" denotes the average expression level of each gene.*

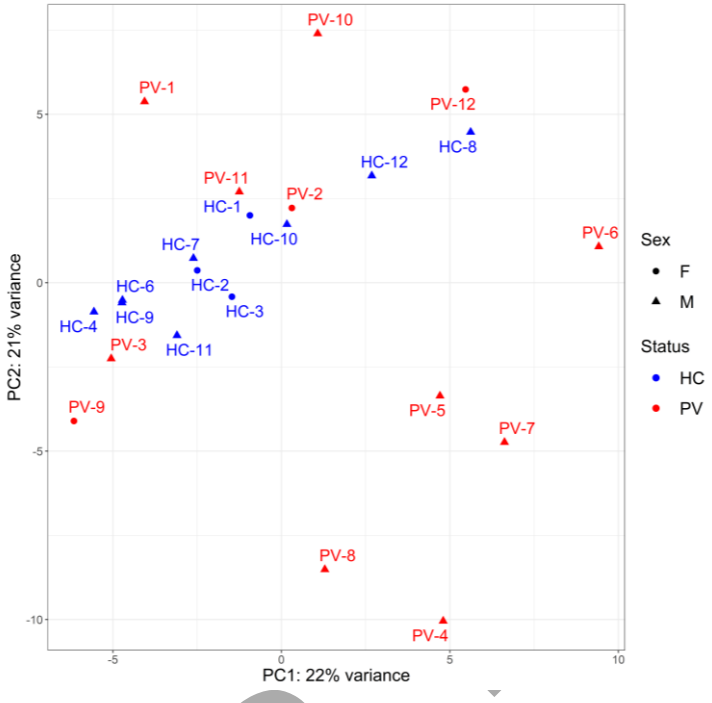

Figure 38. Principal component analysis (PCA) of psoriasis and healthy control samples. *PCA plot showing the distribution of psoriasis vulgaris (PV) and healthy control (HC) samples based on gene expression profiles.*

Upon examining the characteristics of patients in 'PV-A group' (samples showing significant upregulation), and the 'PV-B group', no significant differences were observed in age, PASI score, disease duration, sex, CMV status, or proportions of γδ T subsets within the γδ T compartment. However, to determine whether the differences observed in PV vs. HC comparisons were primarily driven by the PV-A group, patients were stratified into two groups and analyses were performed comparing PV-A vs. HC, PV-B vs. HC, and PV-A vs. PV-B.

The PV-A vs. HC analysis revealed significant differences in gene expression. All genes identified as upregulated in the initial PV vs. HC comparison remained upregulated in the PV-A vs. HC analysis, along with an additional 20 elevated transcripts (Figure 39). The number of downregulated genes also increased, although MX1 and OAS3 were not among them. Notably, the significance of these findings was strengthened, for instance, the adjusted p-value for ZAP70, decreased from 0.001 to 3.78 $x10^{-23}$, and the log_2fold change increased from 2 to 3.01. Conversely, there were no statistically significant differentially expressed genes in the PV-B vs. HC comparison, indicating that the differences observed when comparing total PV vs. HC are primarily driven by the PV-A group. While many of the upregulated genes in the PV-A vs. HC analysis also appeared in the PV-A vs. PV-B analysis, some genes like *SELL*,

CD247, *POLR2A*, *SRGN*, *NKG7*, *CD3D*, *CD3G*, and *STAT6* were not differentially express, implying that these transcripts are present at elevated levels in the PV-B group relative to HC, but not high enough to achieve statistical significance. Overall, the intergroup analysis was performed to discern the unique transcriptomic signature of the PV-A group, however due to the lack of clear biological explanations for the observed variations within the PV group and the small sample sizes of both PV-A and PV-B groups, further interpretation of these results remains uncertain.

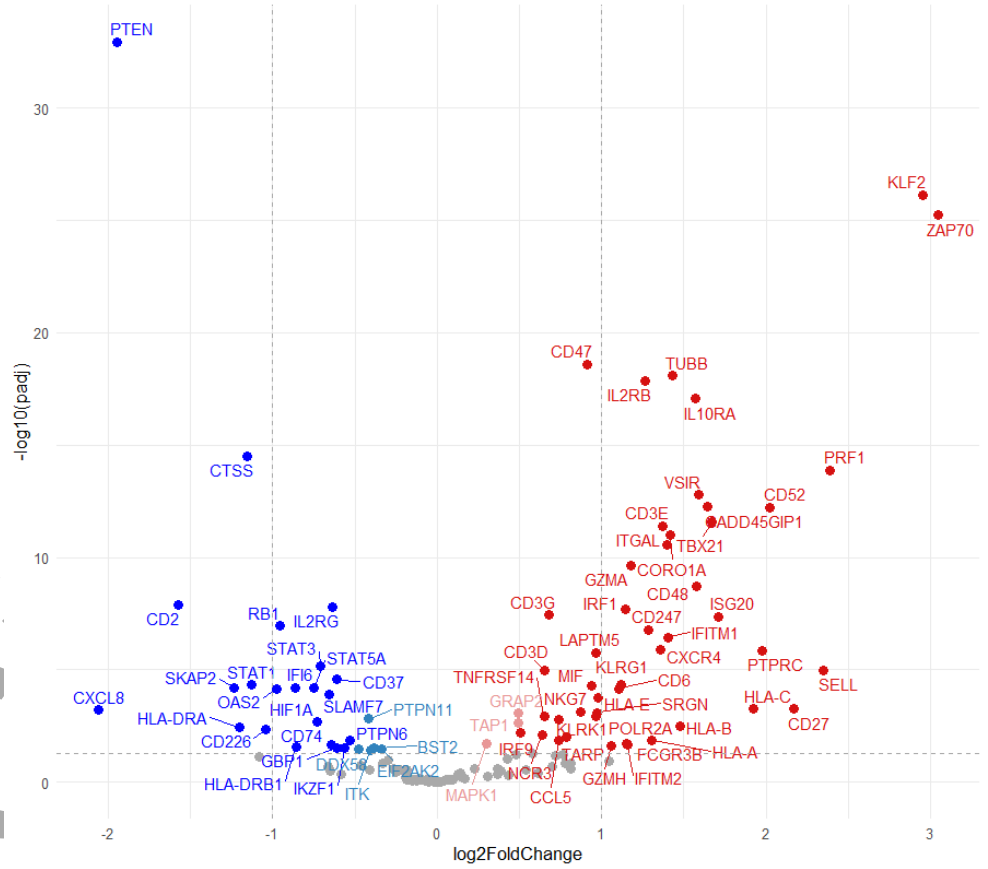

Figure 39. **Differentially expressed genes in γδ T cells from the PV-A subgroup of psoriasis patients versus healthy controls.** *The volcano plot shows log2 fold change (X-axis) and -log10 adjusted p-value (Y-axis). Genes significantly upregulated (log2FC > 1, adj. p-value < 0.05) are in dark red, with less significant upregulated (log2FC > 0, adj. p-value < 0.05) genes in light red. Similarly, significantly downregulated genes (log2FC < –1, adj. p-value < 0.05) are in dark blue; less significant downregulated genes (log2FC < 0, adj. p-value < 0.05) are in light blue. Non-significant genes are grey. Dashed lines indicate thresholds for fold change and adjusted p-value.*

4.4. γδ T cell profiling through high-dimensional spectral flow cytometry

The phenotypic profiles of circulating γδ T cells were further analysed using high-dimensional spectral flow cytometry. This approach incorporated a combination of surface and intracellular staining panels, enabling the detailed characterisation of cell subsets, activation states, and functional markers. For this purpose, peripheral blood mononuclear cells (PBMCs) from a total of 31 participants were included, comprising 12 healthy controls and 19 psoriasis patients. The study groups were balanced with respect to anthropometric and clinical characteristics. Detailed baseline characteristics of the study participants are presented in Table 19.

Table 19. Subjects' baseline characteristics

	PV (N = 19)	**HC (N = 12)**	**P**
Age	47 (36 – 55)	55 (38 – 64)	0.440*
Sex (M/F)	10/9	9/3	0.274**
hsCRP (mg/L)	1.02 (0.53 – 2.94)	1.6 (1.00 – 3.17)	0.373*
L (N x10^9/L)	7.80 (6.25 – 8.90)	7.0 (6.75 – 8.45)	0.982*
CMV IgG (U/mL)	118 (70.7 – 142.6)	96.4 (77.1 – 133)	0.862*
CMV IgG (pos/neg)	15/4	9/0	0.273**
PASI	8.6 (6.7 – 12.6)	-	-
Disease duration (years)	11.5 (4 – 16.5)	-	-

*Continuous data are shown as median (interquartile range). hsCRP – high sensitivity C-reactive protein, L – leukocyte count, CMV – cytomegalovirus; PASI – psoriasis area and severity index, * Mann-Whitney U test, ** Fisher's Exact Test*

The proportion of γδ T cells and their subsets were comparable between psoriasis patients and healthy controls, showing no significant differences in their distribution. However, a significant positive correlation between the proportion of Vγ9Vδ2$^-$ cells and age present in healthy participants (ρ = 0.73, P=0.007, Spearman's rho), was absent in psoriasis group (ρ = 0.12, P=0.62). Interestingly, a notable sex-specific difference was observed within the psoriasis group: women exhibited significantly higher proportions of γδ T cells (Me[IQR]: 4.49 [3.91 – 11.2] % vs. 3.09 [2.28 – 3.60] %, P = 0.037, women vs. men, Mann-Whitney U test) and the Vγ9Vδ2 subset (2.68 [2.09 – 4.44] % vs. 1.35 [0.91 – 2.10] %, P = 0.016) within the CD3$^+$ T cell compartment, whereas men contained higher frequencies of Vδ1 cells (51.15 [29.33 – 59.5] % vs 13.5 [4.64 – 24.8] %, P = 0.030, men vs. women) within the γδ T cells.

4.4.1. γδ T cell subclusters

The analysis of γδ T cell clusters using opt-SNE, a dimensionality reduction method optimized for high-dimensional single-cell data, revealed distinct segregation of these cells based on δ-chain expression into the major Vδ2 and Vδ1 populations. Furthermore, subclusters within the Vδ1, Vδ2, and Vδ3 populations were distinguished by the co-expression of the Vγ9 chain (Figure 40). This segregation underscores the functional and phenotypic diversity of γδ T cells associated with δ- and γ-chain expression, consistent with previous findings (140,141,156).

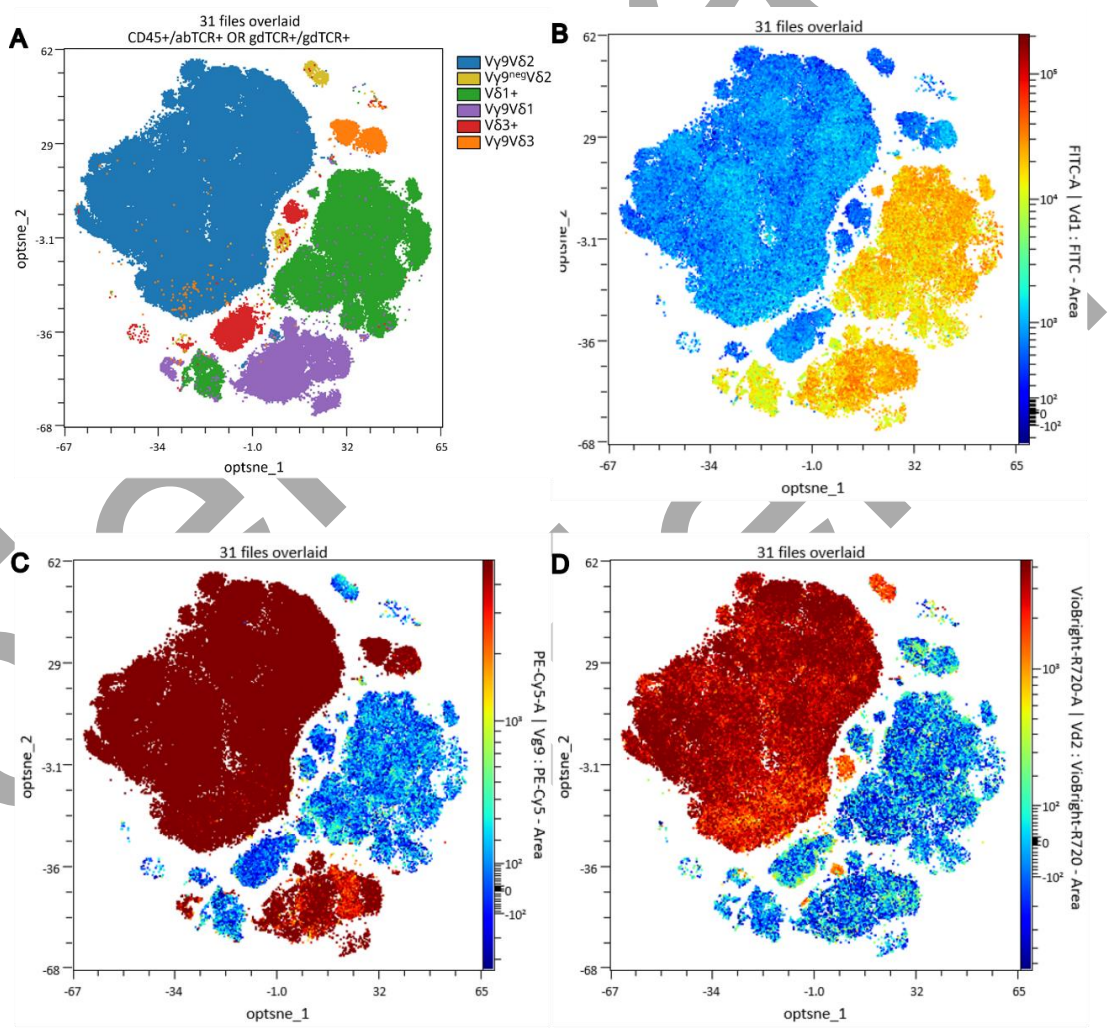

Figure 40. γδ T cells clusters segregate based on Vγ9 and δ chain expression. *A) Opt-SNE visualization of γδ T cells reveals clustering primarily driven by δ and* Vγ9 *chain expression. Fluoresecence signal intensity for B) Vδ1, C)* Vγ9, and D) *Vδ2 populations. The data represents a combined overlay analysis of all samples.*

4.4.2. Skin-homing potential of circulating γδ T cells

The skin-homing potential of circulating γδ T cells was evaluated by the expression of CLA, cutaneous lymphocyte antigen. The highest percentage of CLA^+ cells was observed in Vγ9Vδ2 population, with significantly lower levels observed in the $Vδ3^+$ and $Vδ1^+$ subsets, suggesting that Vγ9Vδ2 cells possess the highest skin-homing potential among γδ T cell subsets (Figure 42). Although CLA^+ cells did not form a distinct cluster of cells on opt-SNE plot, they predominantly grouped with cells expressing markers associated with a naïve-like phenotype, such as CD28, CD27, and CD127 (Figure 41). Direct comparison of CLA^+ and CLA^- cells further supported this observation, demonstrating that the CLA^+ cells were enriched for tissue-homing and naïve-like markers (CD27, CD28, CD127, CD161, and CXCR3), and contained significantly fewer cytotoxic-effector-like markers such as CD57, HLA-DR, CX_3CR_1, and CD16 (Figure 42). When comparing psoriasis patients to healthy controls, the frequency of CLA^+ γδ T cells was similar between the groups. However, within the psoriasis cohort, women exhibited significantly higher proportions of CLA^+ γδ T cells within the T cell population compared to men (Me [IQR]: 0.75 [0.51 – 0.94] vs. 0.33 [0.25 – 0.59], P = 0.025, women vs. men, Mann-Whitney U test).

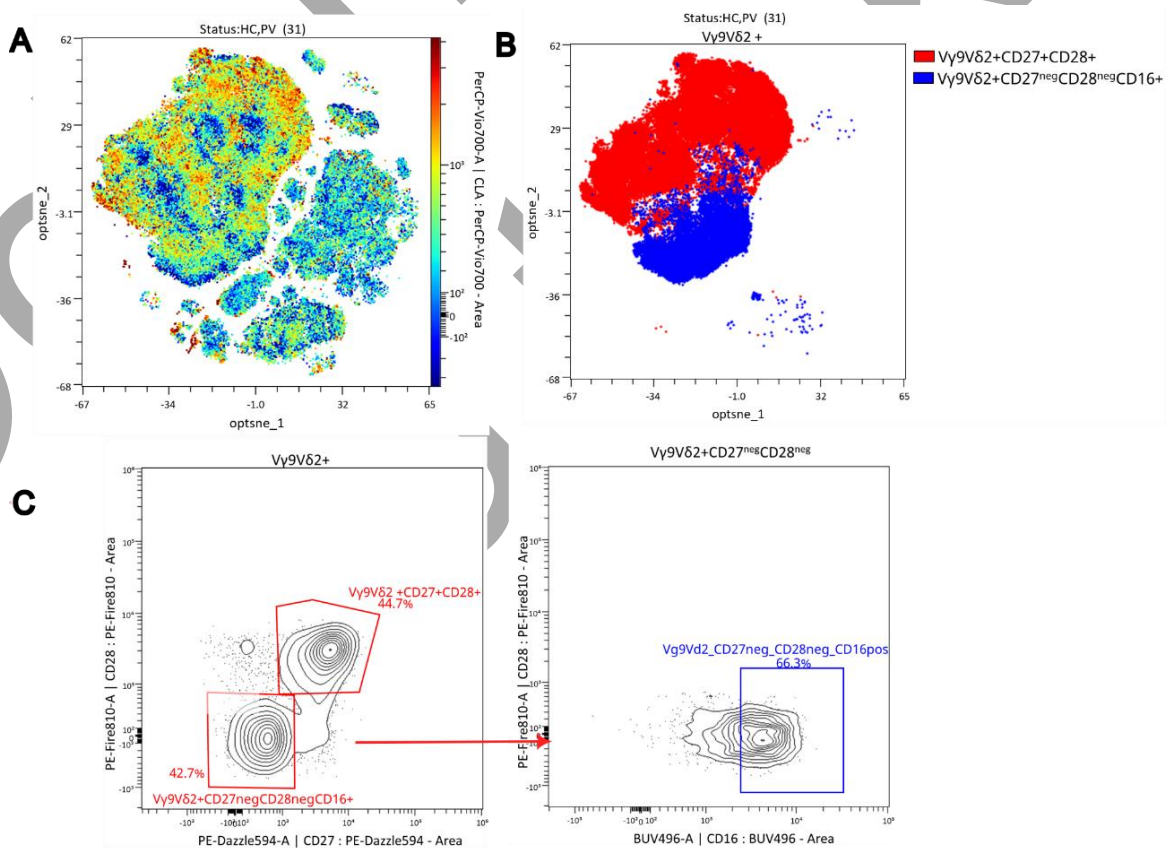

Figure 41. CLA⁺ Vγ9Vδ2 T cells are predominantly naïve-like. *A) Opt-SNE plot showing fluorescence intensity of CLA expression across γδ T cells. B) The distribution of CLA⁺ Vγ9Vδ2 cells aligns primarily with the naïve-like compartment (CD27⁺ CD28⁺), with a smaller association to the effector-like phenotype (CD27⁻CD28⁻CD16⁺). C) Representative gating strategy delineating naïve-like (CD27⁺ CD28⁺) and effector-like (CD27⁻CD28⁻CD16⁺) subsets within Vγ9Vδ2 T cells.*

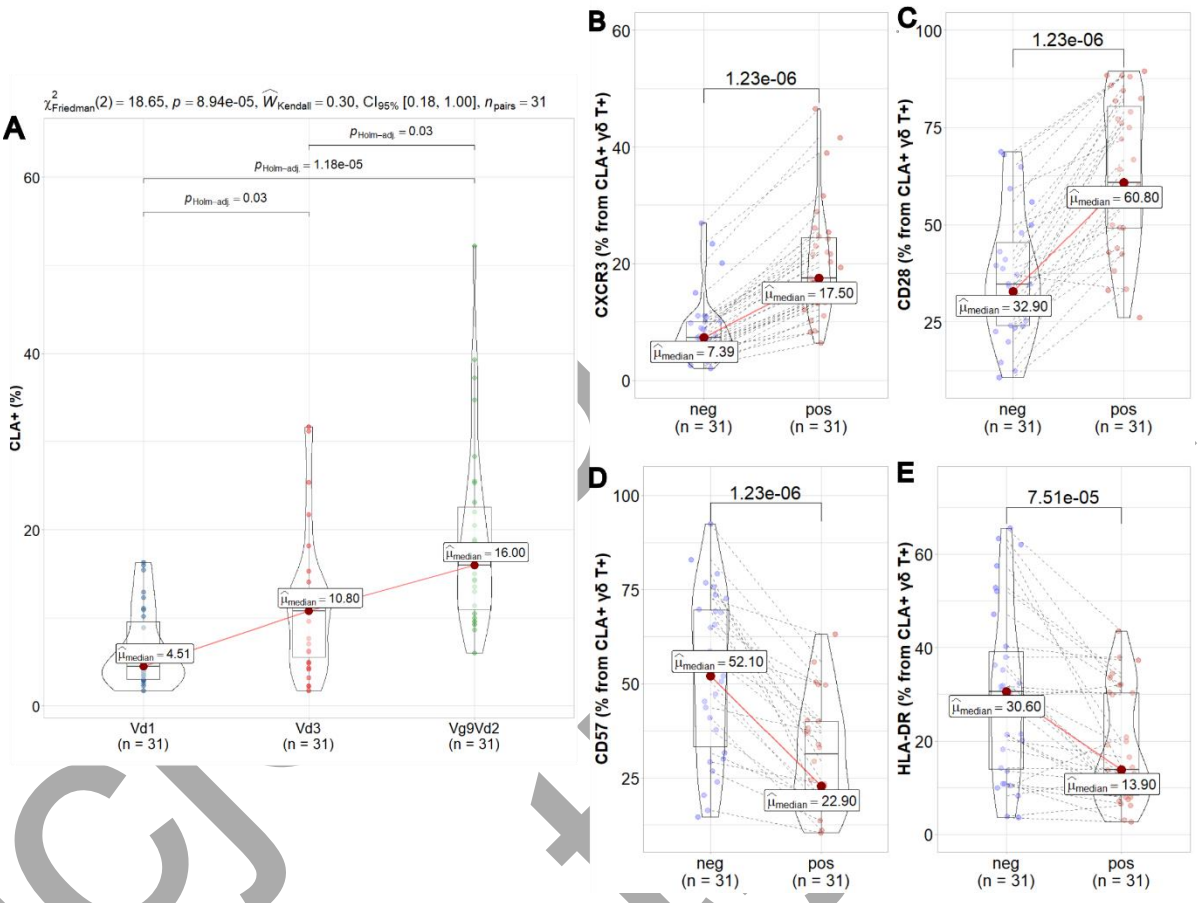

Figure 42. CLA expression on γδ T cells is enriched in Vγ9Vδ2 cells and associated with tissue-homing and naïve-like phenotypes. *A) CLA expression is the highest in Vγ9Vδ2 γδ T cells compared to Vδ3⁺ and Vδ1⁺ subsets. CLA⁺ γδ T cells show increased expression of B) tissue-homing CXCR3 and C) naïve-like marker CD28, with reduced levels of terminal differentiation and effector markers D) CD57 and E) HLA-DR. Dashed lines connect paired CLA⁺ and CLA⁻ samples from the same donors. Statistical significance was assessed using Friedman's test (A) and Wilcoxon signed-rank test (B–E).*

4.4.3. Phenotypic characterisation of γδ T Cells

A total of 28 surface markers were used for a detailed characterisation of γδ T cells. Given the significant heterogeneity among γδ T cell subsets, subsequent analyses were performed using stratification on the most dominant circulating $V\gamma9V\delta2^+$ and $V\gamma9V\delta2^-$ populations, of which the latter was further subdivided into $V\delta1^+$ and $V\delta3^+$ cells.

4.4.3.1. Phenotypic characterisation of Vγ9Vδ2 cells

A case-control comparison of markers expressed on Vγ9Vδ2 cells revealed no statistically significant differences between healthy and psoriasis-affected participants. However, significant correlations emerged between disease characteristics and the expression of several marker on these cells. The percentage of CD56-expressing Vγ9Vδ2 cells showed a significant positive correlation with disease duration ($\rho = 0.531$, $P = 0.019$, Spearman's rho), as did the frequency of $CD56^+$ CLA^+ Vγ9Vδ2 subset ($\rho = 0.472$, $P = 0.041$). Conversely, the frequencies of $CD27^+$ CLA^+ Vγ9Vδ2 cells decreased with disease duration ($\rho = -0.566$, $P = 0.012$), suggesting a shift from a naïve-like state toward higher cytolytic potential with prolonged disease. Furthermore, a significant association was found between PASI scores and the proportion of $CD56^+$ CLA^+ Vγ9Vδ2 cells ($\rho = 0.553$, $P = 0.017$), further underscoring the potential importance of this subset in disease.

Sex-based differences were also identified in the composition of circulating CLA^+ Vγ9Vδ2 T cells. Female psoriasis patients exhibited significantly higher proportions of $CD56^+$, $CD45RA^+$, $CCR7^+$, $CXCR5^+$, and $CX_3CR_1^+$ CLA^+ Vγ9Vδ2 cells within the T cell compartment, reflecting a combination of enhanced cytotoxic capacity, memory-like characteristics and migration potential. In contrast, male patients demonstrated higher proportions of $CD28^+$ CLA^+ T cells, suggesting a more naïve or co-stimulation-dependent phenotype. Furthermore, the percentage of $CD56^+$ CLA^+ Vγ9Vδ2 cells increased significantly with PASI score in male patients, while in female patients this subset increased with longer disease duration (Figure 43 A, C). Moreover, disease duration had differential effects on the Vγ9Vδ2 subset: in male patients, it was negatively associated with the frequency of $CD27^+$ Vγ9Vδ2 cells, reflecting a loss of naïve-like cells, while in females it associated with an overall decrease of Vγ9Vδ2 cells (Figure 43 B, D).

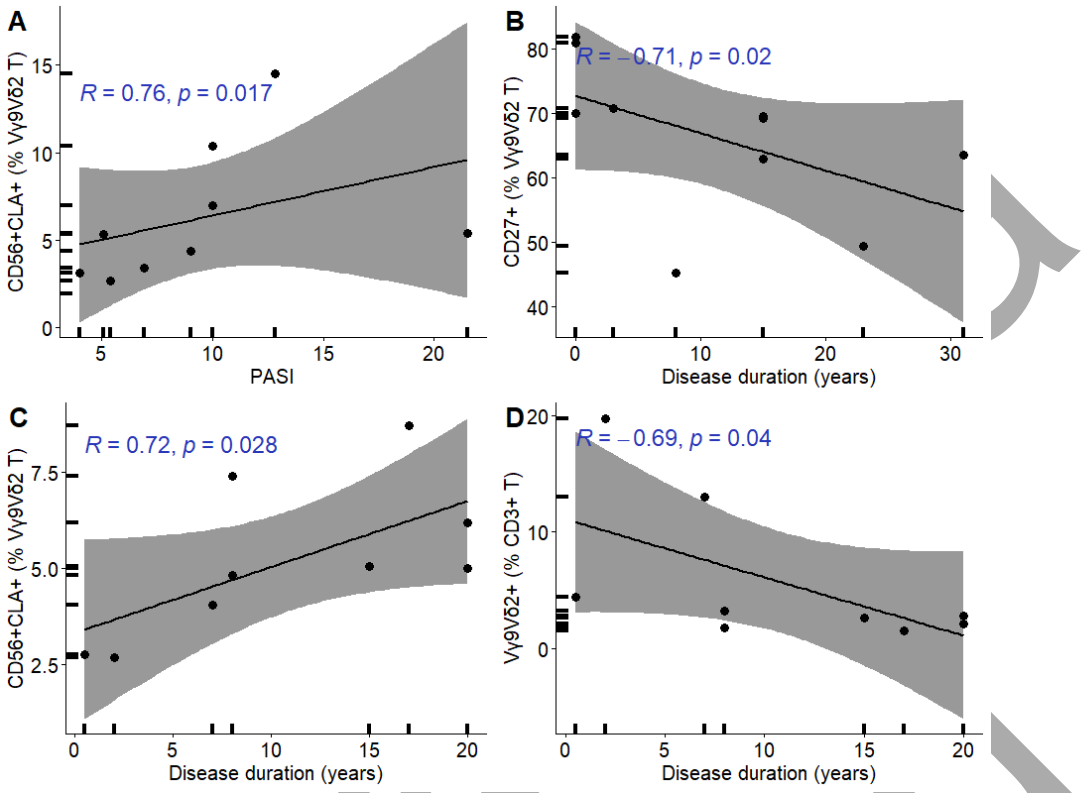

Figure 43. Differential relationships between PASI scores, disease duration, and Vγ9Vδ2 T cell subsets in male and female psoriasis patient. *In male patients: A) higher PASI scores positively correlate with the frequency of CD56⁺CLA⁺ Vγ9Vδ2 T cells within the Vγ9Vδ2 compartment, while B) longer disease duration negatively correlates with the frequency of CD27⁺ Vγ9Vδ2 cells. In female patients: C) longer disease duration positively correlates with the frequency of CD56⁺CLA⁺ Vγ9Vδ2 T cells within the Vγ9Vδ2 compartment, while D) the percentage of Vγ9Vδ2 cells within CD3+ T cell compartment declines. Spearman's correlation coefficient.*

The observed associations between the proportion of CD56⁺ Vγ9Vδ2 cells and both disease duration and PASI scores, along with sex-based differences, prompted further characterisation of CD56⁺ Vγ9Vδ2 cells. These cells exhibited a distinct co-expression profile compared to their CD56⁻ counterparts, highlighting phenotypic and functional divergence. Specifically, CD56⁺ Vγ9Vδ2 cells showed significantly higher expression of CD57, CD16, HLA-DR, CD25, CD11a, and PD-1, markers associated with activation, cytotoxicity, immune regulation, and terminal differentiation. In contrast, CD56⁻ Vγ9Vδ2 cells displayed elevated levels of CD28, CD27, and CD127, consistent with a more naïve-like phenotype (Figure 44). In addition, analysis of intracellular cytotoxic granules and transcription factors revealed that CD56⁺ cells demonstrate significantly higher proportions of perforin expression (Me[IQR]:

59.4 [46.5 – 68.4] % vs. 36.2 [26.4 – 49.6] %, $CD56^+$ vs. $CD56^-$, P=1.31 $x10^{-5}$, Paired Wilcoxon test), along with elevated levels of T-bet, and granzyme B, while $CD56^-$ cells showed higher expression of granzyme K and Eomes**.**

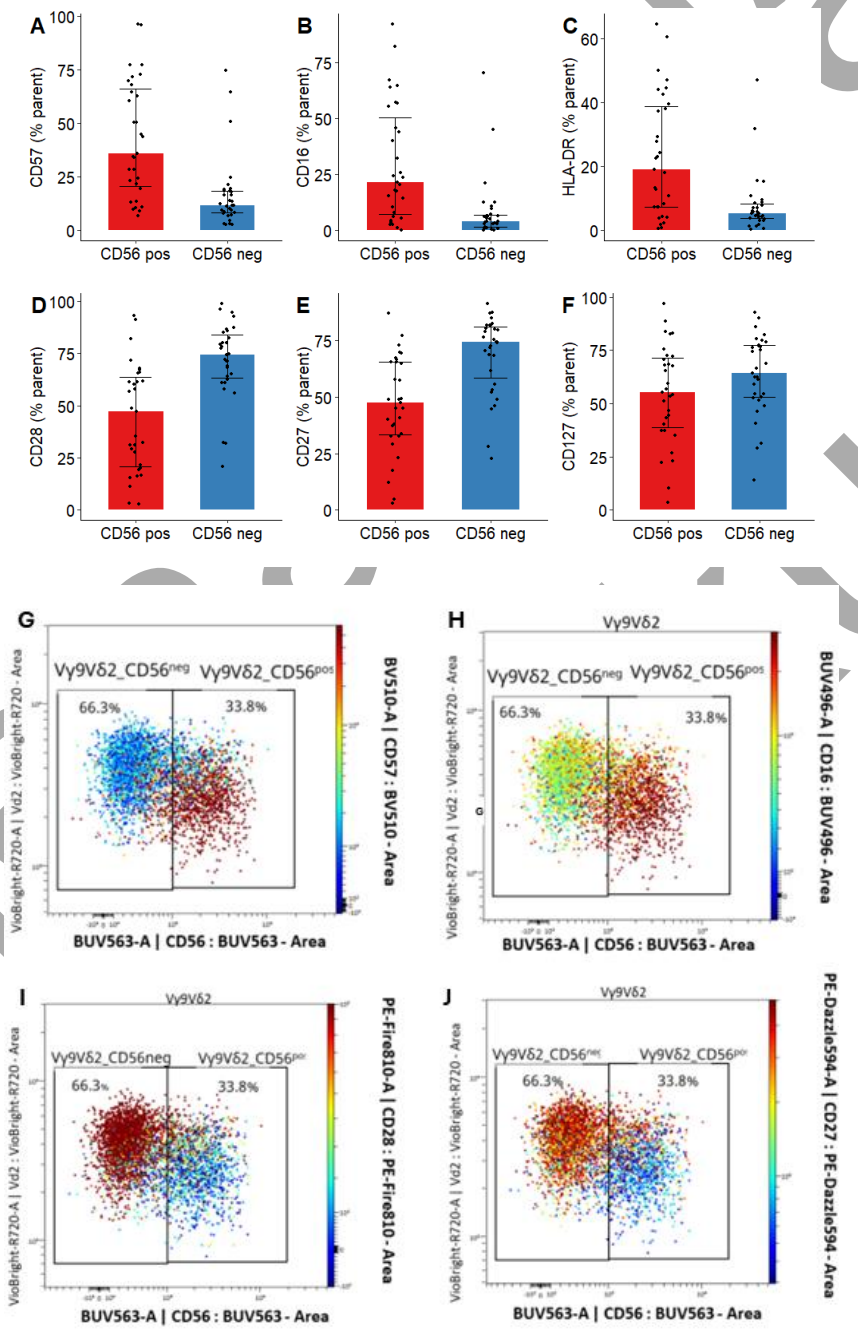

Figure 44. $CD56^+$ Vγ9Vδ2 cells exhibit elevated expression of cytotoxic effector markers and reduced expression of naïve-like markers. *Bar plots show the percentages of A) CD57, B) CD16, C) HLA-DR, D) CD28, E) CD27, and F) CD127 positive cells in $CD56^+$ (pos) and $CD56^-$ (neg) Vγ9Vδ2 subsets. Representative fluorescence intensity plots illustrate the*

distribution of G) CD57, H) CD16, I) CD28, and J) CD27 expression on CD56$^+$ and CD56$^-$ Vγ9Vδ2 T cells.

4.4.3.2. Phenotypic characterisation of Vγ9Vδ2^{neg} cells

In addition to its relevance in Vγ9Vδ2$^+$ cells, CD56 also emerged as an interesting marker in Vγ9Vδ2$^-$ subset. The frequency of CD56$^+$ Vγ9Vδ2$^-$ cells increased significantly with the age of psoriasis patients, a trend entirely absent in healthy group (Figure 45 A). Similar to previous observations in the Vγ9Vδ2$^+$ population, female patients had significantly higher frequencies of CD56-expressing CLA$^+$ Vγ9Vδ2$^-$ cells compared to their male counterparts (Figure 45 C). Interestingly, the relationship between CD56 expression within Vγ9Vδ2$^-$ cells and PASI scores varied by gender. In female patients, the proportion of CD56$^+$ CLA$^+$ in Vγ9Vδ2$^-$ cells positively correlated with PASI scores (Figure 45 B), whereas in male patients, an inverse trend was observed, with the frequency of CD56$^+$ Vγ9Vδ2$^-$ cells within the CD3$^+$ T cell population declining as PASI scores increased ($\rho = -0.686$, $P = 0.041$). Moreover, CD103, an integrin that mediates epithelial adhesion by binding to E-cadherin, was increasingly expressed on Vγ9Vδ2$^-$ cells with increasing PASI scores, particularly in male patients ($\rho = 0.678$, $P = 0.044$), while disease duration was positively associated with elevated CD161 expression on CLA$^+$ Vγ9Vδ2$^-$ cells in female patients ($\rho = 0.706$, $P = 0.003$).

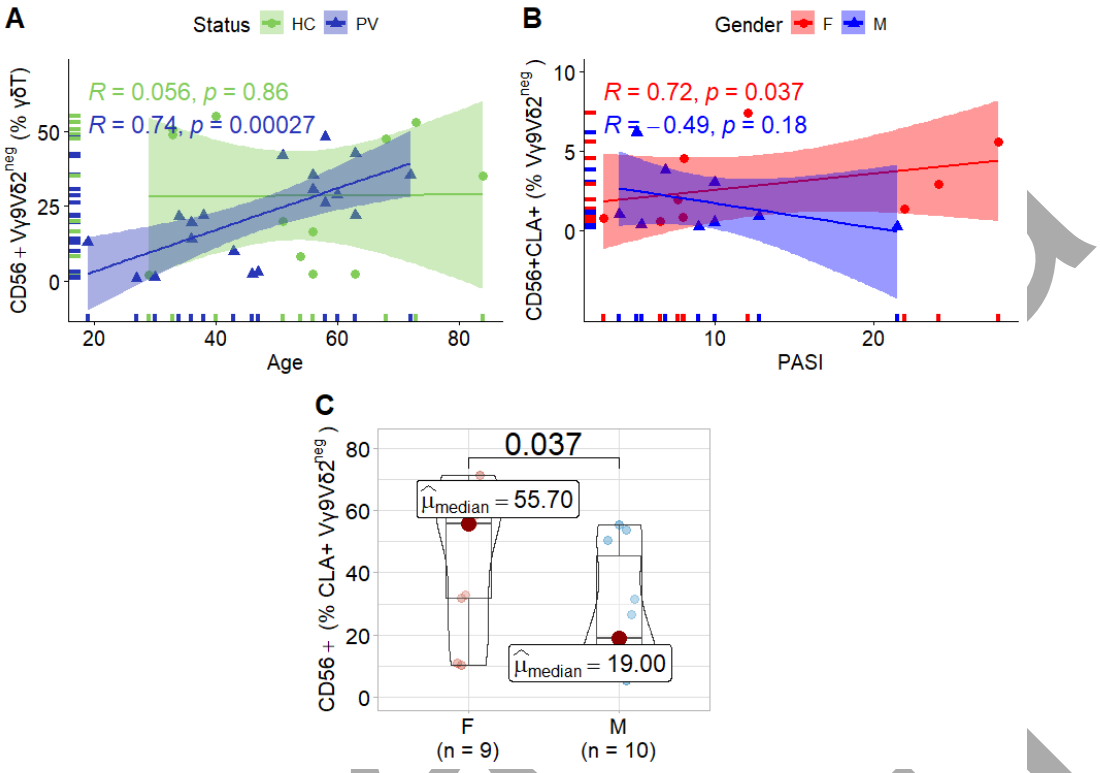

Figure 45. Age, PASI, and gender influence frequencies of CD56⁺ Vγ9Vδ2^{neg} T Cells. *A) The frequencies of CD56⁺ Vγ9Vδ2^{neg} T cells correlate significantly with the age of psoriasis patients. Female patients show B) a significant positive correlation between CD56⁺ CLA⁺ Vγ9Vδ2^{neg} frequencies and PASI score and C) significantly higher frequencies of CD56⁺ Vγ9Vδ2^{neg} T cells compared to male patients. Spearman's correlation coefficient (A, B), Mann-Whitney-U test (C).*

4.4.3.3. Phenotypic characterisation of Vδ1 cells

The analysis of Vδ1 T cells revealed no significant differences in the overall profiles of these cells between healthy controls and individuals with psoriasis. However, sex-related distinctions were observed again in psoriasis cohort. Male patients demonstrated both a higher overall abundance of Vδ1 cells and an increased percentage of CX_3CR_1+ Vδ1 cells (Figure 46 A, B, C), while female patients exhibited higher prevalence of CXCR3⁺ and CD8⁺ CLA⁺ Vδ1 cells. Further analysis indicated that the expression of CD103 on circulating Vδ1 cells positively correlated with PASI scores, especially in affected men. In addition, in men, PASI scores showed a significant negative correlation with the frequency of HLA-DR-expressing CLA⁺ Vδ1 cells, while in female patients, longer disease duration was associated with reduced percentages of CD94⁺, PD-1⁺, and CD25⁺ cells within the CLA⁺ Vδ1 population (Figure 46 E,

F). In addition, age-related changes in psoriasis patients further highlighted an increase in CCR7$^+$ CLA$^+$ Vδ1 cells (Figure 46 D), alongside a decrease in CD38$^+$ CLA, both trends not evident in heathy controls.

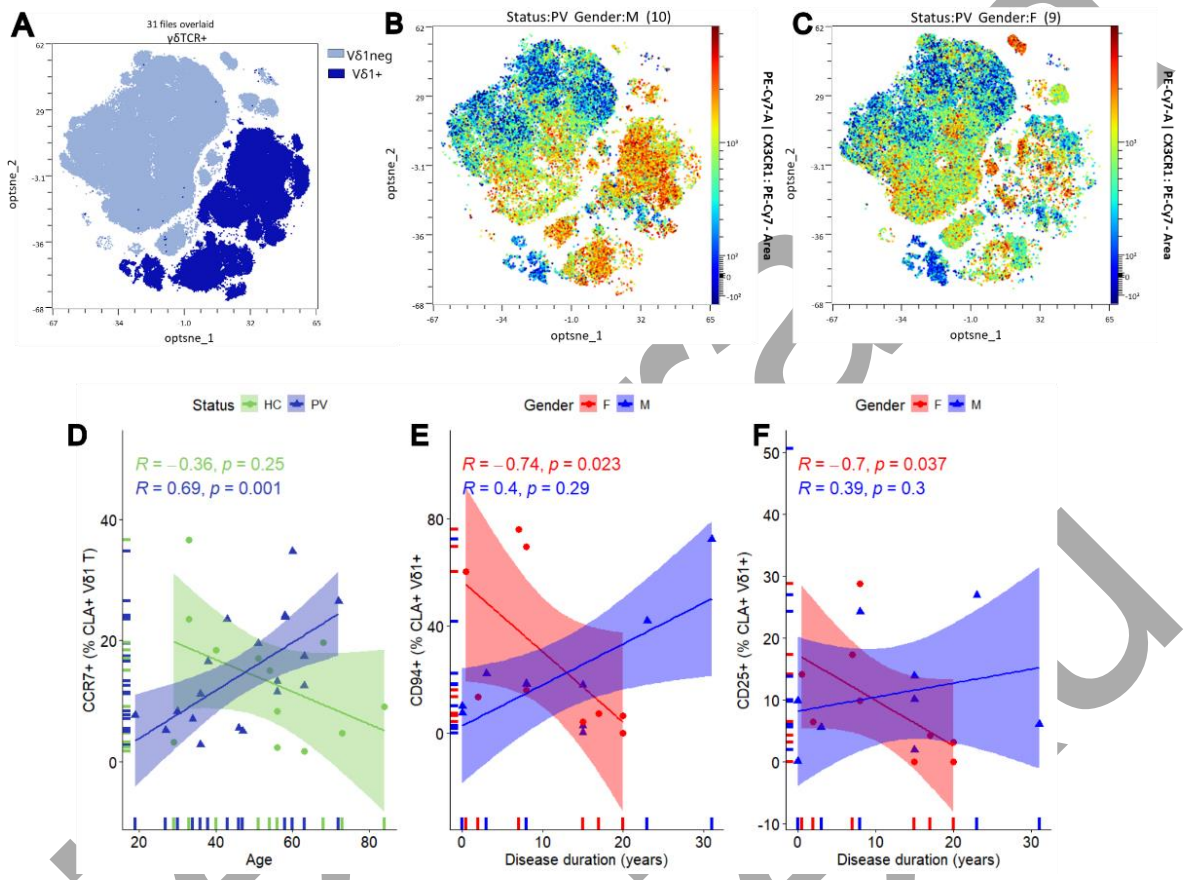

Figure 46. Gender-based phenotypic differences in Vδ1 cells of psoriasis patients. *A) opt-SNE plot of γδ T cells, with Vδ1+ cells highlighted in dark blue. Fluorescence intensity plots showing B) higher CX3CR1 expression in Vδ1+ cells of male patients compared to C) female patients. D) The proportion of CCR7+ cells in CLA+ Vδ1+ increase significantly with age of psoriasis patients. Disease duration associates with E) increased percentage of CD94+ and F) decreased percentage of CD25+ Vδ1cells in female, but not male patients.*

1.1.1.4. Phenotypic characterisation of Vδ3 cells

The analysis of Vδ3 cell characteristics revealed that psoriasis patients had significantly higher percentages of CD38$^+$ CLA$^+$ cells within Vδ3$^+$ population (Figure 47 A), while CD103$^+$ cells in the CLA$^+$ Vδ3 fraction were lower compared to healthy controls (Me [IQR]: 0.28 [0 – 4.81] vs. 6.79 [2.57 – 16.7], P = 0.013, PV vs HC, Mann-Whitney U test). Among the Vγ9Vδ2$^-$

population, the percentage of CD56$^+$ Vδ3$^+$ cells increased with PASI scores (ρ = 0.479, P = 0.044), suggesting that Vδ3$^+$ cells contribute to the previously observed trends in the Vγ9Vδ2$^-$ subset.

Sex-specific differences were also evident. Female patients displayed a strong positive correlation between PASI scores and the percentage of CD56$^+$ Vδ3$^+$ cells in Vγ9Vδ2$^-$ subset (ρ = 0.75, P = 0.025), as well as higher proportions of CD56$^+$ CLA$^+$ Vδ3 cells compared to males (Figure 47 B), mirroring the findings observed in Vγ9Vδ2$^+$ and collectively analysed Vγ9Vδ2$^-$ cells. In contrast, male patients showed a significant decrease in PD-1$^+$ CLA$^+$ Vδ3 cells with increasing PASI scores (ρ = -0.703, P = 0.035). Additionally, CD8$^+$ CLA$^+$ Vδ3 cells were positively associated with disease duration in males (ρ = 0.701, P = 0.035), accompanied by increased expression of CD25$^+$ (Figure 47 C) and CD103$^+$ (ρ = 0.756, P = 0.018) in the total Vδ3 population. In female patients, PASI scores were positively correlated with the levels of CD16$^+$ (Figure 47 D) in the Vδ3 population, as well as CD103 (ρ = 0.679, P = 0.044) on CLA$^+$ Vδ3$^+$ cells. Disease duration was also associated with an increased percentage of CD38$^+$ CLA$^+$ Vδ3 cells in females (ρ = 0.688, P = 0.041). Together, these findings highlight distinct phenotypic profiles of Vδ3 cells in psoriasis patients, pointing to potentially heightened activation states and notable sex-associated differences, with female patients exhibiting higher expression of cytotoxicity-associated markers.

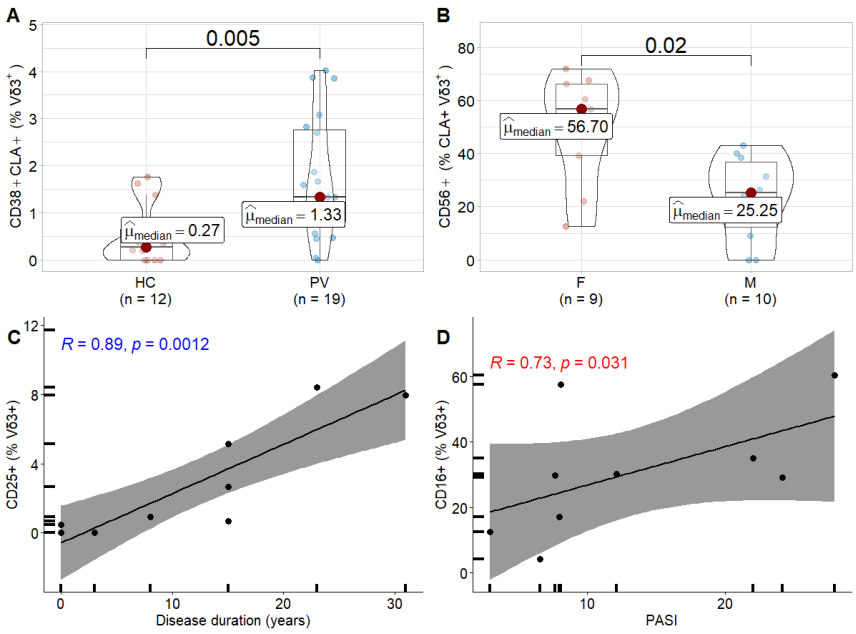

Figure 47. Distinct phenotypic characteristics of Vδ3 cells in psoriasis patients. *A) Psoriasis patients exhibit significantly higher proportions of CD38$^+$ CLA$^+$ cells within the Vδ3 compartment. B) Female psoriasis patients display higher frequencies of CD56+ cells in the*

CLA^+ Vδ3 subset. C) Disease duration associates positively with the percentage of $CD25^+$ $Vδ3^+$ cells in male patients, while D) $CD16^+Vδ3^+$ proportions increase with PASI scores in female patients.

4.4.4. Transcriptional factors and cytolytic granules

The intracellular (IC) staining analysis was performed to assess the cytolytic capacities (GzmA/B/K, perforin, granulysin), transcriptional regulation of effector differentiation (T-bet, Eomes, Blimp-1), exhaustion-related regulation (TOX), and proliferation (Ki67) of γδ T cells. Transcriptomic data previously revealed increased expression of T-bet, perforin, and granzyme A in psoriasis patients, which were corroborated by intracellular staining. Specifically, IC staining confirmed elevated T-bet and perforin expression, while the overall percentage of $GzmA^+$ γδ T cells in psoriasis patients was only marginally higher compared to healthy controls and did not reach statistical significance (Figure 48). However, a subset of psoriasis patients exhibited higher proportions of $GzmA^+$ γδ T cells than any healthy participant, mirroring the transcriptomic data, where subset of patients contributed to significant case-control differences. In addition, psoriasis patients showed increased frequencies of perforin-expressing γδ T, with differential T-bet expression primarily confined to the $Vδ2^+$ subset. Notably, when analysing the entire γδ T cell population, no significant difference in T-bet expression was observed, suggesting that $Vδ2^+$ γδ T cells were the primary contributors to the differences observed in RNA-seq analyses. Furthermore, significant correlations were identified between the percentages of T-bet^+, $Eomes^+$, $GzmA^+$, $GzmB^+$, $GzmK^+$, TOX^+ and $perforin^+$ within the $Vδ2^-$ cells and the age of psoriasis patients, whereas these cytotoxic-effector markers showed no age-related trends in healthy controls (Table 20, Figure 49). These findings suggest that age-associated changes in $Vδ2^-$ γδ T cells may promote the acquisition of cytotoxic and effector-like phenotypes, potentially amplifying inflammatory responses in psoriasis.

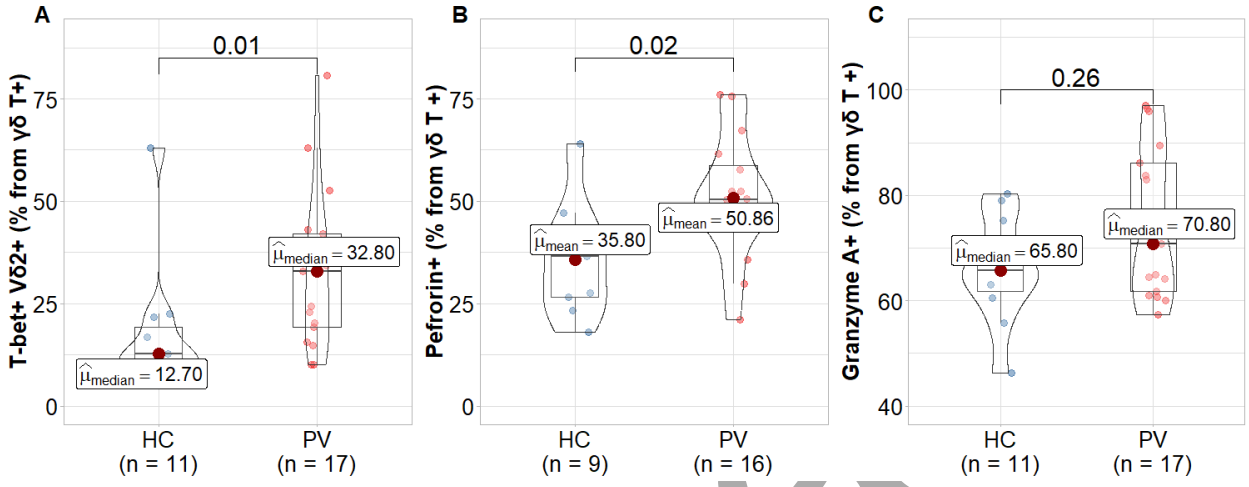

Figure 48. Elevated T-bet and perforin expression in γδ T cells in psoriasis patients, with marginally increased granzyme A levels. *Violin plots depict the percentages of A) T-bet⁺, B) perforin⁺, and C) granzyme A⁺ γδ T cells in healthy controls (HC) and psoriasis patients (PV). Mann-Whitney U test (A, C), Student-t test (B).*

Table 20. Statistically significant correlations between age and marker expression in psoriasis patients.

Marker	Vδ2⁺ correlation (ρ, P)	Vδ2⁻ correlation (ρ, P)
Granzyme A	ρ = -0.503, P = 0.039	ρ = 0.672, P = 0.03
Granzyme B	ρ = -0.637, P = 0.06	ρ = 0.624, P = 0.007
Granzyme K	-	ρ = 0.807, P = 9.15 x 10^{-5}
Granulysin	-	-
Perforin	-	ρ = 0.625, P = 0.009
T-bet	-	ρ = 0.629, P = 0.007
Eomes	-	ρ = 0.554, P = 0.21
TOX	-	ρ = 0.554, P = 0.21
Ki67	-	-

The table presents the Spearman's correlation coefficients (ρ) and corresponding P values for statistically significant correlations between age and the percentage of marker-positive Vδ2⁺ or Vδ2⁻ cells within the γδ T cell population of psoriasis patients. Correlations with no statistical significance (p ≥ 0.05) are denoted by (-).

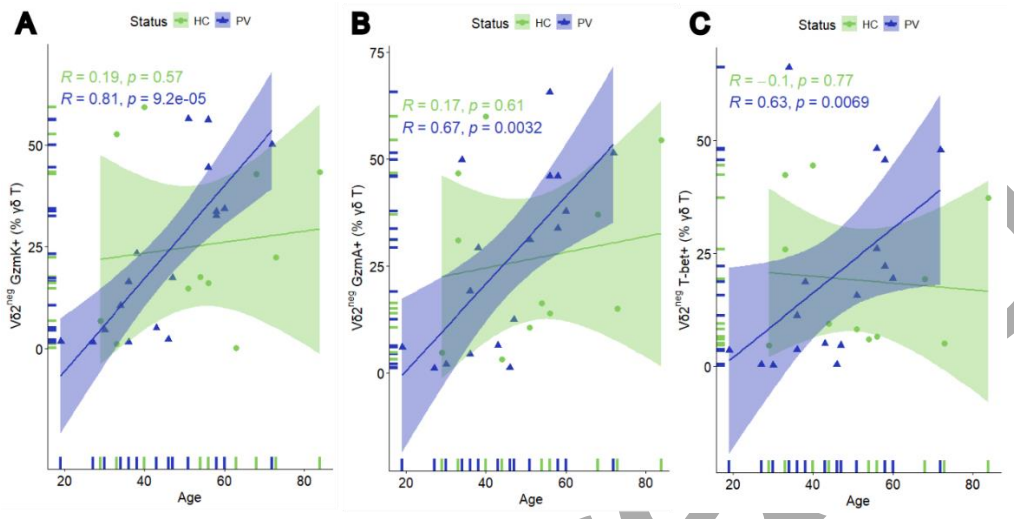

Figure 49. Age-associated increase in cytotoxic granule expression and effector markers in Vγ9Vδ2⁻ cells of psoriasis patients. *The proportion of Vγ9Vδ2⁻ cells expressing A) GzmK, B) GzmA, and C) T-bet within the γδ T cell compartment increases significantly with age in psoriasis patients, but not healthy controls. Sperman's correlation coefficient.*

4.5. Proportion and composition of circulating MAIT cell compartment

The frequencies of mucosal-associated invariant T (MAIT) cells, defined as $CD3^+$MR1-5-OP-RU-$tet^+$$TCRVa7.2^+$ cells, and their $CD8^+$, double-negative (DN, $CD4^-CD8^-$), $CD4^+$, and double-positive (DP, $CD4^+CD8^+$) subsets were evaluated in the same cohort used to examine the γδ T cell compartment. This cohort included 96 participants: 64 psoriasis patients and 32 healthy controls. While demographic and clinical features were largely similar, psoriasis patients exhibited higher BMI, elevated leukocyte counts, and a greater prevalence of smoking and CMV seronegativity. Baseline characteristics are detailed in Chapter 4.1., Table 4.

The median percentage of MAIT cells in $CD3^+$ compartment was 1.92 (Q1–Q3: 0.88 – 3.52) %, aligning with previous reports (181–185). As expected, the $CD8^+$ MAIT subset was the most prevalent, occupying median 68.2 (Q1–Q3: 58.2 – 77.8) % of MAIT cell population, followed by the DN subset (23.1 [15.5 – 36.8] %) and less frequent $CD4^+$ (2.3 [1 – 5.1] %) and DP (1.26 [0.69 – 2.49] %) populations (Figure 50).

The case-control comparison showed no significant differences in the proportion of MAIT cells within $CD3^+$ T lymphocytes, nor in the composition of the MAIT cell subsets. Interestingly, however, the proportion of $CD4^+$ MAIT cells within the T cell pool was significantly lower in psoriasis patients compared to healthy controls (Table 21).

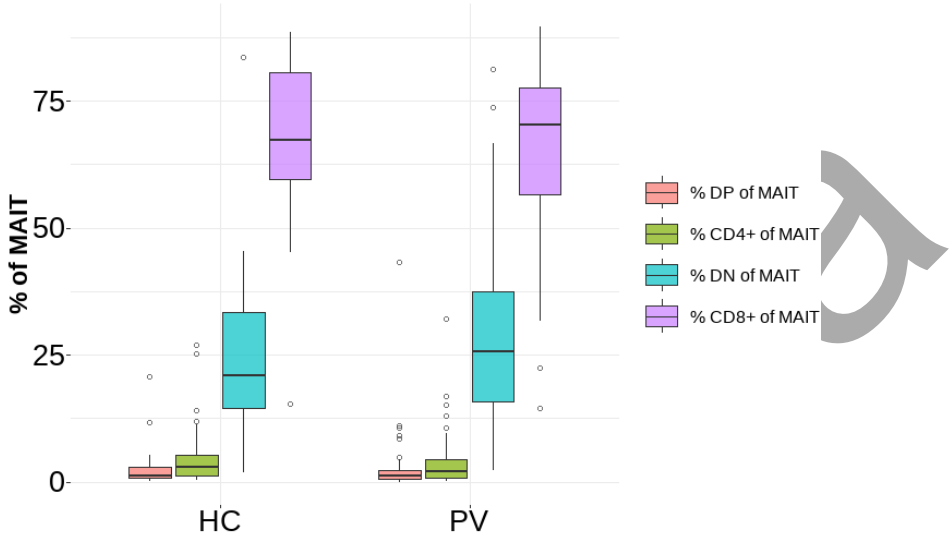

Figure 50. Distribution of MAIT cell subsets in psoriasis patients and healthy controls. *$CD8^+$ MAIT cells are the most abundant, followed by DN ($CD4^-CD8^-$), and less represented CD4+ and DP ($CD4^+CD8^+$) subsets, with no significant differences between healthy controls (HC) and psoriasis patients (PV).*

Table 21. The distribution of peripheral MAIT cells in PV and HC samples

	PV (N = 63)	HC (N = 32)	P
% MAIT of $CD3^+$	1.86 (0.75 – 3.26)	2.41 (0.95 – 3.65)	0.341
% $CD8^+$ MAIT of $CD3^+$	1.07 (0.38 – 2.43)	1.52 (0.65 – 2.26)	0.361
% DN MAIT of $CD3^+$	0.45 (0.16 – 0.91)	0.46 (0.22 – 0.69)	0.777
% $CD4^+$ MAIT of $CD3^+$	0.03 (0.01 – 0.08)	0.07 (0.03 – 0.13)	**0.016**
% DP MAIT of $CD3^+$	0.02 (0.01 – 0.05)	0.03 (0.01 – 0.07)	0.084
% $CD8^+$ of MAIT	70.3 (56.65 – 77.5)	67.2 (59.55 – 80.63)	0.825
% DN of MAIT	25.7 (15.75 – 37.5)	20.95 (14.53 – 33.48)	0.438
% $CD4^+$ of MAIT	2.09 (0.82 – 4.49)	2.9 (1.26 – 5.41)	0.202
% DP of MAIT	1.23 (0.55 – 2.23)	1.29 (0.89 – 2.92)	0.245

Data are shown as median with interquartile range. DP – $CD4^+CD8^+$, DN – $CD4^-CD8^-$. Mann-Whitney U test

In line with previous reports(184,185,193,195), the frequency of MAIT cells declined with advancing age in both psoriasis-affected and healthy individuals. This age-associated reduction was evident in the proportions of predominant $CD8^+$ and DN populations of MAIT cells within the $CD3^+$ T compartment (Figure 51), whereas the frequencies of $CD4^+$ and DP populations did not show significant association with age. In the PV group, significant negative correlations were observed between hsCRP levels and the percentage of MAIT cells, as well

as their $CD8^+$ and DN clusters within $CD3^+$ T cells (Figure 52). A moderate negative association was also identified between the PASI score and the percentage of DN MAIT cells in the $CD3^+$ T cell pool ($\rho = -0.311$, $P = 0.015$).

Given the significant positive correlation between age and hsCRP levels in PV patients ($\rho = 0.518$, $P = 5.28 \times 10^{-4}$), further analysis was conducted to assess whether age and hsCRP exert independent or interactive effects on MAIT cell proportions. A generalized linear model (GLM) with a gamma distribution and a log link function was used to evaluate the individual effects of age and hsCRP on MAIT cell proportions. The model was specified as: $\log(Y)=\beta_0 +\beta_1 Age+\beta_2 hsCRP$, where Y represents the percentage of total MAIT, $CD8^+$ MAIT, or DN MAIT cells within the $CD3^+$T cell population. Both age and hsCRP were found to be significant negative predictors of total MAIT (age: $\beta = -0.028$, $P = 0.006$; hsCRP: $\beta = -0.123$, $P = 0.003$), $CD8^+$ subset (age: $\beta = -0.029$, $P = 0.008$; hsCRP: $\beta = -0.149$, $P = 0.001$), and DN subset (age: $\beta = -0.029$, $P = 0.008$; hsCRP: $\beta = -0.149$, $P = 0.001$) proportions. To explore potential interactive effects of age and hsCRP on MAIT cell proportions, an interaction term (Age × hsCRP) was added to the model: $\log(Y)=\beta 0+\beta 1 Age+\beta 2 hsCRP+\beta 3(Age \times hsCRP)$. The interaction was not found to be significant for total MAIT cells or the CD8+ subset. However, it was significant for the DN cluster ($\beta = -0.005$, $P = 0.039$), suggesting a combined effect of age and hsCRP on the proportion of DN MAIT cells. Altogether, these results indicate that while age and hsCRP independently predict the proportions of total MAIT cells and $CD8^+$ MAIT cells, their combined effects are significant for the DN subset, highlighting distinct impacts of systemic inflammation and aging.

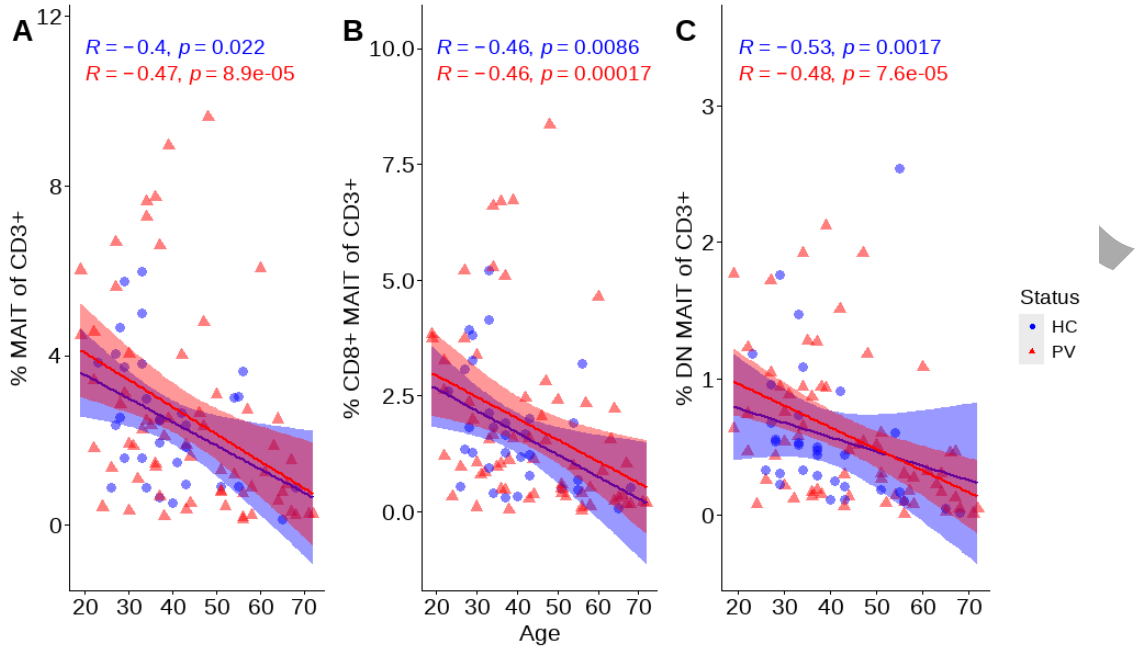

Figure 51. Negative associations between increasing age and the proportion of MAIT cells. *Negative correlation between age and A) total MAIT, B) CD8⁺ MAIT, and C) DN MAIT within the CD3⁺ T cell compartment. Sperman's correlation coefficient. PV (N=63), HC (N=32).*

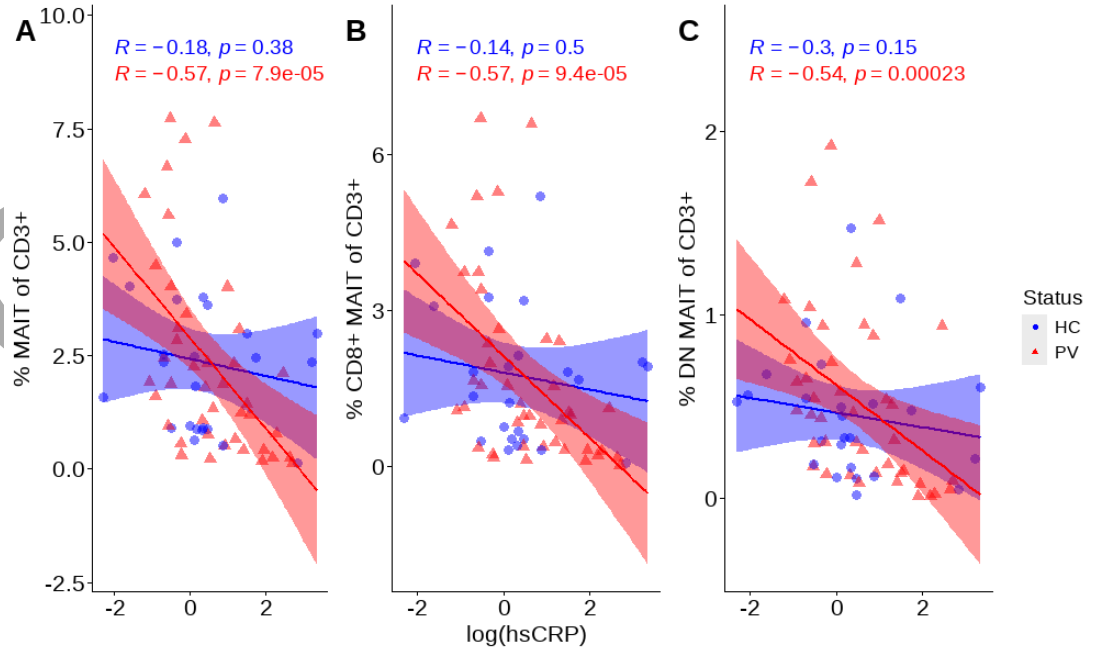

Figure 52. Negative associations between increasing hsCRP levels and the proportion of MAIT cells in psoriasis. *Negative correlation between A) total MAIT, B) CD8⁺ MAIT, and C) DN MAIT within the CD3⁺ T cell compartment. hsCRP levels are presented on a logarithmic scale. Sperman's correlation coefficient. PV (N=42), HC (N=25).*

Upon sex-based stratification, significant differences were observed between healthy and diseased male participants. Namely, psoriasis patients exhibited a significantly lower proportion of total MAIT cells compared to healthy examinees (Me [IQR]: 1.43 [0.7–2.74] vs. 2.53 [1.71–3.77], P = 0.021, PV vs. HC, Mann-Whitney U test), as well as reduced representation of $CD8^+$ (0.98 [0.34–2.15] vs. 1.83 [1.22–2.85], P = 0.039), $CD4^+$ (0.03 [0.01–0.08] vs. 0.07 [0.03–0.13], P = 0.015) and DP (0.02 [0.01–0.04] vs. 0.03 [0.02–0.07], P = 0.026) MAIT cell subsets within the $CD3^+$ T cell population. Given that, unlike in the PV group, there were no participants older than 60 years in the healthy group, a follow-up analysis was conducted on a reduced, age-matched cohort to control for potential age-related biases. This reanalysis confirmed a significantly lower proportion of DP and $CD4^+$ MAIT cell populations within the $CD3^+$ T lymphocyte pool (Figure 53), whereas the differences in the total proportion of MAIT cells and the $CD8^+$ MAIT cell subset loss statistical significance. No significant differences were observed in the comparison of MAIT cell frequencies between healthy and affected female participants. Interestingly, however, healthy women displayed significantly lower proportions of MAIT and $CD8^+$ MAIT cells within the $CD3^+$ T cell population, a finding not observed when female and male psoriasis patients were compared. Of note, there were no significant differences in age between men and women in either healthy or psoriasis group. The significant differences observed in male participants, along with the reduced percentages of MAIT cells in healthy women, resembled patterns seen in γδ T cell proportion analyses. As previous studies have reported MAIT cell frequencies are similar to those of $V\delta2^+$ γδ T cells (184), a correlation analysis was conducted between the proportions of γδ T and MAIT cells. This analysis revealed a positive correlation between the percentage of $CD8^+$ MAIT cells and $V\delta2^+$ γδ T cells within the $CD3^+$ T cell population across all samples ($\rho = 0.304$, P = 0.003) and in the PV group ($\rho = 0.318$, P = 0.012), however the same trend was not present in healthy participants.

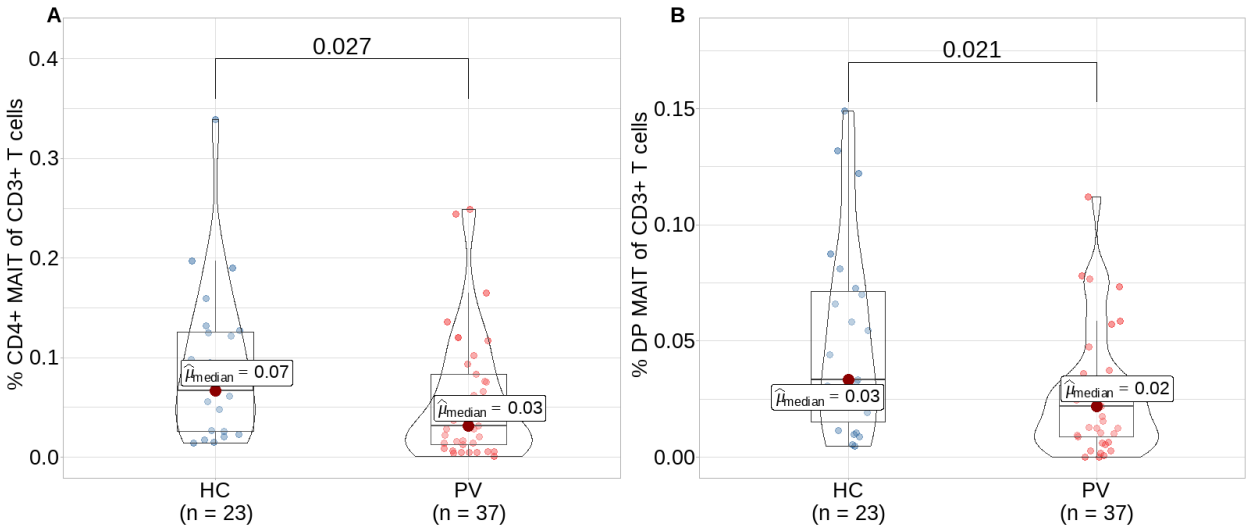

Figure 53. Male psoriasis patients show reduced CD4$^+$ and DP MAIT subsets proportions compared to healthy men. *Proportions of A) CD4$^+$ and B) DP (CD4$^+$CD8$^+$) subsets within CD3$^+$ T in male psoriasis patients (PV) versus healthy male controls (HC). Based on an age-matched cohort of participants under 60 years old. Mann-Whitney U test.*

4.6.Characterisation of the TCR repertoire in circulating MAIT cells

4.6.1. Sequencing quality metrics and participants' characteristics

To assess the TCR repertoire of circulating MAIT cells, sequencing libraries were constructed from 40 RNA samples (27 psoriasis vulgaris patients [PV] and 13 from healthy controls [HC]) obtained from flow-sorted cells. Of these, 39 libraries met the recommended concentration threshold and were sequenced.

All sequenced libraries and the overall sequencing run, satisfied quality control requirements, including read accuracy, sequence length, and coverage depth. The read count and clonotype number did not exhibit correlation pattern, ensuring the clonotype counts were not affected by sequencing depth. However, upon closer investigation of clonotypic characteristics, one sample was excluded from analysis due to significant deviations in basic CDR3 features and skewed gene usage, likely resulting from extreme clonotype expansion attributable to the participant's age (an 84-year-old male). A sequencing metrics summary is provided in Table 22.

Table 22. MAIT TCR sequencing metrics

	PV (N = 26)	HC (N=12)	P
TRA reads	823,018 (686,289–963,435)	730,345 (607,655–814,321)	0.582
TRB reads	911,458 (724,957–1,079,960)	1,098,755 (877,019–1,764,067)	0.081
TRA/TRB reads (%)	91.59 (89.92–93.15)	92.51 (90.87–94.22)	0.484
TRA clonotypes	485 (356–716)	392 (280–604)	0.541
TRB clonotypes	1643 (1102–2448)	1377 (949–2068)	0.623

Data are shown as median with interquartile range. Mann-Whitney U test

There were no statistically significant differences between the psoriasis and healthy control group in terms of age, sex distribution, BMI, hsCRP levels, leukocyte count, CMV IgG levels, or CMV IgG serostatus. Additionally, no significant differences were observed in the phenotypic characteristics of MAIT cells, as assessed by flow cytometry based on the surface expression of CD4/CD8 coreceptors. Baseline characteristics of the 38 participants whose TCR repertoires were analysed are summarised in Table 23.

Table 23. Study participants' characteristics

	PV (N = 26)	HC (N = 12)	P
Age	36 (29 – 47)	33 (29 – 46)	0.949*
Sex (M/F)	19/7	11/1	0.393**
BMI	29.43 (25.67 – 32.22)	27.45 (26.24 – 30.18)	0.627*
hsCRP (mg/L)	0.88 (0.56 – 1.66)	1.4 (0.65 – 1.99)	0.389*
L (N x10^9/L)	7.4 (6.3 – 8.1)	6.35 (5.43 – 7.13)	0.079*
CMV IgG (U/mL)	89.7 (5 – 116)	92.95 (72.3 – 106.6)	0.609*
CMV IgG (pos/neg)	19/7	10/0	0.084**
PASI	9 (5.1 – 23)	-	-
Disease duration (years)	9 (5 – 15)	-	-

*Continuous data are shown as median (interquartile range). BMI - body mass index, hsCRP – high sensitivity C-reactive protein, L – leukocyte count, CMV – cytomegalovirus; PASI – psoriasis area and severity index * Mann-Whitney U test, ** Fisher's Exact Test*

4.6.2. Pre-filtering of clonotypes and sample cohorts

Clonotype filtering based on variable domains was applied to identify clonotypic transcripts encoding the canonical MAIT TCRVα7.2 chain, as well as the most prevalent clonotypes in TCRβ chains. MAIT cells are specifically defined by the TRAV1-2 gene segment within the TCRα chain, distinguishing them from other MR1-reactive (186,207,231) cells,

which commonly express non-TRAV1-2 variants. Therefore, TRAV1-2 clonotypes were extracted and analysed alongside the full TRA repertoire to distinguish MAIT-specific profiles. The TCRβ repertoire of MAIT cells, although diverse, exhibits a preferential enrichment in TRBV6 and TRBV20 gene families. To capture the most common TCRβ features of MAIT cells while preserving a comprehensive view of TRB diversity, analyses were performed across the complete TCRβ repertoire and individually focused on the most frequently represented TRBV segments (TRBV20-1, TRBV6-1, TRBV6-2, TRBV6-4, and TRBV4-2).

For age-related correlation analyses, the three youngest psoriasis patients (younger than any participant in healthy cohort) were excluded to minimize age-related variability and enhance comparability between the psoriasis and control group. In addition, as only one female participant was present in healthy control group, contrasting seven in PV group, additional analyses were carried out on male subjects only, to account for potential sex-related biases.

4.6.3. Gene usage composition in TRA and TRB repertoires

The TRA repertoires exhibited substantial diversity, with 47 distinct TRAV gene segments contributing to the construction of TCRα chains. As expected, the canonical TRAV1-2 variant was predominant, accounting for a median of 77 % of repertoires, ranging from 61 to 94 % across samples. Other frequently observed TRAV variants included TRAV2, TRAV12-1, TRAV13-2, and TRAV1-1 (Table 24, Figure 54 A). Although 47 distinct TRAV segments were identified, only 16 were present in over 90% of samples, of which TRAV1-2, TRAV13-2, and TRAV4 were consistently detected in all repertoires. Similarly, the TRAJ gene segments displayed broad diversity, with 55 distinct segments utilized in the construction of CDR3a loops. The TRAJ33 variant was the most prevalent, followed by TRAJ20 and TRAJ12 (Table 24, Figure 54 B), in line with the preferential pairing of these variants with the canonical TRAV1-2 segment. Unlike the TRAV gene distribution, 30 of the 55 TRAJ segments were present in more than 90 % of the repertoires, with TRAJ33 and TRAJ20 appearing in all samples. Correspondingly, the TRAV1-2-TRAJ33 recombination was the most frequent pairing, followed by TRAV1-2-TRAJ12, and TRAV1-2-TRAJ20 (Figure 55). No significant differences in TRAV or TRAJ gene usage were observed in case-control comparisons.

Table 24. The frequencies of top 5 most frequent TRAV/TRAJ gene segments.

	PV (N = 26)	HC (N = 12)	P
TRAV1-2	77.65 (67.78 – 80.9)	74.85 (71.12 – 81.46)	0.765
TRAV2	4.39 (2.98 – 6.22)	3.99 (2.68 – 6.04)	0.789
TRAV12-1	1.22 (0.71 – 1.88)	1.69 (0.92 – 2.07)	0.695
TRAV13-2	1.33 (0.53 – 1.88)	0.8 (0.49 – 1.7)	0.695
TRAV1-1	1.21 (0.6 – 1.75)	0.79 (0.54 – 1.59)	0.54
TRAJ33	64.73 (55.38 – 70.95)	62.96 (57.79 – 67.51)	0.962
TRAJ20	5.16 (3.92 – 6.52)	6.67 (4.26 – 7.0)	0.323
TRAJ12	4.79 (2.82 – 6.95)	5.72 (2.78 – 7.69)	0.519
TRAJ3	1.56 (0.76 – 2.5)	0.85 (0.63 – 1.85)	0.252
TRAJ10	0.97 (0.63 – 2.27)	0.91 (0.56 – 1.32)	0.388

Data are shown as the median percentage with interquartile range. Mann-Whitney U test

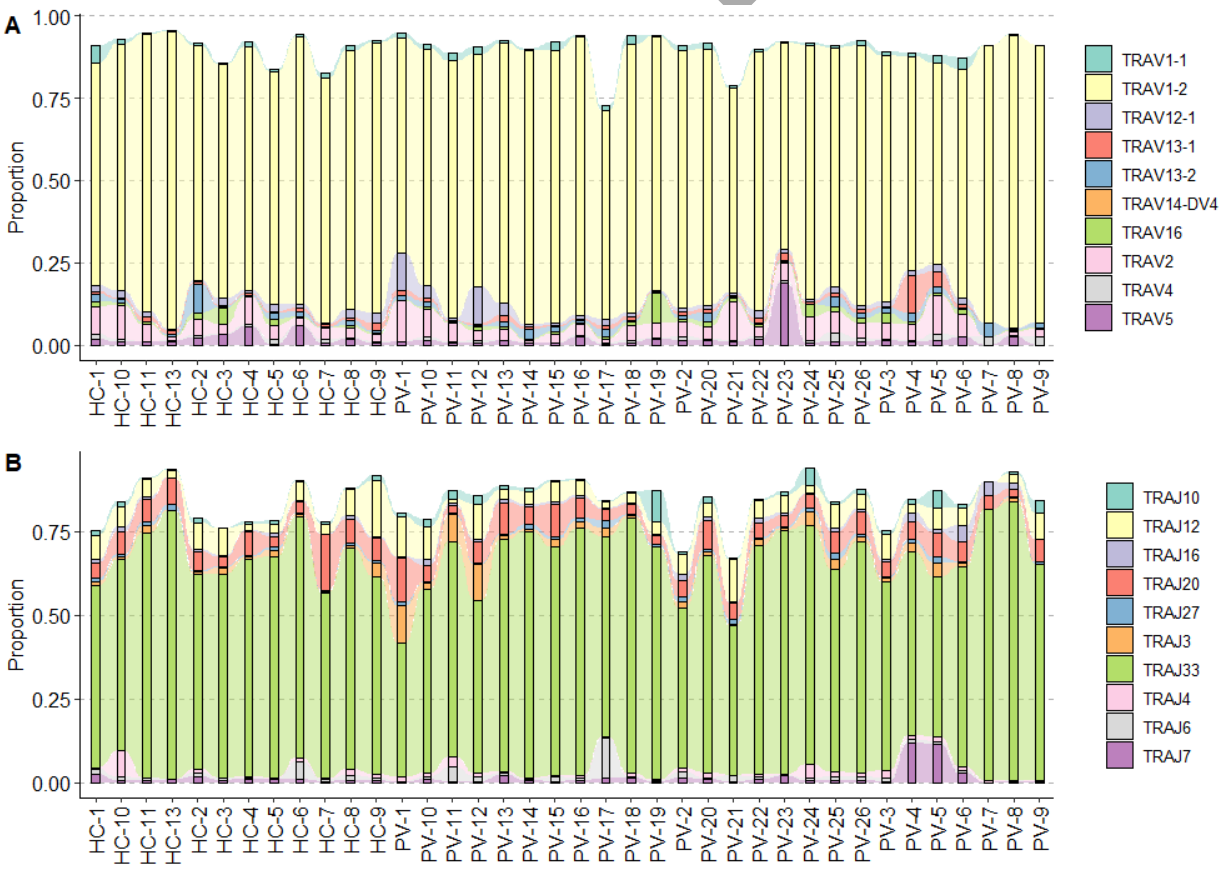

Figure 54. The distribution of the top 10 most frequently observed A) TRAV and B) TRAJ gene segments across all samples.

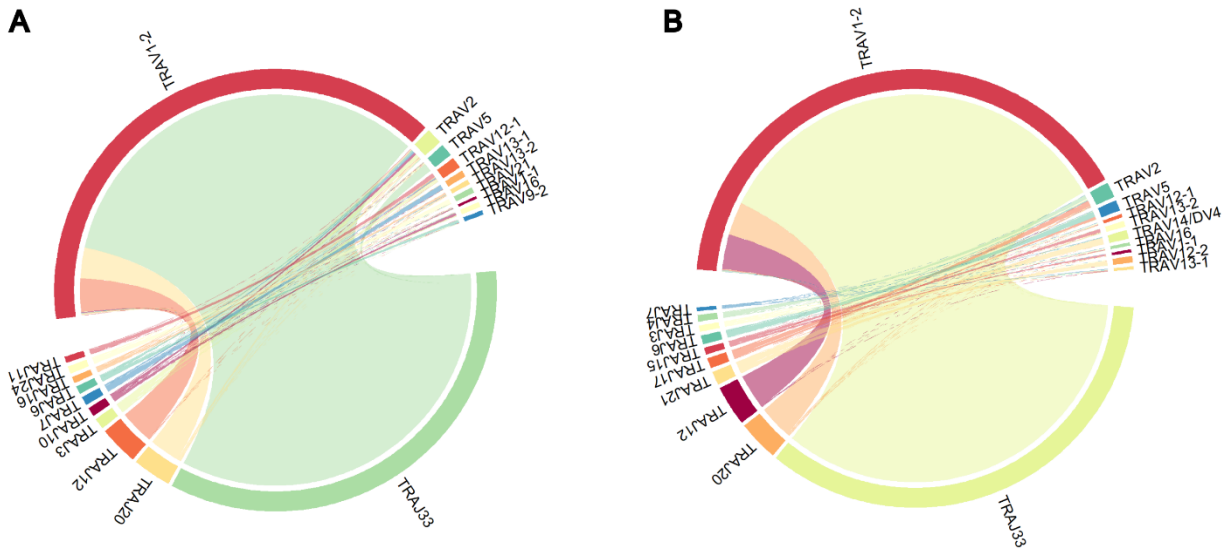

Figure 55. Chord diagram of the top 10 most frequent TRAV and TRAJ variants pairings in A) pooled PV samples, B) pooled HC samples.

In clonotypes containing the canonical TRAV1-2 variant, 47 distinct TRAJ gene segments were found. Consistent with the invariant nature of MAIT TCRα chain, the TRAV1-2 segments predominantly paired with TRAJ33 (Me [IQR]: 84.65 [76.25–88.03]), followed by TRAJ20 (6.28 [4.35–7.51]), and TRAJ12 (6.14 [3.48–9.48]), whereas other TRAJ variants were infrequently recombined, comprising less than 3% of TRAV1-2 clonotypes (Figure 56). These findings align with previous single-cell sequencing analyses of MAIT TCRα TRAV1-2 receptors (184,199).

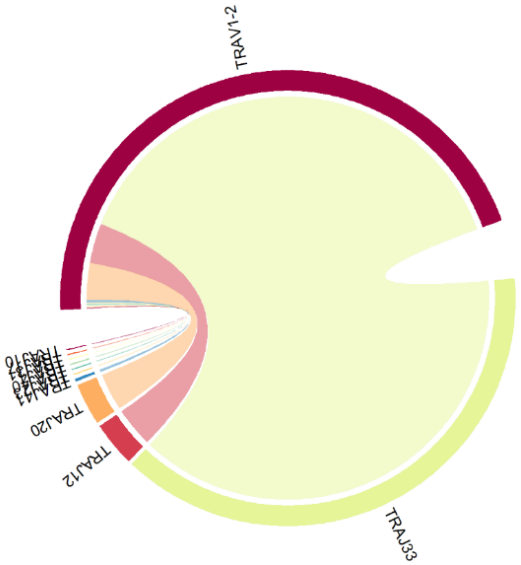

Figure 56. Chord diagram of the top 10 TRAJ gene segment paired with TRAV1-2 variant. *Based on a composite of clonotype data from all participants.*

The TRB repertoires comprised 59 distinct TRBV and 13 TRBJ gene segments, with a notable skewness toward specific TRBV variants. TRBV20-1, TRBV6-4, TRBV6-2, TRBV6-1, and TRBV4-2 were the most frequently represented, collectively comprising over 60% of all TRBV variants within the MAIT TCRβ repertoire, consistent with prior findings (199,205). Among the TRBJ gene segments, those from the TRBJ2 familiy were the most frequently incorporated, with TRBJ2-1 predominating, followed by TRBJ2-7, TRBJ2-2, TRBJ2-3, TRBJ2-3, and TRBJ1-1 (Figure 57). While no statistically significant differences emerged in comparison of TRBV segment usage, the TCRβ repertoires of psoriasis patients displayed higher usage of TRBJ2-7. However, this trend did not remain significant after applying multiple testing correction (Table 25). The most frequently observed TRBV-TRBJ pairings included TRBV6-4-TRBJ2-1, TRBV20-1-TRBJ2-1/1-1/2-7, and TRBV6-2-TRBJ2-1 (Figure 58). Analysis of the rearrangement frequencies between the top 10 TRBV segments and all TRBJ segments revealed significant enrichment of specific pairings in the psoriasis group compared to healthy controls. Notably, TRBV6-4-TRBJ2-4 (Me [IQR]: 0.019 [0.009–0.055] vs. 0 [0–0.006] %, P = 0.003; PV vs. HC), TRBV6-2-TRBJ1-5 (0.675 [0.203–1.046] vs. 0.117 [0.102–0.265] %, P = 0.005), and TRBV6-2-TRBJ1-1 (0.622 [0.348–0.965] vs. 0.263 [0.102–0.417] %, P = 0.013), showed higher representation in psoriasis patients, though these differences did not remain significant after multiple test correction. Further examination of joining segment frequencies paired with the five most common TRBV variants (TRBV20-1, TRBV6-4, TRBV6-2, TRBV6-1, TRBV4-2), revealed significant case-control differences (Table 26). Specifically, TRBV6-4 clonotypes of psoriasis patients contained higher frequencies of TRBJ2-4 and TRBJ1-5, whereas TRBV6-1 clonotypes exhibited reduced pairing with TRBJ2-4 and TRBJ2-6 compaired to healthy repertoires. In addition, TRBV6-2 clonotypes in patients paired more frequently with TRBJ1-5, and TRBV20-1 showed a higher preferential pairing with TRBJ2-7 segment and reduced rearrangement with TRBJ2-1 compared to healthy controls (Figure 58). These findings demonstrate alterations in TRBV-TRBJ pairing frequencies in psoriasis, suggesting potential disease-associated shifts in the TCRβ repertoire.

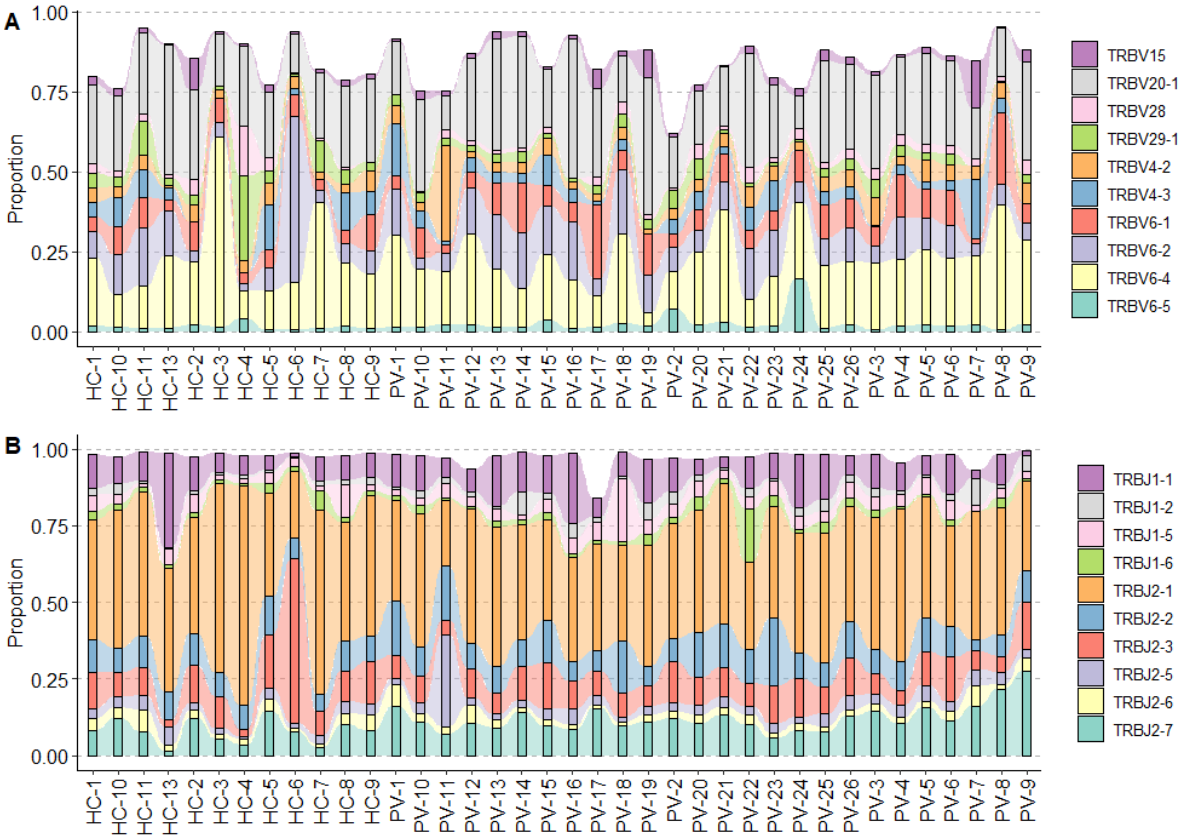

Figure 57. The frequency of top 10 A) TRBV and B) TRBJ segments across all samples.

Table 25. The frequencies of top 10 most frequent TRBV and top 5 TRBJ gene segments.

	PV (N = 26)	HC (N = 12)	P*	P**
TRBV20-1	26.19 (16.62 – 30.36)	24.97 (20.63 – 25.5)	0.626	0.987
TRBV6-4	20.75 (15.75 – 23.78)	18.48 (13.13 – 21.62)	0.540	0.987
TRBV6-2	10.12 (6.54 – 14.58)	7.24 (4.33 – 12.72)	0.265	0.987
TRBV6-1	7.80 (5.83 – 10.34)	6.31 (4.02 – 8.76)	0.128	0.987
TRBV4-2	3.97 (2.94 – 5.33)	3.75 (2.83 – 4.69)	0.561	0.987
TRBV4-3	3.61 (2.84 – 5.22)	4.15 (0 – 8.94)	0.987	0.987
TRBV29-1	2.70 (1.19 – 3.31)	3.60 (2.62 – 6.00)	0.106	0.987
TRBV28	2.16 (1.28 – 3.27)	1.54 (0.56 – 3.28)	0.561	0.987
TRBV15	1.79 (1.32 – 2.52)	1.47 (0.85 – 2.32)	0.405	0.987
TRBV6-5	1.86 (1.33 – 2.16)	1.25 (0.85 – 1.61)	0.062	0.925
TRBJ2-1	38.29 (33.09 – 42.48)	42.67 (38.53 – 50.45)	0.071	0.331
TRBJ2-7	10.86 (9.61 – 14.33)	8.02 (5.01 – 10.58)	**0.01**	0.067
TRBJ2-2	9.46 (7.72 – 13.41)	8.64 (7.82 – 10.34)	0.388	0.679
TRBJ2-3	8.94 (6.99 – 11.95)	10.17 (7.79 – 12.67)	0.480	0.699
TRBJ1-1	9.99 (6.42 – 12.69)	8.01 (6.38 – 9.86)	0.338	0.676

*Data are shown as the median percentage with interquartile range. * Mann-Whitney U test ** Benjamini-Hochberg correction*

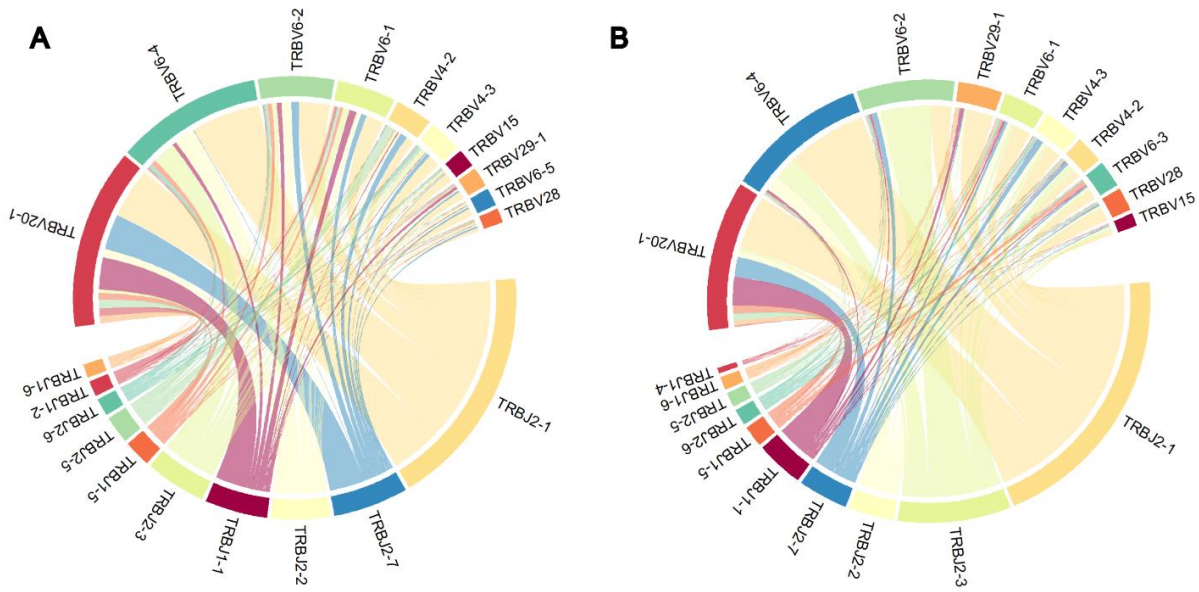

Figure 58. Comparison of TRBV-TRBJ pairing frequencies between psoriasis and healthy repertoires reveals overall similarity with distinct psoriasis-specific alterations. *Chord diagram of pairings between the top 10 TRBV and top 10 TRBJ variants in A) pooled PV (N=26) and B) pooled HC (N=12) samples.*

Table 26. Statistically significant differences in TRBJ pairing frequencies for the four most common TRBV variants

	PV (N = 26)	HC (N = 12)	P
TRBV6-4-TRBJ2-4	0.099 (0.031 – 0.341)	0 (0 – 0.023)	0.007
TRBV6-4-TRBJ1-5	1.546 (0.721 – 3.185)	0.648 (0.289 – 1.305)	0.043
TRBV6-1-TRBJ2-4	0.094 (0 – 0.375)	0.473 (0.155 – 0.758)	0.028
TRBV6-1-TRBJ2-6	1.801 (0.818 – 2.727)	3.830 (2.321 – 5.299)	0.025
TRBV6-2-TRBJ1-5	6.315 (2.341 – 9.086)	3.434 (0.576 – 5.396)	0.034
TRBV20-1-TRBJ2-1	31.174 (24.111 – 37.326)	40.296 (32.939 – 46.422)	0.029
TRBV20-1-TRBJ2-7	21.016 (13.599 – 25.963)	13.646 (9.870 – 18.532)	0.034

Data are shown as the median percentage with interquartile range. Mann-Whitney U test

4.6.4. CDR3α and CDR3β region characteristics in MAIT TCR

The basic repertoire features were assessed through several key metrics such as the count of unique clonotypes for overall diversity, average length of CDR3 regions for antigen-binding specificities, and average clonotype frequency to evaluate distribution. Convergence, reflecting identical amino acid sequences from different nucleotide sequences, was analysed, along with junctional diversity parameters like nucleotide insertions at V-D and D-J junctions and the presence of non-templated nucleotides (NDN) to capture structural variability.

A case-control comparison revealed no significant differences in CDR3α features, either within TRAV1-2 clonotypes or across the entire TCRα repertoire. Similarly, TCRβ repertoire analysis showed no significant differences in clonotypes containing TRBV6-4, TRBV6-2, TRBV6-1, TRBV20-1, or TRBV4-2 segments, nor in the overall TRB repertoire (Table 27).

Spectratyping of TCRα clonotypes showed a broad range of CDR3 lengths, spanning from 9 to 18 amino acids, with a prominent peak at 12 AA (Figure 59 A). Further analysis revealed that this 12-AA peak was primarily due to TRAV1-2 clonotypes (Figure 59 B), consistent with previous findings (206,232). The CDR3 length distributions were similar between psoriasis patients and healthy controls. TCRβ clonotypes ranged from 11 to 20 amino acids, with most concentrated between 13 and 16 AA, peaking at 15 AA (Figure 60 A). TRBV6-4 and TRBV20-1 clonotypes dominated the 13-15 AA range, with CDR3 lengths spanning 13-17 and 12-18 AA, respectively (Figure 60 B, C). TRBV4-2 clonotypes had a narrower distribution, primarily between 14 and 17 AA, with the majority being 15 and 16 AA (Figure 60 D). Similar to TCRα repertoires, no significant differences in CDR3β length were observed between diseased and healthy participants.

Table 27. Basic TRA and TRB repertoire characteristics

	PV (N = 26)	**HC (N = 12)**	**P**
TRA			
Clonotypes (N)	485 (356 – 716)	421 (312 – 641)	0.765
Clonotype frequency (%)	0.21 (0.14 – 0.28)	0.24 (0.16 – 0.32)	0.765
Clonotype geomean frequency (%)	0.05 (0.04 – 0.08)	0.04 (0.04 – 0.06)	0.987
CDR3 length (nt)	36.96 (36.78 – 37.30)	36.71 (36.35 – 37.17)	0.128
NDN size	1.96 (1.78 – 2.18)	1.96 (1.49 – 2.19)	0.672
Convergence	1.205 (1.162 – 1.266)	1.224 (1.204 – 1.228)	0.371
TRB			
Clonotypes (N)	1643 (1102 – 2448)	1640 (1018 – 2186)	0.888
Clonotype frequency (%)	0.06 (0.04 – 0.09)	0.06 (0.05 – 0.09)	0.888
Clonotype geomean frequency (%)	0.02 (0.01 – 0.03)	0.016 (0.015 – 0.018)	0.187
CDR3 length (nt)	43.62 (43.42 – 43.87)	43.77 (43.43 – 43.90)	0.583
Inserted nucleotides (N)	4.04 (3.71 – 4.29)	4.28 (3.92 – 4.85)	0.227
NDN size	12.32 (11.81 – 12.77)	12.43 (11.61 – 12.66)	0.789
Convergence	1.010 (1.008 -1.013)	1.010 (1.007 – 1.018)	0.561

Data are shown as median with interquartile range. NDN- number of nontemplated nucleotides *Mann-Whitney U test*

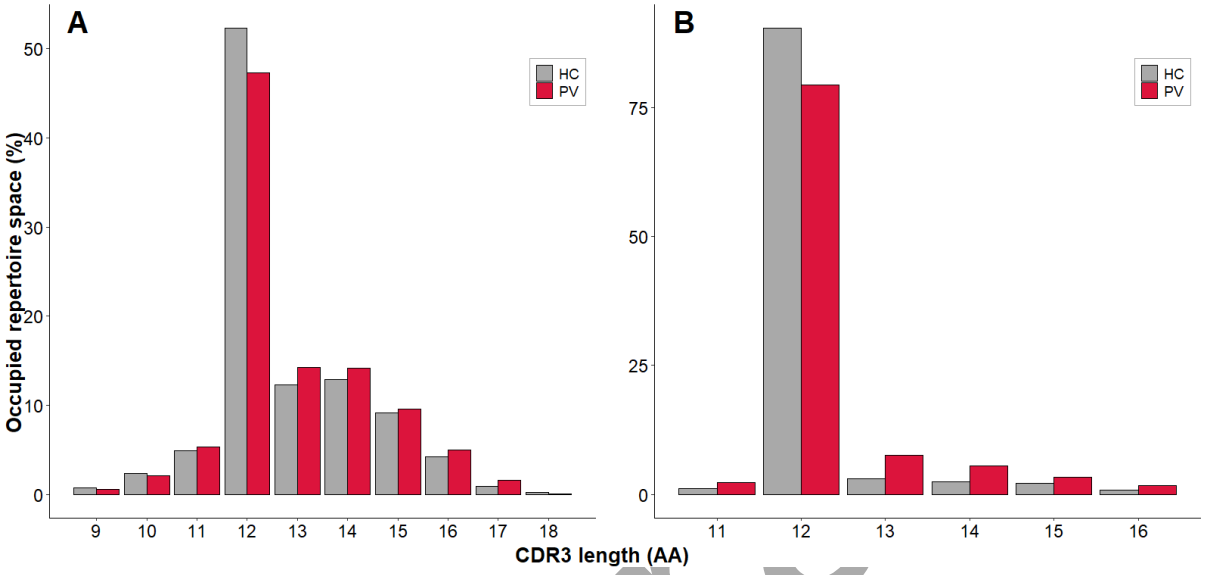

Figure 59. Spectratyping of TCRα clonotypes reveals a dominant 12-amino acid CDR3 region, primarily from TRAV1-2 clonotypes, with similar profiles between psoriasis patients and healthy controls. *A) Spectratype of all TCRα clonotypes, B) Spectratype of TRAV1-2 clonotypes.*

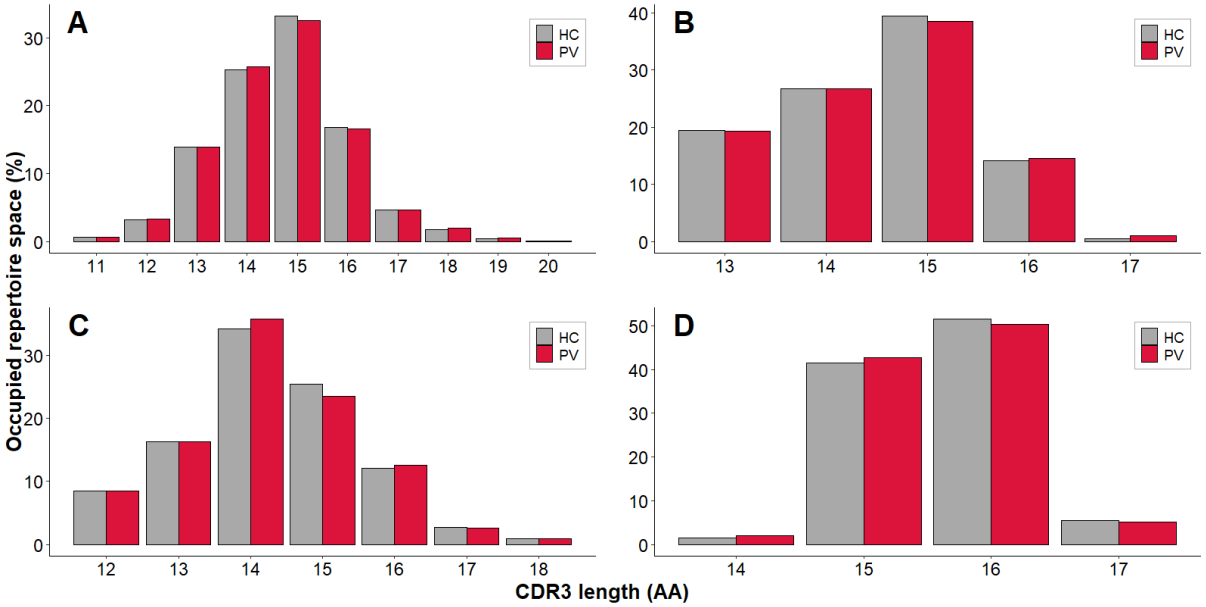

Figure 60. TCRβ clonotypes from psoriasis patients and healthy controls show no differences in CDR3 length, with the TRBV20, TRBV6, and TRBV4 families predominantly contributing to the 13-16 amino acid range. *Spectratype of A) all TCRβ, B) TRBV6-4, C) TRBV20-1, and D) TRBV4-2 clonotypes*

Analysis of the relationship between clinical parameters and clonotype characteristics revealed several significant correlations. In psoriasis patients, a moderate negative correlation was observed between PASI score and the mean number of non-templated nucleotides in TCRα clonotypes (ρ = -0.49, P = 0.013). Further investigation demonstrated a decline in the total count of TCRα and TRAV1-2 clonotypes, which was observed exclusively in male patients, along with a decrease in the CDR3α length of TRAV1-2 clonotypes (Figure 61). Disease severity also displayed a negative trend with the total number of TCRβ clonotypes in male psoriasis patients exclusively, accompanied by a significant reduction in the length of TRBV6-1 clonotypes, driven by a decrease in mean insert size (ρ = -0.518, P = 0.028). Among the five most dominant clonotypic variants, only TRBV6-4 clonotypes displayed a reduction in clonotype number with increasing PASI scores in male patients (Figure 62).

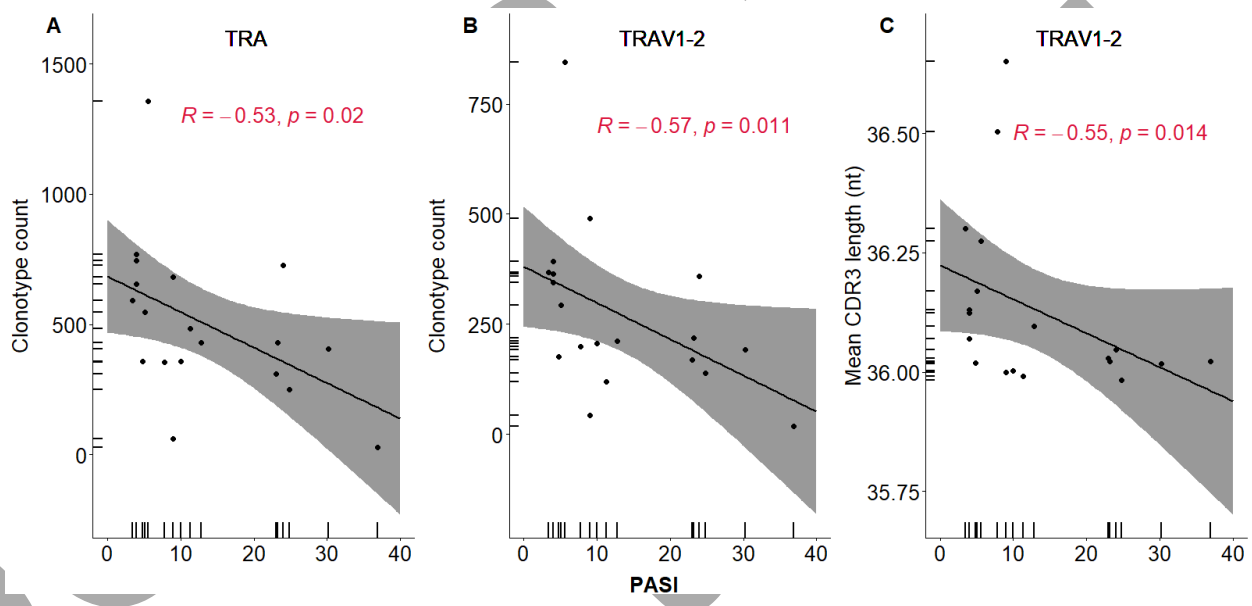

Figure 61. PASI scores in male psoriasis patients correlate negatively with TRA clonotype count and CDR3 length. *PASI scores correlate negatively with A) total TRA clonotype count, B) TRAV1-2 clonotype count, and C) TRAV1-2 mean CDR3 length. Spearman's correlation coefficient*

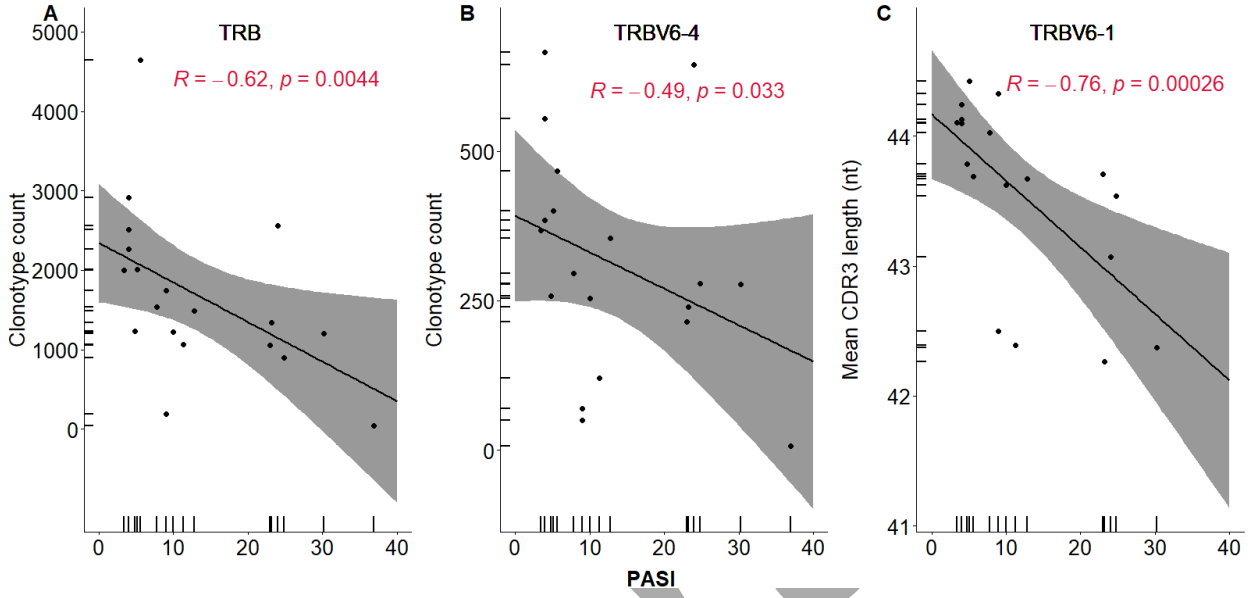

Figure 62. PASI scores correlate negatively with TRB clonotype count and CDR3 length in male psoriasis patients. *PASI scores correlate negatively with A) total TRB clonotype count, B) TRBV6-4 clonotype count, and C) TRBV6-1 mean CDR3 length. Spearman's rank correlation coefficient.*

The TCRβ repertoire showed age-related changes in both psoriasis-affected and healthy participants, with more pronounced effects in the psoriasis cohort. Namely, the number of unique TCRβ clonotypes significantly declined with age in psoriasis patients, while a similar, non-significant trend was seen in healthy individuals (Figure 63 A). Analysis of TRBV subsets revealed significant age-associated reductions in TRBV4-2 (ρ = -0.534, P = 0.009), TRBV6-2 (ρ = -0.491, P = 0.017), TRBV20-1 (ρ = -0.541, P = 0.008), and TRBV6-4 (ρ = -0.631, P = 0.001) clonotypes in psoriasis, with TRBV6-4 also showing a similar decline in healthy participants (ρ = -0.604, P = 0.037). Interestingly, psoriasis patients exhibited a notable age-related decrease in TCRβ clonotype convergence (Figure 63 B), defined as distinct nucleotide sequences encoding identical amino acid sequences. This reduction, absent in healthy participants, was especially marked in TRBV6-4 clonotypes (Figure 63 C). Collectively, these results suggest that aging has a greater impact on the MAIT TCRβ repertoire in psoriasis patients, leading to reduced clonotype diversity and convergence.

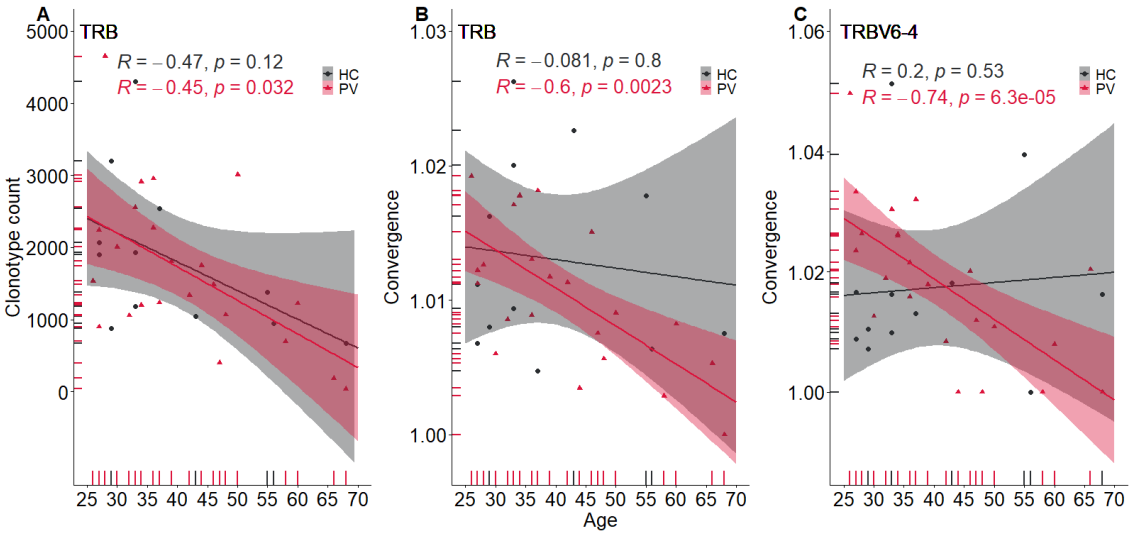

Figure 63. Age-related reduction in TRB clonotype count and convergence in psoriasis vs. healthy controls. *A) Unique TRB clonotype count decreases significantly with age in psoriasis patients (PV) while the decline in healthy controls (HC) remains non-significant. Convergence shows a marked age-related decline in psoriasis patients in B) all TCRβ clonotypes, and C) TRBV6-4 subset. Spearman's rank correlation coefficient.*

4.6.5. Clonal distribution and diversity metrics of TCRα and TCRβ repertoires

The structural complexity of the TCRα and TCRβ repertoires was analysed using a framework similar to that applied for γδ TCR repertoires, incorporating both diversity indices and frequency-based clonotypic classification. Clonotypes were stratified into 'hyperexpanded' (>5%), 'large' (0.5–5%), 'medium' (0.05–0.5%), and 'small' (<0.005%) categories to identify major shifts in repertoire composition, while diversity indices provided a detailed insights into repertoire dynamics. Specifically, Efron-Thisted and Chao1 indices were used to estimate the richness and presence of rare clonotypes, while the Shannon-Wiener, Inverse Simpson, and D50 indices were applied to assess the clonotype distribution, dominance, and clonal expansion.

TCRα repertoires

In the analysis of TCRα repertoires diversity, no statistically significant differences emerged between psoriasis patients and healthy participants. Within the psoriasis cohort, however, age exhibited negative correlations with Efron-Thisted, Chao1, Shannon-Wiener and Inverse Simpson indices, reflecting a reduction in the number of rare clonotypic variants and

an increase in dominant clonotypes (Table 28). Interestingly, these age-associated reductions were not present in age-matched healthy controls. When the clonotypes were examined within specific frequency groups, these age-associated trends were not observed, which suggests that age may influence TCRα repertoire composition more subtly, compatible with the restricted and relatively invariant nature of MAIT TCRα chains. Further analysis of TRAV1-2 clonotypes, a characteristic feature of MAIT cells, displayed only a modest negative correlation between age and Shannon-Wiener index in psoriasis patients, with a gradual reduction specifically within the 'medium' clonotype group. In healthy controls this age-associated decrease was more evident in the 'small' clonotype group (ρ = -0.685, P = 0.014). Disease duration or disease severity, as measured by the PASI score, did not show significant associations with TCRα repertoire diversity in psoriasis patients. Taken together, age-related reductions in TCRα repertoire diversity were more pronounced in psoriasis, suggesting age-associated shifts in PV are not mirrored in healthy aging.

Table 28. Statistically significant correlations between age and diversity indices or frequency groups in total TRA and TRAV1-2 repertoire of psoriasis patients

	Index or frequency group	ρ	P
TRA	Efron-Thisted	-0.560	0.005
	Chao1	-0.545	0.007
	Shannon-Wiener	-0.577	0.004
	Inverse Simpson	-0.430	0.041
TRAV1-2	Shannon-Wiener	-0.427	0.042
	Medium	-0.547	0.007

Spearman correlation analysis, N (PV) =23; excluding the three youngest patients, N(HC)=12

TCRβ repertoires

The TCRβ repertoires showed more pronounced age-associated reshaping compared to TCRα repertoires. In psoriasis patients, age was significantly linked to an increase in hyperexpanded TCRβ clonotypes, unlike in healthy group (Figure 64). This expansion was accompanied by a reduction in the 'small' and 'medium' clonotype groups, suggesting a shift towards clonal dominance (Table 29). This shift was further supported by significant declines in Shannon-Wiener and Inverse Simpson indices, while negative correlations with Efron-Thisted and Chao1 indices highlighted a loss of low frequent clonotype species. Furthermore, in male psoriasis patients, the frequency of hyperexpanded clonotypes also showed a moderate

correlation with higher PASI scores (ρ = 0.475, P = 0.04), suggesting that clonal expansion may, to some extent, be associated with linked severity in this subgroup. Examining specific TRBV clonotypes, age was associated with increased hyperexpanded clonotypes within TRBV6-4, TRBV6-2, and TRBV20-1 clonotypes in the PV cohort, although these associations were less robust than those observed in the overall TCRβ repertoire (Table 29). Consistent with the trend toward clonal dominance, negative correlations were also noted between age and diversity indices (Shannon-Wiener and Inverse Simpson) within these clonotypes, with TRBV20-1 showing the strongest age-related decline in diversity (Figure 65). Interestingly, age-related reductions in diversity were also seen in TRBV6-4 clonotypes among healthy controls, as evidenced by declines in Efron-Thisted (ρ = -0.590, P = 0.043) and Chao1 (ρ = -0.604, P = 0.037) indices, suggesting that constriction in rare TRBV6-4 clonotypic variants may be a normal aspect of ageing. Overall, the TCRβ repertoires in healthy controls did not exhibit significant age-associated diversity changes, underscoring the distinct age-related repertoire alterations in psoriasis compared to healthy individuals.

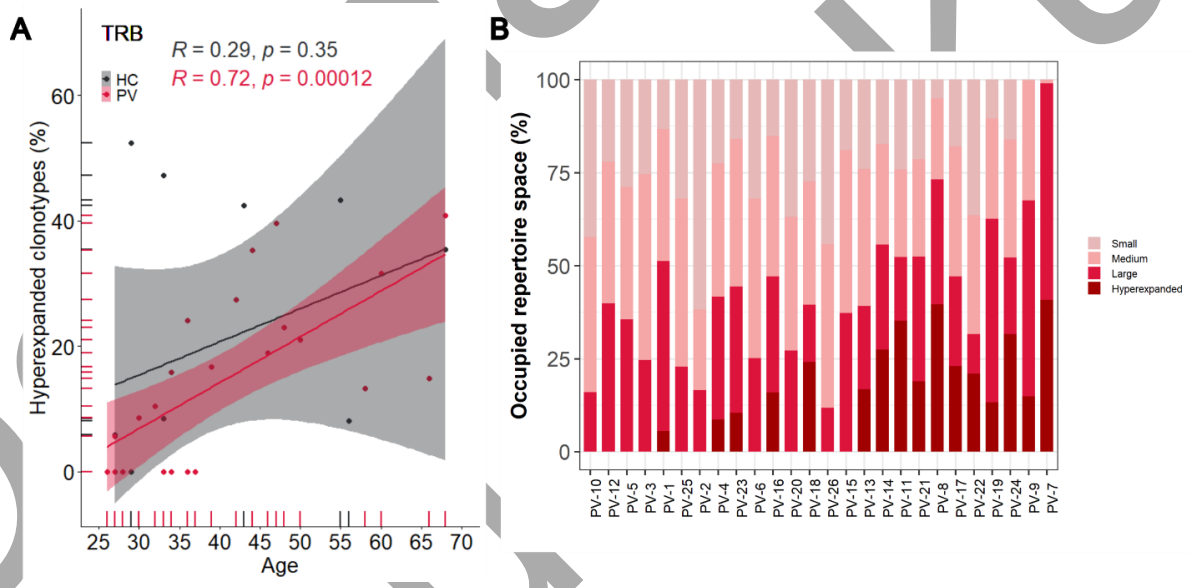

Figure 64. Frequency of hyperexpanded TCRβ clonotypes increases with age in psoriasis patients. *A) Spearman's correlation shows a significant positive association between age and hyperexpanded TCRβ clonotypes frequency in psoriasis (PV), B) Stacked bar plot illustrating clonotype frequency categories ('small' (<0.005%), 'medium' (0.05–0.5%), 'large' (0.5–5%), and 'hyperexpanded' (>5%)) across psoriasis patients, ranked by age.*

Table 29. Statistically significant correlations between age and diversity indices or frequency groups in total TRB and TRBV variants -filtered repertoires of psoriasis patients

	Index or frequency group	ρ	P
TRB	Efron-Thisted	-0.483	0.020
	Chao1	-0.448	0.032
	Shannon-Wiener	-0.676	3.95×10^{-4}
	Inverse Simpson	-0.672	4.46×10^{-4}
	Small	-0.479	0.021
	Medium	-0.625	0.001
	Hyperexpanded	0.717	1.2×10^{-4}
TRBV4-2	Efron-Thisted	-0.494	0.019
	Chao1	-0.465	0.029
	Medium	-0.547	0.007
TRBV6-2	Efron-Thisted	-0.487	0.019
	Chao1	-0.491	0.017
	Shannon-Wiener	-0.461	0.027
	Inverse Simpson	-0.427	0.042
	Medium	-0.491	0.017
	Large	-0.482	0.020
	Hyperexpanded	0.544	0.007
TRBV6-4	Efron-Thisted	-0.618	0.002
	Chao1	-0.631	0.001
	Shannon-Wiener	-0.584	0.003
	Inverse Simpson	-0.486	0.019
	Small	-0.489	0.018
	Medium	-0.676	4×10^{-4}
	Hyperexpanded	0.591	0.003
TRBV20-1	Efron-Thisted	-0.508	0.013
	Chao1	-0.541	0.008
	Shannon-Wiener	-0.666	5.22×10^{-4}
	Inverse Simpson	-0.625	0.010
	Small	-0.429	0.041
	Medium	-0.650	7.84×10^{-4}
	Hyperexpanded	0.563	0.005

Spearman's rank correlation coefficient. N (PV) =23; excluding the three youngest patients, N(HC)=12

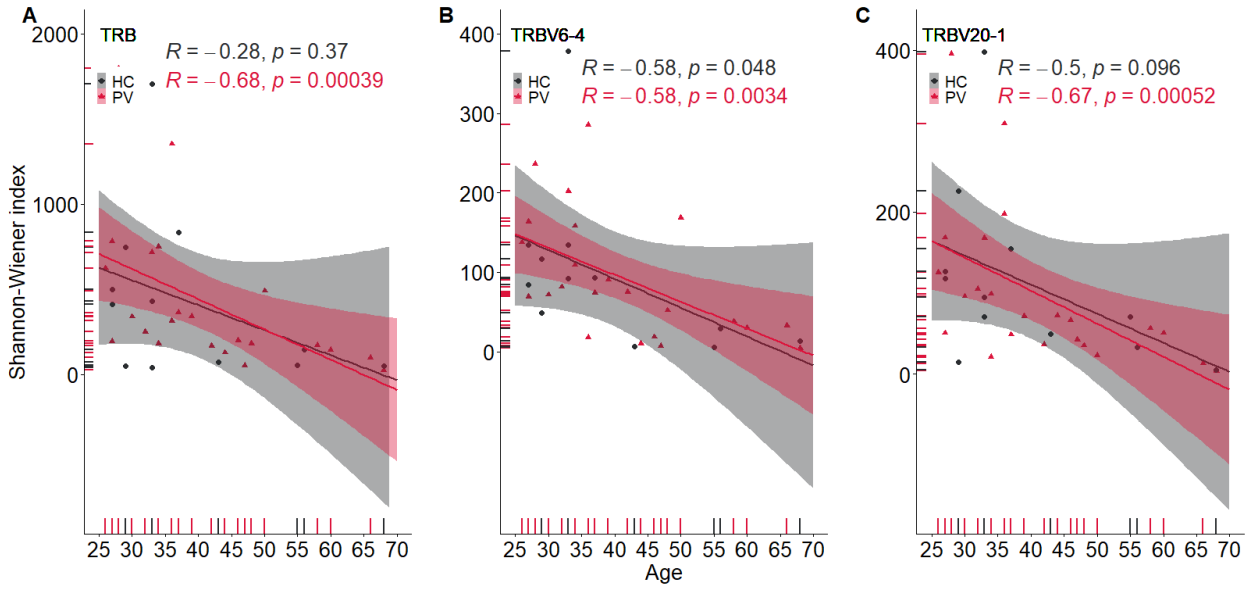

Figure 65. Age-related decline in TCRβ clonotype diversity in psoriasis patients. *Spearman's correlation analysis shows a significant negative association between age and Shannon-Wiener diversity index in psoriasis (PV) and weaker or non-significant correlations in healthy controls (HC) across A) the complete TCRβ repertoire, B) TRBV6-4, and C) TRBV20-1 clonotypes*

4.6.6. The analysis of public and disease-associated TCRα and TCRβ clonotypes

A total of 12,196 unique TCR α clonotypes were identified across all samples, with 8,913 found in PV samples and 3,944 across healthy repertoires. As anticipated, TCRα clonotypes were frequently shared among study participants, with 8.76 % (1069/12196) classified as public clonotypes, appearing in at least two repertoires. The degree of publicness was comparable between the groups, with 8 % (713/8913) shared clonotypes in PV and 7.33 % (289/3944) in healthy group. The ten most frequent clonotypes, present in at least 37 of 38 repertoires, accounted for substantial portions of individual repertoires, cumulatively representing more than 40 % of TCRα sequences (Figure 66 A). Publicness was further assessed using the Jaccard index (JI), which measures the proportion of shared clonotypes between two samples relative to their total clonotype counts. The analysis revealed a median JI value of 0.054, indicating that approximately 5% of TCRα clonotypes were shared between samples (IQR: 0.048 – 0.057) (Figure 66 B). The frequency of shared TRAV1-2 clonotypes was significantly higher, with a median JI value of 0.113 (IQR: 0.101 – 0.119) (Figure 66 C). Five clonotypes were found in all repertoires, characterised by conserved TRAV1-2-TRAJ33, or, in one case, TRAV1-2-TRAJ20 recombination, and a CDR3 length of 12 amino acids, a

hallmark feature of MAIT cells (184). Several clonotypes were detected exclusively in subsets of psoriasis patients and absent in healthy controls; however, a similar pattern of unique clonotypes was also observed in healthy repertoires, indicating no definitive association of specific clonotypes with psoriasis, underscoring the lack of disease-specific MAIT TCRα clonotype signatures.

TCRβ repertoires demonstrated greater diversity than TCRα repertoires, with 60,379 unique clonotypes detected across all samples: 42,267 in psoriasis patients and 20,343 in healthy controls. TCRβ repertoires were slightly more private, with public clonotypes comprising 6.22 % (3757/60379) of all clonotypes, 5.28 % (2230/42267) in PV samples, and 4.33 % (880/20343) in healthy repertoires. Furthermore, the top 10 ten most shared clonotypes (present in at least 20 out of 38 samples) occupied only small proportions of individual repertoires, typically less than 1%, reflecting the high diversity and predominantly private nature of MAIT TCRβ repertoires (Figure 67 A). The median Jaccard index for TRB clonotypes was 0.008 (IQR: 7.58×10^{-3} – 0.010), indicating that, on average, 0.8 % of clonotypes were shared between any two samples. Among the individually analysed TRBV groups, TRBV20-1 clonotypes exhibited the lowest median Jaccard index (Me [IQR]: 0.005 [0.004 – 0.006]) (Figure 67 B). In contrast, TRBV6-4 clonotypes displayed the most public character with a median Jaccard index of 0.017 (IQR: 0.013 – 0.021) (Figure 67 C). The Jaccard index for TRBV4-2, TRBV6-1, and TRBV6-2 clonotypic variants was similar, around 0.006, indicating limited clonotype sharing. No significant differences were found in Jaccard index values across the total TCRβ repertoire or within the most frequently expressed TRBV variants. However, Jaccard index negatively converged with age in psoriasis patients, but not in healthy controls, in total TCRβ ($\rho = -0.677$, $P = 3.9 \times 10^{-4}$), TRBV6-4 ($\rho = -0.692$, $P = 2.56 \times 10^{-4}$), TRBV6-2 ($\rho = -0.681$, $P = 3.5 \times 10^{-4}$), TRBV20-1 ($\rho = -0.589$, $P = 0.003$), and TRBV4-2 ($\rho = -0.643$, $P = 0.001$) clonotypes, pointing to a significant reduction in shared clonotypes with advancing age, which may partially explain the negative association between age and convergence described earlier.

Several clonotypes were more frequently present in a higher number of psoriasis patients (at least 30%) and were either absent or rarely found in healthy controls. One such clonotype, CASSDSGGSYNEQFF, previously identified in our earlier MAIT TCRβ repertoire study as commonly shared among psoriasis patients, was detected in 15 psoriasis samples but only in two healthy repertoires in the current analysis. Additionally, several clonotypes that were more prevalent in psoriasis samples in this analysis had also been reported in previous studies examining the peripheral blood and skin of psoriasis patients (68,95,97,233),

suggesting possible disease-specific clonotypic patterns. Furthermore, four clonotypes classified as 'psoriasis-exclusive' in our earlier study were again more common in psoriasis samples than in healthy controls (4–5/26 in PV vs. 1/12 in HC), with the CASSVTSGGADTQYF clonotype maintaining its PV-exclusive status, appearing in four psoriasis samples and remaining absent in all healthy repertoires. However, Fisher's exact test did not identify any clonotype as significantly enriched in either cohort, suggesting limited statistical power to establish specific clonotypic variants as disease associated. In addition, some clonotypes found to be enriched in healthy repertoires but previously reported in lesional skin (95) or CLA^+ fractions of circulating cells (68) in psoriasis patients complicate the interpretation of disease-specific overlaps (Table 30). Given these complexities, it is important to note that the observed overlap between MAIT clonotypes in this study and those reported in prior studies may reflect similarities with TCRβ clonotypes of conventional T cells rather than true MAIT cell repertoires, warranting caution in interpretation.

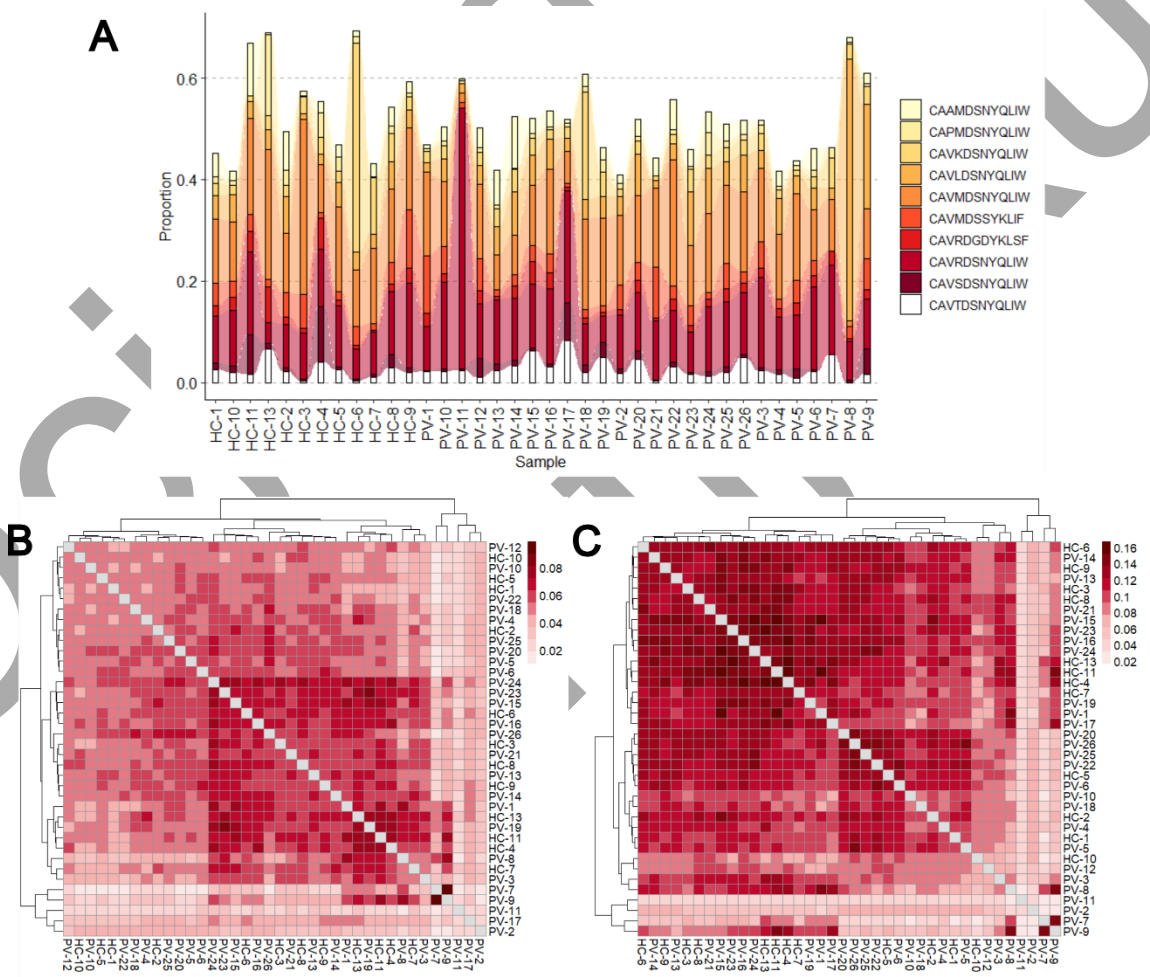

Figure 66. MAIT TRAV1-2 clonotypes are highly shared across repertoires and occupy significant portions of individual repertoires. *A) stacked barplot of the proportion of the top*

10 most frequently shared TRAV1-2 clonotypes across individual repertoires. Heatmap of Jaccard index showing clonotype sharing across B) all TRA and C) TRAV1-2 variants.

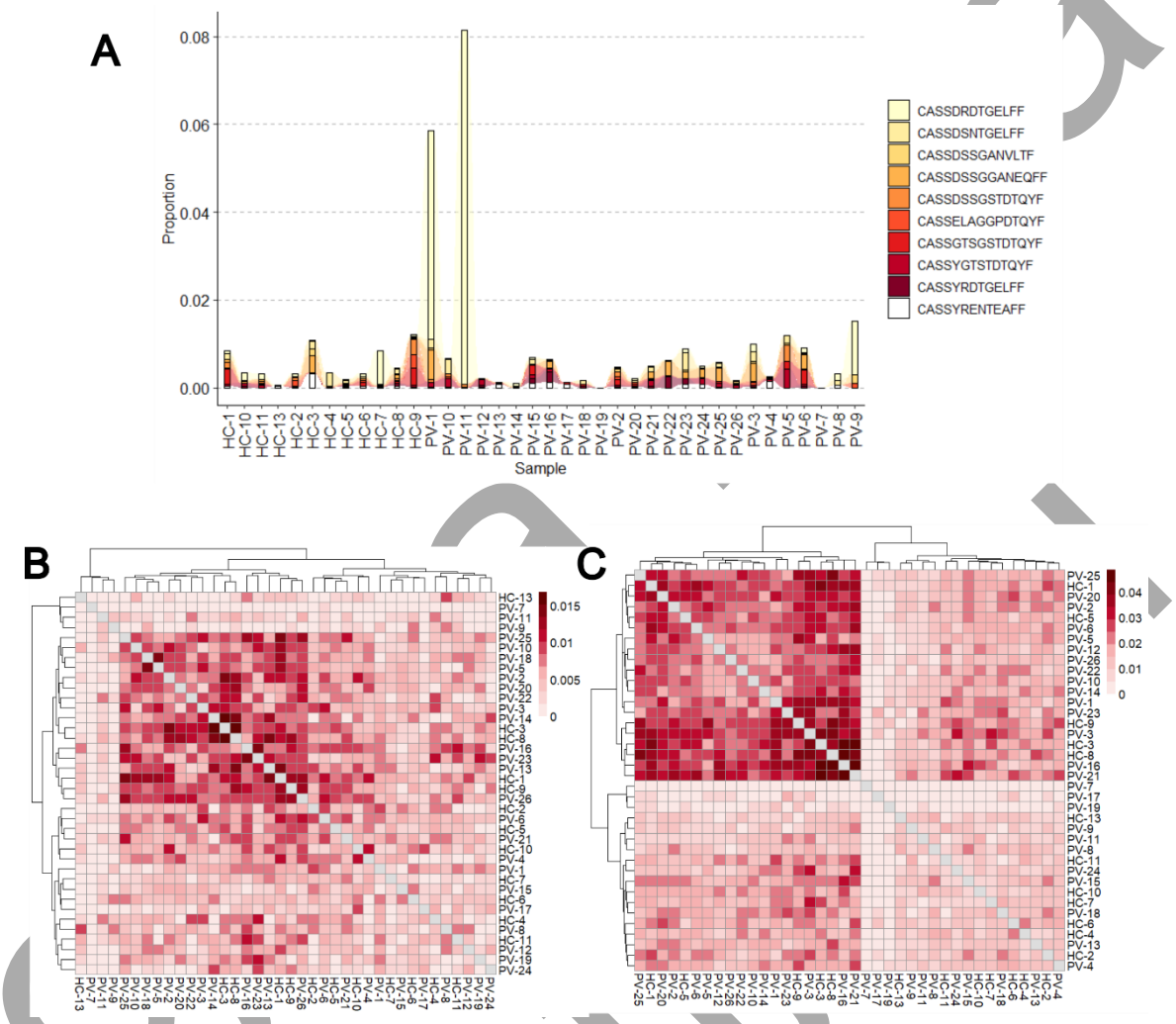

Figure 67. Low-frequency distribution and differential sharing of public MAIT TCRβ clonotypes. *A) Proportion of the top 10 most shared TCRβ clonotypes across individual repertoires. Jaccard index heatmap depicting clonotype sharing patterns for B) TRBV20-1 and C) TRBV6-4 variants.*

Table 30. TCRβ clonotypes with differential presence in psoriatic (PV) versus healthy (HC) repertoires

Clonotype	TRBV	TRBJ	PV frequency	HC frequency	Ref.	Fold change
CASSDSGGSYNEQFF	TRBV6-4	TRBJ2-1	15/26	2/12	(68) †, (205) ‡	3.5*
CASSDSSGGYNEQFF	TRBV6-4	TRBJ2-1	12/26	1/12	-	5.5*
CASSQDRGGQETQYF	TRBV4-2	TRBJ2-5	8/26	0/12	-	NA
CASSGTNTGELFF	TRBV6-4	TRBJ2-2	7/26	0/12	(68) §, (97) #	NA
CSVGTGETEAFF	TRBV29-1	TRBJ1-1	7/26	0/12		NA
CASSQDQGSGANVLTF	TRBV4-3	TRBJ2-6	2/26	7/12	-	7.6**
CASSQRTSGGGTDTQYF	TRBV4-3	TRBJ2-3	0/26	4/12	(95) §	NA
CASSYSEGSGANVLTF	TRBV6-5	TRBJ2-6	0/26	4/12	-	NA
CASSYSSYNEQFF	TRBV6-2	TRBJ2-1	1/26	5/12	(68)†	10.8**

*The fold change represents the ratio of PV to HC prevalence (*PV frequency / HC frequency) or the inverse ratio for HC prevalence (**HC frequency / PV frequency). 'NA' indicates cases where no occurrences were observed in the comparison group. †Clonotypes identified in CLA⁺ circulating T cells, ‡Clonotypes enriched in circulating psoriasis MAIT TCRβ, § Clonotypes found in lesional skin, #Clonotypes found in circulating T cells.*

4.7. Transcriptomic features of circulating MAIT cells

Transcriptomic profiles of circulating MAIT cells were assessed using a commercial panel targeting 395 genes associated with T cell activation, effector functions, adhesion, migration, differentiation, TCR signalling, antigen-presentation, and migration. The sequencing libraries were prepared from 24 RNA samples obtained from flow-sorted MAIT cells of 12 psoriasis patients and 12 healthy controls. Of these, 23 libraries met concentration thresholds and were successfully sequenced. Both the sequencing run and individual samples passed quality control metrics, with an average Phred score >30 for 93.48 ± 0.38 % of bases and an average alignment rate of 76.09 ± 5.55 %. Two healthy control samples were excluded from downstream analysis due to low total read counts (138,589 and 215,844), which were significantly below the average read count of 1,431,200. Detailed sequencing characteristics are provided in Table 31.

Table 31. Basic sequencing metrics

	PV (N = 11)	HC (N = 10)	P*
Sequencing reads	1,520,573 (1,241,288 – 1,764,770)	1,663,668 (1,287,420 – 1,845,607)	0.499
> Q30 bases (%)	93.59 (93.36 – 93.70)	93.37 (92.85 – 93.51)	0.227
Aligned reads (%)	77.59 (73.47 – 81.27)	74.96 (72 – 78.94)	0.414

Data are shown as median (interquartile range). Mann-Whitney U test

The baseline characteristics of the subjects showed no significant differences between the PV and HC groups, however, psoriasis patients in this cohort demonstrated a higher leukocyte count. Descriptive statistics participant characteristics are provided in Table 29.

Table 32. Baseline subjects' characteristics

	PV (N = 11)	HC (N = 10)	P
Age	37 (31.5 – 35)	35 (33 – 40)	0.777
Sex (M/F)	8/3	8/2	1
BMI	27.72 (23.95 – 30.49)	26.44 (26.08 – 27.14)	0.778
hsCRP (mg/L)	0.9 (0.55 – 1.29)	1.4 (0.7 – 2.37)	0.223
L (N x10^9/L)	6.5 (6.05 – 8.45)	5 (4.63 – 6.4)	**0.037**
PASI	5.4 (4.9 – 8.1)	-	-
Disease duration (years)	6 (3 – 10)	-	-

*Continuous data are shown as median (interquartile range). BMI - body mass index, hsCRP – high sensitivity C-reactive protein, L – leukocyte count, PASI – psoriasis area and severity index * Mann-Whitney U test, ** Fisher's Exact Test*

In addition, the composition of the MAIT cell compartment did not differ between the healthy and diseased groups (Table 33).

Table 33. MAIT compartment composition

	PV (N = 11)	HC (N = 11)	P
% $CD8^+$ of MAIT	70.1 (66.8 – 76)	71.4 (66.9 – 82.4)	0.751
% DN of MAIT	25.8 (22.7 – 27.9)	18.9 (15.2 – 28.9)	0.245
% $CD4^+$ of MAIT	1.5 (0.6 – 3.1)	1.9 (1.2 – 3.3)	0.342
% DP of MAIT	0.9 (0.5 – 1.2)	1.1 (0.6 – 1.5)	0.418

Data are shown as median (interquartile range). Mann-Whitney U test

4.7.1. Analysis of differentially expressed genes

Differential expression analysis using DESeq2 began with an essential pre-filtering step to exclude low-count transcripts. Transcripts were retained if they had a minimum of 10 counts

in at least five samples within either the psoriasis or control group. This filtering process reduced the dataset to 298 genes, which were subsequently analysed for differential expression.

The analysis found no statistically significant differences in gene expression in MAIT cells between psoriasis samples and healthy controls. However, further examination uncovered genes strongly linked to age and clinical markers of the disease. Notably, psoriasis patient age showed strong positive links with the expression of *CD70*, *TNRFSF9*, *CDKN2A* (Figure 68), and *CXCR5*, while *EIF2AK2* had a strong negative association. The age-related rise in *CDKN2A*, which encodes $p16^{INK4a}$, a widely recognised marker of cellular senescence (234–236), underscores the potential for aging-related immune dysregulation to manifest earlier in MAIT cells in the context of psoriasis. In addition, the associations of *CD70* and *TNRFSF9* with age suggest that these genes reflect persistent immune activation, characteristic of the chronic inflammatory state observed in psoriasis. Interestingly, gene expression dynamics also reflected changes in disease severity. For example, *GZMB* (granzyme B), a key effector molecule involved in cytotoxicity, demonstrated a significant decline in expression with increasing PASI scores, accompanied by reductions in *HLA-DRB1* and lowly-expressed *CXCR2* (Figure 69).

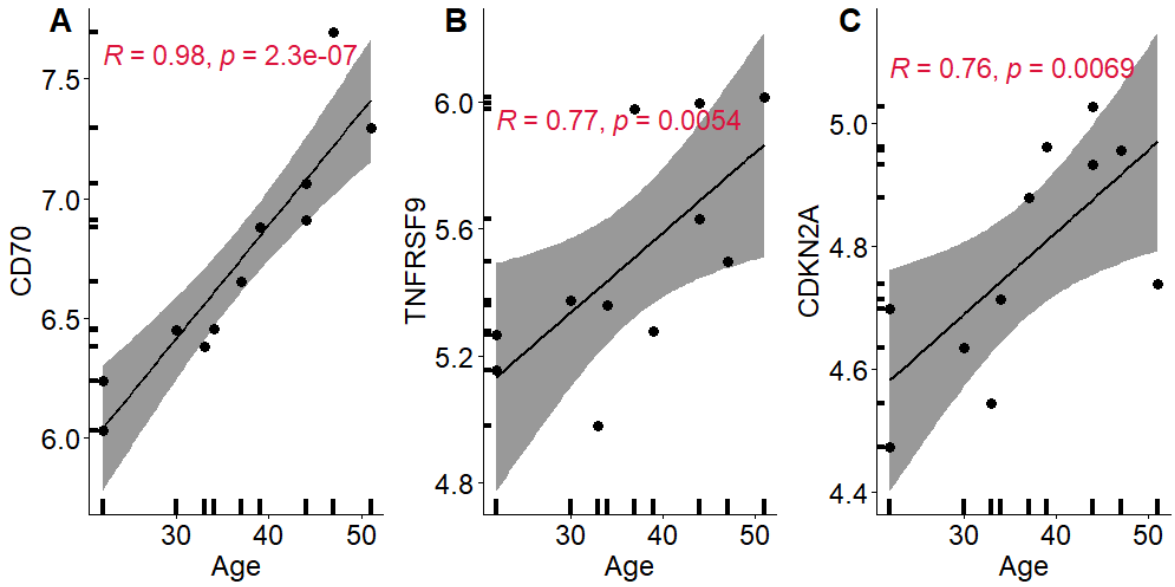

Figure 68. The expression of *CD70*, *TNFRSF9*, and *CDKN2A* increases with age in psoriasis patients. *Correlation plots demonstrate the Spearman's rank correlation between patients' age and the expression levels of A) CD70, B) TNFRSF9, and C) CDKN2A. The y-axis represents regularized log (rlog) normalized gene counts.*

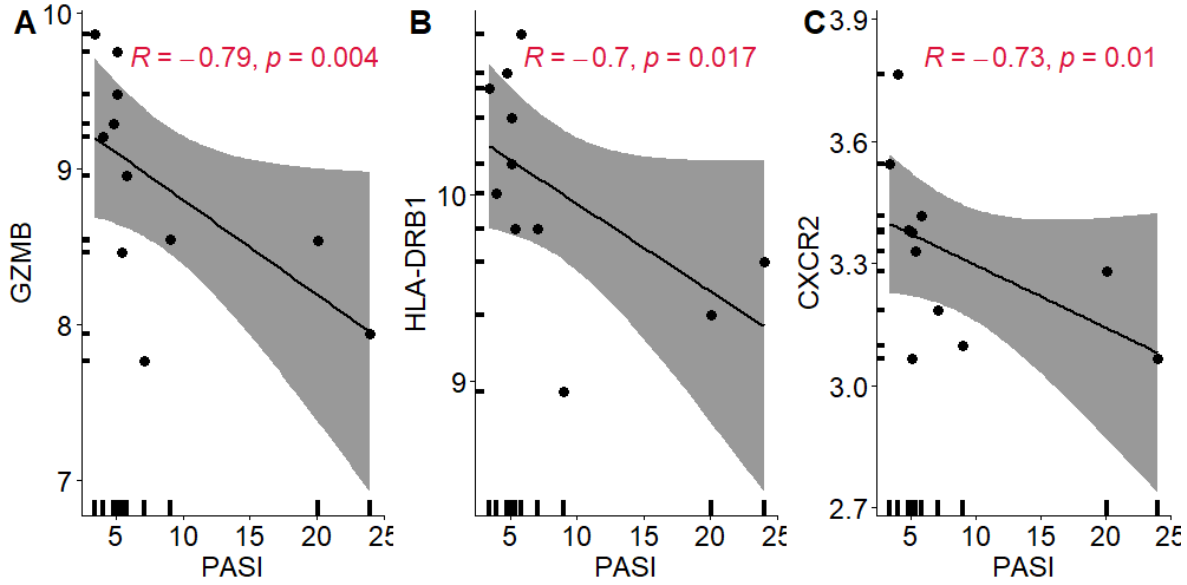

Figure 69. The expression of *GZMB*, *HLA-DRB1*, and *CXCR2* declines with PASI scores. *Correlation plots demonstrate the Spearman's rank correlation between PASI scores and the expression levels of A) GZMB, B) HLA-DRB1, and C) CXCR2. The y-axis represents regularized log (rlog) normalized gene counts.*

4.8. Characterisation of MAIT cells using high-dimensional spectral flow cytometry

The phenotypes of circulating MAIT cells were examined through high-dimensional spectral flow cytometry, enabling precise characterisation of their subsets, with respect to activation, cytotoxic, effector functions and tissue migration potentials. The analysis was performed on the same set of peripheral blood mononuclear cell (PBMC) samples used for the γδ T cell analysis. The study groups did not differ in any anthropometric and clinical characteristics, as outlined in Table 18, chapter 4.4.

MAIT cells (MR1-5-OP-RU-tet$^+$TCRVα7.2$^+$), were of similar frequencies in psoriasis patients and healthy control (Me [IQR]: 1.42 [0.472 – 3.005] vs 1.33 [0.501 – 2.003], PV vs HC, P=0.792, Mann-Whitney U test), comprising a median of 1.42% of circulating T cells. The composition of the MAIT cell compartment was also similar between groups, with CD8$^+$ being expectedly the most abundant subset, followed by DN (CD4$^-$CD8$^-$), CD4$^+$ and DP (CD4$^+$CD8$^+$) subsets. In addition, phenotypic analysis confirmed constitutive expression of CD161, CD28, and CD127, consistent with prior reports (184) (Figure 70).

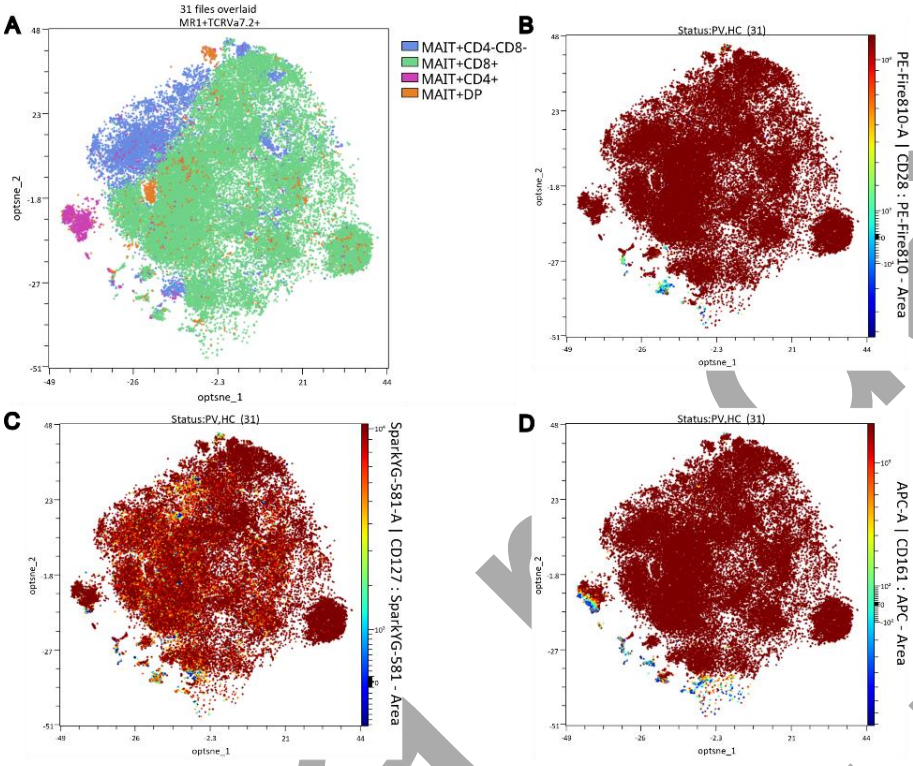

Figure 70. MAIT cells predominantly consist of the CD8+ subset and constitutively express CD28, CD127, and CD161. *A) opt-SNE plot showing MAIT cell subsets categorized as CD8+, CD4+, double-positive (DP), or double-negative (DN). Fluorescence intensity levels of B) CD28, C) CD127, and D) CD161.*

4.8.1. Characterisation of skin-tropic CLA$^+$ MAIT subset

The median percentage of MAIT cells expressing CLA (cutaneous lymphocyte antigen), was 9.55 %, with no significant differences observed between psoriasis patients (PV) and healthy partcipants (HC). Interestingly, the proportions of CLA$^+$CD8$^+$ cells within the MAIT compartment showed a significant positive correlation trend with age in healthy controls ($\rho = 0.66$, $P = 0.02$), but this trend was not observed in psoriasis group ($\rho = -0.098$, $P = 0.689$). Instead, the proportions of CLA$^+$ cells in psoriasis patients were significantly associated with PASI scores, with the strongest correlation observed in DP subset, while CD4$^+$ subset did not display significant correlation trend (Figure 71).

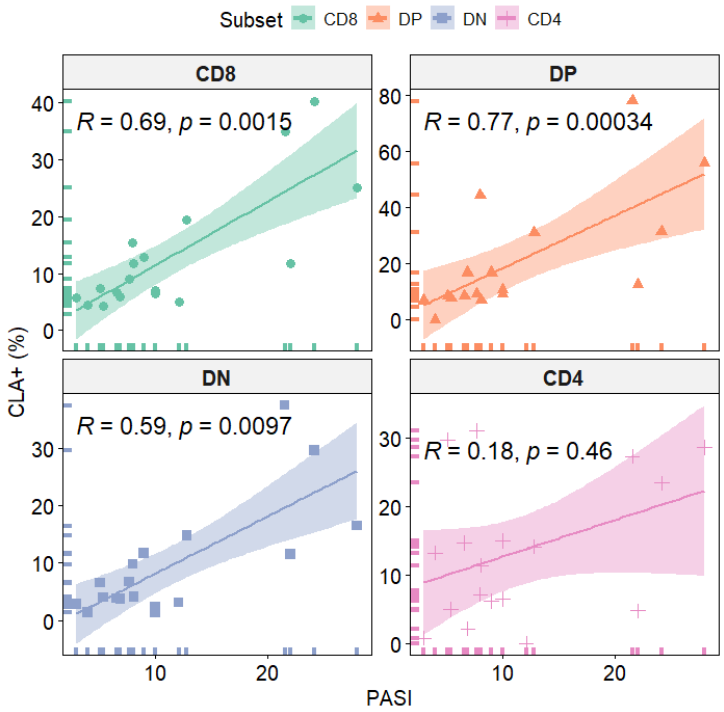

Figure 71. The percentage of CLA$^+$ cells positively correlate with PASI score in all MAIT subsets, without statistical significance for CD4$^+$. *Spearman's correlation coefficient*

Within MAIT cell subsets, rare CD4$^+$ and DP (CD4$^+$CD8$^+$) subsets had the highest proportions of CLA$^+$ cells, whereas the DN (CD4$^-$CD8$^-$) subset exhibited the lowest expression (Figure 72 A). No significant differences in the percentage of CLA$^+$ cells were detected across subsets when comparing PV and HC groups. Further analysis of the unique characteristics of CLA$^+$ MAIT cells, compared to CLA$^-$ cells, revealed distinct phenotypic differences. CLA$^+$ MAIT cells express higher levels of CD45RA, CD103, CXCR3, and PD-1, while showing lower levels of CD69 and CD127 (Figure 72). These findings indicate that ciculating CLA$^+$ MAIT cells exert characteristics related to migration to inflamed epithelial tissues (via CXCR3 and CD103) and may exhibit a less activated or regulated state (lower CD69 and CD127, and higher PD-1), reflecting functional adaptations for tissue-specific immunity.

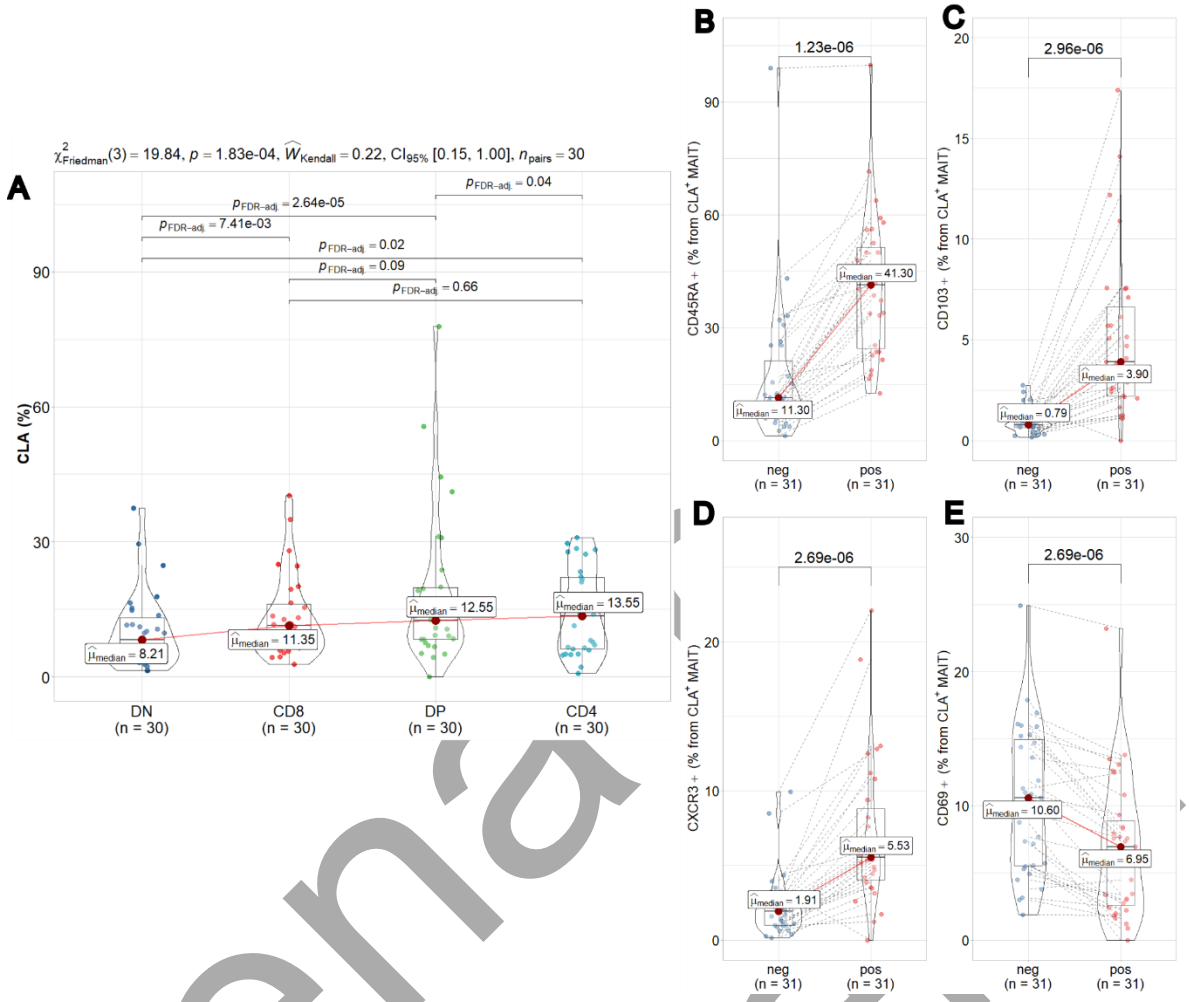

Figure 72. CLA expression on MAIT cells is the highest in CD4⁺ and DP subsets and reflects a tissue-migratory phenotype. *A) CLA expression across MAIT subsets. CLA⁺ MAIT cells show increased expression of B) CD45RA C) CD103, and D) CXCR3, with reduced levels of E) CD69. Dashed lines connect paired CLA⁺ and CLA⁻ samples from the same donors. Friedman's test (A) and Wilcoxon signed-rank test (B–E).*

4.8.2. Phenotypic characteristics of MAIT cells in psoriasis

The comparison of MAIT cell phenotypes between psoriasis patients and healthy controls revealed that MAIT cells in psoriasis patients comprise higher proportions of CD27⁺ Me [IQR]: 78.3 [70.3 – 87.05] % vs. 68.9 [59.2 – 72.9] %, P = 0.024; PV vs. HC, Mann-Whitney U test) and CD69⁺ cells (Figure 73 A), including within the CLA subset. In addition, a closer examination of individual molecule expression in relation to PASI score revealed that PD-1 on CLA⁺ cells increased significantly with disease severity (Figure 73 B), whereas the expression of CCR7⁺ within CLA⁺ cells declined (ρ = -0.649, P = 0.004, Spearman's rho).

Interestingly, the expression of CD56 on CLA^+ cells showed a significant positive correlation with PASI scores in female but not male patients, suggesting sex-based trends resembling those observed in γδ T cells. Given the previously recognised heterogeneity of MAIT cell compartment, further analysis was conducted on MAIT subsets to identify subset-specific perturbations associated with PV.

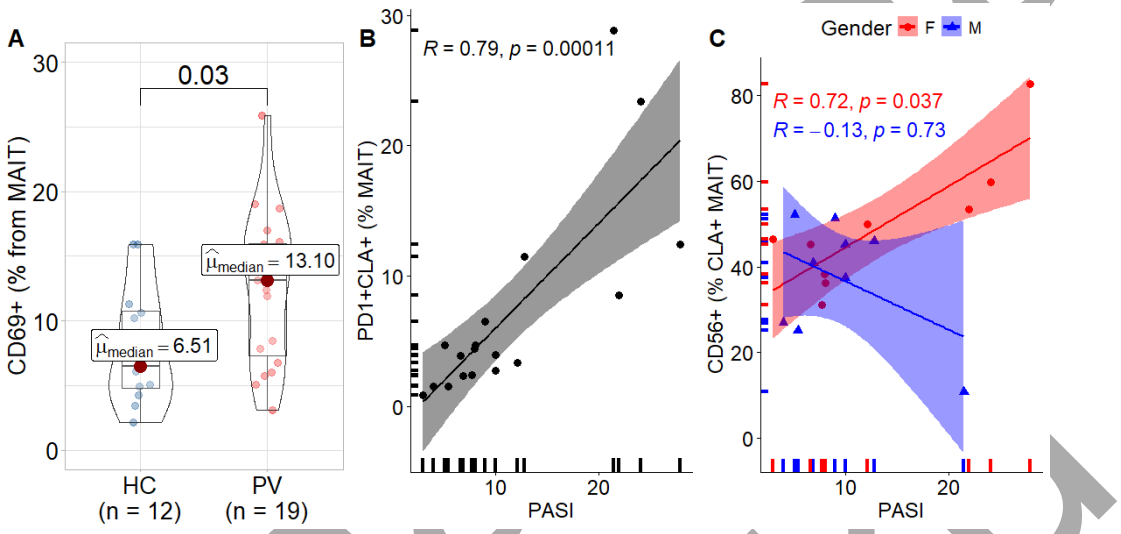

Figure 73. CD69 expression is elevated in MAIT cells of psoriasis patients, with PD-1 CLA^+ cells correlating with disease severity, and $CD56^+$ expression showing sex-specific trend. *A) The frequency of $CD69^+$ cells in psoriasis (PV) versus healthy controls (HC). B) The percentage of PD-1^+ CLA^+ MAIT cells increases with PASI scores. C) CD56 expression on CLA^+ MAIT increases with PASI scores in female patients only. Mann-Whitney U test (A), Spearman's rank correlation coefficient (B, C).*

4.8.2.1. Phenotypic characteristics of $CD8^+$ MAIT subset in psoriasis

As $CD8^+$ MAIT subset is the most dominant, it was expected that the previously described trends observed across the entire MAIT cells would largely reflect the dynamics within the $CD8^+$ compartment. Indeed, $CD8^+$ MAIT cells in psoriasis patients exhibited higher levels of CD69 (8.2 [4.4 – 13] % vs. 3.6 [2.1 – 6.2] %, P = 0.016; PV vs. HC) and CD27 (79.6 [68.5–85.3] % vs. 67.7 [47.8 – 73.5] %, P = 0.039) within the CLA^+ subset, along with an increase in CXCR3 expression (1.9 [1.3– 2.9] % vs. 0.9 [0.6 – 1.8] %, P = 0.026). In addition, the proportion of PD-1^+CLA^+ (Figure 74 B) and $CD56^+CLA^+$ ($\rho = 0.701$, P = 0.001) cells in $CD8^+$ MAIT subset increased significantly with PASI scores, with again more prominent trend observed in female patients. Additionally, it was observed that the proportions of $CD27^+CLA^+$

cells increase significantly with PASI scores in male patients ($\rho = 0.862$, $P = 0.003$), while in female patients the same was true for $CCR7^+$ ($\rho = 0.797$, $P = 0.01$) in $CD8^+$ MAIT subset.

4.8.2.2. Phenotypic characteristics of DN ($CD8^-CD4^-$) MAIT subset in psoriasis

The proportions of PD-1^+ CLA^+ cells in the DN subset, like those in the $CD8^+$ subset, increased significantly with PASI scores (Figure 74 B). However, no significant differences were observed between psoriasis patients and the healthy group. Similar to previously described findings, sex-based differences were also evident in DN subset. In female patients, PASI scores showed a significant positive correlation with the CD38-expressing CLA^+DN MAIT cells ($\rho = 0.842$, $P = 0.004$), whereas in male patients PASI scores associated negatively with the CCR7 ($\rho = -0.904$, $P = 8.27 \times 10^{-4}$) and CD94 ($\rho = -0.795$, $P = 0.01$) CLA^+ DN cells.

4.8.2.3. Phenotypic characteristics of DP ($CD8^+CD4^+$) MAIT subset in psoriasis

The percentage of $CD69^+$ cells within the DP compartment was also significantly higher in PV patients (11.3 [7.2–21.7] % vs. 7.1 [3.0–11] %, $P = 0.028$; PV vs. HC). Additionally, there was a notable increase in HLA-DR expression within the CLA^+ DP subset in PV patients (9.7 [0–15.5] % vs. 0 [0–2.1] %, $P = 0.028$; PV vs. HC). The DP subset showed significant shifts with disease severity, as evidenced by strong positive correlations between PASI scores and the frequency of PD-1^+ (Figure 74 B), $CD27^+$ ($\rho = 0.743$, $P = 6.31 \times 10^{-4}$) $CD127^+$ ($\rho = 0.739$, $P = 6.94 \times 10^{-4}$), and $CD11a^+$ ($\rho = 0.739$, $P = 7.07 \times 10^{-4}$) CLA^+ DP cells. Interestingly, the association between PASI scores and PD-1 expression was notable only in in male patients. Conversely, in female patients, the reshaping of DP compartment appeared to be more closely associated with disease duration, as shown by very strong correlations between the percentage of PD-1^+CLA^+ DP cells, along with $CXCR3^+$ and $CD69^+$ CLA^+ cells within the DP compartment with disease duration. Interestingly, PD-1 showed the highest expression on CLA^+ cells within the DP subset compared to the $CD8^+$ and DN subsets (Figure 74 A).

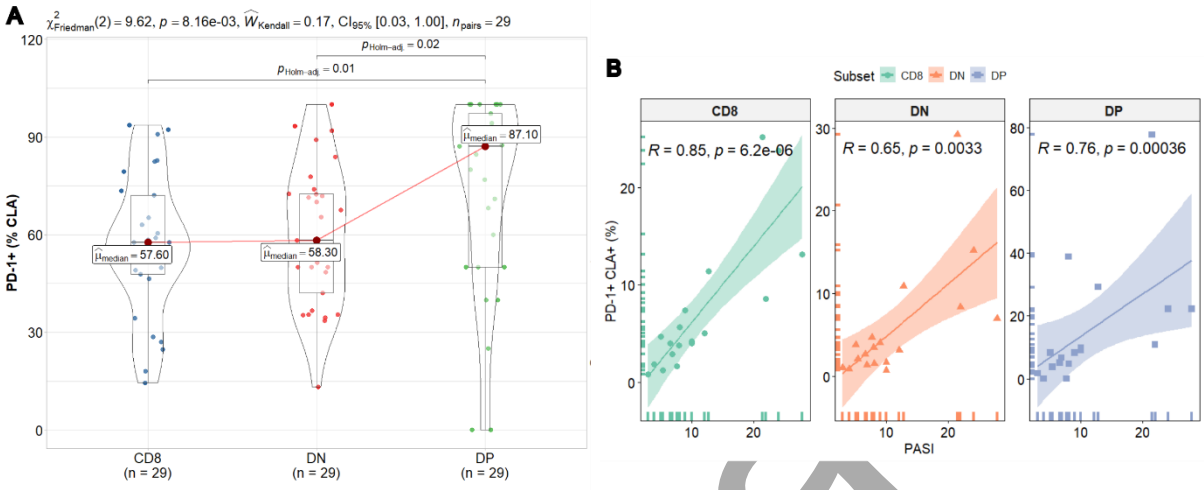

Figure 74. The percentage of PD-1$^+$ CLA$^+$ cells correlates with PASI scores in CD8, DN, and DP subsets, with DP subsets showing the highest expression. *Statistical significance was assessed using Friedman's test (A) and Spearman's correlation coefficient (B).*

1.1.1.4. Phenotypic characteristics of CD4+ MAIT subset in psoriasis

The CD4$^+$ MAIT subset displayed no significant differences or trends indicative of a strong involvement in the disease. This may be explained by the previously described distinctions of the CD4$^+$ subset compared to the CD8$^+$ and DN subset, which exhibit greater cytotoxic potential. However, in female patients, the expression of CD16 ($\rho = 0.81$, $P = 0.015$) and CD69 ($\rho = 0.862$, $P = 0.005$) on CLA$^+$ cells increased with PASI scores, suggesting this subset may, at least partially, be influenced by disease severity in affected women, reflecting heightened activation and cytotoxic potential.

Altogether, these results describe an elevated activation state in MAIT cells of psoriasis patients, as reflected by increased expression of CD69. In addition, the positive associations between the frequency of CLA$^+$ cells and PASI scores suggest higher capacity of these cells for blood-skin recirculation, with upregulation of the co-inhibitory receptor PD-1 on these cells pointing to a role in immune regulation and reflecting prior activation. In addition, the observed sex-associated differences offer new insights into the differential shaping of the MAIT cell compartment in psoriasis, however the trends reported here would require validation through larger cohort studies to confirm their significance and broader applicability.

5. DISCUSSION

5.1. Lower levels of circulating γδ T and Vδ2$^+$ T cells in male psoriasis patients

The investigation into the proportions of γδ T cells and their subsets revealed a significant reduction in γδ T and Vδ2$^+$ cell frequencies exclusively in male psoriasis patients, a pattern not evident in the total sample analysis. This reduction in Vδ2$^+$ cell proportions is consistent with previous studies that reported decreased Vγ9Vδ2 cell frequencies within the peripheral CD3$^+$ cell population of psoriasis patients (105,119). However, these findings have been characterized as inherent to the disease group, with no reported associations with sex differences. While the reduced proportions of Vδ2$^+$ cells in our cohort appears strictly associated with the male population, this interpretation should be approached with caution due to baseline differences in the control group. Notably, female controls displayed significantly lower γδ T and Vδ2$^+$ cell proportions within CD3$^+$ population compared to their male counterparts, which could have masked case-control distinctions when all samples were analysed together. Female patients did not show significantly different proportions of γδ T cells, or their subsets compared to healthy women or affected men, however, their average proportions were slightly elevated, suggesting potential differences that warrant further investigation. Importantly, the number of women in our cohort was three times lower than that of men, thus a focused study with a balanced male-to-female ratio is needed to confirm whether the observed reduction in γδ T and Vδ2$^+$ cells is indeed restricted to male patients.

It is also important to note that in a study by Laggner et al., the reduction in the proportion of circulating Vγ9Vδ2 cells was attributable primarily to the skin-homing CLA$^+$ fraction, with no significant difference observed in the frequencies of Vγ9Vδ2 CLA$^-$ subset (105). This finding suggested enhanced recruitment of Vγ9Vδ2 cells in affected skin, which was further supported by the observation of significantly higher percentages of Vδ2 cells in the lesional skin compared to healthy skin, a result also reported by Zhou et al (119).

Based on these findings, the observed reduction in Vδ2$^+$ cells within male patients may reflect increased trafficking of these cells from the bloodstream to cutaneous lesions, however, future studies incorporating CLA marker and paired skin-blood analyses will provide a clearer understanding of the underlying mechanisms driving the altered frequencies of Vδ2$^+$ cells.

5.2. The TCR repertoires of circulating γδ T cells alter with disease severity and age of psoriasis patients

A significant reduction in repertoire diversity, associated with both disease severity and age, emerged as the primary finding in the investigation of circulating γδ TCR repertoires of psoriasis patients. This reduction was primarily driven by a depletion of rare clonotypic variants, juxtaposed with an expansion of dominant clonotypic variants.

Disease severity, assessed by the PASI score, showed an inverse correlation with the number of unique clonotypes in both TCRγ and TCRδ repertoires, particularly affecting the dominant TRGV9 and TRDV2 variants. This decline in TRGV9 and TRDV2 diversity resulted from an increase in hyperexpanded clonotypes alongside a reduction in low-frequent ones. Moderate negative associations with PASI score also emerged for TRGV4, TRGV2, TRGV8, and TRDV3 clonotypes, while other clonotypic groups appeared unaffected by disease severity. Although previous studies have not included TCR repertoire analyses, findings by Zhou et al. might have indicated increased clonal expansion of Vγ9Vδ2 cells (119). Namely, circulating Vγ9Vδ2 cells of psoriasis patients exhibited skewed phenotypic profiles, with decreased $CD27^{+}CD45RA^{-}$ and enriched $CD27^{-}CD45RA^{+}$ cell frequencies, with these subsets showing significant negative and positive association with disease severity, respectively. This loss of CD27 expression has been linked to clonotypic amplification of Vγ9Vδ2 cells (140,159), implying that the phenotypic changes reported by Zhou et al. may reflect clonotypic expansions. Given that Vγ9Vδ2 cells are the predominant γδ T cell subset in peripheral blood, the observed loss of TRGV9 and TRDV2 clonotypic diversity may indicate a selective expansion of specific Vγ9Vδ2 clonotypes, potentially aligning with Zhou et al.'s findings. However, this interpretation should be approached with caution, as bulk RNA sequencing does not provide information on the pairing of γ and δ chains.

The age of psoriasis patients showed an even more pronounced effect on the contraction of TCRγ and TCRδ repertoires, most notable in the TRGV9 and TRDV2 repertoires, though detectable across all clonotypic variants. Interestingly, the age-related reshaping of γδ TCR repertoires in psoriasis patients differed significantly from that observed in age-matched healthy participants, indicating chronic inflammation or other disease-related factors may drive an alternate reorganisation of γδ TCR clonotypes in psoriasis. Specifically, while the counts of TRGV2 and TRDV1 clonotypes increased significantly with age in healthy controls, consistent with previous reports (237), psoriasis patients exhibited a significant decrease in the diversity of TRGV2, TRDV1, and other TRGV and TRDV variants with advancing age, attributed

primarily to a marked loss of low-frequency variants.

Disease duration also influenced TRG and TRD repertoires, with longer disease courses associated with a higher percentage of TRGV4 clonotypes, particularly TRGV4-TRGJ2 and TRGV4-TRGJP rearrangements. In addition, a negative correlation between disease duration and D50 values for TRGV4 clonotypes, along with an increase in medium-frequency TRGV4 clonotypes (0.05–0.5% of the repertoire), suggested that expansion within this frequency range contributes to gradual TCR repertoire remodelling. Similarly, although to a lesser extent, prolonged disease was associated with an increase in medium-frequency TRDV3 clonotypes. These repertoire shifts, previously unreported, may result from repeated exposure to skin-associated antigens, persistent inflammatory signalling, or potentially from increased migration of TRGV4 clonotypes from skin lesions into the bloodstream. However, other mechanisms may also drive this observed expansion, warranting further investigation to clarify the factors influencing TRGV4 dynamics in disease progression.

The observed contraction in TRGV9 and TRDV2 repertoires with increasing age and disease severity resembles the features of 'late-stage differentiated' $CD27^{-}CD28^{-}$ $CD16^{+}$ Vγ9Vδ2 cells (159). Specifically, $CD27^{-}$ subsets show significantly fewer clonotypes and lower diversity in their TCRδ repertoires compared to their $CD27^{+}$ ($CD27^{+}CD28^{+}$) counterparts (140,159), suggesting that patients with more severe disease and advanced age may have a higher representation of cytotoxic γδ T cells. Furthermore, seven PV patients with a high cumulative frequency of the top 10 clonotypes showed low Jaccard index values for TRDV2 clonotypes (PV-2, PV-10, PV-11, PV-13, PV-18, PV-19 and PV-21), aligning with Vyborova et al.'s reports indicating that the loss of common public sequences accompanies the transition from a $CD27^{+}$ to a $CD27^{-}$ phenotype (159). Thus, it is plausible that the alterations in TCR repertoire observed in our patient cohort reflect a shift toward a 'late-stage' differentiated state. In further support of this hypothesis, phenotyping using spectral cytometry showed an increased percentage of cytotoxic $CD56^{+}$ γδ T cells with both age and disease severity. Together, these findings suggest that disease progression and aging may drive γδ T cells toward a cytotoxic phenotype coupled with restricted TCR diversity. However, future studies utilizing single-cell sequencing that integrates TCR profiling and transcriptomic analysis are essential to clarify the link between γδTCR repertoire contraction, phenotypic differentiation, and disease severity.

5.3. Circulating γδ T cells in psoriasis patients display differential transcriptomic signatures attributable to patient subgroup heterogeneity

The upregulated genes in the γδ T cells of the psoriasis cohort indicate an increased activation, enhanced effector state, a type-1 immune response signature, increased migratory capacity, cytotoxic potential, and improved survival. The activated profile is reflected in the elevated expression of genes involved in T cell receptor (TCR) signalling, including CD3 complex components (*CD3E*, *CD3G*, *CD3D*, and *CD247*) and the tyrosine kinase *ZAP70*. Increased expression of CD48, a signalling lymphocyte activation marker (SLAM) family member, further confirms the activated state of γδ T cells. *CD48* is upregulated in activated cells (238), particularly under inflammatory conditions driven by cytokines like IFN-α, IFN-β, and IFN-γ (239) and enhances TCR signalling through Lck, promoting the production of IL-2 (240). In addition, the increased expression of *IL2RB*, encoding the IL-2 receptor beta chain, suggests enhanced responsiveness to IL-2 and IL-15, as IL-2Rβ is a shared subunit of these receptors. Both IL-2 and IL-15 promote the type 1 cytotoxic γδ T cell differentiation by upregulating key effectors like perforin and transcription factors T-bet and Eomes, important for IFN-γ production and Th1 polarization (241).

Complementing this, *TBX21*, which encodes T-bet, was significantly increased, further reflecting the effector profile of γδ T cells. T-bet is constitutively expressed in Vγ9Vδ2 cells and upregulated upon the TCR-induced transition of $V\delta1^+$ cells from a naïve state (142). In parallel, the upregulation of *IRF1*, a transcription factor induced by IFN-γ and needed for Th1 differentiation, points to a coordinated transcriptional network promoting a type-1 immune response. The increased production of IFN-γ is further supported by the upregulation of *GADD45G*, a member of the growth arrest and DNA-damage-induced 45 family, which is induced during T cell activation and known to enhance IFN-γ production (242,243). Moreover, the elevation of *IFITM1* and *ISG20*, both IFN-γ-induced genes, further highlights the downstream effects of IFN-γ signalling.

The cytolytic potential of γδ T cells was also enhanced, as evidenced from the upregulation of cytotoxic hallmark genes, including *PRF1* (perforin), *GZMA* (granzyme A), *SRGN* (serglycin), and *NKG7* (natural killer cell granule protein 7). The expression of cytotoxic genes *PRF1*, *GZMA*, and *NKG7* is closely associated with the effector profiles of γδ T cells (140,142) and is consistently identified as a signature of upregulated genes in T cells from psoriasis patients (97,118,244).

Moreover, the transcriptional signature of peripheral γδ T cells in psoriasis suggests a

heightened potential for migration to inflamed tissues, as demonstrated by the upregulation of *KLF2*, *SELL*, and *CXCR4*. Krüppel-like factor 2 (KLF2) is crucial for lymphocyte trafficking, as it maintains expression of *SELL* (CD62L or L-selectin), which mediates the T cell homing to secondary lymphoid tissues (245,246). KLF2 also modulates the expression of transcription factors T-bet, GATA3, and Blimp-1 (247). Upregulated *CXCR4*, a chemokine receptor, enhances migratory capacity by directing γδ T cells toward CXCL12, which is abundant in inflamed tissues (248). Notably, CXCR4 expression was found elevated in both active and resolved (244) psoriatic skin lesions, predominantly in the dermis (249), and was found to be constitutively expressed on dermal γδ T cells (120). Furthermore, increased *ITGAL* expression, encoding CD11a indicates enhanced motility of γδ T cells in this condition, as CD11a is needed for adhesion to endothelial and epithelial cells (250).

In addition, γδ T cells from psoriasis patients exhibit upregulation of genes associated with cell survival and protection, including *CORO1A*, *CD47*, and *HLA-E*. Coronin-1A (*CORO1A*) enhances T cell survival by modulating immune synapse dynamics and promoting intracellular Ca^{2+} mobilization, which supports activation and cytokine production (251). CD47 serves as a "don't eat me" signal by inhibiting phagocytosis through interaction with the SIRPα receptor on phagocytes (252), while HLA-E engages with the inhibitory receptors CD94/NKG2A on natural killer (NK) cells and certain T cell subsets, delivering anti-lysis signals that protect γδ T cells from NK cell-mediated cytotoxicity (253).

Furthermore, the upregulation of *TUBB* (beta-tubulin) suggests enhanced cytoskeletal dynamics, necessary for processes such as proliferation, cytokine production, and motility. Concurrently, increased expression of *POLR2A*, encoding the RNA polymerase II complex, reflects elevated transcriptional activity aligned with amplified immune activation and effector functionality. Furthermore, *GPR18* (G-Protein Coupled Receptor 18), typically expressed on intraepithelial γδ T cells, was also upregulated. *GPR18* has been associated with epithelial retention (254) and effector memory T cell maintenance (255), thereby in this context potentially indicating an activated or memory-like phenotype primed for tissue migration. Similarly, *MIF* (Macrophage Migration Inhibitory Factor), a pro-inflammatory mediator often upregulated in inflammatory conditions such as psoriasis, rheumatoid arthritis, and inflammatory bowel disease (256), suggests a role in amplifying inflammatory responses. The increased expression of *CD52*, a therapeutic target in multiple sclerosis, implies potential immunoregulatory functions, as new evidence indicates it may inhibit antigen-specific activation by disrupting TCR-MHC interactions (257). Upregulation of *PTPN7* (Protein Tyrosine Phosphatase, Non-Receptor Type 7) may also serve as a feedback regulator,

modulating the amplitude of immune responses by negatively regulating T cell activation pathways to prevent overactivation (258). Lastly, the upregulation of *STAT6*, typically associated with Th2 differentiation, introduces a contrasting profile to Th1 markers, suggesting nuanced immune response dynamics.

The downregulation of *IL2RG* (interleukin-2 receptor gamma chain), a key component of several interleukin receptors (IL-2R, IL-4R, IL-7R, IL-9R, IL-15R, and IL-21R) (259), coupled with reduced ICOS expression, a co-stimulatory molecule essential for T cell activation and differentiation (260), suggests diminished T cell activation. However, this downregulation could potentially reflect a shift in γδ T cells from a state of high dependence on cytokine and co-stimulatory signals to a more specialized, self-sustaining effector state, suggesting a reduced reliance on extensive activation signals. In addition, the downregulation of *MTOR*, a central regulator of cell growth, metabolism, and memory CD8 T-cell differentiation (261,262) further supports this notion of altered cellular dynamics. This decline is accompanied by the downregulation of *MX1*, *OAS3*, and *IFI44L*, genes known to play roles in antiviral responses (263–265), suggesting a diminished capacity to manage viral infections. However, it is important to consider that these differences may also reflect upregulated antiviral profiles in the transcriptomes of healthy individuals, underscoring the dynamic nature of immune responses across different physiological contexts.

This distinct set of upregulated genes resonates with those identified in earlier studies focused on psoriasis-associated T cell responses. Among the genes found to be upregulated here, *CD247*, *GZMA*, *CXCR4*, and *CD52* have previously been shown to be elevated in peripheral T cells in psoriasis, while *ISG20*, *IFITM1*, *PRF1*, *GZMA*, *NKG7*, and *SELL* were similarly upregulated in T cells from psoriatic lesions (97). Interestingly, the persistent elevation of *CD48*, *GZMA*, *IRF1*, *CXCR4*, and *ISG20* even after clinical improvement (244), suggests their potential role in maintaining sustained inflammatory activity in psoriasis. Moreover, the heightened activation state and type-1 immune signature identified in this study align with prior research showing that peripheral γδ T cells in psoriasis patients exhibit hyperactivation characterised by enhanced IFN-γ and TNF-α production, along with gene enrichment in pathways related to T cell activation, proliferation, and IFN-γ response (119). Collectively, the alignment of the γδ T cell transcriptomic profile with findings from previous studies, particularly concerning the sustained elevation of key genes post-treatment, suggests the active role of γδ T cells in the chronic inflammatory processes of psoriasis.

The transcriptomic profile observed in the psoriasis cohort indicates an enrichment of effector-like gene signatures in γδ T cells, aligning with previously observed expression patterns in Vδ1 effector (*GZMA*, *PRF1*, *NKG7*, *IL2RB*, *CD3D*, *CD3G*, *CD3E*, *CD247*, *ITGAL*, *TBX21*)(142), and innate-like Vγ9Vδ2 effector cells (*GZMA*, *PRF1*, *NKG7*, *IL2RB*, *TBX21*, *CD247*, *CD48*) (140,266). Given that Vγ9Vδ2 and Vδ1 cells are dominant in peripheral blood, it is plausible that the observed transcriptomic differences arise primarily from the effector subsets of these populations. However, as the analysis encompassed the total γδ T cell population without detailed phenotypic characterization, distinguishing the specific contributions of γδ T cell subsets remains challenging. Accordingly, single-cell resolution studies are necessary to uncover the distinct transcriptomic changes within these subsets and clarify their roles in the pathophysiology of psoriasis.

The heterogenous response within the psoriasis group, with differential expression primarily attributed to a specific subset of patients, suggests diverse immune dynamics of γδ T cells in the disease. The overlap of differentially expressed genes (DEG) between the PV-A vs. HC and total PV vs. HC analyses, alongside the absence of overlap in the PV-B vs. HC comparison, confirmed that the PV-A group is primarily responsible for the differential expression observed. However, the increased number of DEGs should be interpreted with caution, as these results might be inflated due to high variability in gene expression, particularly given the small sample size of five patients in PV-A group. In addition, while the results suggest significant deviations in one segment of the PV group, the available patient data do not provide an explanation for these findings. Nevertheless, previous studies have uncovered "hidden heterogeneity" within psoriasis vulgaris patients by identifying diverse molecular and cellular profiles which have enabled the categorization of patients into distinct subtypes according to varying inflammatory signatures, disease severity, and different responses to therapeutic interventions (267–271). In light of this evidence, it can be hypothesized that the involvement of γδ T cells in psoriasis vulgaris is also heterogenous and may vary not only between patients but also within the same individual over the course of their disease. Therefore, further investigation with a larger sample size and longitudinal tracking of disease progression and therapeutic response might provide deeper insights into the significance of the heterogenous profiles of circulating γδ T cells observed here.

5.4. Phenotypic and functional profiling of γδ T cells in psoriasis highlights CD56 as a marker of sex- and disease-driven alterations

The multi-dimensional profiling of γδ T cells using spectral flow cytometry has provided deeper insights into the phenotypic and functional profiles of γδ T cell subsets in psoriasis. While initial case-control comparisons did not reveal significant differences, a more nuanced disease-driven effect was uncovered when disease duration, severity and sex were taken into the equation. Notably, CD56 or neural cell adhesion molecule (NCAM), emerged as a key marker, with its expression correlating positively with both disease severity (PASI) and duration. Intriguingly, CD56 expression was consistently higher in female patients across both $V\gamma9V\delta2^+$ and $V\gamma9V\delta2^-$ subsets. In these subsets, CD56 levels were associated with disease duration ($V\gamma9V\delta2^+$) and PASI scores ($V\gamma9V\delta2^-$) in females, while in male patients CD56 expression increased on $V\gamma9V\delta2^+$ T cells as disease worsened. In addition, CD56 expression on $V\gamma9V\delta2^-$ cells increased with age in psoriasis patients, a trend absent in healthy aging, suggesting a disease-specific effect.

$CD56^+$ γδ T cells exhibited distinct functional profiles. The $V\gamma9V\delta2^+$ $CD56^+$ subset demonstrated heightened cytotoxic potential, characterised by co-expression of CD16, perforin, and granzyme B. These cells also expressed activation and late-stage differentiation markers, such as CD57, HLA-DR, CD25, CD11a, PD-1, and T-bet, aligning with prior studies characterising $CD56^+$ T cells as potent cytotoxic effectors with enhanced Th1-like responses and IFN-γ production (272–276). Interestingly, CD56 expression in γδ T cells is significantly upregulated in response to isopentenyl pyrophosphate (IPP), a phosphoantigen derived from the mevalonate pathway, which accumulates in metabolically stressed cells. Furthermore, IL-15, a cytokine implicated in psoriasis pathogenesis (277,278) has been shown to enhance CD56 expression in γδ T cells (274–276). These observations point to a potential mechanism where prolonged IL-15 stimulation and IPP accumulation in hyperproliferative keratinocytes drive the upregulation of CD56 in γδ T cells, particularly in the context of psoriasis severity and duration. However, this hypothesis requires further validation, as the mechanistic interplay between IL-15, IPP, and CD56 expression in psoriasis have not been defined.

Sexual dimorphism also emerged as a significant feature of γδ T cells in psoriasis, with female patients consistently exhibiting higher CD56 expression across γδ T cell subsets, reinforcing prior findings that women generally have greater effector responses, higher Th1 cytokine production, and enhanced cytotoxic T cell activity (51–53). Elevated expression of

CX_3CR_1 and CXCR5 on CLA^+ $V\gamma9V\delta2^+$ T cells further support greater cytotoxic potential in female patients. An additional intriguing observation was the increased expression of CXCR3 on CLA^+ Vδ1 cells in females. This X-linked gene, which may escape X-chromosome inactivation (282), has been associated with autoimmune diseases that disproportionately affect women (283). Its increased expression has been associated with IFN-γ signalling and Th1-dominant immune responses (56), and as $CXCR3^+$ T cells are enriched in psoriatic lesions (285), these finding may suggest that $CXCR3^+$ CLA^+ Vδ1 cells contribute to autoinflammatory processes in female patients.

Altered CD103 expression on $V\gamma9V\delta2^-$ cells also emerged as a disease-associated feature. CD103, known as the αE integrin, binds to E-cadherin on epithelial cells, facilitating the entry of T cells into the skin (286). The CD103 expression was significantly lower among circulating CLA^+ $V\delta3^+$ cells in psoriasis patients, plausibly suggesting enhanced homing of these cells to the skin. Conversely, its increased expression with disease severity may reflect the enhanced recirculation of previously skin-resident T cells, consistent with earlier findings that circulating $CD4^+$ CLA^+ $CD103^+$ cells originate from former skin-resident $CD69^+CD103^+$ populations (113). In addition to these CD103 dynamics, the Vδ3 subset in PV exhibited an increased proportion of cells expressing the activation marker CD38, which was almost entirely absent in healthy samples. Moreover, CD16 and CD25 also showed increased expression with disease duration or severity, suggesting that the Vδ3 subset may be involved in disease progression. These findings point to a potentially distinct and underexplored role for Vδ3 cells in psoriasis, which warrants further exploration, particularly given their poor characterisation in current literature.

An intriguing finding of this study was the identification of previously undescribed phenotype of CLA^+ γδ T cells. These cells exhibited increased expression of co-stimulatory molecules CD28 and CD27, alongside lower levels of CD57 compared to their CLA^- counterparts, suggesting a non-immunosenescent and highly active state. The expression of CD27 and CD28 highlights their enhanced functional capacity, as these molecules are associated with improved survival and responsiveness to stimulatory signals. This phenotype aligns with findings in αβ T cells, where CLA^+ cells have been identified as non-ageing, maintaining consistent telomere length and sustained CD28 expression over time, in contrast to CLA^- cells, which show declining CD28 expression and progressive exhaustion with age (287). This phenotype is particularly relevant in the context of psoriasis, where the persistence of activated and exhaustion-resistant CLA^+ T cells likely contribute to chronic inflammation

and disease maintenance. Additionally, CLA^+ γδ T cells were found to express higher levels of CXCR3, a chemokine receptor associated with Th1 responses and enhanced skin-homing capacity. This is consistent with the known enrichment of CLA^+ and $CXCR3^+$ cells in psoriatic lesions (102,285), supporting the idea that CLA^+ γδ T cells may contribute to sustaining the inflammatory environment within psoriatic skin.

Importantly, the elevated expression of T-bet and perforin in γδ T cells of psoriasis patients, previously identified at the transcriptomic level, was validated by intracytoplasmic staining, confirming the transcriptional findings at the protein level. While the expression of granzyme A was not statistically significant, it was elevated in psoriasis patients, with a subset of patients exhibiting levels surpassing those observed in any healthy control, reflecting the within-patient heterogeneity observed at the transcriptomic level. Interestingly, the expression of cytotoxic and effector markers such as granzymes, perforin, T-bet, Eomes and TOX increased significantly with age in $V\gamma9V\delta2^-$ cells of psoriasis patients, but remained unchanged in healthy controls, suggesting a distinct immune aging trajectory in psoriasis, potentially contributing to disease persistence and severity with advancing age.

In summary, the profiling of γδ T cells uncovered significant disease- and sex-associated dynamics in psoriasis, offering valuable insights into their potential contributions to disease pathogenesis. However, the study is limited by the low representation of female participants in the healthy cohort, which restricts the ability to fully investigate sex-driven responses. In addition, a greater representation of patients with severe disease, particularly among male participants, would strengthen the analysis of disease progression. Therefore, to validate these findings and gain a more comprehensive understanding, future research on larger cohorts and incorporated paired analyses of blood and skin samples will provide a more comprehensive understanding.

5.5. Decreased $CD4^+$ and DP MAIT cells in peripheral blood of male psoriasis patients and inflammation-dependent decline of $CD8^+$ and DN subsets

The distribution of MAIT cells in the peripheral blood of psoriasis patients was generally comparable to that observed in healthy participants, with similar proportions across the $CD8^+$, DN, $CD4^+$, and DP subsets. However, when examining the proportions of these subsets within the $CD3^+$ T cell compartment, psoriasis patients showed a significant reduction in $CD4^+$ MAIT cells, particularly in male patients, who also exhibited significantly lower proportions of DP MAIT cells. These findings are consistent with previous study conducted on smaller cohort, which similarly reported that a reduction in $CD4^+$ and DP MAIT cells was a characteristic feature of male psoriasis patients (1). Therefore, these results suggests that sex-specific factors may influence the distribution and function of MAIT cells in psoriasis, warranting further investigation the underlying mechanisms driving these differential patterns.

The MAIT cell compartment is predominantly composed of $CD8^+$ and DN subsets, which are recognised for their potent cytotoxic properties (184,198). In contrast, $CD4^+$ and DP MAIT cells, which typically represent a smaller fraction (less than 5%) of the MAIT cell population, exhibit distinct functional characteristics. $CD4^+$ MAIT cells are generally less cytotoxic than their $CD8^+$ and DN counterparts and are marked by the increased expression of molecules such as CCR7, SELL, FOXP3, and CD25, indicative of enhanced tissue migration potential and shared phenotypic similarities with regulatory T cells (Tregs) (198). In addition, compared to other subsets, $CD4^+$ MAIT cells produce significantly higher levels of IL-2, (184) a cytokine critical for maintaining Treg populations and promoting immunoregulation (3). Thus, the observed reduction in $CD4^+$ MAIT cells may suggest a diminished capacity of these cells to contribute to immune homeostasis, potentially exacerbating the inflammatory milieu in psoriasis. It is also possible that the reduced presence of $CD4^+$ MAIT cells in peripheral blood reflects their migration to inflamed skin, as observed in other autoimmune diseases where a reduction in circulating MAIT cells is accompanied by increased infiltration into lesional sites (192,212). Interestingly, MAIT cell numbers were previously not found to be enriched in psoriatic lesional skin (4), suggesting that the reduction in $CD4^+$ and DP MAIT cells in peripheral blood may not solely be a consequence of tissue migration. However, no study to date has specifically investigated the frequencies of individual MAIT cell subsets within psoriatic skin, and given the low percentage of $CD4^+$ and DP MAIT cells within the compartment, it is possible that, even if these cells preferentially infiltrate perturbed skin, their presence would not significantly alter the overall MAIT cell proportions in the lesional skin.

Furthermore, the reduction of circulating MAIT cells in autoimmune and chronic inflammatory conditions has been frequently associated with increased activation marker CD69 expression and activation-induced cell death (192,212). The CD69 expression was indeed elevated on the DP subset in psoriasis, however, whether activation-induced cell death or increased migration to the skin contribute to their reduced proportion in peripheral blood remains to be investigated.

While the frequencies of total MAIT cells, $CD8^+$ and DN subsets were not significantly different between psoriasis patients and healthy controls, their levels correlated negatively with high-sensitivity C-reactive protein (hsCRP), a marker of systemic inflammation. Consistent with the concept of inflammageing (289), a positive correlation between hsCRP levels and age was observed in both psoriasis patients and healthy controls, reflecting the chronic, low-grade inflammation associated with aging. Importantly, the association between elevated hsCRP levels and reduced proportions of total MAIT cells, as well as $CD8^+$ and DN subsets, was specific to the psoriasis cohort, suggesting that systemic inflammation may have a pronounced impact on MAIT cells dynamics in psoriasis, possibly reflecting disease-specific immune dysregulation.

In conclusion, the altered distribution of circulating DP and $CD4^+$ MAIT cell subsets in psoriasis highlights their potential role in shaping disease progression, with sex-based differences emerging as a critical avenue for exploration. Moreover, the observed relationship between elevated hsCRP levels and reductions in $CD8^+$ and DN MAIT cells raises intriguing questions about whether this decrease is driven by activation-induced depletion, impaired homeostatic maintenance, or a shift toward increased tissue residency. Addressing these questions could illuminate the role of MAIT cells in local and systemic inflammation, offering fresh perspectives on their contribution to the complex immunopathology of psoriasis.

5.6. Age-associated loss of diversity and convergence in MAIT TCR repertoires of psoriasis patients, with disease severity-related remodelling in male examinees

The MAIT TCRα and TCRβ repertoires of psoriasis patients did not exhibit significant differences in diversity, CDR3 length or variable (V) and joining (J) gene usage compared to healthy controls. However, detailed analysis revealed distinct patterns, suggesting underlying differences in repertoire organization. Specifically, psoriasis patients exhibited subtle enrichment of certain V-J gene segment pairings and more pronounced age-related alterations, with disease severity influencing repertoire composition primarily in male patients.

On average, 77% of TCRα transcripts contained the TRAV1-2 segment, consistent with the canonical MAIT cell TCR usage. However, notable diversity in TCRα transcripts was observed, despite the high post-sorting purity and a gating strategy designed to isolate TCRVα7.2 (TRAV1-2)$^{+}$ MR1-5-OP-RU-tet^{+} cells. This diversity may partly reflect the inclusivity of the sorting strategy, which could have allowed the capture of MR1-restricted cells lacking TRAV1-2 (186,290). Additionally, cells with low to intermediate MR1 binding intensity, included within the sorted population, have been reported to express dual TCRα receptors (291), further complicating the interpretation of TCR repertoire composition. Moreover, transcript-level data do not always correspond to surface protein expression, and non-TRAV1-2 transcripts may represent transcriptionally active but untranslated chains. Nevertheless, the proportional binding affinities of TRAV1-2 to TRAJ33, TRAJ12, and TRAJ20 variants align with prior reports (184,232), reducing the likelihood that the observed diversity arises from conventional non-MR1 binding subsets.

Age emerged as a significant determinant in shaping the MAIT TCRβ repertoires and, to a lesser extent, the TCRα repertoires, with a more pronounced impact in psoriasis patients compared to healthy individuals, consistent with our previous findings (205). Increasing age of psoriasis patients was associated with a marked decline in unique TCRβ clonotypes, an increase in hyperexpanded clonotypes and a reduced proportion of smaller, less dominant ones. These alterations were consistent across the most prevalent TRBV variants, including TRBV4-2, TRBV6-2, TRBV6-4, and TRBV20-1, while TRBV6-1 clonotypes appeared resistant to age-related changes. The loss of TCRβ clonotype diversity with age is well-documented in the general population and is attributed to cumulative antigen exposure and thymic involution, which skew the TCR repertoire toward expanded clonotypes (292,293). In healthy MAIT repertoires, similar age-related reductions were observed but often failed to reach statistical

significance, which may partly be due to the smaller sample size (N = 12 for healthy controls vs. N = 26 for psoriasis patients). However, the observed age-related decline in TRBV6-4 clonotypes number in healthy controls may indicate that this reduction is a normal consequence of aging, independent of disease.

By contrast, the significant reduction in TCRβ convergence with increasing age was specific to psoriasis patients, highlighting a distinct feature of MAIT repertoire remodelling under chronic inflammation. Convergent recombination, the process by which distinct nucleotide sequences produce identical CDR3 regions, enables genetically distinct T cell clones to recognise the same antigenic epitope, thereby contributing to the formation of public clonotypes shared across individuals. This decline in convergence suggests a diminished capacity in psoriasis patients to generate and maintain these shared clonotypes with age. Indeed, public clonotype frequency, quantified by Jaccard index, significantly declined with age in psoriasis patients, a trend absent in healthy participants. Collectively, these results suggest an accelerated reshaping of MAIT TCR repertoires in psoriasis, characterised by the loss of convergently recombined clonotypes. This loss likely reduces the proportion of public clonotypes, with a shift toward private repertoires marked by the expansion of antigen-specific clonotypes and a concurrent decline in rare variants.

Compared to γδ TCR repertoires, the associations between disease duration or severity, assessed by PASI score, and MAIT TCR repertoire metrics were either absent or considerably weaker, at least when the entire PV cohort was examined. However, significant correlations between PASI score and TRA and TRB clonotype counts were observed exclusively in male psoriasis patients, pointing to potential sex-based differences in the reshaping of the MAIT TCR repertoire. These findings, along with the observed male-specific reductions in $CD4^+$ and DP MAIT subsets, indicate that sex hormones or sex-linked genetic factors may differentially impact MAIT cell biology in psoriasis, however, further studies are needed to dissect the underlying molecular drivers.

In summary, these findings reveal a complex interplay between ageing, chronic inflammation, and sex-specific factors in shaping the MAIT TCR repertoire in psoriasis. These insights open new avenues for further research to uncover the mechanisms driving these changes, with expanded sample sizes and robust sex-based stratification necessary to validate and extend these findings.

5.7. Transcriptomic profiles of circulating MAIT cells in mild psoriasis show no distinct features compared to healthy controls but reveal perturbations linked to age and disease severity

The transcriptomic landscape of circulating MAIT cells in psoriasis patients showed no discernible differences compared to healthy participants. However, closer examination revealed significant associations between the expression of several genes and key clinical parameters, including patient age and disease severity as measured by PASI score.

The expression of three genes declined significantly with increasing PASI scores, with *GZMB*, encoding granzyme B, displaying the strongest trend. Granzyme B is typically expressed at low levels in resting MAIT cells (208) but is upregulated upon TCR- or cytokine-driven activation (210). Studies have reported lower *GZMB* expression in IL-17-producing subset of MAIT cells (199), suggesting the observed decline in its expression might reflect a shift toward MAIT17 phenotype in more severe forms of psoriasis. However, as IL-17 transcripts were almost entirely absent across the PV samples, the presence of a MAIT17 phenotype can largely be excluded. Instead, the loss of *GZMB* may indicate functional impairment or stagnation of MAIT cells associated with increased disease severity. This interpretation is partially supported by the reduction in *HLA-DRB1* expression, which encodes a key component of the HLA-DR molecule, a marker associated with late-stage activation. Furthermore, *CXCR2* expression also declined with disease severity, however, given the minimal baseline expression of *CXCR2* in MAIT cells, the functional relevance of this decrease is likely limited in this context. Taken together, these findings suggest that MAIT cells in severe psoriasis may have reduced functional capacity or activation, potentially contributing to immune dysregulation. However, the associations with disease severity should be interpreted with caution and require further validation, as the cohort primarily consisted of patients with mild disease, with only 2 out of 11 individuals meeting the criteria for severe disease.

Building on these findings, age-related gene expression patterns observed specifically in psoriasis patients reveal additional insights into potential mechanism of cellular senescence, even within the narrow age range of 22 to 51 years. Among these, the strongest positive correlation was observed with *CD70*, a ligand for CD27 primarily associated with antigen-presenting cells but also upregulated on activated T cells, where it serves as a co-stimulatory molecule to enhance immune responses (294). Interestingly, CD70 overexpression has been linked to autoimmune conditions like rheumatoid arthritis (RA), systemic lupus erythematosus, Sjögren's syndrome, and systemic sclerosis, underscoring its role in promoting

autoinflammatory responses (295). In RA, increased CD70 expression is particularly notable in $CD4^{+}CD28^{-}$ cells, a subset associated with immune aging. This dysregulated expression of CD70 was associated with a lower TCR activation threshold, potentially driving self-reactive T cell activation and exacerbating autoimmune pathology (296). Furthermore, the age-associated upregulation of *TNFRSF9*, encoding 4-1BB (CD137), another co-stimulatory receptor expressed by activated T cells, further exploits heightened activation and possibly exhaustion in MAIT cells in psoriasis. TNFRSF9 is strongly induced by TCR activation in MAIT cells (199,210), and has been linked to the expansion and differentiation of exhausted T cells (13). Further evidence of accelerated senescence in MAIT cells in psoriasis comes from the significant association between patients' age and the expression of *CDKN2A*, the gene encoding the tumour suppressor $p16^{INK4a}$. This protein plays a critical role in maintaining cell cycle arrest and is widely recognised as a biomarker of cellular ageing (234–236). Its upregulation in T cells is observed following repeated stimulations and is closely tied to the development of an exhaustion phenotype (236). Together, these findings suggest that age-related changes in gene expression may compound the functional decline of MAIT cells in psoriasis, contributing to disease progression and immune dysregulation.

Clear differences in MAIT cell phenotypes seen in case-control comparisons via spectral flow cytometry, contrasted with the lack of differences at the transcriptomic level, raise questions about factors that may have affected the transcriptomic analysis, including sample selection. The selection of RNA samples was limited by availability and concentration, resulting in a psoriasis cohort mostly consisting of patients with mild disease (9 out of 11 had PASI scores below 10) and a median disease duration of 6 years. These characteristics suggest the transcriptomic profiles of circulating MAIT cells may not display clear differences in early or mild disease stages. While contamination from co-sorted conventional or other MR1-reactive subsets could also explain the lack of transcriptional differences, it is likely a minor factor compared to cohort composition, given the satisfactory post-sort purity. The narrow PASI scores and age range further limit the scope and interpretability of correlation analyses. However, the narrow age range hint at early senescence-related changes in psoriasis, though this requires validation in larger, more diverse sample sets. Therefore, future studies with broader PASI scores and age ranges are needed to better understand the transcriptomic and phenotypic profiles of MAIT cells in psoriasis and to explain the notable protein-level differences identified through spectral flow cytometry.

5.8. Circulating MAIT cells in psoriasis patients show CD69 upregulation and increased expression of CLA and PD-1 with disease severity

The multi-dimensional phenotypic analysis of circulating MAIT cells in psoriasis provided novel insights into their activation and potential contributions to disease pathogenesis. Psoriasis patients exhibited a pronounced increase in the expression of early activation marker CD69, along with elevated levels of skin-homing cutaneous lymphocyte antigen (CLA) and the co-inhibitory receptor PD-1 in patients with more severe disease.

The heightened expression of CD69 on MAIT cells, while not previously reported in psoriasis, aligns with findings from several studies investigating MAIT cells in other autoimmune disorders. Increased frequencies of $CD69^+$ MAIT cells have been documented in systemic lupus erythematosus, autoimmune liver disease, inflammatory bowel disease, ankylosing spondylitis, systemic sclerosis, and multiple sclerosis (211,212,298). Similarly, the upregulation of CD69 on conventional T cells within psoriatic lesions has been associated with their persistent activation (299). Together, these findings establish CD69 as a consistent marker of MAIT cell activation across autoimmune and autoinflammatory diseases, and its identification in psoriasis provides novel evidence of circulating MAIT cell involvement in disease pathogenesis.

The enrichment of CLA^+ MAIT cells in patients with severe psoriasis highlights their increased capacity for skin homing, suggesting a role in disease pathophysiology. This pattern mirrors previous findings where the frequency of conventional CLA^+ T cells correlated with PASI scores (106), supporting the hypothesis that MAIT cells actively participate in psoriasis immunopathology. In addition, the elevated proportion of circulating CLA^+ MAIT cells may represent cells re-entering the bloodstream after contributing to local inflammation in psoriatic skin, reflecting dynamic trafficking between tissue and systemic compartments. Of particular interest is the strong correlation between the frequency of $PD\text{-}1^+$ CLA^+ MAIT cells and disease severity. PD-1, a co-inhibitory receptor commonly upregulated during T cell activation, becomes increasingly expressed with chronic antigen exposure, marking persistent activation (300). At advanced disease stages, the increased frequency of $PD\text{-}1^+$ CLA^+ MAIT cells likely reflects prolonged inflammatory stimulation. In addition, enhanced PD-1 expression can be interpreted as a regulatory mechanism to limit excessive activation, but it could also signal immune exhaustion. In other autoimmune diseases, PD-1 overexpression on MAIT cells has been linked to reduced cell numbers and impaired IFN-γ production, raising the possibility that

chronic activation leads to functional dysregulation or cell death (301–303). Interestingly, however, PD-1$^+$CD8$^+$CD103$^+$ T cells enriched in psoriatic lesion were shown to produce significantly high levels of IL-17A, key driver of psoriasis pathogenesis. In addition, the number of these PD-1$^+$ T cells, but not their PD-1-negative counterparts, correlated positively with PASI scores and decreased with treatment, suggests that PD-1$^+$ cells are functionally active and contribute to inflammation in psoriasis. Similarly, PD-1$^+$ CLA$^+$ MAIT cells in circulation may represent a subset of chronically activated but functional cells, capable of driving systemic inflammation. These findings position PD-1$^+$ CLA$^+$ MAIT cells as potential biomarkers of systemic inflammation in psoriasis, though further studies are required to clarify their precise roles and functional status.

Another intriguing observation is the parallel expression patterns of CD69, PD-1, and CLA across the rare double-positive (CD4$^+$CD8$^+$, DP) MAIT subset and the more common CD8$^+$ and DN subsets. The high expression of CLA on DP MAIT subset suggests a strong propensity for skin homing, while the significant upregulation of HLA-DR further marks their activated state. In contrast, the CD4$^+$ subset did not display similar changes, potentially reflecting their distinct functional roles and reduced pro-inflammatory activity (184,198). Interestingly, significant correlations between PASI scores and CD69$^+$ or CD16$^+$ CD4$^+$ MAIT cells in female patients suggest possible sex-specific immune perturbations, however these observations, together with similar trends noted in other subsets, warrant further investigation in larger cohorts to better understand the biological basis of these sex-associated difference.

The expansion of CD56-expressing CD8$^+$ MAIT cells with disease severity introduces a new perspective on their activation mechanisms. CD56$^+$ MAIT cells are known to be more responsive to cytokine-driven activation than TCR-mediated stimulation (199,304), implying that their increase in severe psoriasis reflects an adaptation to the cytokine-rich inflammatory environment characteristic of the disease.

In summary, this study provides novel and previously unrecognised characteristics of circulating MAIT cells in psoriasis, providing compelling evidence of their contribution to disease pathogenesis. Future research should aim to elucidate the functional roles of these activated MAIT cells, particularly their contributions to cytokine production, immune regulation, and lesion development. Furthermore, a deeper understanding of the interplay between circulating and tissue-resident MAIT cells will be crucial for defining their precise roles in psoriasis pathophysiology.

6. CONCLUSIONS

1. Male psoriasis patients exhibit a significant reduction in the proportions of γδ T and Vδ2$^+$ γδ T cells within the circulating CD3$^+$ T cell compartment compared to healthy men.
2. The diversity of the T cell receptor (TCR) repertoire in circulating γδ T cells contracts significantly with higher disease severity (PASI scores) and patient age, driven by the loss of rare clonotypic variants alongside an expansion of dominant clonotypes.
3. In psoriasis patients, age-related reshaping of γδ TCR repertoires differs significantly from the patterns observed in healthy controls, with the strongest decline in diversity occurring in the TRGV9 and TRDV2 repertoires.
4. The proportion of TRGV4 clonotypes increases significantly with disease duration, most prominently within the medium-frequency range (0.05–0.5% of the repertoire).
5. Circulating γδ T cells in psoriasis exhibit a transcriptome enriched with gene transcripts associated with activation, enhanced effector functions, greater migratory capacity, heightened cytotoxic potential, and improved survival.
6. Transcriptional profile of circulating γδ T cells can vary between PV patients with no discernible clinical or anthropometric differences.
7. The percentage of CD56$^+$ cells within the Vγ9Vδ2 subset increases significantly with higher PASI scores, particularly in female patients, who also exhibit higher CD56$^+$ cell percentages across both Vγ9Vδ2$^+$ and Vγ9Vδ2$^-$ subsets.
8. In the Vγ9Vδ2$^-$ subset, the percentage of CD56$^+$ cells, along with the expression of T-bet, Eomes, Tox, perforin, and granzyme A/B/K, increase significantly with age in psoriasis patients, while remaining stable in age-matched healthy controls.
9. CLA$^+$ γδ T cells exhibit higher expression of co-stimulatory molecules (e.g. CD27, CD28) and lower levels of markers associated with terminal differentiation and prior activation/exhaustion (e.g. CD57, HLA-DR) compared to CLA$^-$ cells.
10. The proportions of CD4$^+$ and DP (CD4$^+$CD8$^+$) MAIT cell subsets within the CD3$^+$ T cell population is significantly lower in male psoriasis patients compared to healthy male controls.
11. The frequencies of CD8$^+$ and DN (CD4$^-$CD8$^-$) MAIT subsets decline significantly with increasing hsCRP levels in psoriasis patients.
12. Ageing in psoriasis patients is associated with a decline in unique TCRβ clonotypes in MAIT cells, driven by an increase in hyperexpanded clonotypes and a reduction in

smaller, less dominant ones. This patter is consistent across major TRBV variants (TRBV4-2, TRBV6-2, TRBV6-4, and TRBV20-1), except for TRBV6-1.

13. In male psoriasis patients, disease severity is significantly associated with the contraction of the TCRβ repertoire in MAIT cells.
14. Increasing age in psoriasis patients correlates with a significant reduction in TCRβ convergence, along with a decline in the Jaccard index, reflecting the loss of convergently recombined clonotypes and reduced publicness of the TCR repertoire.
15. The transcriptomic landscape of circulating MAIT cells in psoriasis patients shows no discernible differences compared to healthy participants, most likely owing to mild disease phenotype across the majority of patients.
16. The expression of several genes in MAIT cells is associated with PASI scores and age, suggesting a loss of functional capacity, immune exhaustion, chronic activation, and cellular senescence.
17. The percentage of activated $CD69^+$ MAIT cell subsets ($CD8^+$, DN, and DP) is significantly increased in psoriasis patients compared to healthy individuals.
18. The proportion of circulating CLA^+ MAIT cell subsets ($CD8^+$, DN, and DP), including $PD\text{-}1^+CLA^+$ MAIT cells, increase significantly with disease activity.
19. The DP MAIT cell subset contains the highest proportion of CLA^+ cells and a significantly higher proportion of $HLA\text{-}DR^+$ cells in psoriasis, while the CD56 expression increases significantly with disease severity in the $CD8^+$ subset.

7. LITERATURE

1. Man A-M, Orăsan MS, Hoteiuc O-A, Olănescu-Vaida-Voevod M-C, Mocan T. Inflammation and Psoriasis: A Comprehensive Review. *Int J Mol Sci* (2023) 24:16095. doi: 10.3390/ijms242216095

2. Yan B-X, Chen X-Y, Ye L-R, Chen J-Q, Zheng M, Man X-Y. Cutaneous and Systemic Psoriasis: Classifications and Classification for the Distinction. *Front Med* (2021) 8:649408. doi: 10.3389/fmed.2021.649408

3. Raharja A, Mahil SK, Barker JN. Psoriasis: a brief overview. *Clin Med* (2021) 21:170–173. doi: 10.7861/clinmed.2021-0257

4. Boehncke W-H, Schön MP. Psoriasis. *The Lancet* (2015) 386:983–994. doi: 10.1016/S0140-6736(14)61909-7

5. Greb JE, Goldminz AM, Elder JT, Lebwohl MG, Gladman DD, Wu JJ, Mehta NN, Finlay AY, Gottlieb AB. Psoriasis. *Nat Rev Dis Primer* (2016) 2:16082. doi: 10.1038/nrdp.2016.82

6. Raychaudhuri SK, Maverakis E, Raychaudhuri SP. Diagnosis and classification of psoriasis. *Autoimmun Rev* (2014) 13:490–495. doi: 10.1016/j.autrev.2014.01.008

7. Fredriksson T, Pettersson U. Oral Treatment of Pustulosis Palmo-Plantaris with a New Retinoid, Ro 10-9359. *Dermatologica* (1979) 158:60–64. doi: 10.1159/000250744

8. Manchanda Y, De A, Das S, Chakraborty D. Disease Assessment in Psoriasis. *Indian J Dermatol* (2023) 68:278–281. doi: 10.4103/ijd.ijd_420_23

9. Feldman SR. Psoriasis assessment tools in clinical trials. *Ann Rheum Dis* (2005) 64:ii65–ii68. doi: 10.1136/ard.2004.031237

10. Finlay AY, Khan GK. Dermatology Life Quality Index (DLQI)-a simple practical measure for routine clinical use. *Clin Exp Dermatol* (1994) 19:210–216. doi: 10.1111/j.1365-2230.1994.tb01167.x

11. Parisi R, Symmons DPM, Griffiths CEM, Ashcroft DM. Global Epidemiology of Psoriasis: A Systematic Review of Incidence and Prevalence. *J Invest Dermatol* (2013) 133:377–385. doi: 10.1038/jid.2012.339

12. World Health Organization. *Global report on psoriasis*. Geneva: World Health Organization. (2016). https://iris.who.int/handle/10665/204417 [Accessed September 11, 2024]

13. Perera GK, Di Meglio P, Nestle FO. Psoriasis. *Annu Rev Pathol Mech Dis* (2012) 7:385–422. doi: 10.1146/annurev-pathol-011811-132448

14. Gmeiner T, Grzelj J, Strukelj B, Stopar L, Marko PB. Psoriasis: A Comprehensive Review on the Aetiopathogenesis and Recent Advances in Long-Term Management of

Patients with Plaque Psoriasis. *Pharmacol Amp Pharm* (2020) 11:373–401. doi: 10.4236/pp.2020.1112030

15. AlQassimi S, AlBrashdi S, Galadari H, Hashim MJ. Global burden of psoriasis – comparison of regional and global epidemiology, 1990 to 2017. *Int J Dermatol* (2020) 59:566–571. doi: 10.1111/ijd.14864

16. Bronckers IMGJ, Paller AS, van Geel MJ, van de Kerkhof PCM, Seyger MMB. Psoriasis in Children and Adolescents: Diagnosis, Management and Comorbidities. *Pediatr Drugs* (2015) 17:373–384. doi: 10.1007/s40272-015-0137-1

17. Langley RGB. Psoriasis: epidemiology, clinical features, and quality of life. *Ann Rheum Dis* (2005) 64:ii18–ii23. doi: 10.1136/ard.2004.033217

18. Griffiths CEM, Armstrong AW, Gudjonsson JE, Barker JNWN. Psoriasis. *The Lancet* (2021) 397:1301–1315. doi: 10.1016/S0140-6736(20)32549-6

19. Henseler T, Christophers E. Psoriasis of early and late onset: Characterization of two types of psoriasis vulgaris. *J Am Acad Dermatol* (1985) 13:450–456. doi: 10.1016/S0190-9622(85)70188-0

20. Iskandar IYK, Parisi R, Griffiths CEM, Ashcroft DM, the Global Psoriasis Atlas. Systematic review examining changes over time and variation in the incidence and prevalence of psoriasis by age and gender*. *Br J Dermatol* (2021) 184:243–258. doi: 10.1111/bjd.19169

21. Napolitano M, Mastroeni S, Fania L, Pallotta S, Fusari R, Uras C, Panebianco A, Cavani A, Sampogna F, Abeni D. Sex- and gender-associated clinical and psychosocial characteristics of patients with psoriasis. *Clin Exp Dermatol* (2020) 45:705–711. doi: 10.1111/ced.14218

22. Hägg D, Sundström A, Eriksson M, Schmitt-Egenolf M. Severity of Psoriasis Differs Between Men and Women: A Study of the Clinical Outcome Measure Psoriasis Area and Severity Index (PASI) in 5438 Swedish Register Patients. *Am J Clin Dermatol* (2017) 18:583–590. doi: 10.1007/s40257-017-0274-0

23. Na SJ, Jo SJ, Youn JI. Clinical study on psoriasis patients for past 30 years (1982–2012) in S eoul N ational U niversity H ospital P soriasis C linic. *J Dermatol* (2013) 40:731–735. doi: 10.1111/1346-8138.12224

24. Hägg D, Eriksson M, Sundström A, Schmitt-Egenolf M. The Higher Proportion of Men with Psoriasis Treated with Biologics May Be Explained by More Severe Disease in Men. *PLoS ONE* (2013) 8:e63619. doi: 10.1371/journal.pone.0063619

25. Daugaard C, Iversen L, Hjuler KF. Comorbidity in Adult Psoriasis: Considerations for the Clinician. *Psoriasis Targets Ther* (2022) Volume 12:139–150. doi: 10.2147/PTT.S328572

26. Yamazaki F. Psoriasis: Comorbidities. *J Dermatol* (2021) 48:732–740. doi: 10.1111/1346-8138.15840

27. Alinaghi F, Calov M, Kristensen LE, Gladman DD, Coates LC, Jullien D, Gottlieb AB, Gisondi P, Wu JJ, Thyssen JP, et al. Prevalence of psoriatic arthritis in patients with psoriasis: A systematic review and meta-analysis of observational and clinical studies. *J Am Acad Dermatol* (2019) 80:251-265.e19. doi: 10.1016/j.jaad.2018.06.027

28. Boehncke W-H, Menter A. Burden of Disease: Psoriasis and Psoriatic Arthritis. *Am J Clin Dermatol* (2013) 14:377–388. doi: 10.1007/s40257-013-0032-x

29. Armstrong EJ, Harskamp CT, Armstrong AW. Psoriasis and Major Adverse Cardiovascular Events: A Systematic Review and Meta-Analysis of Observational Studies. *J Am Heart Assoc Cardiovasc Cerebrovasc Dis* (2013) 2:e000062. doi: 10.1161/JAHA.113.000062

30. Wu JJ, Nguyen TU, Poon K-YT, Herrinton LJ. The association of psoriasis with autoimmune diseases. *J Am Acad Dermatol* (2012) 67:924–930. doi: 10.1016/j.jaad.2012.04.039

31. Jm G, Ab T, Jd L, Sk K, Db S, X W, Dj M, Bl S. The risk of mortality in patients with psoriasis: results from a population-based study. *Arch Dermatol* (2007) 143: doi: 10.1001/archderm.143.12.1493

32. Wu JJ, Suryavanshi M, Davidson D, Patel V, Jain A, Seigel L. Economic Burden of Comorbidities in Patients with Psoriasis in the USA. *Dermatol Ther* (2022) 13:207–219. doi: 10.1007/s13555-022-00832-9

33. Yu AP, Tang J, Xie J, Wu EQ, Gupta SR, Bao Y, M. Mulani P. Economic burden of psoriasis compared to the general population and stratified by disease severity. *Curr Med Res Opin* (2009) 25:2429–2438. doi: 10.1185/03007990903185557

34. Ha D, Lee J, Kim D, Oh I-S, Lee E-K, Shin J-Y. Healthcare utilization and medical expenditure of Korean psoriasis patients: A descriptive result using a health insurance database. *Medicine (Baltimore)* (2018) 97:e11070. doi: 10.1097/MD.0000000000011070

35. Lønnberg AS, Skov L, Skytthe A, Kyvik KO, Pedersen OB, Thomsen SF. Heritability of psoriasis in a large twin sample. *Br J Dermatol* (2013) 169:412–416. doi: 10.1111/bjd.12375

36. Ogawa K, Okada Y. The current landscape of psoriasis genetics in 2020. *J Dermatol Sci* (2020) 99:2–8. doi: 10.1016/j.jdermsci.2020.05.008

37. Huang Y-H, Kuo C-F, Huang L-H, Hsieh M-Y. Familial Aggregation of Psoriasis and Co-Aggregation of Autoimmune Diseases in Affected Families. *J Clin Med* (2019) 8:115. doi: 10.3390/jcm8010115

38. Duffy DL, Spelman LS, Martin NG. Psoriasis in Australian twins. *J Am Acad Dermatol* (1993) 29:428–434. doi: 10.1016/0190-9622(93)70206-9

39. Schön MP, Boehncke W-H. Psoriasis. *N Engl J Med* (2005) 352:1899–1912. doi: 10.1056/NEJMra041320

40. Morris A, Rogers M, Fischer G, Williams K. Childhood Psoriasis: A Clinical Review of 1262 Cases. *Pediatr Dermatol* (2001) 18:188–198. doi: 10.1046/j.1525-1470.2001.018003188.x

41. Nair RP, Stuart PE, Nistor I, Hiremagalore R, Chia NVC, Jenisch S, Weichenthal M, Abecasis GR, Lim HW, Christophers E, et al. Sequence and Haplotype Analysis Supports HLA-C as the Psoriasis Susceptibility 1 Gene. *Am J Hum Genet* (2006) 78:827–851. doi: 10.1086/503821

42. Mahil SK, Capon F, Barker JN. Genetics of Psoriasis. *Dermatol Clin* (2015) 33:1–11. doi: 10.1016/j.det.2014.09.001

43. Guðjónsson JE, Valdimarsson H, Kárason A, Antonsdóttir AA, Hjaltey Rúnarsdóttir E, Gulcher JR, Stefánsson K. HLA-Cw6-Positive and HLA-Cw6-Negative Patients with Psoriasis Vulgaris have Distinct Clinical Features. *J Invest Dermatol* (2002) 118:362–365. doi: 10.1046/j.0022-202x.2001.01656.x

44. Thorleifsdottir RH, Sigurdardottir SL, Sigurgeirsson B, Olafsson JH, Petersen H, Sigurdsson MI, Gudjonsson JE, Johnston A, Valdimarsson H. HLA-Cw6 homozygosity in plaque psoriasis is associated with streptococcal throat infections and pronounced improvement after tonsillectomy: A prospective case series. *J Am Acad Dermatol* (2016) 75:889–896. doi: 10.1016/j.jaad.2016.06.061

45. Farber EM, Nall ML, Watson W. Natural History of Psoriasis in 61 Twin Pairs.

46. Gudjonsson JE, Thorarinsson AM, Sigurgeirsson B, Kristinsson KG, Valdimarsson H. Streptococcal throat infections and exacerbation of chronic plaque psoriasis: a prospective study. *Br J Dermatol* (2003) 149:530–534. doi: 10.1046/j.1365-2133.2003.05552.x

47. Kamiya K, Kishimoto M, Sugai J, Komine M, Ohtsuki M. Risk Factors for the Development of Psoriasis. *Int J Mol Sci* (2019) 20:4347. doi: 10.3390/ijms20184347

48. Fry L, Baker BS. Triggering psoriasis: the role of infections and medications. *Clin Dermatol* (2007) 25:606–615. doi: 10.1016/j.clindermatol.2007.08.015

49. Thorleifsdottir RH, Sigurdardottir SL, Sigurgeirsson B, Olafsson JH, Sigurdsson MI, Petersen H, Arnadottir S, Gudjonsson JE, Johnston A, Valdimarsson H. Improvement of Psoriasis after Tonsillectomy Is Associated with a Decrease in the Frequency of Circulating T Cells That Recognize Streptococcal Determinants and Homologous Skin Determinants. *J Immunol* (2012) 188:5160–5165. doi: 10.4049/jimmunol.1102834

50. Valdimarsson H, Thorleifsdottir RH, Sigurdardottir SL, Gudjonsson JE, Johnston A. Psoriasis – as an autoimmune disease caused by molecular mimicry. *Trends Immunol* (2009) 30:494–501. doi: 10.1016/j.it.2009.07.008

51. Diluvio L, Vollmer S, Besgen P, Ellwart JW, Chimenti S, Prinz JC. Identical TCR beta-chain rearrangements in streptococcal angina and skin lesions of patients with psoriasis vulgaris. *J Immunol Baltim Md 1950* (2006) 176:7104–7111. doi: 10.4049/jimmunol.176.11.7104

52. Visser MJE, Kell DB, Pretorius E. Bacterial Dysbiosis and Translocation in Psoriasis Vulgaris. *Front Cell Infect Microbiol* (2019) 9:7. doi: 10.3389/fcimb.2019.00007

53. Fyhrquist N, Muirhead G, Prast-Nielsen S, Jeanmougin M, Olah P, Skoog T, Jules-Clement G, Feld M, Barrientos-Somarribas M, Sinkko H, et al. Microbe-host interplay in atopic dermatitis and psoriasis. *Nat Commun* (2019) 10:4703. doi: 10.1038/s41467-019-12253-y

54. Chen L, Li J, Zhu W, Kuang Y, Liu T, Zhang W, Chen X, Peng C. Skin and Gut Microbiome in Psoriasis: Gaining Insight Into the Pathophysiology of It and Finding Novel Therapeutic Strategies. *Front Microbiol* (2020) 11:589726. doi: 10.3389/fmicb.2020.589726

55. Arias-Santiago S, Espiñeira-Carmona MJ, Aneiros-Fernández J. The Koebner phenomenon: psoriasis in tattoos. *Can Med Assoc J* (2013) 185:585–585. doi: 10.1503/cmaj.111299

56. Jin Y, Yang S, Zhang F, Kong Y, Xiao F, Hou Y, Fan X, Zhang X. Combined effects of *HLA-Cw6* and cigarette smoking in psoriasis vulgaris: A hospital-based case–control study in China. *J Eur Acad Dermatol Venereol* (2009) 23:132–137. doi: 10.1111/j.1468-3083.2008.02951.x

57. Di Meglio P, Perera GK, Nestle FO. The Multitasking Organ: Recent Insights into Skin Immune Function. *Immunity* (2011) 35:857–869. doi: 10.1016/j.immuni.2011.12.003

58. Murphy M, Kerr P, Grant-Kels JM. The histopathologic spectrum of psoriasis. *Clin Dermatol* (2007) 25:524–528. doi: 10.1016/j.clindermatol.2007.08.005

59. Bowcock AM, Krueger JG. Getting under the skin: the immunogenetics of psoriasis. *Nat Rev Immunol* (2005) 5:699–711. doi: 10.1038/nri1689

60. Lowes MA, Bowcock AM, Krueger JG. Pathogenesis and therapy of psoriasis. *Nature* (2007) 445:866–873. doi: 10.1038/nature05663

61. Billi AC, Gudjonsson JE, Voorhees JJ. Psoriasis: Past, Present, and Future. *J Invest Dermatol* (2019) 139:e133–e142. doi: 10.1016/j.jid.2019.08.437

62. Arakawa A, Siewert K, Stöhr J, Besgen P, Kim S-M, Rühl G, Nickel J, Vollmer S, Thomas P, Krebs S, et al. Melanocyte antigen triggers autoimmunity in human psoriasis. *J Exp Med* (2015) 212:2203–2212. doi: 10.1084/jem.20151093

63. Fuentes-Duculan J, Bonifacio KM, Hawkes JE, Kunjravia N, Cueto I, Li X, Gonzalez J, Garcet S, Krueger JG. Autoantigens ADAMTSL5 and LL37 are significantly upregulated in active Psoriasis and localized with keratinocytes, dendritic cells and other leukocytes. *Exp Dermatol* (2017) 26:1075–1082. doi: 10.1111/exd.13378

64. Lande R, Botti E, Jandus C, Dojcinovic D, Fanelli G, Conrad C, Chamilos G, Feldmeyer L, Marinari B, Chon S, et al. The antimicrobial peptide LL37 is a T-cell autoantigen in psoriasis. *Nat Commun* (2014) 5:5621. doi: 10.1038/ncomms6621

65. Ten Bergen LL, Petrovic A, Aarebrot AK, Appel S. Current knowledge on autoantigens and autoantibodies in psoriasis. *Scand J Immunol* (2020) 92:e12945. doi: 10.1111/sji.12945

66. Kim J, Krueger JG. Highly Effective New Treatments for Psoriasis Target the IL-23/Type 17 T Cell Autoimmune Axis. *Annu Rev Med* (2017) 68:255–269. doi: 10.1146/annurev-med-042915-103905

67. Guo J, Zhang H, Lin W, Lu L, Su J, Chen X. Signaling pathways and targeted therapies for psoriasis. *Signal Transduct Target Ther* (2023) 8:437. doi: 10.1038/s41392-023-01655-6

68. Roesner LM, Farag AK, Pospich R, Traidl S, Werfel T. T-cell receptor sequencing specifies psoriasis as a systemic and atopic dermatitis as a skin-focused, allergen-driven disease. *Allergy* (2022) 77:2737–2747. doi: 10.1111/all.15272

69. Korman NJ. Management of psoriasis as a systemic disease: what is the evidence? *Br J Dermatol* (2020) 182:840–848. doi: 10.1111/bjd.18245

70. Di Meglio P, Nestle FO. "Immunopathogenesis of Psoriasis.," In: Gaspari AA, Tyring SK, Kaplan DH, editors. *Clinical and Basic Immunodermatology*. Cham: Springer International Publishing (2017). p. 373–395 doi: 10.1007/978-3-319-29785-9_21

71. Lande R, Chamilos G, Ganguly D, Demaria O, Frasca L, Durr S, Conrad C, Schröder J, Gilliet M. Cationic antimicrobial peptides in psoriatic skin cooperate to break innate tolerance to self-DNA. *Eur J Immunol* (2015) 45:203–213. doi: 10.1002/eji.201344277

72. Lande R, Gregorio J, Facchinetti V, Chatterjee B, Wang Y-H, Homey B, Cao W, Wang Y-H, Su B, Nestle FO, et al. Plasmacytoid dendritic cells sense self-DNA coupled with antimicrobial peptide. *Nature* (2007) 449:564–569. doi: 10.1038/nature06116

73. Johnson-Huang LM, Suárez-Fariñas M, Pierson KC, Fuentes-Duculan J, Cueto I, Lentini T, Sullivan-Whalen M, Gilleaudeau P, Krueger JG, Haider AS, et al. A single intradermal injection of IFN-γ induces an inflammatory state in both non-lesional psoriatic and healthy skin. *J Invest Dermatol* (2012) 132:1177–1187. doi: 10.1038/jid.2011.458

74. Schlaak JF, Buslau M, Jochum W, Hermann E, Girndt M, Gallati H, Meyer zum Büschenfelde KH, Fleischer B. T cells involved in psoriasis vulgaris belong to the Th1 subset. *J Invest Dermatol* (1994) 102:145–149. doi: 10.1111/1523-1747.ep12371752

75. Uyemura K, Yamamura M, Fivenson DF, Modlin RL, Nickoloff BJ. The cytokine network in lesional and lesion-free psoriatic skin is characterized by a T-helper type 1 cell-mediated response. *J Invest Dermatol* (1993) 101:701–705. doi: 10.1111/1523-1747.ep12371679

76. Hawkes JE, Yan BY, Chan TC, Krueger JG. Discovery of the IL-23/IL-17 Signaling Pathway and the Treatment of Psoriasis. *J Immunol* (2018) 201:1605–1613. doi: 10.4049/jimmunol.1800013

77. Keijsers RRMC, Joosten I, Van Erp PEJ, Koenen HJPM, Van De Kerkhof PeterCM. Cellular sources of IL -17 in psoriasis: a paradigm shift? *Exp Dermatol* (2014) 23:799–803. doi: 10.1111/exd.12487

78. Šahmatova L, Sügis E, Šunina M, Hermann H, Prans E, Pihlap M, Abram K, Rebane A, Peterson H, Peterson P, et al. Signs of innate immune activation and premature immunosenescence in psoriasis patients. *Sci Rep* (2017) 7:7553. doi: 10.1038/s41598-017-07975-2

79. Ehst B, Wang Z, Leitenberger J, McClanahan D, De La Torre R, Sawka E, Ortega-Loayza AG, Strunck J, Greiling T, Simpson E, et al. Synergistic induction of IL-23 by TNFα, IL-17A, and EGF in keratinocytes. *Cytokine* (2021) 138:155357. doi: 10.1016/j.cyto.2020.155357

80. Chaudhari U, Romano P, Mulcahy LD, Dooley LT, Baker DG, Gottlieb AB. Efficacy and safety of infliximab monotherapy for plaque-type psoriasis: a randomised trial. *Lancet Lond Engl* (2001) 357:1842–1847. doi: 10.1016/s0140-6736(00)04954-0

81. Mease PJ, Goffe BS, Metz J, VanderStoep A, Finck B, Burge DJ. Etanercept in the treatment of psoriatic arthritis and psoriasis: a randomised trial. *The Lancet* (2000) 356:385–390. doi: 10.1016/S0140-6736(00)02530-7

82. Ten Bergen LL, Petrovic A, Krogh Aarebrot A, Appel S. The TNF/IL-23/IL-17 axis—Head-to-head trials comparing different biologics in psoriasis treatment. *Scand J Immunol* (2020) 92:e12946. doi: 10.1111/sji.12946

83. Honda H, Umezawa Y, Kikuchi S, Yanaba K, Fukuchi O, Ito T, Nobeyama Y, Asahina A, Nakagawa H. Switching of biologics in psoriasis: Reasons and results. *J Dermatol* (2017) 44:1015–1019. doi: 10.1111/1346-8138.13860

84. Hu Y, Chen Z, Gong Y, Shi Y. A Review of Switching Biologic Agents in the Treatment of Moderate-to-Severe Plaque Psoriasis. *Clin Drug Investig* (2018) 38:191–199. doi: 10.1007/s40261-017-0603-3

85. Zhang P, Su Y, Li S, Chen H, Wu R, Wu H. The roles of T cells in psoriasis. *Front Immunol* (2023) 14:1081256. doi: 10.3389/fimmu.2023.1081256

86. Masson Regnault M, Konstantinou M-P, Khemis A, Poulin Y, Bourcier M, Amelot F, Bulaï Livideanu C, Paul C. Early relapse of psoriasis after stopping brodalumab: a retrospective cohort study in 77 patients. *J Eur Acad Dermatol Venereol JEADV* (2017) 31:1491–1496. doi: 10.1111/jdv.14387

87. Tokura Y, Phadungsaksawasdi P, Kurihara K, Fujiyama T, Honda T. Pathophysiology of Skin Resident Memory T Cells. *Front Immunol* (2021) 11:618897. doi: 10.3389/fimmu.2020.618897

88. Gallais Sérézal I, Classon C, Cheuk S, Barrientos-Somarribas M, Wadman E, Martini E, Chang D, Xu Landén N, Ehrström M, Nylén S, et al. Resident T Cells in Resolved Psoriasis Steer Tissue Responses that Stratify Clinical Outcome. *J Invest Dermatol* (2018) 138:1754–1763. doi: 10.1016/j.jid.2018.02.030

89. Kurihara K, Fujiyama T, Phadungsaksawasdi P, Ito T, Tokura Y. Significance of IL-17A-producing CD8+CD103+ skin resident memory T cells in psoriasis lesion and their possible relationship to clinical course. *J Dermatol Sci* (2019) 95:21–27. doi: 10.1016/j.jdermsci.2019.06.002

90. Liu G, Wang Z, Li S. Heterogeneity and plasticity of tissue-resident memory T cells in skin diseases and homeostasis: a review. *Front Immunol* (2024) 15:1378359. doi: 10.3389/fimmu.2024.1378359

91. Liu J, Chang H-W, Huang Z-M, Nakamura M, Sekhon S, Ahn R, Munoz-Sandoval P, Bhattarai S, Beck KM, Sanchez IM, et al. Single-cell RNA sequencing of psoriatic skin identifies pathogenic Tc17 cell subsets and reveals distinctions between CD8+ T cells in autoimmunity and cancer. *J Allergy Clin Immunol* (2021) 147:2370–2380. doi: 10.1016/j.jaci.2020.11.028

92. Lowes MA, Kikuchi T, Fuentes-Duculan J, Cardinale I, Zaba LC, Haider AS, Bowman EP, Krueger JG. Psoriasis vulgaris lesions contain discrete populations of Th1 and Th17 T cells. *J Invest Dermatol* (2008) 128:1207–1211. doi: 10.1038/sj.jid.5701213

93. Johnston A, Gudjonsson JE, Sigmundsdottir H, Love TJ, Valdimarsson H. Peripheral blood T cell responses to keratin peptides that share sequences with streptococcal M proteins are largely restricted to skin-homing CD8+ T cells. *Clin Exp Immunol* (2004) 138:83–93. doi: 10.1111/j.1365-2249.2004.00600.x

94. Cheung KL, Jarrett R, Subramaniam S, Salimi M, Gutowska-Owsiak D, Chen Y-L, Hardman C, Xue L, Cerundolo V, Ogg G. Psoriatic T cells recognize neolipid antigens generated by mast cell phospholipase delivered by exosomes and presented by CD1a. *J Exp Med* (2016) 213:2399–2412. doi: 10.1084/jem.20160258

95. Harden JL, Hamm D, Gulati N, Lowes MA, Krueger JG. Deep Sequencing of the T-cell Receptor Repertoire Demonstrates Polyclonal T-cell Infiltrates in Psoriasis. *F1000Research* (2015) 4:460. doi: 10.12688/f1000research.6756.1

96. Matos TR, O'Malley JT, Lowry EL, Hamm D, Kirsch IR, Robins HS, Kupper TS, Krueger JG, Clark RA. Clinically resolved psoriatic lesions contain psoriasis-specific IL-17-producing αβ T cell clones. *J Clin Invest* (2017) 127:4031–4041. doi: 10.1172/JCI93396

97. Zhang B, Roesner LM, Traidl S, Koeken VACM, Xu C-J, Werfel T, Li Y. Single-cell profiles reveal distinctive immune response in atopic dermatitis in contrast to psoriasis. *Allergy* (2023) 78:439–453. doi: 10.1111/all.15486

98. Ferran M, Romeu ER, Rincón C, Sagristà M, Giménez Arnau AM, Celada A, Pujol RM, Holló P, Jókai H, Santamaria-BabÍ LF. Circulating CLA + T lymphocytes as peripheral cell biomarkers in T -cell-mediated skin diseases. *Exp Dermatol* (2013) 22:439–442. doi: 10.1111/exd.12154

99. Fuhlbrigge RC, Kieffer JD, Armerding D, Kupper TS. Cutaneous lymphocyte antigen is a specialized form of PSGL-1 expressed on skin-homing T cells. *Nature* (1997) 389:978–981. doi: 10.1038/40166

100. Clark RA, Chong B, Mirchandani N, Brinster NK, Yamanaka K, Dowgiert RK, Kupper TS. The Vast Majority of CLA+ T Cells Are Resident in Normal Skin. *J Immunol* (2006) 176:4431–4439. doi: 10.4049/jimmunol.176.7.4431

101. De Jesús-Gil C, Ruiz-Romeu E, Ferran M, Chiriac A, Deza G, Hóllo P, Celada A, Pujol RM, Santamaria-Babí LF. CLA+ T Cell Response to Microbes in Psoriasis. *Front Immunol* (2018) 9:1488. doi: 10.3389/fimmu.2018.01488

102. De Jesús-Gil C, Sans-de San Nicolàs L, García-Jiménez I, Ferran M, Pujol RM, Santamaria-Babí LF. Human CLA+ Memory T Cell and Cytokines in Psoriasis. *Front Med* (2021) 8:731911. doi: 10.3389/fmed.2021.731911

103. Picker LJ, Michie SA, Rott LS, Butcher EC. A unique phenotype of skin-associated lymphocytes in humans. Preferential expression of the HECA-452 epitope by benign and malignant T cells at cutaneous sites. *Am J Pathol* (1990) 136:1053–1068.

104. Cordiali-Fei P, Bianchi L, Bonifati C, Trento E, Ruzzetti M, Francesconi F, Bultrini S, D'Agosto G, Bordignon V, Francavilla V, et al. Immunologic Biomarkers for Clinical and Therapeutic Management of Psoriasis. *Mediators Inflamm* (2014) 2014:1–11. doi: 10.1155/2014/236060

105. Laggner U, Meglio PD, Perera GK, Hundhausen C, Lacy KE, Ali N, Smith CH, Hayday AC, Nickoloff BJ, Nestle FO. Identification of a Novel Proinflammatory Human Skin-Homing Vγ9Vδ2 T Cell Subset with a Potential Role in Psoriasis. *J Immunol* (2011) 187:2783–2793. doi: 10.4049/jimmunol.1100804

106. Sigmundsdóttir H, Gudjónsson JE, Jónsdóttir I, Lúdvíksson BR, Valdimarsson H. The frequency of CLA+ CD8+ T cells in the blood of psoriasis patients correlates closely with the severity of their disease. *Clin Exp Immunol* (2008) 126:365–369. doi: 10.1046/j.1365-2249.2001.01688.x

107. Teunissen MBM, Yeremenko NG, Baeten DLP, Chielie S, Spuls PI, de Rie MA, Lantz O, Res PCM. The IL-17A-Producing CD8 + T-Cell Population in Psoriatic Lesional Skin Comprises Mucosa-Associated Invariant T Cells and Conventional T Cells. *J Invest Dermatol* (2014) 134:2898–2907. doi: 10.1038/jid.2014.261

108. Davison SC, Ballsdon A, Allen MH, Barker JNWN. Early migration of cutaneous lymphocyte-associated antigen (CLA) positive T cells into evolving psoriatic plaques. *Exp Dermatol* (2001) 10:280–285. doi: 10.1034/j.1600-0625.2001.100408.x

109. Harper EG, Simpson EL, Takiguchi RH, Boyd MD, Kurtz SE, Bakke AC, Blauvelt A. Efalizumab therapy for atopic dermatitis causes marked increases in circulating effector memory CD4+ T cells that express cutaneous lymphocyte antigen. *J Invest Dermatol* (2008) 128:1173–1181. doi: 10.1038/sj.jid.5701169

110. Vugmeyster Y, Kikuchi T, Lowes MA, Chamian F, Kagen M, Gilleaudeau P, Lee E, Howell K, Bodary S, Dummer W, et al. Efalizumab (anti-CD11a)-induced increase in peripheral blood leukocytes in psoriasis patients is preferentially mediated by altered trafficking of memory CD8+ T cells into lesional skin. *Clin Immunol* (2004) 113:38–46. doi: 10.1016/j.clim.2004.06.001

111. Eysteinsdóttir JH, Sigurgrímsdóttir H, Einarsdóttir HK, Freysdottir J, Agnarsson BA, Ólafsson JH, Sigurgeirsson B, Lúðvíksson BR. Effective treatment with balneophototherapy and narrowband UVB monotherapy reduces skin homing Th17/Tc17 and Th22/Tc22 effector cells in peripheral blood in patients with psoriasis. *J Dermatol Sci* (2019) 96:110–112. doi: 10.1016/j.jdermsci.2019.10.001

112. Diani M, Galasso M, Cozzi C, Sgambelluri F, Altomare A, Cigni C, Frigerio E, Drago L, Volinia S, Granucci F, et al. Blood to skin recirculation of CD4+ memory T cells associates with cutaneous and systemic manifestations of psoriatic disease. *Clin Immunol Orlando Fla* (2017) 180:84–94. doi: 10.1016/j.clim.2017.04.001

113. Klicznik MM, Morawski PA, Höllbacher B, Varkhande SR, Motley S, Kuri-Cervantes L, Goodwin E, Rosenblum MD, Long SA, Brachtl G, et al. Human CD4 $^{+}$ CD103 $^{+}$ cutaneous resident memory T cells are found in the circulation of healthy subjects. (2018) doi: 10.1101/361758

114. Kagami S, Rizzo HL, Lee JJ, Koguchi Y, Blauvelt A. Circulating Th17, Th22, and Th1 Cells Are Increased in Psoriasis. *J Invest Dermatol* (2010) 130:1373–1383. doi: 10.1038/jid.2009.399

115. Prpić Massari L, Kaštelan M, Laškarin G, Zamolo G, Massari D, Rukavina D. Analysis of perforin expression in peripheral blood and lesions in severe and mild psoriasis. *J Dermatol Sci* (2007) 47:29–36. doi: 10.1016/j.jdermsci.2007.02.007

116. Lee BH, Bang YJ, Lim SH, Kang S-J, Kim SH, Kim-Schulze S, Park C-G, Kim HJ, Kim T-G. High-dimensional profiling of regulatory T cells in psoriasis reveals an impaired skin-trafficking property. *eBioMedicine* (2024) 100:104985. doi: 10.1016/j.ebiom.2024.104985

117. Cao X, Wa Q, Wang Q, Li L, Liu X, An L, Cai R, Du M, Qiu Y, Han J, et al. High throughput sequencing reveals the diversity of TRB-CDR3 repertoire in patients with psoriasis vulgaris. *Int Immunopharmacol* (2016) 40:487–491. doi: 10.1016/j.intimp.2016.10.004

118. Prpić L, Strbo N, Sotosek V, Gruber F, Podack ER, Rukavina D. Assessment of perforin expression in peripheral blood lymphocytes in psoriatic patients during exacerbation of disease. *Acta Derm Venereol Suppl (Stockh)* (2000)14–16. doi: 10.1080/00015550050500059

119. Zhou J, Zhang J, Tao L, Peng K, Zhang Q, Yan K, Luan J, Pan J, Su X, Sun J, et al. Up-regulation of BTN3A1 on CD14+ cells promotes Vγ9Vδ2 T cell activation in psoriasis. *Proc Natl Acad Sci U S A* (2022) 119:e2117523119. doi: 10.1073/pnas.2117523119

120. Cai Y, Shen X, Ding C, Qi C, Li K, Li X, Jala VR, Zhang H, Wang T, Zheng J, et al. Pivotal role of dermal IL-17-producing γδ T cells in skin inflammation. *Immunity* (2011) 35:596–610. doi: 10.1016/j.immuni.2011.08.001

121. Kurioka A, Klenerman P. Aging unconventionally: γδ T cells, iNKT cells, and MAIT cells in aging. *Semin Immunol* (2023) 69:101816. doi: 10.1016/j.smim.2023.101816

122. Constantinides MG, Belkaid Y. Early-life imprinting of unconventional T cells and tissue homeostasis. *Science* (2021) 374:eabf0095. doi: 10.1126/science.abf0095

123. Mayassi T, Barreiro LB, Rossjohn J, Jabri B. A multilayered immune system through the lens of unconventional T cells. *Nature* (2021) 595:501–510. doi: 10.1038/s41586-021-03578-0

124. Gully BS, Rossjohn J, Davey MS. Our evolving understanding of the role of the γδ T cell receptor in γδ T cell mediated immunity. *Biochem Soc Trans* (2021) 49:1985–1995. doi: 10.1042/BST20200890

125. Liu N, Qin H, Cai Y, Li X, Wang L, Xu Q, Xue F, Chen L, Ding C, Hu X, et al. Dynamic trafficking patterns of IL-17-producing γδ T cells are linked to the recurrence of skin inflammation in psoriasis-like dermatitis. *eBioMedicine* (2022) 82:104136. doi: 10.1016/j.ebiom.2022.104136

126. Turner SJ, Doherty PC, McCluskey J, Rossjohn J. Structural determinants of T-cell receptor bias in immunity. *Nat Rev Immunol* (2006) 6:883–894. doi: 10.1038/nri1977

127. Arunkumar M, Zielinski CE. T-Cell Receptor Repertoire Analysis with Computational Tools—An Immunologist's Perspective. *Cells* (2021) 10:3582. doi: 10.3390/cells10123582

128. Rosati E, Dowds CM, Liaskou E, Henriksen EKK, Karlsen TH, Franke A. Overview of methodologies for T-cell receptor repertoire analysis. *BMC Biotechnol* (2017) 17:61. doi: 10.1186/s12896-017-0379-9

129. Sender R, Weiss Y, Navon Y, Milo I, Azulay N, Keren L, Fuchs S, Ben-Zvi D, Noor E, Milo R. The total mass, number, and distribution of immune cells in the human body. *Proc Natl Acad Sci* (2023) 120:e2308511120. doi: 10.1073/pnas.2308511120

130. Sofou E, Vlachonikola E, Zaragoza-Infante L, Brüggemann M, Darzentas N, Groenen PJTA, Hummel M, Macintyre EA, Psomopoulos F, Davi F, et al. Clonotype definitions for immunogenetic studies: proposals from the EuroClonality NGS Working Group. *Leukemia* (2023) 37:1750–1752. doi: 10.1038/s41375-023-01952-7

131. Weng N-P. Numbers and odds: TCR repertoire size and its age changes impacting on T cell functions. *Semin Immunol* (2023) 69:101810. doi: 10.1016/j.smim.2023.101810

132. Hayday AC, Saito H, Gillies SD, Kranz DM, Tanigawa G, Eisen HN, Tonegawa S. Structure, organization, and somatic rearrangement of T cell gamma genes. *Cell* (1985) 40:259–269. doi: 10.1016/0092-8674(85)90140-0

133. Chien YH, Iwashima M, Kaplan KB, Elliott JF, Davis MM. A new T-cell receptor gene located within the alpha locus and expressed early in T-cell differentiation. *Nature* (1987) 327:677–682. doi: 10.1038/327677a0

134. Rhodes DA, Chen H-C, Price AJ, Keeble AH, Davey MS, James LC, Eberl M, Trowsdale J. Activation of Human γδ T Cells by Cytosolic Interactions of BTN3A1 with Soluble Phosphoantigens and the Cytoskeletal Adaptor Periplakin. *J Immunol* (2015) 194:2390–2398. doi: 10.4049/jimmunol.1401064

135. Sandstrom A, Peigné C-M, Léger A, Crooks JE, Konczak F, Gesnel M-C, Breathnach R, Bonneville M, Scotet E, Adams EJ. The intracellular B30.2 domain of butyrophilin 3A1 binds phosphoantigens to mediate activation of human Vγ9Vδ2 T cells. *Immunity* (2014) 40:490–500. doi: 10.1016/j.immuni.2014.03.003

136. Uldrich AP, Le Nours J, Pellicci DG, Gherardin NA, McPherson KG, Lim RT, Patel O, Beddoe T, Gras S, Rossjohn J, et al. CD1d-lipid antigen recognition by the γδ TCR. *Nat Immunol* (2013) 14:1137–1145. doi: 10.1038/ni.2713

137. Harly C, Joyce SP, Domblides C, Bachelet T, Pitard V, Mannat C, Pappalardo A, Couzi L, Netzer S, Massara L, et al. Human γδ T cell sensing of AMPK-dependent metabolic tumor reprogramming through TCR recognition of EphA2. *Sci Immunol* (2021) 6:eaba9010. doi: 10.1126/sciimmunol.aba9010

138. Willcox CR, Pitard V, Netzer S, Couzi L, Salim M, Silberzahn T, Moreau J-F, Hayday AC, Willcox BE, Déchanet-Merville J. Cytomegalovirus and tumor stress surveillance by binding of a human γδ T cell antigen receptor to endothelial protein C receptor. *Nat Immunol* (2012) 13:872–879. doi: 10.1038/ni.2394

139. Marlin R, Pappalardo A, Kaminski H, Willcox CR, Pitard V, Netzer S, Khairallah C, Lomenech A-M, Harly C, Bonneville M, et al. Sensing of cell stress by human γδ TCR-dependent recognition of annexin A2. *Proc Natl Acad Sci* (2017) 114:3163–3168. doi: 10.1073/pnas.1621052114

140. Davey MS, Willcox CR, Hunter S, Kasatskaya SA, Remmerswaal EBM, Salim M, Mohammed F, Bemelman FJ, Chudakov DM, Oo YH, et al. The human Vδ2+ T-cell compartment comprises distinct innate-like Vγ9+ and adaptive Vγ9- subsets. *Nat Commun* (2018) 9:1760. doi: 10.1038/s41467-018-04076-0

141. Davey MS, Willcox CR, Joyce SP, Ladell K, Kasatskaya SA, McLaren JE, Hunter S, Salim M, Mohammed F, Price DA, et al. Clonal selection in the human Vδ1 T cell repertoire indicates γδ TCR-dependent adaptive immune surveillance. *Nat Commun* (2017) 8:14760. doi: 10.1038/ncomms14760

142. McMurray JL, von Borstel A, Taher TE, Syrimi E, Taylor GS, Sharif M, Rossjohn J, Remmerswaal EBM, Bemelman FJ, Vieira Braga FA, et al. Transcriptional profiling of human Vδ1 T cells reveals a pathogen-driven adaptive differentiation program. *Cell Rep* (2022) 39:110858. doi: 10.1016/j.celrep.2022.110858

143. Davey MS, Willcox CR, Baker AT, Hunter S, Willcox BE. Recasting Human Vδ1 Lymphocytes in an Adaptive Role. *Trends Immunol* (2018) 39:446–459. doi: 10.1016/j.it.2018.03.003

144. Ravens S, Schultze-Florey C, Raha S, Sandrock I, Drenker M, Oberdörfer L, Reinhardt A, Ravens I, Beck M, Geffers R, et al. Human γδ T cells are quickly reconstituted after stem-cell transplantation and show adaptive clonal expansion in response to viral infection. *Nat Immunol* (2017) 18:393–401. doi: 10.1038/ni.3686

145. Hu Y, Hu Q, Li Y, Lu L, Xiang Z, Yin Z, Kabelitz D, Wu Y. γδ T cells: origin and fate, subsets, diseases and immunotherapy. *Signal Transduct Target Ther* (2023) 8:434. doi: 10.1038/s41392-023-01653-8

146. Provine NM, Binder B, FitzPatrick MEB, Schuch A, Garner LC, Williamson KD, Van Wilgenburg B, Thimme R, Klenerman P, Hofmann M. Unique and Common Features of Innate-Like Human Vδ2+ γδT Cells and Mucosal-Associated Invariant T Cells. *Front Immunol* (2018) 9:756. doi: 10.3389/fimmu.2018.00756

147. Davey MS, Willcox CR, Hunter S, Oo YH, Willcox BE. Vδ2+ T Cells—Two Subsets for the Price of One. *Front Immunol* (2018) 9:2106. doi: 10.3389/fimmu.2018.02106

148. Gutierrez-Arcelus M, Teslovich N, Mola AR, Polidoro RB, Nathan A, Kim H, Hannes S, Slowikowski K, Watts GFM, Korsunsky I, et al. Lymphocyte innateness defined by transcriptional states reflects a balance between proliferation and effector functions. *Nat Commun* (2019) 10:687. doi: 10.1038/s41467-019-08604-4

149. IMGT, the international ImMunoGeneTics information system - PubMed. https://pubmed.ncbi.nlm.nih.gov/18978023/ [Accessed October 3, 2024]

150. Carding SR, Egan PJ. Gammadelta T cells: functional plasticity and heterogeneity. *Nat Rev Immunol* (2002) 2:336–345. doi: 10.1038/nri797

151. Willcox CR, Davey MS, Willcox BE. Development and Selection of the Human Vγ9Vδ2+ T-Cell Repertoire. *Front Immunol* (2018) 9:1501. doi: 10.3389/fimmu.2018.01501

152. Puan K-J, Jin C, Wang H, Sarikonda G, Raker AM, Lee HK, Samuelson MI, Marker-Hermann E, Pasa-Tolic L, Nieves E, et al. Preferential recognition of a microbial metabolite by human V 2V 2 T cells. *Int Immunol* (2007) 19:657–673. doi: 10.1093/intimm/dxm031

153. Ashihara E, Munaka T, Kimura S, Kanai M, Abe H, Hirai H, Shoji S, Maekawa T. Isopentenyl Pyrophosphate (IPP), a Metabolite produced in Myeloma Cells Induces the Chemotaxis of γδT Cells. *Blood* (2010) 116:2766. doi: 10.1182/blood.V116.21.2766.2766

154. Karunakaran MM, Subramanian H, Jin Y, Mohammed F, Kimmel B, Juraske C, Starick L, Nöhren A, Länder N, Willcox CR, et al. A distinct topology of BTN3A IgV and B30.2 domains controlled by juxtamembrane regions favors optimal human γδ T cell phosphoantigen sensing. *Nat Commun* (2023) 14:7617. doi: 10.1038/s41467-023-41938-8

155. Vavassori S, Kumar A, Wan GS, Ramanjaneyulu GS, Cavallari M, El Daker S, Beddoe T, Theodossis A, Williams NK, Gostick E, et al. Butyrophilin 3A1 binds phosphorylated antigens and stimulates human γδ T cells. *Nat Immunol* (2013) 14:908–916. doi: 10.1038/ni.2665

156. Sanz M, Mann BT, Ryan PL, Bosque A, Pennington DJ, Hackstein H, Soriano-Sarabia N. Deep characterization of human γδ T cell subsets defines shared and lineage-specific traits. *Front Immunol* (2023) 14:1148988. doi: 10.3389/fimmu.2023.1148988

157. Glatzel A, Wesch D, Schiemann F, Brandt E, Janssen O, Kabelitz D. Patterns of Chemokine Receptor Expression on Peripheral Blood γδ T Lymphocytes: Strong Expression of CCR5 Is a Selective Feature of Vδ2/Vγ9 γδ T Cells1. *J Immunol* (2002) 168:4920–4929. doi: 10.4049/jimmunol.168.10.4920

158. Aj N, H T, Sr M, T H, K S, K Y, M N. Clinical evaluation of autologous gamma delta T cell-based immunotherapy for metastatic solid tumours. *Br J Cancer* (2011) 105: doi: 10.1038/bjc.2011.293

159. Vyborova A, Janssen A, Gatti L, Karaiskaki F, Yonika A, van Dooremalen S, Sanders J, Beringer DX, Straetemans T, Sebestyen Z, et al. γ9δ2 T-Cell Expansion and Phenotypic Profile Are Reflected in the CDR3δ Repertoire of Healthy Adults. *Front Immunol* (2022) 13:915366. doi: 10.3389/fimmu.2022.915366

160. Ryan PL, Sumaria N, Holland CJ, Bradford CM, Izotova N, Grandjean CL, Jawad AS, Bergmeier LA, Pennington DJ. Heterogeneous yet stable Vδ2(+) T-cell profiles define distinct cytotoxic effector potentials in healthy human individuals. *Proc Natl Acad Sci U S A* (2016) 113:14378–14383. doi: 10.1073/pnas.1611098113

161. Kallemeijn MJ, Boots AMH, Van Der Klift MY, Brouwer E, Abdulahad WH, Verhaar JAN, Van Dongen JJM, Langerak AW. Ageing and latent CMV infection impact on maturation, differentiation and exhaustion profiles of T-cell receptor gammadelta T-cells. *Sci Rep* (2017) 7: doi: 10.1038/s41598-017-05849-1

162. Wistuba-Hamprecht K, Frasca D, Blomberg B, Pawelec G, Derhovanessian E. Age-associated alterations in γδ T-cells are present predominantly in individuals infected with Cytomegalovirus. *Immun Ageing A* (2013) 10:26. doi: 10.1186/1742-4933-10-26

163. Hunter S, Willcox CR, Davey MS, Kasatskaya SA, Jeffery HC, Chudakov DM, Oo YH, Willcox BE. Human liver infiltrating γδ T cells are composed of clonally expanded circulating and tissue-resident populations. *J Hepatol* (2018) 69:654–665. doi: 10.1016/j.jhep.2018.05.007

164. Qu G, Wang S, Zhou Z, Jiang D, Liao A, Luo J. Comparing Mouse and Human Tissue-Resident γδ T Cells. *Front Immunol* (2022) 13:891687. doi: 10.3389/fimmu.2022.891687

165. Reijneveld JF, Ocampo TA, Shahine A, Gully BS, Vantourout P, Hayday AC, Rossjohn J, Moody DB, Van Rhijn I. Human γδ T cells recognize CD1b by two distinct mechanisms. *Proc Natl Acad Sci U S A* (2020) 117:22944–22952. doi: 10.1073/pnas.2010545117

166. Spada FM, Grant EP, Peters PJ, Sugita M, Melián A, Leslie DS, Lee HK, van Donselaar E, Hanson DA, Krensky AM, et al. Self-recognition of CD1 by gamma/delta T cells: implications for innate immunity. *J Exp Med* (2000) 191:937–948. doi: 10.1084/jem.191.6.937

167. Le Nours J, Gherardin NA, Ramarathinam SH, Awad W, Wiede F, Gully BS, Khandokar Y, Praveena T, Wubben JM, Sandow JJ, et al. A class of γδ T cell receptors recognize the underside of the antigen-presenting molecule MR1. *Science* (2019) 366:1522–1527. doi: 10.1126/science.aav3900

168. Wu J, Groh V, Spies T. T Cell Antigen Receptor Engagement and Specificity in the Recognition of Stress-Inducible MHC Class I-Related Chains by Human Epithelial γδ T Cells. *J Immunol* (2002) 169:1236–1240. doi: 10.4049/jimmunol.169.3.1236

169. Falk MC, Ng G, Zhang GY, Fanning GC, Kamath KR, Knight JF. Predominance of T cell receptor V delta 3 in small bowel biopsies from coeliac disease patients. *Clin Exp Immunol* (1994) 98:78–82. doi: 10.1111/j.1365-2249.1994.tb06610.x

170. Tuengel J, Ranchal S, Maslova A, Aulakh G, Papadopoulou M, Drissler S, Cai B, Mohsenzadeh-Green C, Soudeyns H, Mostafavi S, et al. Characterization of Adaptive-like γδ T Cells in Ugandan Infants during Primary Cytomegalovirus Infection. *Viruses* (2021) 13:1987. doi: 10.3390/v13101987

171. Taupin JL, Halary F, Déchanet J, Peyrat MA, Ragnaud JM, Bonneville M, Moreau JF. An enlarged subpopulation of T lymphocytes bearing two distinct gammadelta TCR in an HIV-positive patient. *Int Immunol* (1999) 11:545–552. doi: 10.1093/intimm/11.4.545

172. Ravens S, Hengst J, Schlapphoff V, Deterding K, Dhingra A, Schultze-Florey C, Koenecke C, Cornberg M, Wedemeyer H, Prinz I. Human γδ T Cell Receptor Repertoires in Peripheral Blood Remain Stable Despite Clearance of Persistent Hepatitis C Virus Infection by Direct-Acting Antiviral Drug Therapy. *Front Immunol* (2018) 9: doi: 10.3389/fimmu.2018.00510

173. Mangan BA, Dunne MR, O'Reilly VP, Dunne PJ, Exley MA, O'Shea D, Scotet E, Hogan AE, Doherty DG. Cutting Edge: CD1d Restriction and Th1/Th2/Th17 Cytokine Secretion by Human Vδ3 T Cells. *J Immunol* (2013) 191:30–34. doi: 10.4049/jimmunol.1300121

174. Rice MT, von Borstel A, Chevour P, Awad W, Howson LJ, Littler DR, Gherardin NA, Le Nours J, Giles EM, Berry R, et al. Recognition of the antigen-presenting molecule MR1 by a Vδ3+ γδ T cell receptor. *Proc Natl Acad Sci U S A* (2021) 118:e2110288118. doi: 10.1073/pnas.2110288118

175. Robak E, Niewiadomska H, Robak T, Bartkowiak J, Błoński JZ, Woźniacka A, Pomorski L, Sysa-Jedrezejowska A. Lymphocyctes Tgammadelta in clinically normal skin and peripheral blood of patients with systemic lupus erythematosus and their correlation with disease activity. *Mediators Inflamm* (2001) 10:179–189. doi: 10.1080/09629350124724

176. Qi C, Wang Y, Li P, Zhao J. Gamma Delta T Cells and Their Pathogenic Role in Psoriasis. *Front Immunol* (2021) 12:627139. doi: 10.3389/fimmu.2021.627139

177. Singh TP, Zhang HH, Hwang ST, Farber JM. IL-23- and Imiquimod-Induced Models of Experimental Psoriasis in Mice. *Curr Protoc Immunol* (2019) 125:e71. doi: 10.1002/cpim.71

178. Plužarić V, Štefanić M, Mihalj M, Tolušić Levak M, Muršić I, Glavaš-Obrovac L, Petrek M, Balogh P, Tokić S. Differential Skewing of Circulating MR1-Restricted and γδ T Cells in Human Psoriasis Vulgaris. *Front Immunol* (2020) 11:572924. doi: 10.3389/fimmu.2020.572924

179. Chen Y, Fu Q, Ma Y, Wang N, Yang J, Liang Q, Wang K, Gao L. Identification of the immune repertoire of γδ T-cell receptors in psoriasis. *Immunol Cell Biol* (2024) 102:570–577. doi: 10.1111/imcb.12765

180. Nel I, Bertrand L, Toubal A, Lehuen A. MAIT cells, guardians of skin and mucosa? *Mucosal Immunol* (2021) 14:803–814. doi: 10.1038/s41385-021-00391-w

181. Dusseaux M, Martin E, Serriari N, Péguillet I, Premel V, Louis D, Milder M, Le Bourhis L, Soudais C, Treiner E, et al. Human MAIT cells are xenobiotic-resistant, tissue-targeted, CD161hi IL-17-secreting T cells. *Blood* (2011) 117:1250–1259. doi: 10.1182/blood-2010-08-303339

182. Kurioka A, Jahun AS, Hannaway RF, Walker LJ, Fergusson JR, Sverremark-Ekström E, Corbett AJ, Ussher JE, Willberg CB, Klenerman P. Shared and Distinct Phenotypes and Functions of Human CD161++ Vα7.2+ T Cell Subsets. *Front Immunol* (2017) 8:1031. doi: 10.3389/fimmu.2017.01031

183. Magalhaes I, Pingris K, Poitou C, Bessoles S, Venteclef N, Kiaf B, Beaudoin L, Silva JD, Allatif O, Rossjohn J, et al. Mucosal-associated invariant T cell alterations in obese and type 2 diabetic patients. *J Clin Invest* (2015) 125:1752. doi: 10.1172/JCI78941

184. Gherardin NA, Souter MN, Koay H, Mangas KM, Seemann T, Stinear TP, Eckle SB, Berzins SP, d'Udekem Y, Konstantinov IE, et al. Human blood MAIT cell subsets defined using MR1 tetramers. *Immunol Cell Biol* (2018) 96:507–525. doi: 10.1111/imcb.12021

185. Lee O-J, Cho Y-N, Kee S-J, Kim M-J, Jin H-M, Lee S-J, Park K-J, Kim T-J, Lee S-S, Kwon Y-S, et al. Circulating mucosal-associated invariant T cell levels and their cytokine levels in healthy adults. *Exp Gerontol* (2014) 49:47–54. doi: 10.1016/j.exger.2013.11.003

186. Gherardin NA, Keller AN, Woolley RE, Le Nours J, Ritchie DS, Neeson PJ, Birkinshaw RW, Eckle SBG, Waddington JN, Liu L, et al. Diversity of T Cells Restricted by the MHC Class I-Related Molecule MR1 Facilitates Differential Antigen Recognition. *Immunity* (2016) 44:32–45. doi: 10.1016/j.immuni.2015.12.005

187. Kjer-Nielsen L, Patel O, Corbett AJ, Le Nours J, Meehan B, Liu L, Bhati M, Chen Z, Kostenko L, Reantragoon R, et al. MR1 presents microbial vitamin B metabolites to MAIT cells. *Nature* (2012) 491:717–723. doi: 10.1038/nature11605

188. Eckle SBG, Birkinshaw RW, Kostenko L, Corbett AJ, McWilliam HEG, Reantragoon R, Chen Z, Gherardin NA, Beddoe T, Liu L, et al. A molecular basis underpinning the T cell receptor heterogeneity of mucosal-associated invariant T cells. *J Exp Med* (2014) 211:1585–1600. doi: 10.1084/jem.20140484

189. Corbett AJ, Eckle SBG, Birkinshaw RW, Liu L, Patel O, Mahony J, Chen Z, Reantragoon R, Meehan B, Cao H, et al. T-cell activation by transitory neo-antigens derived from distinct microbial pathways. *Nature* (2014) 509:361–365. doi: 10.1038/nature13160

190. Reantragoon R, Corbett AJ, Sakala IG, Gherardin NA, Furness JB, Chen Z, Eckle SBG, Uldrich AP, Birkinshaw RW, Patel O, et al. Antigen-loaded MR1 tetramers define T cell receptor heterogeneity in mucosal-associated invariant T cells. *J Exp Med* (2013) 210:2305–2320. doi: 10.1084/jem.20130958

191. Ussher JE, Bilton M, Attwod E, Shadwell J, Richardson R, de Lara C, Mettke E, Kurioka A, Hansen TH, Klenerman P, et al. CD161++ CD8+ T cells, including the MAIT cell subset, are specifically activated by IL-12+IL-18 in a TCR-independent manner. *Eur J Immunol* (2014) 44:195–203. doi: 10.1002/eji.201343509

192. Godfrey DI, Koay H-F, McCluskey J, Gherardin NA. The biology and functional importance of MAIT cells. *Nat Immunol* (2019) 20:1110–1128. doi: 10.1038/s41590-019-0444-8

193. Novak J, Dobrovolny J, Novakova L, Kozak T. The Decrease in Number and Change in Phenotype of Mucosal-Associated Invariant T cells in the Elderly and Differences in Men and Women of Reproductive Age. *Scand J Immunol* (2014) 80:271–275. doi: 10.1111/sji.12193

194. Chen P, Deng W, Li D, Zeng T, Huang L, Wang Q, Wang J, Zhang W, Yu X, Duan D, et al. Circulating Mucosal-Associated Invariant T Cells in a Large Cohort of Healthy Chinese Individuals From Newborn to Elderly. *Front Immunol* (2019) 10: doi: 10.3389/fimmu.2019.00260

195. Loh L, Gherardin NA, Sant S, Grzelak L, Crawford JC, Bird NL, Koay H-F, van de Sandt CE, Moreira ML, Lappas M, et al. Human Mucosal-Associated Invariant T Cells in Older Individuals Display Expanded TCRαβ Clonotypes with Potent Antimicrobial Responses. *J Immunol* (2020) 204:1119–1133. doi: 10.4049/jimmunol.1900774

196. Dias J, Boulouis C, Gorin J-B, van den Biggelaar RHGA, Lal KG, Gibbs A, Loh L, Gulam MY, Sia WR, Bari S, et al. The CD4−CD8− MAIT cell subpopulation is a functionally distinct subset developmentally related to the main CD8+ MAIT cell pool. *Proc Natl Acad Sci U S A* (2018) 115:E11513–E11522. doi: 10.1073/pnas.1812273115

197. Brozova J, Karlova I, Novak J. Analysis of the Phenotype and Function of the Subpopulations of Mucosal-Associated Invariant T Cells. *Scand J Immunol* (2016) 84:245–251. doi: 10.1111/sji.12467

198. Vorkas CK, Krishna C, Li K, Aubé J, Fitzgerald DW, Mazutis L, Leslie CS, Glickman MS. Single-Cell Transcriptional Profiling Reveals Signatures of Helper, Effector, and Regulatory MAIT Cells during Homeostasis and Activation. *J Immunol Baltim Md 1950* (2022) 208:1042–1056. doi: 10.4049/jimmunol.2100522

199. Garner LC, Amini A, FitzPatrick MEB, Lett MJ, Hess GF, Filipowicz Sinnreich M, Provine NM, Klenerman P. Single-cell analysis of human MAIT cell transcriptional, functional and clonal diversity. *Nat Immunol* (2023) 24:1565–1578. doi: 10.1038/s41590-023-01575-1

200. Rahimpour A, Koay HF, Enders A, Clanchy R, Eckle SBG, Meehan B, Chen Z, Whittle B, Liu L, Fairlie DP, et al. Identification of phenotypically and functionally heterogeneous mouse mucosal-associated invariant T cells using MR1 tetramers. *J Exp Med* (2015) 212:1095–1108. doi: 10.1084/jem.20142110

201. Lefranc M-P, Giudicelli V, Ginestoux C, Jabado-Michaloud J, Folch G, Bellahcene F, Wu Y, Gemrot E, Brochet X, Lane J, et al. IMGT, the international ImMunoGeneTics

information system. *Nucleic Acids Res* (2009) 37:D1006-1012. doi: 10.1093/nar/gkn838

202. Reantragoon R, Kjer-Nielsen L, Patel O, Chen Z, Illing PT, Bhati M, Kostenko L, Bharadwaj M, Meehan B, Hansen TH, et al. Structural insight into MR1-mediated recognition of the mucosal associated invariant T cell receptor. *J Exp Med* (2012) 209:761–774. doi: 10.1084/jem.20112095

203. Patel O, Kjer-Nielsen L, Le Nours J, Eckle SBG, Birkinshaw R, Beddoe T, Corbett AJ, Liu L, Miles JJ, Meehan B, et al. Recognition of vitamin B metabolites by mucosal-associated invariant T cells. *Nat Commun* (2013) 4:2142. doi: 10.1038/ncomms3142

204. Lepore M, Kalinichenko A, Colone A, Paleja B, Singhal A, Tschumi A, Lee B, Poidinger M, Zolezzi F, Quagliata L, et al. Parallel T-cell cloning and deep sequencing of human MAIT cells reveal stable oligoclonal TCRβ repertoire. *Nat Commun* (2014) 5:3866. doi: 10.1038/ncomms4866

205. Jirouš Drulak M, Grgić Z, Plužarić V, Šola M, Opačak-Bernardi T, Viljetić B, Glavaš K, Tolušić-Levak M, Periša V, Mihalj M, et al. Characterization of the TCRβ repertoire of peripheral MR1-restricted MAIT cells in psoriasis vulgaris patients. *Sci Rep* (2023) 13:20990. doi: 10.1038/s41598-023-48321-z

206. Held K, Beltrán E, Moser M, Hohlfeld R, Dornmair K. T-cell receptor repertoire of human peripheral CD161hiTRAV1-2+ MAIT cells revealed by next generation sequencing and single cell analysis. *Hum Immunol* (2015) 76:607–614. doi: 10.1016/j.humimm.2015.09.002

207. Gherardin NA, McCluskey J, Rossjohn J, Godfrey DI. The Diverse Family of MR1-Restricted T Cells. *J Immunol Baltim Md 1950* (2018) 201:2862–2871. doi: 10.4049/jimmunol.1801091

208. Kurioka A, Ussher JE, Cosgrove C, Clough C, Fergusson JR, Smith K, Kang Y-H, Walker LJ, Hansen TH, Willberg CB, et al. MAIT cells are licensed through granzyme exchange to kill bacterially sensitized targets. *Mucosal Immunol* (2015) 8:429–440. doi: 10.1038/mi.2014.81

209. Gibbs A, Leeansyah E, Introini A, Paquin-Proulx D, Hasselrot K, Andersson E, Broliden K, Sandberg JK, Tjernlund A. MAIT cells reside in the female genital mucosa and are biased towards IL-17 and IL-22 production in response to bacterial stimulation. *Mucosal Immunol* (2017) 10:35–45. doi: 10.1038/mi.2016.30

210. Lamichhane R, Schneider M, De La Harpe SM, Harrop TWR, Hannaway RF, Dearden PK, Kirman JR, Tyndall JDA, Vernall AJ, Ussher JE. TCR- or Cytokine-Activated CD8+ Mucosal-Associated Invariant T Cells Are Rapid Polyfunctional Effectors That Can Coordinate Immune Responses. *Cell Rep* (2019) 28:3061-3076.e5. doi: 10.1016/j.celrep.2019.08.054

211. Fan Q, Nan H, Li Z, Li B, Zhang F, Bi L. New insights into MAIT cells in autoimmune diseases. *Biomed Pharmacother* (2023) 159:114250. doi: 10.1016/j.biopha.2023.114250

212. Chiba A, Murayama G, Miyake S. Mucosal-Associated Invariant T Cells in Autoimmune Diseases. *Front Immunol* (2018) 9:1333. doi: 10.3389/fimmu.2018.01333

213. Li J, Reantragoon R, Kostenko L, Corbett AJ, Varigos G, Carbone FR. The frequency of mucosal-associated invariant T cells is selectively increased in dermatitis herpetiformis. *Australas J Dermatol* (2017) 58:200–204. doi: 10.1111/ajd.12456

214. Fredriksson T, Pettersson U. Severe psoriasis--oral therapy with a new retinoid. *Dermatologica* (1978) 157:238–244. doi: 10.1159/000250839

215. Plužarić V, Štefanić M, Mihalj M, Tolušić Levak M, Muršić I, Glavaš-Obrovac L, Petrek M, Balogh P, Tokić S. Differential Skewing of Circulating MR1-Restricted and γδ T Cells in Human Psoriasis Vulgaris. *Front Immunol* (2020) 11:572924. doi: 10.3389/fimmu.2020.572924

216. Caccamo N, Dieli F, Wesch D, Jomaa H, Eberl M. Sex-specific phenotypical and functional differences in peripheral human Vγ9/Vδ2 T cells. *J Leukoc Biol* (2006) 79:663–666. doi: 10.1189/jlb.1105640

217. The Galaxy Community, Abueg LAL, Afgan E, Allart O, Awan AH, Bacon WA, Baker D, Bassetti M, Batut B, Bernt M, et al. The Galaxy platform for accessible, reproducible, and collaborative data analyses: 2024 update. *Nucleic Acids Res* (2024) 52:W83–W94. doi: 10.1093/nar/gkae410

218. Dobin A, Davis CA, Schlesinger F, Drenkow J, Zaleski C, Jha S, Batut P, Chaisson M, Gingeras TR. STAR: ultrafast universal RNA-seq aligner. *Bioinformatics* (2013) 29:15–21. doi: 10.1093/bioinformatics/bts635

219. Love MI, Huber W, Anders S. Moderated estimation of fold change and dispersion for RNA-seq data with DESeq2. *Genome Biol* (2014) 15: doi: 10.1186/s13059-014-0550-8

220. Ashburner M, Ball CA, Blake JA, Botstein D, Butler H, Cherry JM, Davis AP, Dolinski K, Dwight SS, Eppig JT, et al. Gene Ontology: tool for the unification of biology. *Nat Genet* (2000) 25:25–29. doi: 10.1038/75556

221. The Gene Ontology Consortium, Aleksander SA, Balhoff J, Carbon S, Cherry JM, Drabkin HJ, Ebert D, Feuermann M, Gaudet P, Harris NL, et al. The Gene Ontology knowledgebase in 2023. *GENETICS* (2023) 224: doi: 10.1093/genetics/iyad031

222. Kanehisa M, Goto S. KEGG: kyoto encyclopedia of genes and genomes. *Nucleic Acids Res* (2000) 28:27–30. doi: 10.1093/nar/28.1.27

223. Liberzon A, Birger C, Thorvaldsdóttir H, Ghandi M, Mesirov JP, Tamayo P. The Molecular Signatures Database Hallmark Gene Set Collection. *Cell Syst* (2015) 1:417–425. doi: 10.1016/j.cels.2015.12.004

224. Subramanian A, Tamayo P, Mootha VK, Mukherjee S, Ebert BL, Gillette MA, Paulovich A, Pomeroy SL, Golub TR, Lander ES, et al. Gene set enrichment analysis: A knowledge-based approach for interpreting genome-wide expression profiles. *Proc Natl Acad Sci* (2005) 102:15545–15550. doi: 10.1073/pnas.0506580102

225. Bolotin DA, Poslavsky S, Mitrophanov I, Shugay M, Mamedov IZ, Putintseva EV, Chudakov DM. MiXCR: software for comprehensive adaptive immunity profiling. *Nat Methods* (2015) 12:380–381. doi: 10.1038/nmeth.3364

226. Shugay M, Bagaev DV, Turchaninova MA, Bolotin DA, Britanova OV, Putintseva EV, Pogorelyy MV, Nazarov VI, Zvyagin IV, Kirgizova VI, et al. VDJtools: Unifying Post-analysis of T Cell Receptor Repertoires. *PLOS Comput Biol* (2015) 11:e1004503. doi: 10.1371/journal.pcbi.1004503

227. Bioinformatics Analysis of T-Cell and B-Cell Immune Repertoires • immunarch. https://immunarch.com/ [Accessed July 26, 2023]

228. Cairo C, Armstrong CL, Cummings JS, Deetz CO, Tan M, Lu C, Davis CE, Pauza CD. Impact of age, gender, and race on circulating γδ T cells. *Hum Immunol* (2010) 71:968–975. doi: 10.1016/j.humimm.2010.06.014

229. Pitard V, Roumanes D, Lafarge X, Couzi L, Garrigue I, Lafon M-E, Merville P, Moreau J-F, Déchanet-Merville J. Long-term expansion of effector/memory Vδ2− γδ T cells is a specific blood signature of CMV infection. *Blood* (2008) 112:1317–1324. doi: 10.1182/blood-2008-01-136713

230. Deng L, Harms A, Ravens S, Prinz I, Tan L. Systematic pattern analyses of Vδ2+ TCRs reveal that shared "public" Vδ2+ γδ T cell clones are a consequence of rearrangement bias and a higher expansion status. *Front Immunol* (2022) 13: doi: 10.3389/fimmu.2022.960920

231. Meermeier EW, Laugel BF, Sewell AK, Corbett AJ, Rossjohn J, McCluskey J, Harriff MJ, Franks T, Gold MC, Lewinsohn DM. Human TRAV1-2-negative MR1-restricted T cells detect S. pyogenes and alternatives to MAIT riboflavin-based antigens. *Nat Commun* (2016) 7:12506. doi: 10.1038/ncomms12506

232. Garner LC, Amini A, FitzPatrick MEB, Provine NM, Klenerman P. Human MAIT cells show clonal diversity but transcriptional and functional homogeneity. [preprint]. Immunology. (2022). doi: 10.1101/2022.02.26.482031

233. Liu J, Chang H-W, Grewal R, Cummins DD, Bui A, Beck KM, Sekhon S, Yan D, Huang Z-M, Schmidt TH, et al. Transcriptomic Profiling of Plaque Psoriasis and Cutaneous T-Cell Subsets during Treatment with Secukinumab. *JID Innov* (2022) 2:100094. doi: 10.1016/j.xjidi.2021.100094

234. Coppé J-P, Rodier F, Patil CK, Freund A, Desprez P-Y, Campisi J. Tumor Suppressor and Aging Biomarker p16INK4a Induces Cellular Senescence without the Associated Inflammatory Secretory Phenotype. *J Biol Chem* (2011) 286:36396–36403. doi: 10.1074/jbc.M111.257071

235. Baker DJ, Wijshake T, Tchkonia T, LeBrasseur NK, Childs BG, Van De Sluis B, Kirkland JL, Van Deursen JM. Clearance of p16Ink4a-positive senescent cells delays ageing-associated disorders. *Nature* (2011) 479:232–236. doi: 10.1038/nature10600

236. Janelle V, Neault M, Lebel M-È, De Sousa DM, Boulet S, Durrieu L, Carli C, Muzac C, Lemieux S, Labrecque N, et al. p16INK4a Regulates Cellular Senescence in PD-1-

Expressing Human T Cells. *Front Immunol* (2021) 12:698565. doi: 10.3389/fimmu.2021.698565

237. Kallemeijn MJ, Kavelaars FG, van der Klift MY, Wolvers-Tettero ILM, Valk PJM, van Dongen JJM, Langerak AW. Next-Generation Sequencing Analysis of the Human TCRγδ+ T-Cell Repertoire Reveals Shifts in Vγ- and Vδ-Usage in Memory Populations upon Aging. *Front Immunol* (2018) 9:448. doi: 10.3389/fimmu.2018.00448

238. McArdel SL, Terhorst C, Sharpe AH. Roles of CD48 in regulating immunity and tolerance. *Clin Immunol* (2016) 164:10–20. doi: 10.1016/j.clim.2016.01.008

239. Tissot C, Rebouissou C, Klein B, Mechti N. Both human alpha/beta and gamma interferons upregulate the expression of CD48 cell surface molecules. *J Interferon Cytokine Res Off J Int Soc Interferon Cytokine Res* (1997) 17:17–26. doi: 10.1089/jir.1997.17.17

240. Patel VP, Moran M, Low TA, Miceli MC. A molecular framework for two-step T cell signaling: Lck Src homology 3 mutations discriminate distinctly regulated lipid raft reorganization events. *J Immunol Baltim Md 1950* (2001) 166:754–764. doi: 10.4049/jimmunol.166.2.754

241. Ribot JC, Ribeiro ST, Correia DV, Sousa AE, Silva-Santos B. Human γδ thymocytes are functionally immature and differentiate into cytotoxic type 1 effector T cells upon IL-2/IL-15 signaling. *J Immunol Baltim Md 1950* (2014) 192:2237–2243. doi: 10.4049/jimmunol.1303119

242. Chi H, Lu B, Takekawa M, Davis RJ, Flavell RA. GADD45β/GADD45γ and MEKK4 comprise a genetic pathway mediating STAT4-independent IFNγ production in T cells. *EMBO J* (2004) 23:1576–1586. doi: 10.1038/sj.emboj.7600173

243. Liu L, Tran E, Zhao Y, Huang Y, Flavell R, Lu B. Gadd45β and Gadd45γ are critical for regulating autoimmunity. *J Exp Med* (2005) 202:1341–1348. doi: 10.1084/jem.20051359

244. Suárez-Fariñas M, Fuentes-Duculan J, Lowes MA, Krueger JG. Resolved Psoriasis Lesions Retain Expression of a Subset of Disease-Related Genes. *J Invest Dermatol* (2011) 131:391–400. doi: 10.1038/jid.2010.280

245. Bai A, Hu H, Yeung M, Chen J. Krüppel-Like Factor 2 Controls T Cell Trafficking by Activating L-Selectin (CD62L) and Sphingosine-1-Phosphate Receptor 1 Transcription. *J Immunol* (2007) 178:7632–7639. doi: 10.4049/jimmunol.178.12.7632

246. Odumade OA, Weinreich MA, Jameson SC, Hogquist KA. Krüppel-like factor 2 regulates trafficking and homeostasis of gammadelta T cells. *J Immunol Baltim Md 1950* (2010) 184:6060–6066. doi: 10.4049/jimmunol.1000511

247. Lee J-Y, Skon CN, Lee YJ, Oh S, Taylor JJ, Malhotra D, Jenkins MK, Rosenfeld MG, Hogquist KA, Jameson SC. The Transcription Factor KLF2 Restrains CD4 + T Follicular Helper Cell Differentiation. *Immunity* (2015) 42:252–264. doi: 10.1016/j.immuni.2015.01.013

248. García-Cuesta EM, Santiago CA, Vallejo-Díaz J, Juarranz Y, Rodríguez-Frade JM, Mellado M. The Role of the CXCL12/CXCR4/ACKR3 Axis in Autoimmune Diseases. *Front Endocrinol* (2019) 10:585. doi: 10.3389/fendo.2019.00585

249. Zgraggen S, Huggenberger R, Kerl K, Detmar M. An Important Role of the SDF-1/CXCR4 Axis in Chronic Skin Inflammation. *PLoS ONE* (2014) 9:e93665. doi: 10.1371/journal.pone.0093665

250. Guttman-Yassky E, Vugmeyster Y, Lowes MA, Chamian F, Kikuchi T, Kagen M, Gilleaudeau P, Lee E, Hunte B, Howell K, et al. Blockade of CD11a by Efalizumab in Psoriasis Patients Induces a Unique State of T-Cell Hyporesponsiveness. *J Invest Dermatol* (2008) 128:1182–1191. doi: 10.1038/jid.2008.4

251. Mueller P, Massner J, Jayachandran R, Combaluzier B, Albrecht I, Gatfield J, Blum C, Ceredig R, Rodewald H-R, Rolink AG, et al. Regulation of T cell survival through coronin-1–mediated generation of inositol-1,4,5-trisphosphate and calcium mobilization after T cell receptor triggering. *Nat Immunol* (2008) 9:424–431. doi: 10.1038/ni1570

252. Kelley SM, Ravichandran KS. Putting the brakes on phagocytosis: "don't-eat-me" signaling in physiology and disease. *EMBO Rep* (2021) 22:e52564. doi: 10.15252/embr.202152564

253. Lee N, Llano M, Carretero M, Ishitani A, Navarro F, López-Botet M, Geraghty DE. HLA-E is a major ligand for the natural killer inhibitory receptor CD94/NKG2A. *Proc Natl Acad Sci* (1998) 95:5199–5204. doi: 10.1073/pnas.95.9.5199

254. Wang X, Sumida H, Cyster JG. GPR18 is required for a normal CD8αα intestinal intraepithelial lymphocyte compartment. *J Exp Med* (2014) 211:2351–2359. doi: 10.1084/jem.20140646

255. Sumida H, Cyster JG. G-Protein Coupled Receptor 18 Contributes to Establishment of the CD8 Effector T Cell Compartment. *Front Immunol* (2018) 9:660. doi: 10.3389/fimmu.2018.00660

256. Stosic-Grujicic S, Stojanovic I, Nicoletti F. MIF in autoimmunity and novel therapeutic approaches. *Autoimmun Rev* (2009) 8:244–249. doi: 10.1016/j.autrev.2008.07.037

257. Liu T, Wu G, Gudd CLC, Trovato FM, Barbera T, Liu Y, Triantafyllou E, McPhail MJW, Thursz MR, Khamri W. Cis-interaction between CD52 and T cell receptor complex interferes with CD4+ T cell activation in acute decompensation of cirrhosis. *eBioMedicine* (2024) 108:105336. doi: 10.1016/j.ebiom.2024.105336

258. Stanford SM, Rapini N, Bottini N. Regulation of TCR signalling by tyrosine phosphatases: from immune homeostasis to autoimmunity. *Immunology* (2012) 137:1–19. doi: 10.1111/j.1365-2567.2012.03591.x

259. Leonard WJ, Lin J-X, O'Shea JJ. The γc Family of Cytokines: Basic Biology to Therapeutic Ramifications. *Immunity* (2019) 50:832–850. doi: 10.1016/j.immuni.2019.03.028

260. Wikenheiser DJ, Stumhofer JS. ICOS Co-Stimulation: Friend or Foe? *Front Immunol* (2016) 7:304. doi: 10.3389/fimmu.2016.00304

261. Araki K, Turner AP, Shaffer VO, Gangappa S, Keller SA, Bachmann MF, Larsen CP, Ahmed R. mTOR regulates memory CD8 T-cell differentiation. *Nature* (2009) 460:108–112. doi: 10.1038/nature08155

262. Saxton RA, Sabatini DM. mTOR Signaling in Growth, Metabolism, and Disease. *Cell* (2017) 168:960–976. doi: 10.1016/j.cell.2017.02.004

263. Verhelst J, Hulpiau P, Saelens X. Mx Proteins: Antiviral Gatekeepers That Restrain the Uninvited. *Microbiol Mol Biol Rev MMBR* (2013) 77:551. doi: 10.1128/MMBR.00024-13

264. Li Y, Banerjee S, Wang Y, Goldstein SA, Dong B, Gaughan C, Silverman RH, Weiss SR. Activation of RNase L is dependent on OAS3 expression during infection with diverse human viruses. *Proc Natl Acad Sci U S A* (2016) 113:2241–2246. doi: 10.1073/pnas.1519657113

265. DeDiego ML, Martinez-Sobrido L, Topham DJ. Novel Functions of IFI44L as a Feedback Regulator of Host Antiviral Responses. *J Virol* (2019) 93:e01159. doi: 10.1128/JVI.01159-19

266. Tan L, Fichtner AS, Bruni E, Odak I, Sandrock I, Bubke A, Borchers A, Schultze-Florey C, Koenecke C, Förster R, et al. A fetal wave of human type 3 effector γδ cells with restricted TCR diversity persists into adulthood. *Sci Immunol* (2021) 6:eabf0125. doi: 10.1126/sciimmunol.abf0125

267. Liu Y, Wang H, Cook C, Taylor MA, North JP, Hailer A, Shou Y, Sadik A, Kim E, Purdom E, et al. Defining Patient-Level Molecular Heterogeneity in Psoriasis Vulgaris Based on Single-Cell Transcriptomics. *Front Immunol* (2022) 13:842651. doi: 10.3389/fimmu.2022.842651

268. Zhang S, Chang M, Zheng L, Wang C, Zhao R, Song S, Hao J, Zhang L, Wang C, Li X. Deep analysis of skin molecular heterogeneities and their significance on the precise treatment of patients with psoriasis. *Front Immunol* (2024) 15:1326502. doi: 10.3389/fimmu.2024.1326502

269. Swindell WR, Xing X, Stuart PE, Chen CS, Aphale A, Nair RP, Voorhees JJ, Elder JT, Johnston A, Gudjonsson JE. Heterogeneity of Inflammatory and Cytokine Networks in Chronic Plaque Psoriasis. *PLoS ONE* (2012) 7:

270. Wang G, Miao Y, Kim N, Sweren E, Kang S, Hu Z, Garza LA. Association of the Psoriatic Microenvironment With Treatment Response. *JAMA Dermatol* (2020) 156:1057–1065. doi: 10.1001/jamadermatol.2020.2118

271. Ainali C, Valeyev N, Perera G, Williams A, Gudjonsson JE, Ouzounis CA, Nestle FO, Tsoka S. Transcriptome classification reveals molecular subtypes in psoriasis. *BMC Genomics* (2012) 13:472. doi: 10.1186/1471-2164-13-472

272. Correia MP, Costa AV, Uhrberg M, Cardoso EM, Arosa FA. IL-15 induces CD8+ T cells to acquire functional NK receptors capable of modulating cytotoxicity and

cytokine secretion. *Immunobiology* (2011) 216:604–612. doi: 10.1016/j.imbio.2010.09.012

273. Chan WK, Rujkijyanont P, Neale G, Yang J, Bari R, Das Gupta N, Holladay M, Rooney B, Leung W. Multiplex and Genome-Wide Analyses Reveal Distinctive Properties of KIR+ and CD56+ T Cells in Human Blood. *J Immunol* (2013) 191:1625–1636. doi: 10.4049/jimmunol.1300111

274. Van Acker HH, Anguille S, Willemen Y, Van Den Bergh JM, Berneman ZN, Lion E, Smits EL, Van Tendeloo VF. Interleukin-15 enhances the proliferation, stimulatory phenotype, and antitumor effector functions of human gamma delta T cells. *J Hematol OncolJ Hematol Oncol* (2016) 9:101. doi: 10.1186/s13045-016-0329-3

275. Gruenbacher G, Nussbaumer O, Gander H, Steiner B, Leonhartsberger N, Thurnher M. Stress-related and homeostatic cytokines regulate Vγ9Vδ2 T-cell surveillance of mevalonate metabolism. *Oncoimmunology* (2014) 3:e953410. doi: 10.4161/21624011.2014.953410

276. Murday AS, Chaudhry S, Pauza CD. Interleukin-18 activates Vγ9Vδ2+ T cells from HIV-positive individuals: recovering the response to phosphoantigen. *Immunology* (2017) 151:385–394. doi: 10.1111/imm.12735

277. Elder JT. IL-15 and Psoriasis: Another Genetic Link to Th17? *J Invest Dermatol* (2007) 127:2495–2497. doi: 10.1038/sj.jid.5700855

278. De Jesús-Gil C, Ruiz-Romeu E, Ferran M, Sagristà M, Chiriac A, García P, Celada A, Pujol RM, Santamaria-Babí LF. IL-15 and IL-23 synergize to trigger Th17 response by CLA^+ T cells in psoriasis. *Exp Dermatol* (2020) 29:630–638. doi: 10.1111/exd.14113

279. Layug PJ, Vats H, Kannan K, Arsenio J. Sex differences in $CD8^+$ T cell responses during adaptive immunity. *WIREs Mech Dis* (2024) 16:e1645. doi: 10.1002/wsbm.1645

280. Hewagama A, Patel D, Yarlagadda S, Strickland FM, Richardson BC. Stronger inflammatory/cytotoxic T-cell response in women identified by microarray analysis. *Genes Immun* (2009) 10:509–516. doi: 10.1038/gene.2009.12

281. Klein SL, Flanagan KL. Sex differences in immune responses. *Nat Rev Immunol* (2016) 16:626–638. doi: 10.1038/nri.2016.90

282. Oghumu S, Varikuti S, Stock JC, Volpedo G, Saljoughian N, Terrazas CA, Satoskar AR. Cutting Edge: CXCR3 Escapes X Chromosome Inactivation in T Cells during Infection: Potential Implications for Sex Differences in Immune Responses. *J Immunol* (2019) 203:789–794. doi: 10.4049/jimmunol.1800931

283. Hewagama A, Gorelik G, Patel D, Liyanarachchi P, McCune WJ, Somers E, Gonzalez-Rivera T, Michigan Lupus Cohort, Strickland F, Richardson B. Overexpression of X-linked genes in T cells from women with lupus. *J Autoimmun* (2013) 41:60–71. doi: 10.1016/j.jaut.2012.12.006

284. Groom JR, Luster AD. CXCR3 in T cell function. *Exp Cell Res* (2011) 317:620–631. doi: 10.1016/j.yexcr.2010.12.017

285. Chen S-C, De Groot M, Kinsley D, Laverty M, McClanahan T, Arreaza M, Gustafson EL, Teunissen MBM, De Rie MA, Fine JS, et al. Expression of chemokine receptor CXCR3 by lymphocytes and plasmacytoid dendritic cells in human psoriatic lesions. *Arch Dermatol Res* (2010) 302:113–123. doi: 10.1007/s00403-009-0966-2

286. Hardenberg J-HB, Braun A, Schön MP. A Yin and Yang in Epithelial Immunology: The Roles of the αE(CD103)β7 Integrin in T Cells. *J Invest Dermatol* (2018) 138:23–31. doi: 10.1016/j.jid.2017.05.026

287. Neuber K, Schmidt S, Mensch A. Telomere length measurement and determination of immunosenescence-related markers (CD28, CD45RO, CD45RA, interferon-γ and interleukin-4) in skin-homing T cells expressing the cutaneous lymphocyte antigen: indication of a non-ageing T-cell subset. *Immunology* (2003) 109:24–31. doi: 10.1046/j.1365-2567.2003.01640.x

288. Malek TR. The main function of IL-2 is to promote the development of T regulatory cells. *J Leukoc Biol* (2003) 74:961–965. doi: 10.1189/jlb.0603272

289. Ferrucci L, Fabbri E. Inflammageing: chronic inflammation in ageing, cardiovascular disease, and frailty. *Nat Rev Cardiol* (2018) 15:505–522. doi: 10.1038/s41569-018-0064-2

290. Awad W, Meermeier EW, Sandoval-Romero ML, Le Nours J, Worley AH, Null MD, Liu L, McCluskey J, Fairlie DP, Lewinsohn DM, et al. Atypical TRAV1-2− T cell receptor recognition of the antigen-presenting molecule MR1. *J Biol Chem* (2020) 295:14445–14457. doi: 10.1074/jbc.RA120.015292

291. Suliman S, Kjer-Nielsen L, Iwany SK, Lopez Tamara K, Loh L, Grzelak L, Kedzierska K, Ocampo TA, Corbett AJ, McCluskey J, et al. Dual TCR-α Expression on Mucosal-Associated Invariant T Cells as a Potential Confounder of TCR Interpretation. *J Immunol Baltim Md 1950* (2022) 208:1389–1395. doi: 10.4049/jimmunol.2100275

292. Britanova OV, Putintseva EV, Shugay M, Merzlyak EM, Turchaninova MA, Staroverov DB, Bolotin DA, Lukyanov S, Bogdanova EA, Mamedov IZ, et al. Age-Related Decrease in TCR Repertoire Diversity Measured with Deep and Normalized Sequence Profiling. *J Immunol* (2014) 192:2689–2698. doi: 10.4049/jimmunol.1302064

293. Britanova OV, Shugay M, Merzlyak EM, Staroverov DB, Putintseva EV, Turchaninova MA, Mamedov IZ, Pogorelyy MV, Bolotin DA, Izraelson M, et al. Dynamics of Individual T Cell Repertoires: From Cord Blood to Centenarians. *J Immunol* (2016) 196:5005–5013. doi: 10.4049/jimmunol.1600005

294. Verma K, Croft W, Margielewska-Davies S, Pearce H, Stephens C, Diaconescu D, Bevington S, Craddock C, Amel-Kashipaz R, Zuo J, et al. CD70 identifies alloreactive T cells and represents a potential target for prevention and treatment of acute GVHD. *Blood Adv* (2024) 8:4900–4912. doi: 10.1182/bloodadvances.2024012909

295. Han BK, Olsen NJ, Bottaro A. The CD27–CD70 pathway and pathogenesis of autoimmune disease. *Semin Arthritis Rheum* (2016) 45:496–501. doi: 10.1016/j.semarthrit.2015.08.001

296. Lee W-W, Yang Z-Z, Li G, Weyand CM, Goronzy JJ. Unchecked CD70 Expression on T Cells Lowers Threshold for T Cell Activation in Rheumatoid Arthritis. *J Immunol* (2007) 179:2609–2615. doi: 10.4049/jimmunol.179.4.2609

297. Pichler AC, Carrié N, Cuisinier M, Ghazali S, Voisin A, Axisa P-P, Tosolini M, Mazzotti C, Golec DP, Maheo S, et al. TCR-independent CD137 (4-1BB) signaling promotes CD8+-exhausted T cell proliferation and terminal differentiation. *Immunity* (2023) 56:1631-1648.e10. doi: 10.1016/j.immuni.2023.06.007

298. Carnero Contentti E, Farez MF, Correale J. Mucosal-Associated Invariant T Cell Features and TCR Repertoire Characteristics During the Course of Multiple Sclerosis. *Front Immunol* (2019) 10:2690. doi: 10.3389/fimmu.2019.02690

299. Ferenczi K, Burack L, Pope M, Krueger JG, Austin LM. CD69, HLA-DR and the IL-2R Identify Persistently Activated T Cells in Psoriasis Vulgaris Lesional Skin: Blood and Skin Comparisons by Flow Cytometry. *J Autoimmun* (2000) 14:63–78. doi: 10.1006/jaut.1999.0343

300. Sharpe AH, Pauken KE. The diverse functions of the PD1 inhibitory pathway. *Nat Rev Immunol* (2018) 18:153–167. doi: 10.1038/nri.2017.108

301. Cho Y-N, Kee S-J, Kim T-J, Jin HM, Kim M-J, Jung H-J, Park K-J, Lee S-J, Lee S-S, Kwon Y-S, et al. Mucosal-Associated Invariant T Cell Deficiency in Systemic Lupus Erythematosus. *J Immunol* (2014) 193:3891–3901. doi: 10.4049/jimmunol.1302701

302. Rouxel O, Da silva J, Beaudoin L, Nel I, Tard C, Cagninacci L, Kiaf B, Oshima M, Diedisheim M, Salou M, et al. Cytotoxic and regulatory roles of mucosal-associated invariant T cells in type 1 diabetes. *Nat Immunol* (2017) 18:1321–1331. doi: 10.1038/ni.3854

303. Ju JK, Cho Y-N, Park K-J, Kwak HD, Jin H-M, Park S-Y, Kim HS, Kee S-J, Park Y-W. Activation, Deficiency, and Reduced IFN-γ Production of Mucosal-Associated Invariant T Cells in Patients with Inflammatory Bowel Disease. *J Innate Immun* (2020) 12:422–434. doi: 10.1159/000507931

304. Dias J, Leeansyah E, Sandberg JK. Multiple layers of heterogeneity and subset diversity in human MAIT cell responses to distinct microorganisms and to innate cytokines. *Proc Natl Acad Sci* (2017) 114: doi: 10.1073/pnas.1705759114

8. SUMMARY

Introduction: Psoriasis vulgaris is a chronic autoinflammatory dermatosis with systemic implications. Its pathogenesis involves a complex interplay of immune and non-immune cells, with T lymphocytes playing a central role in driving the formation of skin plaques and systemic inflammation. While the roles of conventional T cells are well-described, the phenotypes and functions of unconventional T cells, such as mucosal-associated invariant T (MAIT) and γδ T cells, remain poorly characterised, and their specific contributions to the disease are still elusive. This study aimed to address these gaps by comprehensively characterising circulating MAIT and γδ T lymphocytes.

Methods: The proportions of γδ T and MAIT cells and their subsets were fist analysed using conventional flow cytometry. Circulating MAIT and γδ T lymphocytes were FACS sorted, and RNA extracted from these cells was used as input for sequencing. Transcriptomic profiles (395 genes) were analysed through targeted amplicon-based RNA sequencing (Immune Response panel, Illumina), while TCR sequencing (Archer Immunoverse, Invitae) was used to assess TCR gene segment usage, diversity, and clonality of αβ and γδ TCR repertoires. Furthermore, detailed profiling of MAIT and γδ T cells was performed using spectral flow cytometry, analysing 34 surface and 10 intracellular markers.

Results: Male psoriasis patients exhibited reduced proportions of γδ T and $V\delta2^+$ cells, as well as $CD4^+$ and DP MAIT subsets within the $CD3^+$ T cell compartment compared to healthy men. The diversity of TCR repertoires in both MAIT and γδ T cells declined significantly with patient age, however, these alterations were more pronounced and disease-specific in the sγδ TCR repertoires, as similar changes were not observed in healthy controls. Disease severity and duration also influenced γδTCR repertoires across all patients, while the impact on TCRβ repertoires of MAIT cells was milder and restricted to male patients. Transcriptomic profiling revealed significant upregulation of genes associated with activation, cytotoxicity, and type-1 effector functions in circulating γδ T cells, with heterogeneous patterns across patients. Protein-level validation using spectral flow cytometry confirmed increased expression of T-bet and perforin, along with an expansion of $CD56^+$ $V\gamma9V\delta2^+$ cells in patients with advanced disease. Sex-specific differences were also observed, with female patients displaying higher CD56 expression in both $V\gamma9V\delta2^+$ and $V\gamma9V\delta2^-$ subsets. Transcriptomic analysis of MAIT cells showed no significant difference between mildly affected psoriasis patients and healthy

controls. However, correlations between several gene expression patterns and PASI scores or patient age suggested features of exhaustion, chronic activation, and cellular senescence. Multi-dimensional cytometric profiling revealed a significant upregulation of CD69 on circulating MAIT cells in psoriasis patients. In addition, the proportion of circulating CLA^+ MAIT cells, including PD-1^+CLA^+ MAIT cells, increased significantly with disease activity across $CD8^+$, DN, and DP subsets.

Conclusion: This thesis uncovers novel, previously uncharacterised alterations in the frequencies, transcriptional landscapes, TCR repertoires, and phenotypic and functional properties of circulating MAIT and γδ T cells in psoriasis vulgaris. These perturbations are influenced by the presence of the disease, as well as its duration, severity, sex and age. The findings emphasize accelerated age-associated reshaping of TCR repertoires, heightened activation states, increased cytotoxic capacities and sex-specific differences across both MAIT and γδ T cell subsets. Altogether, these results suggest significant contributions of these unconventional T cells to disease pathogenesis, paving the way for further investigations.

9. SAŽETAK

Uvod: Psorijaza vulgaris kronična je autoupalna dermatoza sa sustavnim implikacijama. Patogeneza ove bolesti temelji se na složenim interakcijama imunoloških i neimunoloških stanica, pri čemu limfociti T imaju ključnu ulogu u poticanju stvaranja kožnih plakova i sustavne upale. Iako su uloge konvencionalnih T stanica dobro istražene, fenotip i funkcije nekonvencionalnih T stanica, poput sluznici pridruženih invarijantnih T (MAIT) i γδ T stanica, još uvijek nisu dovoljno istraženi, a njihov specifičan doprinos bolesti ostaje nejasan. Ovaj rad usmjeren je na popunjavanje tih praznina sveobuhvatnom karakterizacijom cirkulirajućih MAIT i γδ T limfocita.

Metode: Udio γδ T i MAIT stanica te njihovih subpopulacija analiziran je najprije konvencionalnom protočnom citometrijom. Cirkulirajući MAIT i γδ T limfociti izolirani su metodom FACS sortiranja, nakon čega je iz njih izdvojena RNA za daljnje sekvenciranje. Transkriptomski profili (395 gena) analizirani su ciljanim RNA sekvenciranjem amplikona (Immune Response panel, Illumina), dok je TCR sekvenciranje (Archer Immunoverse, Invitae) korišteno za procjenu uporabe genskih segmenata TCR-a, raznolikosti i klonalnosti αβ i γδ TCR repertoara. Nadalje, detaljna analiza MAIT i γδ T stanica provedena je spektralnom protočnom citometrijom, kojom su istražena 34 površinska i 10 unutarstaničnih markera.

Rezultati: U muških pacijenata s psorijazom zabilježeno je smanjenje udjela γδ T i $V\delta2^+$ stanica, kao i $CD4^+$ i DP MAIT subpopulacija unutar $CD3^+$ T stanične populacije u usporedbi sa zdravim muškarcima. Raznolikost TCR repertoara MAIT i γδ T stanica značajno se smanjivala s dobi pacijenata, međutim, te su promjene bile izraženije i specifične za bolest u γδ TCR repertoarima, budući da slične promjene nisu uočene kod zdravih kontrola. Trajanje i težina bolesti također su utjecali na γδTCR repertoare pacijenata, dok je utjecaj na TCRβ repertoare MAIT stanica bio blaži i ograničen na oboljele muškarce. Transkriptomsko profiliranje otkrilo je povišen izražaj gena povezanih s aktivacijom, citotoksičnošću i tip-1 efektorskim funkcijama u cirkulirajućim γδ T stanicama, uz heterogene obrasce unutar skupine oboljelih. Na proteinskoj razini, spektralnom protočnom citometrijom potvrđena je povećana ekspresija T-bet i perforina, kao i ekspanzija $CD56^+$ $V\gamma9V\delta2^+$ stanica kod pacijenata s uznapredovalom bolešću. Uočene su i spolno specifične razlike, pri čemu su oboljele žene izražavale višu ekspresiju CD56 u $V\gamma9V\delta2^+$ i $V\gamma9V\delta2^-$ subpopulacijama. Transkriptomska analiza MAIT stanica nije pokazala značajne razlike između pacijenata s blagim oblikom

bolesti i zdravih kontrola. Međutim, korelacija između obrazaca ekspresije gena i PASI indeksa ili dobi pacijenata ukazala je na značajke iscrpljenosti, kronične aktivacije i staničnog starenja. Višedimenzionalnim citometrijskim profiliranjem otkrivena je značajno povišena ekspresija CD69 na cirkulirajućim MAIT stanicama u pacijenata s psorijazom, dok je udio cirkulirajućih CLA^+ MAIT stanica, uključujući PD-1^+CLA^+ MAIT stanice, značajno rastao s progresijom bolesti u $CD8^+$, DN i DP podskupinama.

Zaključak: Ova studija otkriva nove, dosad neokarakterizirane promjene u učestalosti, transkriptomskim profilima, TCR repertoarima te fenotipskim i funkcionalnim svojstvima cirkulirajućih MAIT i γδ T stanica u psorijazi vulgaris. Uočene promjene povezane su s težinom i trajanjem bolesti, kao i dobi i spolom pacijenata. Rezultati naglašavaju ubrzano preoblikovanje TCR repertoara povezano s dobi, pojačanu aktivaciju te spolno specifične razlike unutar MAIT i γδ T staničnih podskupina. Sveukupno, ovi rezultati sugeriraju značajan doprinos ovih nekonvencionalnih T stanica u patogenezi psorijaze te otvaraju nove smjerove za daljnja istraživanja.

10. SUPPLEMENTARY MATERIALS

10.1. List of abbreviations

ADAMTSL5 – A Disintegrin and Metalloproteinase with Thrombospondin Motifs-Like 5

BATF – Basic Leucine Zipper ATF-Like Transcription Factor

BLIMP-1 – B-Lymphocyte-Induced Maturation Protein 1

BUV – Brilliant Ultraviolet

BV – Brilliant Violet

BMI – Body Mass Index

BP – Biological process

BTN – Butyrophilin

BTN3A1 – Butyrophilin Subfamily 3 Member A1

BTN3A2 – Butyrophilin Subfamily 3 Member A2

CC – Cellular Component

CCL – C-C Motif Chemokine Ligand

CCR – C-C Motif Chemokine Receptor

CD – Cluster of Differentiation

CDKN2A – Cyclin-Dependent Kinase Inhibitor 2A

CLA – Cutaneous Lymphocyte-Associated Antigen

CMV – Cytomegalovirus

CORO1A – Coronin-1A

CTLA4 – Cytotoxic T-Lymphocyte-Associated Protein 4

CX3CR1 – C-X3-C Motif Chemokine Receptor 1

CXCL – C-X-C Motif Chemokine Ligand

DEG – Differentially expressed gene

DETC – Dendritic Epidermal T Cells

DLQI – Dermatology Life Quality Index

DMSO – Dimethyl Sulfoxide

DN – Double Negative

DNA – Deoxyribonucleic Acid

DP – Double Positive

EGR – Early Growth Response Protein

EOMES – Eomesodermin

ERAP – Endoplasmic Reticulum Aminopeptidase

ESR – Erythrocyte Sedimentation Rate

FACS – Fluorescence-Activated Cell Sorting

FBS – Fetal Bovine Serum

FITC – Fluorescein Isothiocyanate

FMO – Fluorescence Minus One

GADD45G – Growth Arrest and DNA Damage Inducible Gamma

GATA3 – GATA-Binding Protein 3

GNLY – Granulysin

GO – Gene Ontology

GPR18 – G Protein-Coupled Receptor 18

GSEA – Gene Set Enrichment Analysis

Gzm – Granzyme

HBcAg – Hepatitis B Core Antigen

HBeAg – Hepatitis B e Antigen

HBsAg – Hepatitis B Surface Antigen

HC – Healthy Control

HCV – Hepatitis C Virus

HEPES – 4-(2-Hydroxyethyl)-1-piperazineethanesulfonic Acid

HIV – Human Immunodeficiency Virus

HLA – Human Leukocyte Antigen

HMB-PP – (E)-4-Hydroxy-3-methyl-but-2-enyl pyrophosphate

hsCRP – High-sensitivity C-Reactive Protein

ICOS – Inducible T-Cell Costimulator

IFI44L – Interferon-Induced Protein 44-Like

IFIH1 – Interferon Induced with Helicase C Domain 1

IFITM1 – Interferon-Induced Transmembrane Protein 1

IFNG – Interferon Gamma (IFN-γ)

Ig – Immunoglobulin

IKZF1 – IKAROS Family Zinc Finger 1

IL – Interleukin

IMGT – International ImMunoGeneTics Information System

iNKT – Invariant Natural Killer T Cells

IPP – Isopentenyl Pyrophosphate

IRF1 – Interferon Regulatory Factor 1

ISG20 – Interferon-Stimulated Gene 20

ITGAL – Integrin Subunit Alpha L (CD11a)

JAK2 – Janus Kinase 2

JAML – Junctional Adhesion Molecule-Like Protein

KEGG – Kyoto Encyclopedia of Genes and Genomes

KIR – Killer-cell Immunoglobulin-like Receptors

KLF2 – Kruppel-Like Factor 2

KLRK1 – Killer Cell Lectin-like Receptor Subfamily K, Member 1 (NKG2D)

LEF1 – Lymphoid Enhancer-binding Factor 1

MAIT – Mucosal-associated Invariant T Cells

MBC – Molecular barcode

mDCs – Myeloid Dendritic Cells

MF – Molecular Function

MHC – Major Histocompatibility Complex

MICA – MHC Class I Polypeptide-related Sequence A

MICB – MHC Class I Polypeptide-related Sequence B

MIF – Macrophage Migration Inhibitory Factor

MR1 – Major Histocompatibility Complex Class I-related Protein 1

MSigDB – Molecular Signatures Database

MX1 – MX Dynamin-Like GTPase 1

MTOR – Mechanistic Target of Rapamycin

NaCl – Sodium Chloride

NF-kb – Nuclear Factor Kappa-light-chain-enhancer of Activated B Cells

NFATC1 – Nuclear Factor of Activated T-cells, Cytoplasmic 1

NGS – Next-Generation Sequencing

NIR – Near-infrared

NK – Natural Killer Cells

NKG2A – Natural Killer Group 2 Member A

NKG2D – Natural Killer Group 2 Member D

NKG7 – Natural Killer Cell Granule Protein 7

NKT – Natural Killer T Cells

OAS3 – 2'-5'-Oligoadenylate Synthetase 3

OP-RU – 5-(E)-2-Isopentenyl-4-hydroxy-3-methyl-but-2-enyl pyrophosphate

OX40 – Tumor Necrosis Factor Receptor Superfamily Member 4 (TNFRSF4)

pAg - phosphoantigen

PASI – Psoriasis Area and Severity Index

PBMC – Peripheral Blood Mononuclear Cells

PBS – Phosphate Buffered Saline

PCR – Polymerase Chain Reaction

PD-1 – Programmed Cell Death Protein 1

pDCs – Plasmacytoid Dendritic Cells

PE – Phycoerythrin

PE-Cy – Phycoerythrin-Cyanine

PD-1 – Programmed Cell Death Protein 1

PLA2G4D – Phospholipase A2 Group IVD

PLZF – Promyelocytic Leukemia Zinc Finger Protein

POLR2A – RNA Polymerase II Subunit A

PRF1 – Perforin 1

PSGL-1 – P-selectin Glycoprotein Ligand 1

PSORS – Psoriasis Susceptibility

PTPN7 – Protein Tyrosine Phosphatase, Non-Receptor Type 7

PV – Psoriasis Vulgaris

QC – Quality Control

RA – Rheumatoid Arthritis

RB – Rhodamine B

RNA – Ribonucleic Acid

RNA-seq – RNA Sequencing

ROR – RAR-related Orphan Receptors

RORC – RAR-related Orphan Receptor C

RT-qPCR – Reverse Transcription Quantitative Polymerase Chain Reaction

RUNX – Runt-related Transcription Factor

SAV – Sequencing Analysis Viewer

S100A7 – S100 Calcium-binding Protein A7 (Psoriasin)

SELL – Selectin L (L-Selectin)

SELPLG – Selectin P Ligand

SIRP – Signal-Regulatory Protein

SLAM – Signaling Lymphocytic Activation Molecule

SLE – Systemic Lupus Erythematosus

SRGN – Serglycin

STAT – Signal Transducer and Activator of Transcription

TAGAP – T-cell Activation GTPase-activating Protein

TBX21 – T-box Transcription Factor 21 (T-bet)

TCF7 – Transcription Factor 7

TCR – T-cell Receptor

TCR-seq – T-cell Receptor Sequencing

TCRV – T-cell Receptor Variable Region

TEMRA – Terminally Differentiated Effector Memory T Cells Re-expressing CD45RA

TBE – Tris-Borate-EDTA

TE – Tris-EDTA

TIGIT – T-cell Immunoreceptor with Ig and ITIM Domains

TNF-α– Tumor Necrosis Factor Alpha

TNFAIP3 – TNF Alpha-induced Protein 3

TNFRSF4 – Tumor Necrosis Factor Receptor Superfamily, Member 4 (OX40)

TNFRSF9 – Tumor Necrosis Factor Receptor Superfamily, Member 9 (4-1BB)

TNIP1 – TNFAIP3 Interacting Protein 1

TRA – T-cell Receptor Alpha Chain

TRAJ – T-cell Receptor Alpha Joining Gene

TRAV – T-cell Receptor Alpha Variable Region

TRB – T-cell Receptor Beta Chain

TRD – T-cell Receptor Delta Chain

TRG – T-cell Receptor Gamma Chain

TRM – Tissue-resident Memory T Cells

TUBB – Tubulin Beta Chain

TYK2 – Tyrosine Kinase 2

UV – Ultraviolet

ZBTB16 – Zinc Finger and BTB Domain-containing Protein 16 (PLZF)

11. CURRICULUM VITAE AND PUBLICATION LIST

First and last name: Maja Jirouš Drulak

Date and place of birth: 08/09/1995, Virovitica

E-mail: mjirous@mefos.hr, majajirous@gmail.com

WORK EXPERIENCE

- Research assistant - PhD candidate [11/02/2021 –]
    - Department of Medical Chemistry, Biochemistry and Clinical Chemistry, Faculty of Medicine Osijek
    - research project "NGS analysis of MAIT and γδ T cell transcriptome: phenotype, function and TCR repertoire in the aetiology of psoriasis vulgaris", funded by Croatian Science Foundation (UIP-2019-04-3494, PI: Assoc. Prof. Stana Tokić)

EDUCATION

- **Postgraduate Interdisciplinary Doctoral Study Molecular Biosciences** [20/04/2022 –]
    - J. J. Strossmayer University of Osijek, University of Dubrovnik, Ruđer Bošković Institute
- **Graduate University Study of Medical Laboratory Diagnostics** [01/10/2017 – 15/05/2020]
    - Faculty of Medicine Osijek, J. J. Strossmayer University of Osijek

Undergraduate University Study of Medical Laboratory Diagnostics [01/10/2014 – 19/09/2017]

Faculty of Medicine Osijek, J. J. Strossmayer University of Osijek

RESEARCH AND TRAINING FELLOWSHIPS

- **EFIS-IL Short Term Fellowship** [10/06/2024 – 05/07/2024]
    - Division of Biomedical Sciences, Warwick Medical School, UK
    - detailed phenotypic and functional profiling of MAIT and γδ T lymphocytes in psoriasis vulgaris using spectral cytometry and single-cell RNA sequencing
    - Supervisor: Assoc. Prof. Martin Davey

- **Croatian Science Foundation "Mobility Programme - Outbound Mobility of Research Assistants"** [20/12/2023 – 20/03/2024]
    - Division of Biomedical Sciences, Warwick Medical School, UK
    - detailed phenotypic and functional profiling of MAIT and γδ T lymphocytes in psoriasis vulgaris using spectral cytometry and single-cell RNA sequencing
    - Supervisor: Assoc. Prof. Martin Davey

- **Erasmus+ Mobility Program** [15/05/2023-13/06/2023]
    - Department of Immunology and Biotechnology, University of Pécs Medical School, Hungary
    - monoclonal antibody production by hybridoma technology
    - Supervisor: Prof. Péter Balogh

- **Erasmus+ Mobility Program** [21/06/2021 – 02/07/2021]
    - Department of Immunology and Biotechnology, University of Pécs Medical School, Hungary
    - flow cytometry and fluorescence-activated cell sorting
    - Supervisor: Prof. Péter Balogh

- **Erasmus+ Traineeship for Students** [02/03/2020-13/03/2020]
    - Department of Medical Biology and Central Electron Microscopic Laboratory, University of Pécs Medical School, Hungary
    - *In vitro* testing of the biological effects of compounds on tumor cells
    - Supervisor: Assoc. Prof. Hajnalka Abraham

AWARDS AND GRANTS

- **Croatian Immunological Society, "Bright Sparks" Award**
  For Presentation of Scientific Work at The Annual Meeting of the Croatian Immunological Society 2024, Sisak [11/10/2024 – 13/10/2024]

- **EFIS-EJI Travel Grant Scholarship**
    - for participation in the 7th European Congress of Immunology (ECI 2024), Dublin, Ireland [01/09/2024–04/09/2024]

- **FEBS Bursary Scholarship**
    - for participation in the 22nd Young Scientist's Forum and the 47th FEBS Conference, Tours, France [06/07/2023–12/07/2023]

- **Rector's Award for outstanding academic achievement**
    - J. J. Strossmayer University of Osijek [28/05/2018].

PUBLICATIONS

Jirouš Drulak, Maja; Grgić, Zvonimir; Plužarić, Vera; Šola, Marija; Opačak-Bernardi, Teuta; Viljetić, Barbara; Glavaš, Kristina; Tolušić-Levak, Maja; Periša, Vlatka; Mihalj, Martina, Štefanić, Mario; Tokić, Stana. Characterization of the TCRβ repertoire of peripheral MR1-restricted MAIT cells in psoriasis vulgaris patients // Scientific reports, 13 (2023), 13; 20990, 14. doi: https://doi.org/10.1038/s41598-023-48321-z

Krstulović, Luka; Leventić, Marijana; Rastija, Vesna; Starčević, Kristina; **Jirouš, Maja**; Janić, Ivana; Karnaš, Maja; Lasić, Kornelija; Bajić, Miroslav; Glavaš-Obrovac, Ljubica. Novel 7-chloro-4-aminoquinoline-benzimidazole hybrids as inhibitors of cancer cells growth: synthesis, antiproliferative activity, in silico ADME predictions, and docking // Molecules, 28 (2023), 28020540, 28. doi: 10.3390/ molecules28020

Tokić, Stana; **Jirouš, Maja**; Plužarić, Vera; Mihalj, Martina; Šola, Marija; Tolušić Levak, Maja; Glavaš, Kristina; Balogh, Peter; Štefanić, Mario. The miR-20a/miR-92b Profile Is Associated with Circulating γδ T-Cell Perturbations in Mild Psoriasis // International journal of molecular sciences, 24(5) (2023), 4323; 1-15. doi: 10.3390/ijms24054323

CONFERENCE ABSTRACTS

Jirouš Drulak, Maja; Štefanić, Mario; Plužarić, Vera; Šola, Marija; Mihalj, Martina; Tokić, Stana. The TCR repertoire of circulating γδ T lymphocytes in psoriasis vulgaris varies with age and disease severity // European journal of immunology, 54, S1, 2024. str. 988-988. doi: 10.1002/eji.202470200 – **poster presentation (presenter)**

Tokić, Stana; **Jirouš Drulak, Maja**; Plužarić, Vera; Šola, Marija, Mihalj, Martina; Štefanić, Mario. The peripheral MAIT cell TCRα/β repertoires alter with age of psoriasis vulgaris patients // European journal of immunology, 54, S1, 2024. str. 986-986. doi: 10.1002/eji.202470200 – **poster presentation (co-author)**

Jirouš, Maja; Grgić, Zvonimir; Opačak-Bernardi, Teuta; Viljetić, Barbara; Šola, Marija; Plužarić, Vera; Tolušić-Levak, Maja; Glavaš, Kristina; Štefanić, Mario; Tokić, Stana Peripheral MAIT cells of psoriasis vulgaris patients express diverse TCRβ clonal repertoire with specific CDR3 peptide variants // FEBS Open Bio, 2023. str. 244-244. doi: 10.1002/2211-5463.13646 - **poster presentation (presenter)**

Plužarić, Vera; **Jirouš Drulak, Maja**; Glavaš, Kristina; Viljetić, Barbara; Opačak Bernardi, Teuta; Šola, Marija; Tolušić Levak, Maja; Mihalj, Martina; Tokić, Stana; Štefanić, Mario. The peripheral MAIT cell transcriptome is enriched in cytotoxic and memory-effector markers, and associated with differences in cell lineage, not psoriasis vulgaris. // JEADV. Journal of the European academy of dermatology and venereology, XXXVII (2023), 10; 4439- **poster presentation (co-author)**

Tokić, Stana; **Jirouš Drulak, Maja**; Glavaš, Kristina; Plužarić, Vera; Šola, Marija; Opačak Bernardi, Teuta; Viljetić, Barbara; Tolušić Levak, Maja; Štefanić, Mario. Type I/II immunity and cytotoxicity signature genes mark transcriptional programs of peripheral γδ T cells in

untreated psoriasis vulgaris. // Abstract Book EADV Congress 2023. Berlin: European Academy of Dermatology and Venerology, 2023, 2765, 594 – **poster presentation (co-author)**

Jirouš, Maja; Glavaš, Kristina; Plužarić, Vera; Viljetić, Barbara; Opačak-Bernardi, Teuta; Šola, Marija; Tolušić Levak, Maja; Štefanić, Mario; Glavaš-Obrovac, Ljubica; Tokić, Stana RNASeq analysis of TCR repertoire in flow-sorted MAIT and yδ T cells of psoriasis vulgaris patients // 5. kongres Strukovnog razreda medicinsko laboratorijske djelatnosti Hrvatske komore zdravstvenih radnika s međunarodnim sudjelovanjem MEDICINSKO-LABORATORIJSKA DJELATNOST I SUVREMENA DIJAGNOSTIKA, Jesmo li sustigli budućnost? / Glavaš-Obrovac, Ljubica (ur.). Zagreb: Hrvatska komora zdravstvenih radnika, Strukovni razred medicinsko laboratorijske djelatnosti, 2023. str. 36-36 – **invited lecture (presenter)**

Glavaš, Kristina; Viljetić, Barbara; Opačak Bernardi, Teuta; **Jirouš Drulak, Maja**; Plužarić, Vera; Šola, Marija; Tolušić Levak, Maja; Tokić, Stana Comparative analysis of staining of MAIT cellsin skin with two MR1 tetramers // Dubrovnik Summer School on Molecular Biosciences in Medicine with the International Oxidative Stress Symposium - Book of Abstracts. Dubrovnik: Sveučilište u Dubrovniku, 2023. str. 43-43 – **poster presentation (co-author)**

Tokić, Stana; **Jirouš Drulak, Maja**; Grgić, Zvonimir; Plužarić, Vera; Šola, Marija; Opačak Bernardi, Teuta; Viljetić, Barbara; Glavaš, Kristina; Tolušić Leva, Maja; Mihalj, Martina et al. Assessment of T-cell Receptor Repertoire and Immunotranscriptome of Peripheral Innate-like T cells for the Advancement of Psoriasis Diagnostics and Immunotheraphy // The KEMOMIND Science Conference 2023 - Book of Abstracts / Kokondoska Grgič, Vesna; Vuga, Andrej (ur.). – **invited lecture (co-author)**

Viljetić, Barbara; **Jirouš, Maja**; Opačak-Bernardi, Teuta; Plužarić, Vera; Šola, Marija; Glavaš, Kristina; Tolušić Levak, Maja; Štefanić, Mario; Tokić, Stana. Immunostaining of MAIT and γδT cells in psoriatic lesions // Book of Abstracts of the Congress of the Croatian Society of Biochemistry and Molecular Biology HDBMB22: From Science to Knowledge. Zagreb: Hrvatsko Društvo za Biotehnologiju, 2022. str. 154-154 – **poster presentation (co-author)**

Jirouš, Maja; Štefanić, Mario; Plužarić, Vera; Mihalj, Martina; Grujin, Valentina; Tolušić Levak, Maja; Šola, Marija; Viljetić, Barbara; Opačak Bernardi, Teuta; Balogh, Peter et al. Deregulated miR-20a/miR-92b circuit underlies changes in circulating γδT cell proportions in psoriasis vulgaris // HLA: Immune Response Genetics Special Issue: Abstracts for the Joint 35th European Immunogenetics and Histocompatibility Conference Amsterdam, the Netherlands, May 17–20, 2022. 2022. str. 536-536. doi: 10.1111/tan.14606 – **poster presentation (presenter)**

Jirouš, Maja; Štefanić, Mario; Plužarić, Vera; Šola, Marija; Viljetić, Barbara; Opačak-Bernardi, Teuta; Tolušić Levak, Maja; Balogh, Péter; Tokić, Stana. An altered distribution of MR1-restricted mucosal- associated invariant T cells (MAIT) in blood and skin of vulgar psoriasis patients // 6th International Cholnoky Symposium. Pečuh, 2022. str. 8-8 – **oral presentation (presenter)**

Jirouš, Maja; Zidar, Ana; Glavaš, Kristina; Mihalj, Martina; Štefanić, Mario; Tokić, Stana. Comparison of RNA yield and purity from small cell numbers following TRI reagent, Direct-zol RNA Microprep and NucleoSpin RNA XS extraction. 2021. str. 332-332. doi: 10.1002/2211-5463.13205 – **poster presentation (presenter)**

Tokić, Stana; Šola, Marija; Opačak-Bernardi, Teuta; Viljetić, Barbara; **Jirouš, Maja**; Glavaš, Kristina; Plužarić, Vera; Mihalj, Martina; Štefanić, Mario. The proportions of MR1-restricted TCRVa7.2+ and VcVd1-d2-TCR subtypes are altered in human psoriatic skin and vary with age // FEBS Open Bio, 2021. str. 457-457 - **poster presentation (co-author)**

Jirouš, Maja; Štefanić, Mario; Šola, Marija; Viljetić, Barbara; Opačak-Bernardi, Teuta; Plužarić, Vera, Mihalj, Martina; Glavaš, Kristina; Tolušić Levak, Maja; Balogh, Peter; Tokić, Stana. The γδhi and γδint T cell subsets are disproportionally altered in blood and skin of vulgar psoriasis patients // 3rd Young Scientists' Day – Book of Abstracts. 2021. str. 36-36 – **oral presentation (presenter)**

Čupić, Mateo; **Jirouš, Maja;** Knežević, Marija; Radman, Ana; Macan, Marija; Štefanić, Mario; Tokić, Stana. EFFICIENCY ASSESMENT OF CHELEX® AND QIAGEN® METHODS FOR BLOOD AND BUCCAL DNA ISOLATION AND STR ANALYSIS // 11th ISABS Conference on Forensic and Anthropologic Genetics and Mayo Clinic Lectures in Individual Medicine. Zagreb: Printera Grupa, 2019. str. 278-278 – **poster presentation (presenter)**

Jirouš, Maja; Rugani, Bruno; Jukić, Marijana; Krstulović, Luka; Bajić, Miroslav; Glavaš-Obrovac, Ljubica. Antitumorska aktivnost novosintetiziranih kinolinskih hibrida na tumorskim stanicama in vitro // Simpozij „Prvih 10 godina HDIR-a"– knjiga sažetaka. Zagreb: Hrvatsko društvo za istraživanje raka (HDIR), 2019. str. 11-11 – **oral presentation (presenter)**